PTNSS

195(4), 2023

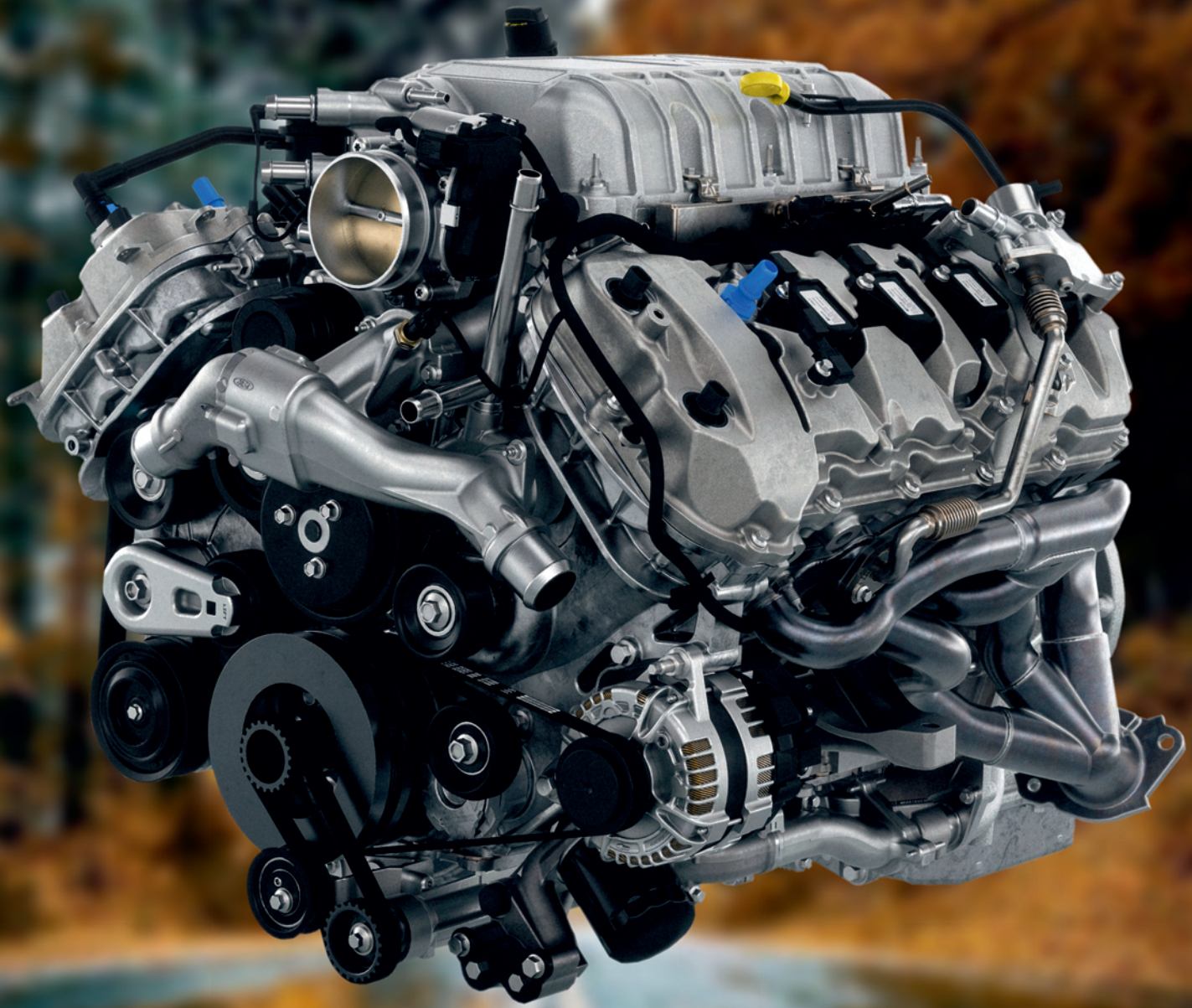

COMBUSTION ENGINES

AIR FORCE INSTITUTE OF TECHNOLOGY
INSTYTUT TECHNICZNY WOJSK LOTNICZYCH

ul. Księcia Bolesława 6, 01-494 Warszawa, Poland
tel.: +48 261 851 300; fax: +48 261 851 313
www.itwl.pl e-mail: poczta@itwl.pl

SUPPORTING OPERATIONS & MAINTENANCE OF AERONAUTICAL ENGINEERING:

- tribological diagnostics of lubrication systems in power units and hydraulic systems
- endoscopic examinations of power units
- measurements of operation parameters of power units using one's own and company systems and their analysis

DEVISING AND DEVELOPING NEW DIAGNOSTIC METHODS:

- CT examinations – V/tome/X CT system
- blade vibration measurements using the tip-timing method

NEW TECHNOLOGIES FOR UNMANNED AERIAL VEHICLES:

- technical condition monitoring system of mini jet engine
- hybrid drive of unmanned aerial vehicle

Due to the dynamic development of machine and vehicle powertrains, the "Combustion Engines" scientific journal, while retaining its historical title, currently publishes works related not only to internal combustion engines, but also other powertrains, including hybrid drives, electric drives and fuel cells.

PTNSS Supporting Members
Członkowie wspierający PTNSS

BOSMAL Automotive Research and Development Institute Ltd
Instytut Badań i Rozwoju Motoryzacji BOSMAL Sp. z o.o

Motor Transport Institute
Instytut Transportu Samochodowego

Institute of Aviation
Sieć Badawcza Łukasiewicz – Instytut Lotnictwa

Automotive Industry Institute
Sieć Badawcza Łukasiewicz – Przemysłowy Instytut Motoryzacji

Sieć Badawcza Łukasiewicz – Poznański Instytut Technologiczny

AVL List GmbH

Solaris Bus & Coach S.A.

Air Force Institute of Technology
Instytut Techniczny Wojsk Lotniczych

Military Institute of Armoured & Automotive Technology
Wojskowy Instytut Techniki Pancernej i Samochodowej

Toyota Motor Poland Ltd. Sp. z o.o.

RADWAG Balances and Scales
RADWAG Wagi Elektroniczne

MS Mechatronic Solutions Group

FOGO Sp. z o.o.

COMBUSTION ENGINES
A Scientific Magazine

2023, 195(4)

Year LXII

PL ISSN 2300-9896
PL eISSN 2658-1442

Publisher:
Polish Scientific Society of Combustion Engines
60-965 Poznan, pl. M. Skłodowskiej-Curie 5, Poland
tel.: +48 61 6475966, fax: +48 61 6652204
E-mail: sekretariat@ptnss.pl
WebSite: http://www.ptnss.pl
Papers available on-line: http://combustion-engines.eu

Contents

Publisher:

Polish Scientific Society of Combustion Engines
60-965 Poznan, pl. M. Sklodowskiej-Curie 5, Poland
tel.: +48 61 6475966, fax: +48 61 6652204
E-mail: sekretariat@ptnss.pl
WebSite: http://www.ptnss.pl

Subscriptions
Send subscription requests to the Publisher's address.
Cost of a single issue PLN 65.

Preparation for print
ARS NOVA Publishing House
60-782 Poznan, ul. Grunwaldzka 17/10A

Circulation: 60 copies

Printing and binding

Zakład Poligraficzny Moś i Łuczak, sp. j.,
Poznań, ul. Piwna 1

The journal is under the patronage of the Transport Committee of the Polish Academy of Sciences

The journal is registered and listed in the Polish and international database

Papers published in the
Combustion Engines
quarterly receive 100 points as stated by the Notification of the Minister of Education and Science dated 17 July 2023.

Declaration of the original version
The original version of the Combustion Engines journal is the printed version.

Cover
I – 5.2L V8 Ford Mustang GTD *(performance.ford.com)*;
background *(Wet Road, autumn, fall, leaves, nature, rainy, road, tree – www.peakpx.com)*
IV – Garrett's Electrified Turbos (E-Turbos)
(www.garrettmotion.com)

Article citation info:
Lasota M, Zabielska A, Jacyna M, Żak J. Research and analysis of the operation of vehicles with various propulsion systems, including costs and CO_2 emissions. Combustion Engines. 2023;195(4):3-13. https://doi.org/10.19206/CE-169845

Michał LASOTA
Aleksandra ZABIELSKA
Marianna JACYNA
Jolanta ŻAK

Combustion Engines
Polish Scientific Society of Combustion Engines

Research and analysis of the operation of vehicles with various propulsion systems, including costs and CO_2 emissions

ARTICLE INFO

Received: 6 June 2023
Revised: 14 July 2023
Accepted: 20 July 2023
Available online: 5 September 2023

The article analyzes and evaluates costs, transport time and CO_2 emissions by selected vans. The research was carried out on the example of three models of Iveco Daily vehicles powered by: diesel oil, electricity and compressed natural gas (CNG). The result of the research presented in the article is the determination of the operating costs of vehicles powered by various energy sources and the level of CO_2 emissions. The comparative analysis was carried out on real data for the established transport task. Vehicles with engines powered by compressed natural gas are characterized by the highest savings in terms of transport costs. As the authors pointed out, this may be due to the fact that this type of engines, despite the low interest of buyers at the moment, may gain much more popularity in the future. On the other hand, in relation to vehicles with electric motors, the cost of transport is the highest, which means that this type of technology is ineffective in relation to long-distance transport.

Key words: *combustion engine, electric motor, exhaust emissions, comparative analysis, operation*

1. Introduction

The operation of combustion, electric and compressed natural gas vehicles is a topic that attracts a lot of interest among both scientists and practitioners from the automotive industry. In recent years, with the increase in the ecological awareness of the society, this issue has become even more topical due to the need to reduce the emission of harmful substances into the atmosphere.

In this context, the so-called alternative drives. As indicated by the author of the work [29], alternative drives are all drives whose overriding goal is to reduce the consumption of fossil fuels. In the initial stage of the idea, the introduction of this type of drive units was to make the world independent of the availability of crude oil. Today, however, the goal is a bit broader and much more ambitious: vehicles with alternative drives generally emit less harmful exhaust gases, and thus are more environmentally friendly and contribute less to the progressing climate change [15].

This applies not only to limited carbon dioxide emissions, but also, for example, nitrogen oxides or hydrocarbons, which can contribute to the development of serious diseases, such as cardiovascular diseases or cancer. One of the basic impulses that draw the attention of vehicle manufacturers and users to new technical solutions is also the need for vehicles to meet strictly defined technical requirements [26]. These requirements must be met both at the design stage and at the operational stage. Legislative centers of individual countries or organizations deal with defining new guidelines and setting deadlines for their implementation. Legal acts currently in force in Poland must comply with the guidelines of the European Commission or the European Parliament [3].

The dynamically growing demand for goods generates a constantly growing demand for transport services, which in turn translates into the need to develop technologies in the area of broadly understood transport and logistics. With the progressive development of automotive technologies, more and more attention is paid to alternative sources of vehicle propulsion [42]. One of the biggest challenges in the field of transport is to reduce emissions of harmful substances and limit the impact of the transport sector on climate change. In this context, electric motors and motors powered by alternative energy sources are gaining popularity as a potential alternative to traditional internal combustion engines [37].

Engineers working on modern technological solutions in the field of vehicles powered by alternative energy sources are trying to design transport devices that provide relatively increasing transport efficiency while minimizing costs, which are influenced by factors such as reliability of manufactured devices, fuel/electricity demand or ease of use. The growing problem related to the stringent regulations on exhaust gas emission levels and the increasingly difficult situation with the workforce generates the need for systematic development of this field [3]. From the point of view of employers, an indispensable aspect in the case of designing new technologies in the field of road freight transport is the development of new transport devices, the operation of which requires the involvement of a relatively smaller number of people, and the development of technologies to ensure a greater range of the vehicle on a single charge/refuelling [4].

The main purpose of the study is to analyze and compare the latest technologies available in the field of domestic cargo distribution using delivery vehicles. The performed analysis focuses on the comparison of delivery vehicles powered by different power sources.

The article presents research on the operation of combustion, electric and compressed natural gas-powered vehicles. The authors analyzed the operating costs of selected vehicles in the implementation of transport tasks annually. Attention was focused on taking into account the costs related to CO_2 emissions.

2. Literature analysis

The literature analysis on the operation of internal combustion, electric and CNG vehicles may cover many aspects. The topic of internal combustion vehicles covers primarily issues related to the repair and maintenance of internal combustion engines and diagnostic tests. Among them, one can distinguish the assessment of the technical condition of internal combustion engines and their components, optimization of engine operation in terms of efficiency and economy, or research on exhaust emissions and the impact of internal combustion engines on the natural environment.

Internal combustion vehicle technology is related to the systems and components used in internal combustion engines, which are the main source of propulsion in traditional cars [13, 40]. Combustion engines are based on the principle of combustion of a mixture of fuel and air inside the cylinder, which generates the mechanical energy needed to move the vehicle [42]. The most common internal combustion engines are reciprocating engines, including gasoline and diesel engines. The technology of internal combustion vehicles also includes fuel supply systems, cooling, exhaust and drive systems [1, 6]. Each of these components plays an important role in the proper functioning of the internal combustion engine and ensures optimal performance. The technology is constantly improved in order to improve efficiency, reduce pollutant emissions and increase the economy [13].

In recent years, various innovations have been introduced, such as direct fuel injection systems, turbochargers, stop-start systems or hybrid drive systems to increase efficiency and reduce the negative impact on the environment [22]. However, the disadvantage of internal combustion engines is still the emission of pollutants such as nitrogen oxides and carbon dioxide, which harm the environment and human health. There are many sources of literature that focus on research on internal combustion vehicles. The authors of the work [25] analyzed the assessment of the impact of the temperature management strategy on engine warm-up in modern spark engines. The article presents techniques such as thermal insulation, the use of thermoactive pumps or cooling system control in order to assess the impact of these strategies on engine warm-up time, its efficiency, fuel consumption and exhaust emissions. The authors of the publication [14] examined the influence of the type of fuel on the emission of pollutants from a compression-ignition engine (diesel engine).

In the article [38], experimental studies related to the efficiency and emission characteristics of a turbocharged diesel engine, which is fueled with fuel mixtures consisting of aviation kerosene and diesel oil, were carried out. The aim was to evaluate the application potential and to understand the effect of the kerosene-oil mixture on engine performance and pollutant emissions. In publication [39], optimization of the compression ratio of a spark engine fueled with mixtures of methanol and gasoline was carried out. The study was based on the use of a multi-criteria method that takes into account various quality indicators, such as combustion efficiency, power, torque and pollutant emissions.

Despite many years of development of internal combustion vehicle technology, interest in alternative power sources, such as electric drive, has recently increased. Literature on electric vehicles focuses mainly on issues related to their power supply or maintenance in proper technical conditions. The discussed topics concern the design and operation of power supply systems, energy management in vehicles and their charging, safety issues during operation or the comparison of the costs of using internal combustion and electric vehicles [31, 32].

Electric vehicles use accumulators or batteries to store electricity that drives the engine [18]. The cars are characterized by low emissions of exhaust gases and carbon dioxide, which makes them environmentally friendly. Electric motors are characterized by quiet engine operation, which allows for a more comfortable ride. The constantly growing interest in electric vehicles contributes to the development of the charging infrastructure [2, 24]. More and more public and private places offer charging stations.

However, despite the continuous development of electric vehicles, the issue of the limited driving range on a single charge remains a big challenge. This is still a big problem for some users. This creates some challenges, extending the charging time compared to refueling and limiting the availability of charging stations in some areas [20]. Despite this, electric vehicles contribute to reducing greenhouse gases and improving air quality [26]. There are many scientific publications that analyze various aspects of electric vehicles. In the article [24], the authors examine issues related to electromobility, such as charging infrastructure, batteries, or power grids.

Many publications, e.g. [12, 42] refer to research related to the emission of harmful substances from the drive system. The papers show that emissions are dependent on the source of electricity, but even with a fossil fuel-based energy mix, emissions from electric vehicles tend to be lower than those of internal combustion vehicles. Publication [17] focuses on the study of CO_2 emissions generated by internal combustion and electric vehicles in car-sharing systems. Position [5] focuses on the analysis of the impact of the network effect on profits and social welfare related to the introduction of electric vehicles. In [8], an effective approach to estimating energy consumption by electric vehicles is presented, which is important when planning and optimizing the fleet of vehicles, as well as managing energy costs in service companies.

The literature on cars powered by compressed natural gas (CNG) provides information on the efficiency, emissions, infrastructure availability and economic aspects related to this type of propulsion. Natural gas is compressed to reduce its volume and increase its density. It is then used as fuel to power the vehicle's engine. In order to use CNG, cars must be equipped with appropriate gas supply systems [35]. Articles [33] or [19] present the current situation of air pollution caused by vehicles powered by compressed natural gas and possible technologies for reducing these emissions. Similarly, [37] provides conclusions and data related to the ecological and economic benefits resulting from the use of CNG power systems in small wood shredders. This is important because small internal combustion engines often generate a significant amount of harmful emissions. The publication [16] analyzes the emission of the particle

number (PN – Particle Number) generated by various types of vehicles, including light vehicles powered by CNG while driving in real road conditions. The aim was to compare the PN emissions for different types of cars, which is important for assessing their impact on air quality. CNG is one of the alternative fuels used to reduce pollutant emissions and reduce the negative impact of transport on the environment. Vehicles powered by compressed natural gas are considered more environmentally friendly than vehicles powered by traditional fuels.

3. Costs of the transport task

3.1. General remarks

The factor that plays an important role in the development of transport technology is the cost of carrying out transport tasks. Transport activity incurs costs that can be divided into fixed and variable costs. Fixed costs do not depend directly on the level of production or sales. These are costs that occur regardless of whether the enterprise is fully operational or has no activity at all [11]. Variable costs are directly related to the level of production or sales. Increasing the company's activity, such as selling more goods, leads to an increase in variable costs. If, on the other hand, the company's activity decreases, variable costs also decrease [11, 23].

Fixed and variable costs will be analyzed in the article for individual vehicles (variants).

Fixed costs:

- depreciation costs of means of transport
- costs of taxes on means of transport (vehicles up to 3.5 tons are not taxed)
- costs of insurance of means of transport
- driver salary costs.

Variable costs:

- road toll costs (vehicles with a GVM up to 3.5 tons are not subject to tolls and there are no motorway tolls in the analyzed section)
- fuel consumption costs
- parking costs of electric cars at charging stations
- costs of environmental fees (for delivery vehicles meeting the EURO VI emission standard, the rate of fees for the introduction of gases and dust is not provided)
- drivers' allowance costs
- costs of servicing means of transport
- costs of replacing tires in means of transport.

3.2. Depreciation costs of means of transport

The Accounting Act [33] and the Corporate Income Tax Act [32] provide information that means of transport are subject to depreciation as fixed assets with a useful life longer than one year when calculating their initial value. The depreciation rate for vans is 20% in accordance with the Classification of Fixed Assets.

$$K_{AP} = K_{A1P} \cdot L_{poj}\ [\text{PLN/year}] \tag{1}$$

where: K_{AP} – annual depreciation costs for the total number of vehicles, K_{A1P} – annual depreciation costs for one vehicle, L_{poj} – number of vehicles (on an annual basis).

The annual depreciation cost of the vehicle was calculated using the formula:

$$K_{A1P} = W_{PD} \cdot \alpha_D [\text{PLN/year}] \tag{2}$$

where: W_{PD} – initial value of the delivery vehicle, α_D – annual depreciation rate for the car.

3.3. Costs of insurance of means of transport

Commercial vehicle insurance includes various types of policies that provide financial protection in the event of damage [43]. The insurance of the analyzed vehicles includes OC, AC and accident insurance. Liability insurance is obligatory and covers damage caused to third parties as a result of an accident caused by a van. Another insurance that applies to the analyzed vehicles is AC (auto-casco), which protects against situations such as accident, theft, fire and unforeseen events.

The AC policy covers the costs of repair or replacement of a delivery vehicle as a result of undesirable damage. The last type of insurance is NNW (Accidental Consequences), which provides financial protection in the event of personal injury that may be suffered by the driver or passenger. Such policies cover all analyzed vehicles – internal combustion, electric, and CNG-powered.

The total annual cost of insurance is calculated from the following relationship:

$$K_{UP} = K_{U1P} \cdot L_{poj}\ [\text{PLN/year}] \tag{3}$$

where: K_{U1P} – annual costs of insurance of the delivery vehicle.

3.4. Driver salary costs

In the enterprise, drivers are employed on the basis of an employment contract. The costs of drivers' remuneration include net remuneration and overheads for remuneration and benefits – social security contributions (pension, accident and disability pension), as well as write-offs to the Labor Fund (FP) and the Guaranteed Employee Benefits Fund (FGŚP). The number of drivers needed to perform a transport task results from the number of vehicles that are necessary for this purpose. In addition, one reserve driver is employed.

The number of drivers can be calculated using the formula:

$$L_k = L_{KP} + L_{KR}\ [\text{drivers}] \tag{4}$$

where: L_{KP} – number of employed drivers, $L_{KP} = L_{poj}$, L_{KR} – number of reserve drivers, $L_{KR} = 1$.

The monthly total remuneration costs of drivers can be determined using the following relationship:

$$K_{WK} = (K_{WP} + K_{NW}) \cdot L_K\ [\text{PLN/month}] \tag{5}$$

where: K_{WP} – monthly salary costs of the employed driver [PLN/month], K_{NW} – monthly costs of mark-ups on the driver's remuneration [PLN/month].

3.5. Fuel/energy costs

The cost of fuel consumption depends on the average fuel consumption of the vehicle and the price of this fuel.

Annual fuel consumption costs are calculated for the total number of means of transport:

$$K_{RRP} = K_{ZP} \cdot L_{poj}\ [\text{PLN/year}] \tag{6}$$

where: K_{ZP} – annual costs of fuel consumption for one vehicle [PLN/year].

$$K_{ZP} = \frac{Z_p \cdot C_p}{100} \cdot L_{RP} \text{ [PLN/year]} \quad (7)$$

where: Z_p – average fuel/energy consumption of a delivery vehicle [dm^3/100 km]/[kWh/100 km]/[m^3], C_p – average net price of fuel/energy [PLN/l]/[PLN/kWh]/[PLN/m^3], L_{RP} – annual vehicle mileage [km], $L_{RP} = L_{MP} \cdot 12$, L_{MP} – monthly vehicle mileage in km.

3.6. Costs of parking electric cars at charging stations

The cost of parking an electric car at charging stations may vary depending on many factors, such as location, charging station operator, type of charger, parking time and service charges. In the case of multiple stations, fees may be charged based on the time of stoppage or the amount of energy delivered. The amount of charging rates and parking fees for electric cars is presented in Table 1.

Table 1. Charge rates and parking fees for electric cars [27]

Charger type	Charging rate [PLN/kWh]
AC	1.89
DC (≤ 50 kW)	2.69
DC (50 kW < x ≤ 125 kW)	2.89
DC (> 125 kW)	3.19
The rate for parking is 0.40 [PLN/min] – charged after 45 minutes from the start of charging for DC connectors.	

In the analyzed case, due to the greatest availability of DC chargers with a power of ≤ 50 kW, selected locations for charging electric vehicles have such devices. Therefore, the power supply is carried out using DC chargers with the specified power.

The cost of parking an electric car at a charging station in a transport relation is expressed by the following formula:

$$K_{PSE} = \gamma_P \cdot t_ł \cdot n_ł \text{ [PLN]} \quad (8)$$

where: γ_P – the rate for parking at the charging station [PLN/min], $t_ł$ – electric vehicle charging time (reduced by 45 minutes) [min], $n_ł$ – number of loads in a transport task.

The total cost for parking cars at charging stations is:

$$K_{ŁP} = K_{PSE} \cdot d_r \cdot L_{poj} \text{ [PLN/year]} \quad (9)$$

where: d_r – number of working days, $d_r = 250$.

3.7. Driver allowance costs

The Regulation of the Minister of Labor and Social Policy of 2022 [30] states that drivers are entitled to a business travel allowance. Domestic travel is considered in the analyzed case. The diet is granted for food costs and currently amounts to PLN 45 per day of travel. According to the regulation, when the trip is shorter than a day and amounts to:

- up to 8 hours – the diet is not due
- from 8 to 12 hours – 50% of the diet is due
- over 12 hours – 100% of the diet is due.

Considering the above, the transport route for a combustion vehicle and a CNG-powered vehicle is from 8 to 12 hours, therefore the value of the business trip allowance is 50%. In the case of electric cars, the entire route (including charging) will be over 12 hours, which means that the driver is entitled to 100% of the allowance. The amount of the annual cost of business travel allowances can be determined by the following formula:

$$K_{DK} = K_{DK}^{PL} \cdot 12 \text{ [PLN/year]} \quad (10)$$

where: K_{DK}^{PL} – monthly costs of allowances for 1 driver [PLN/year].

The rate of annual business trip allowance costs for the total number of drivers carrying out the transport can be calculated from the following relationship:

$$K_{CDK} = K_{DK} \cdot L_{KP} \text{[PLN/year]} \quad (11)$$

3.8. Vehicle service and tire replacement costs

The costs of services include the costs of replacement of operating fluids, as well as the costs of servicing vehicles resulting from wear and tear, as well as breakdowns and repairs. Annual service costs for the total number of vehicles are expressed as follows:

$$K_{SP} = K_{S1P} \cdot L_{poj} \text{ [PLN/year]} \quad (12)$$

K_{S1P} – annual cost of servicing one vehicle [PLN/year].

The annual costs of replacing tires depend on the rate of their wear. For the purposes of the analysis, it was assumed that tires are replaced every 100,000 km. The cost of tires for the total number of vehicles is:

$$K_{ZO} = K_{Z1O} \cdot L_{poj} \text{ [PLN]} \quad (13)$$

where: K_{Z1O} – cost of a set of tires for one delivery vehicle [PLN].

The total number of tire changes per year is 3.

4. Analysis of transport costs and CO_2 emissions based on real data

4.1. Determining the parameters of the cargo to be transported

For the purposes of the analysis, it was assumed that the transported load would be the engine oil filter. It is characterized by high transport susceptibility and relatively low weight. The analyzed pallet load unit consists of collective packaging in the form of 24 cartons, the contents of which include 12 filters. The retail unit is, in turn housed in a unit package. Figure 1 shows the scheme of creating a pallet load unit being the subject of transport.

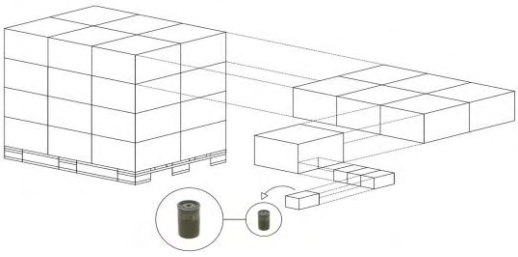

Fig. 1. Scheme of creating a pallet load unit being the subject of transport [own elaboration based on AutoCAD]

One transport includes four pallet load units, which means that the total weight of the load on the vehicle is 800 kg. Transport is carried out once a day, which directly translates into the need for one vehicle to carry out a transport task.

4.2. Technical and operational parameters of vehicles

The selection of the right vehicle for the transport task is a key element of effective logistics and can have a significant impact on the costs, efficiency or equivalence of transport operations. Before making a choice, several important factors should be taken into account [9]:

- Load requirements – The first and most important step is to correctly understand the characteristics and individual requirements of the load itself. Estimate the weight, external dimensions, weather sensitivity, value and any special transport requirements.
- Transport route – a very important aspect is the distance to be covered as part of the transport task and the nature of the route. If the transport will be performed over short distances within the city, electric vehicles may be more appropriate. On the other hand, for long distances, where the range and availability of charging places are important factors, combustion vehicles may be a better alternative.
- Fuel efficiency – When it comes to minimizing vehicle operating costs, the fuel efficiency of different types of vehicles should be considered. In the case of traditional internal combustion engines, attention should be paid to fuel consumption, and thus also to the level of emission of harmful substances into the atmosphere. In the case of electric vehicles, fuel savings may be greater, and the transit time may be adversely affected due to the long charging time of the battery.
- Infrastructure and availability – The availability of refueling/charging infrastructure is also an important factor. While the availability of petrol stations is very high, the situation with vehicle charging stations and available charging stations is a bit more complicated.
- Operating costs – An analysis of operating costs is an indispensable element when choosing a vehicle. When planning, the costs of purchase, maintenance, repairs, insurance and fuel or electricity should be taken into account.

Transport will be carried out using delivery vehicles with a maximum weight of up to 3.5 tons powered by three energy sources. The paper presents the technical parameters of vehicles powered by diesel oil (variant 1), electricity (variant 2) and compressed natural gas (CNG) (variant 3). The vehicle under analysis is the IVECO Daily in the following versions: standard, electric and natural power. The maximum permissible weight of each vehicle is 3.5 tonnes. The engine power of the vehicle powered by diesel oil and compressed natural gas is respectively 136 horsepower, while the electric vehicle generates 110 horsepower. Each of the vehicles is equipped with "Back Sleeper" type sleeping cabins, enabling rest during the transport. Due to the clearly defined technical parameters of the shipment and for the needs of the cargo, whose transportability is relatively high, a vehicle with a box body was selected. The company carries out domestic transport in various relations. The analyzed route has one dedicated vehicle and one driver. One transport cycle is carried out in one day. In the case of variant one and variant 3, the duration of the journey does not include the driver's daily rest, while in variant 2 the daily rest is carried out in the vehicle cabin while the vehicle's battery is being charged. The table below summarizes the basic data of the transport task.

Individual parameters were determined on the basis of the vehicle configurator available on the manufacturer's website. The work assumes the speed of travel on highways up to 90 km/h. Favorable weather conditions and no capacity disturbances on the analyzed section of the route were assumed. In Table 3 presents the technical data of the analyzed vehicles.

Table 3. Vehicle technical data [7]

Parameter \ Vehicle type	Variant 1	Variant 2	Variant 3
Max. range [km]	900	200	350
Refueling/charging time [min]	2	150	5
CO_2 emissions per 100 km [kg]	26.8	0	22.8
Cost of traveling 100 km [PLN]	67	81	51
Noise emission [dB]	85	50	70
Exhaust emission standard	EURO VI	–	EURO VI

4.3. Determination of routes and locations of vehicle power supply points

The article outlines the route from Warsaw to Wroclaw. The return route was also taken into account when designing the journey. Transportation will be performed using combustion, electric and compressed natural gas vehicles. During the planning of the route, power points for the above-mentioned types of vehicles were determined. On the basis of the outlines containing the technical data of the analyzed vehicles, the range of a given vehicle on one refueling/charging was analysed. Due to the above, it was possible to determine at what kilometer intervals the supply points should be considered. Attention was paid to refueling/charging cars before reaching the reserve. Appropriate level of energy/fuel and their regular monitoring ensures smooth driving and a guarantee of delivering the load in accordance with the guidelines. Determining the location of vehicle charging points required an analysis of available charging/refueling points on the road, types of chargers, availability, opening hours and prices.

Figure 2 shows the course of the transport route for a combustion vehicle, taking into account petrol stations, loading and unloading places.

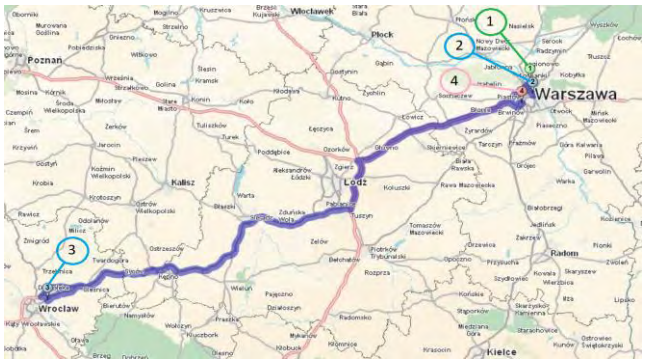

Fig. 2. The course of the route for a combustion vehicle [own elaboration based on PTV Map&Guide]

The next diagram (Fig. 3) shows the course of the road for an electric vehicle, including charging points and places of delivery/collection of the charge.

Fig. 3. Transport route for an electric vehicle [own elaboration based on PTV Map&Guide]

Figure 4 illustrates the transport relation for a vehicle powered by compressed natural gas, taking into account the place of refueling and delivery and collection of the cargo.

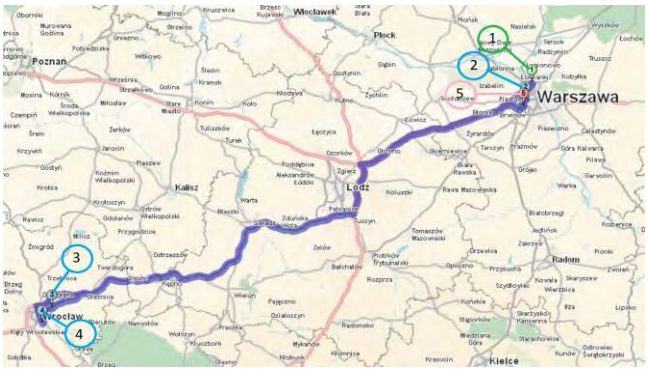

Fig. 4. Transport route for a CNG-powered vehicle [own elaboration based on PTV Map&Guide]

The numbers used in the figures are discussed in Tables 4 and 5.

Table 4. Locations of loading, refueling/loading and unloading points for vehicles on the Warsaw–Wroclaw route

Warszawa – Wroclaw route			
Combustion vehicle	Designation	Location	Operation
	1	Panttoni Europe Warsaw Odlewnicza 6	Loading
	2	Gas station ORLEN al. 3maja 1a	Refueling
	3	DHL Wrocław, Bierutowska 75	Unloading
Electric vehicle	1	Panttoni Europe Warsaw Odlewnicza 6	Loading
	2	Gas station ORLEN al. 3maja 1a	Charging
	3	Gas station ORLEN Sięganów 79d	Charging
	4	DHL Wrocław, Bierutowska 75	Unloading
CNG-powered vehicle	1	Panttoni Europe Warsaw Odlewnicza 6	Loading
	2	Station PGNiG CNG I. Prądzyńskiego 16	Refueling
	3	DHL Wrocław, Bierutska 75	Unloading

Table 5. Locations of loading, refueling/loading and unloading points for vehicles on the Wroclaw–Warsaw route

Wroclaw–Warszawa route			
Combustion vehicle	Designation	Location	Operation
	3	DHL Wrocław, Bierutowska 75	Loading
	4	Warsaw, Krakowiaków 44	Unloading
Electric vehicle	4	DHL Wrocław, Bierutowska 75	Loading
	5	Gas station ORLEN Maślicka 218	Charging
	6	Service Station, Paprotnia 26a	Charging
	7	Warsaw, Krakowiaków 44	Unloading
CNG-powered vehicle	3	DHL Wrocław, Bierutowska 75	Loading
	4	Gas station Wrocław, Gazowa 3	Refueling
	5	Warsaw, Krakowiaków 44	Unloading

Electric vehicle users can choose to charge their vehicles using two basic types of chargers. These are chargers that generate alternating current (AC chargers) and direct current (DC chargers). A given type of charger is characterized by charging speed and the cost of 1 kWh. AC chargers are a more common type found in versions for personal use (in the so-called Wallboxes) as well as commercial ones. At home, the power of chargers of this type is usually from 3.6 to 22 kW. They use single-phase (230 V) or three-phase (400 V) voltage. The charging time of a vehicle with a battery with a standard capacity of 50 kWh with this type of charger varies from 3 to 5 hours.

DC chargers located in service areas, parking lots or petrol stations are often a better choice for drivers on the road. This is primarily due to the fact that their power is much higher compared to AC, ranging from 50 to 150 kW, but can also have a higher power. In the case of this work, the analysis took into account the charging of vehicles at petrol stations belonging to the Orlen Concern, which has DC chargers with a capacity of 50 kW and 100 kW. The charging time of the battery with a capacity of 75 kWh in the used vehicle is approx. 2.5 hours.

5. Comparative analysis of costs and selected vehicle parameters

5.1. Summary list of fixed and variable costs

The considered case assumes that 2023 the vehicle will be operated for 250 days, because this is the number of working days. The work assumes that the length of the route in one transport cycle is approx. 750 km. The daily fuel consumption for a diesel vehicle is approx. 83 liters, for electricity, it is 225 kWh, while the consumption for a CNG vehicle is 113 m^3 of compressed natural gas. Outlays presented in the work are gross costs.

Based on the adopted assumptions, calculations of individual cost components were made, which are summarized in Table 6.

Table 6. Aggregate data relating to the analyzed costs

Parameter \ Variant	Variant 1	Variant 2	Variant 3
The initial value of the vehicle [thousand PLN]	210	180	190
OC, AC, NNW [PLN/year] (delivery vehicle)	3,500	4,000	4,200
Average fuel consumption	11 [dm^3/100 km]	30 [kWh/100 km]	15 [m^3/100 km]
Fuel/energy price	6.09 [PLN/l]	2.69 [PLN/kWh]	3.40 [PLN/m^3]
Employee allowance cost [PLN]	22.5 (up to 8 hours)	45 (up to 12 hours)	22.5 (up to 8 hours)
Net salary (1 driver) [PLN/month]	5,000	5,000	5,000
Total cost of overheads (1 driver) [PLN/month]	1,014	1,014	1,014
Total gross salary cost (1 driver) [PLN/month]	6,014	6,014	6,014
Cost of servicing one vehicle [PLN/year]	60,000	50,400	60,000
The cost of a set of 4 tires [PLN]	2,400	2,400	2,400

Based on the technical data from section 4.2 and calculations for individual vehicles in section 3, fixed and variable costs were estimated on an annual basis.

Table 7. Fixed and variable costs, detailing the costs related to CO_2 emissions for individual variants

Type cost \ Variant		Variant 1	Variant 2	Variant 3
Fixed costs	Depreciation costs [PLN/year]	42,000	36,000	38,000
	Insurance costs [PLN/year]	3,500	4,000	4,200
	Driver salary costs [PLN/year]	12,028	12,028	12,028
	Total [PLN/year]	**57,528**	**52,028**	**54,228**
Variable costs	Costs of fuel/energy consumption [PLN/year]	126,370	151,313	95,625
	Parking costs at refueling/charging stations [PLN/year]	0	42,000	0
	Costs of drivers' allowances [PLN/year]	5,670	11,250	5,670
	Service costs [PLN/year]	60,000	50,400	60,000
	Tire replacement costs [PLN/year]	7,200	7,200	7,200
	Total [PLN/year]	**193,095**	**256,583**	**162,825**

5.2. Discussion of the results of the conducted empirical research

Freight cost benchmarking is the process of evaluating various cost factors to determine the most cost-effective option. A summary of the fixed costs for individual vehicles, which include the costs of depreciation, insurance and drivers' salaries, is shown in the chart (Fig. 5).

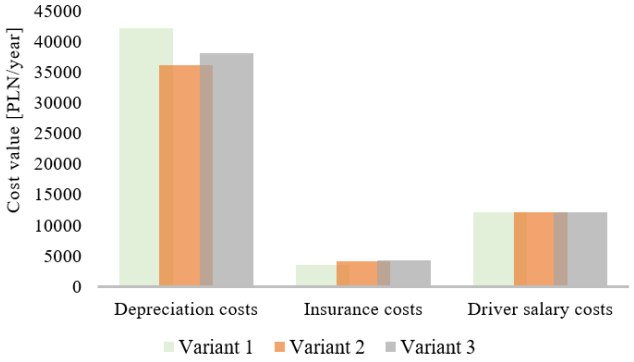

Fig. 5. The structure of fixed costs per year for individual variants

The largest part of fixed costs are vehicle depreciation costs. The electric vehicle with the lowest initial value performed best. For all the analyzed variants, the drivers' remuneration costs are the same. The last cost of insurance differs in small values between given design solutions. The lowest insurance rate is assigned to a combustion engine vehicle, and the highest to a CNG-powered vehicle.

Figure 6 shows a summary of variable costs for the analyzed variants on an annual basis. They include: costs of fuel consumption, parking at charging/refueling stations, drivers' allowances, service and tire replacement.

When analyzing variable costs, it can be seen that the most extensive cost is the cost of fuel/energy consumption of vehicles. For combustion vehicles on an annual basis, it amounted to PLN 126,370 for a given transport task, and PLN 151,313 for an electric vehicle.

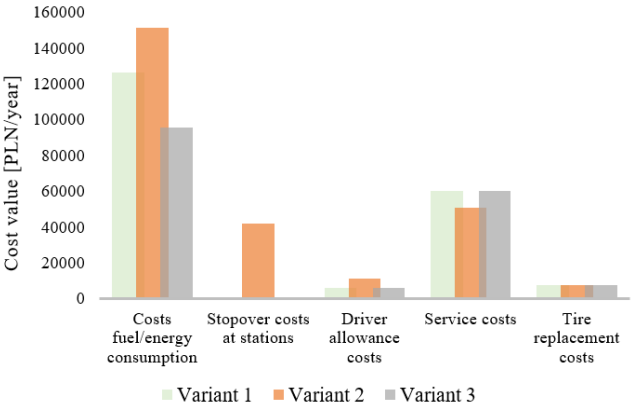

Fig. 6. The structure of variable costs per year for individual variants

In connection with the above, it is determined that this cost for a combustion vehicle is almost 17% lower than for an electric vehicle. Going further, when analyzing the cost of fuel consumption for a CNG-powered vehicle, large fluctuations in value differences with the other two types of vehicles are observed. The cost of fuel consumption of a vehicle powered by compressed natural gas is almost 24% lower than in the case of a combustion vehicle and less than 37% lower compared to an electric vehicle.

Another cost is the cost of parking cars at charging/refueling points. According to the data posted on the websites of selected locations of vehicle charging points, the total cost of parking for electric vehicles was determined, the

cost does not apply to combustion and CNG vehicles. Subsequently, the cost of drivers' allowances was also included for all types of vehicles. The total working time of an electric vehicle is over 12 hours, therefore the cost of the daily allowance is PLN 45, which gives a value of PLN 11,250 per year for one driver. In the case of combustion and CNG-powered vehicles, the cost is PLN 5,670 per year.

Vehicle service costs were determined after contacting the local IVECO dealer, and the highest were allocated ex aequo for a combustion engine vehicle and a CNG-powered vehicle. The last factor analyzed is the cost of tire replacement, which was also discussed with the IVECO dealer and it was estimated that the tire replacement per year will be PLN 7,200 for each vehicle, taking into account that they will be changed three times.

In addition to costs, other aspects of the analyzed vehicles will also be compared, which affect the quality of transport services, as well as the natural environment [36]. The analysis takes into account the time of cargo transport on the selected route for given types of vehicles. Determining this parameter involved determining the distance between the starting point and the destination, the average speed of the vehicle, any stops related to loading or refueling the car, or the time of unloading/loading the goods. Data on the time of carrying out the transport task of individual vehicles are presented in Table 8.

Table 8. Time of carrying out the transport task for the analyzed vehicles

Parameter \ Variant	Variant 1	Variant 2	Variant 3
Time of carrying out the transport task [min]	540	990	540

Another parameter is the noise level in selected vehicles. A car with an internal combustion engine that runs on diesel fuel is notorious for making noise. The noise level of combustion vehicles depends on the type of engine, technical condition, driving speed or noise generated as a result of fuel explosion in the combustion chamber [41]. Electric vehicles typically generate less noise than vehicles powered by internal combustion engines. This is the result of the operation of electric motors, which do not use the fuel explosion to generate propulsion, and instead use the rotating motion of the magnet [41]. In addition, electric vehicles have better sound insulation, which contributes to noise reduction [21]. Cars powered by compressed natural gas (CNG) also generate lower noise levels compared to combustion vehicles. This is due to the fact that CNG engines create less vibrations, in addition, the exhaust system is equipped with noise silencers, which work to reduce the noise generated by vehicle exhaust emissions [10]. The aspect of vehicle noise level is very important, considering its impact on the environment and human health. Long-term exposure to high noise levels in humans can lead to hearing damage, sleep disorders or stress. In addition, the noise generated by the vehicle can have a negative impact on fauna and the natural environment, e.g. disrupt the communication of animals and disturb the balance of ecosystems. Table 3 of the article specifies the noise emission parameters of the analyzed vehicles expressed in decibels.

The last indicator is the analysis of harmful components emitted by selected vehicles. Trucks, vans and passenger cars powered by fossil fuel are associated with high emissions of greenhouse gases, especially CO_2 [22]. Substances contribute to the increase in the greenhouse effect, smog and negatively affect air quality and human health. Electric vehicles do not directly emit exhaust gases or pollutants while driving. However, emissions related to the production of electricity used to charge electric cars can contribute to CO_2 emissions if the energy comes from non-renewable sources, e.g. coal power plants [12]. When using renewable energy, such as solar or wind power, emissions directly related to vehicles are minimal. Cars powered by compressed natural gas (CNG) emit less CO_2 than combustion cars. Combustion of natural gas in the engine causes lower emissions of particulate matter and sulfur compounds compared to traditional fuels [37]. CO_2 emission levels for the purposes of the article were taken from the vehicle manufacturer's outlines. The table below presents data on annual carbon dioxide emissions for selected vehicles based on the data in Table 3.

Table 9. Carbon dioxide (CO_2) emissions on an annual basis

Parameter \ Variant	Variant 1	Variant 2	Variant 3
Annual carbon dioxide emissions [t/year]	67	0	57

6. Summary

The analyzed design variants are defined as the type of delivery vehicles used with engines powered by: diesel oil (in variant 1), electricity (in variant 2) and compressed natural gas (in variant 3). The main point of the article was to determine the route taking into account loading/unloading points and refueling/battery charging points, divided into individual design variants. For the purposes of the research, the elements influencing the operating costs of individual types of vehicles were specified. In addition, the compared parameters were: the duration of the journey and the level of noise emission.

Comparison of vehicles powered by internal combustion engines and those powered by electricity and compressed natural gas can be made on the basis of various criteria, such as: environmental performance, energy efficiency, operating costs, noise emissions and availability of filling stations/charging stations. The article estimates the operating costs of vehicles, broken down into fixed and variable costs of the transport service. The cost of depreciation of means of transport has the greatest impact on the amount of fixed costs.

In the case of variable costs, the largest overheads fall on the costs of fuel consumption. It is worth noting that the highest cost of energy consumption for an electric vehicle is largely due to market fluctuations caused by the economic crisis, which is currently affecting most European Union countries. At the moment, the prices of fuel and gas are slightly falling, so vehicles powered by these resources are taking the lead in the list proposed in this article. Another fact adversely affecting the attractiveness of electric vehicles is the obligation to pay for parking in a parking space that allows free charging of the battery. In terms of finan-

cial savings, the most advantageous variant turned out to be a vehicle powered by compressed gas (CNG). The favorable overtones of this type of transport are largely due to the price of gas, which directly translates into the lowest cost per kilometer of the route.

In the case of long-distance cargo transport, an indisputable aspect requiring comparison is also the maximum range of the vehicle on a single refueling/charging. This parameter is extremely important for entrepreneurs operating in the transport industry, because it directly affects the costs related to employees' salaries and allowances. In addition, the large range generates the ability to quickly and efficiently deliver the load to the destination. In this ranking, the electric vehicle is in last place, while the combustion vehicle is the most advantageous solution. The range of a combustion vehicle is more than four times greater than that of an electric vehicle and almost three times greater in relation to a CNG–powered vehicle.

Another analyzed parameter is the total time of carrying out the transport task. This amount is extremely important in the case of carriers performing transport, because it directly translates into wages for employees. In the case of transport performed using an electric vehicle, the transport time is almost twice as long as in the other two variants, which also has a very negative impact on the choice of this means of transport. The main factors influencing such a large discrepancy are: the maximum range on a single charge (for an electric vehicle it is up to 200 km) and the battery charging time, which is about 2.5 using a charger with a power of up to 50 kW, providing direct current during charging.

To sum up: it is definitely too early to minimize the impact of freight transport using internal combustion vehicles on the environment, because the current technologies of powering vehicles with electricity and the capacity of modern batteries are insufficient to effectively and conveniently carry out long-distance transport. With the increase in the capacity of batteries available in electric vehicles and the possibilities of chargers, this type of alternative to internal combustion vehicles may become a very beneficial solution. On the other hand, the method of powering vehicle engines with compressed natural gas is currently a very advantageous solution, ensuring a relatively high range of the vehicle and a favorable price for covering 1 km of the route. Taking into account the main analyzed parameters, such as transport costs, range, travel time or fuel replenishment time, vehicles powered by internal combustion engines continue to lead the way.

The aim achieved by the authors is to indicate the most advantageous variant among the vehicles used for load distribution in terms of transport costs, emissions of harmful substances and the level of emitted noise. The authors, conducting a comparative analysis of three variants of transport, determined that in the case of domestic transport for longer distances, combustion vehicles are still the most advantageous alternative. This is mainly due to the cost of purchasing such vehicles and the time of transport. For electric vehicles, the biggest barrier to long-distance deployment is the relatively low range. Analyzing the criterion of carbon dioxide emission and noise, the most advantageous alternative is an electric vehicle. It is impossible to draw a final conclusion, because the choice of a vehicle is mainly conditioned by the individual economic, technical and technological preferences of the buyer.

Nomenclature

AC	alternating current
AC	auto casco
CNG	compressed natural gas
CO_2	carbon dioxide
DC	direct current
NNW	accidental consequences
OC	liability insurance

Bibliography

[1] Ahmed Z, Ahmad M, Rjoub H, Kalugina OA, Hussain N. Economic growth, renewable energy consumption, and ecological footprint: exploring the role of environmental regulations and democracy in sustainable development. Sustain Dev. 2022;30(4):595-605. https://doi.org/10.1002/sd.2251

[2] Al-Hanahi, B., Ahmad, I., Habibi, D., & Masoum, M. A. Charging infrastructure for commercial electric vehicles: Challenges and future works. IEEE Access, 2021;9;121476-121492. https://doi.org/10.1109/ACCESS.2021.3108817

[3] Andrych-Zalewska M, Chłopek Z, Merkisz J, Pielecha J. Analysis of the operation states of internal combustion engine in the Real Driving Emissions test. Archives of Transport. 2023;61(1)71-88. https://doi.org/10.5604/01.3001.0015.8162

[4] Greene DL, Ogden JM, Lin Z. Challenges in the designing, planning and deployment of hydrogen refueling infrastructure for fuel cell electric vehicles. ETransportation. 2020;6:100086. https://doi.org/10.1016/j.etran.2020.100086

[5] Hou R, Lei L, Jin K, Lin X, Xiao L. Introducing electric vehicles? Impact of network effect on profits and social welfare. Energy. 2022;243:123002. https://doi.org/10.1016/j.energy.2021.123002

[6] Iodice P, Cardone M. Ethanol/gasoline blends as alternative fuel in last generation spark-ignition engines: a review on CO and HC engine out emissions. Energies. 2021;14(13): 4034. https://doi.org/10.3390/en14134034

[7] IVECO Poland Home Page. https://www.iveco.com/poland/Pages/Home-Page.aspx

[8] Izdebski M, Jacyna M. An efficient hybrid algorithm for energy expenditure estimation for electric vehicles in urban service enterprises. Energies. 2021;14(7):2004. https://doi.org/10.3390/en14072004

[9] Izdebski M, Jacyna-Gołda I, Nivette M, Szczepański E. Selection of a fleet of vehicles for tasks based on the statistical characteristics of their operational parameters. Eksploat Niezawodn. 2022;24(3). https://doi.org/10.17531/ein.2022.3.2

[10] Jacyna M, Szczepański E, Lewczuk K, Izdebski M, Jacyna-Gołda I, Kłodawski M et al. Noise pollution from transport. 2021. https://doi.org/10.1016/B978-0-08-102671-7.10723-7
[11] Jacyna M, Wasiak M. Costs of road transport depending on the type of vehicles. Combustion Engines. 2015;162(3):85-90. https://doi.org/10.19206/CE-116868
[12] Jacyna M, Żochowska R, Sobota A, Wasiak M. Scenario analyses of exhaust emissions reduction through the introduction of electric vehicles into the city. Energies. 2021; 14(7):2030. https://doi.org/10.3390/en14072030
[13] Kałużny J, Waligorski M, Szymański GM, Merkisz J, Różżański J, Nowicki M et al. Reducing friction and engine vibrations with trace amounts of carbon nanotubes in the lubricating oil. Tribol Int. 2020;151:106484. https://doi.org/10.1016/j.triboint.2020.106484
[14] Karagoz M, Uysal C, Agbulut U, Saridemir S. Energy, exergy, economic and sustainability assessments of a compression ignition diesel engine fueled with tire pyrolytic oil−diesel blends. J Clean Prod. 2020;264:121724. https://doi.org/10.1016/j.jclepro.2020.121724
[15] Kluschke P, Gnann T, Plötz P, Wietschel M. Market diffusion of alternative fuels and powertrains in heavy-duty vehicles: a literature review. Energy Reports. 2019;5:1010-1024. https://doi.org/10.1016/j.egyr.2019.07.017
[16] Kontses A, Triantafyllopoulos G, Ntziachristos L, Samaras Z. Particle number (PN) emissions from gasoline, diesel, LPG, CNG and hybrid-electric light-duty vehicles under real-world driving conditions. Atmos Environ. 2020;222: 117126. https://doi.org/10.1016/j.atmosenv.2019.117126
[17] Kubik A, Turoń K, Folęga P, Chen F. CO_2 emissions—evidence from internal combustion and electric engine vehicles from car-sharing systems. Energies. 2023;16(5):2185. https://doi.org/10.3390/en16052185
[18] Liu Z, Song J, Kubal J, Susarla N, Knehr KW et al. Comparing total cost of ownership of battery electric vehicles and internal combustion engine vehicles. Energy Policy. 2021; 158:112564. https://doi.org/10.1016/j.enpol.2021.112564
[19] Lv Z, Wu L, Yang Z, Yang L, Fang T, Mao H. Comparison on real-world driving emission characteristics of CNG, LNG and hybrid-CNG buses. Energy. 2023;262:125571. https://doi.org/10.1016/j.energy.2022.125571
[20] Macioszek E, Sierpiński G. Charging stations for electric vehicles-current situation in Poland. Research and the Future of Telematics: 20th International Conference on Transport Systems Telematics, TST 2020, Kraków, Poland, October 27-30, 2020, Springer International Publishing. https://doi.org/10.1007/978-3-030-59270-7_10
[21] Miconi F, Dimitri GM. A machine learning approach to analyse and predict the electric cars scenario: The Italian case. PloS one. 2023;18(1):e0279040. https://doi.org/10.1371/journal.pone.0279040
[22] Min D, Song Z, Chen H, Wang T, Zhang T. Genetic algorithm optimized neural network based fuel cell hybrid electric vehicle energy management strategy under start-stop condition. Appl Energ. 2022;306:118036. https://doi.org/10.1016/j.apenergy.2021.118036
[23] Moosavi-Nezhad M, Salehi R, Aliniaeifard S, Winans KS, Nabavi-Pelesaraei A. An analysis of energy use and economic and environmental impacts in conventional tunnel and LED-equipped vertical systems in healing and acclimatization of grafted watermelon seedlings. J Clean Prod. 2022; 361:132069. https://doi.org/10.1016/j.jclepro.2022.132069
[24] Mutarraf MU, Guan Y, Xu L, Su CL, Vasquez JC, Guerrero JM. Electric cars, ships, and their charging infrastructure – a comprehensive review. Sustainable Energy Technologies and Assessments. 2022;52:102177. https://doi.org/10.1016/j.seta.2022.102177
[25] Naderi A, Qasemian A, Shojaeefard MH, Samiezadeh S, Younesi M, Sohani A et al. A smart load-speed sensitive cooling map to have a high- performance thermal management system in an internal combustion engine. Energy. 2021;229:120667. https://doi.org/10.1016/j.energy.2021.120667
[26] Neugebauer M, Żebrowski A, Esmer O. Cumulative emissions of CO_2 for electric and combustion cars: a case study on specific models. Energies. 2022;15(7):2703. https://doi.org/10.3390/en15072703
[27] ORLEN | Nasze ładowarki. www.orlencharge.pl
[28] Patterson R. Compendium of accounting in Polish & English. Warsaw 2015.
[29] Pyza D, Jacyna-Gołda I, Gołda P, Gołębiowski P. Alternative fuels and their impact on reducing pollution of the natural environment. Rocznik Ochrona Środowiska. 2018;20.
[30] Rozporządzenie Ministra Rodziny i Polityki Społecznej z dnia 25 października 2022 r. zmieniające rozporządzenie w sprawie należności przysługujących pracownikowi zatrudnionemu w państwowej lub samorządowej jednostce sfery budżetowej z tytułu podróży służbowej (Regulation of the Minister of Family and Social Policy of October 25, 2022 amending the regulation on the amounts due to an employee employed in a state or local government budgetary unit for a business trip).
[31] Shafique M, Azam A, Rafiq M, Luo X. Life cycle assessment of electric vehicles and internal combustion engine vehicles: a case study of Hong Kong. Res Transp Econ. 2022; 91:101112. https://doi.org/10.1016/j.retrec.2021.101112
[32] Tang B, Xu Y, Wang M. Life cycle assessment of battery electric and internal combustion engine vehicles considering the impact of electricity generation mix: a case study in China. Atmosphere. 2022;13(2):252. https://doi.org/10.3390/atmos13020252
[33] Trivedi S, Prasad R, Mishra A, Kalam A, Yadav P. Current scenario of CNG vehicular pollution and their possible abatement technologies: an overview. Environ Sci Pollut R. 2020;27:39977-40000. https://doi.org/10.1007/s11356-020-10361-7
[34] Ustawa o podatku dochodowych od osób prawnych (Corporate Income Tax Act) z dnia 15 lutego 1992 (Dz. U. z 2023 r. poz. 185, 326, 412).
[35] Ustawa o rachunkowości (Accounting Act) z dnia 29 września 1994 (Dz.U. z 2023 r. poz. 120, t.j.).
[36] Ustawa Prawo ochrony środowiska (Environmental Protection Act) z dnia 27 kwietnia 2001 (Dz.U. z 2023 r. poz. 877 z późn. zm.)
[37] Warguła Ł, Kukla M, Lijewski P, Dobrzyński M, Markiewicz F. Impact of compressed natural gas (CNG) fuel systems in small engine woodchippers on exhaust emissions and fuel consumption. Energies. 2020;13(24):6709. https://doi.org/10.3390/en13246709
[38] Wei S, Sun L, Wu L, Yu Z, Zhang Z. Study of combustion characteristics of diesel, kerosene (RP-3) and kerosene-ethanol blends in a compression ignition engine. Fuel. 2022; 317:123468. https://doi.org/10.1016/j.fuel.2022.123468
[39] Yaman H, Yesilyurt MK, Uslu S. Simultaneous optimization of multiple engine parameters of a 1-heptanol/gasoline fuel blends operated a port-fuel injection spark-ignition engine using response surface methodology approach. Energy. 2022;238:122019. https://doi.org/10.1016/j.energy.2021.122019
[40] Yang Z, Wang B, Jiao K. Life cycle assessment of fuel cell, electric and internal combustion engine vehicles under different fuel scenarios and driving mileages in China. Energy. 2020;198:117365. https://doi.org/10.1016/j.energy.2020.117365

[41] Zhu L, Zhong X, Wang H, Qiu X, Wu S, Mao D. An objective and subjective study on global active control of engine noise in a car. J Vib Control. 2023;10775463231174730. https://doi.org/10.1177/10775463231174730

[42] Zimakowska-Laskowska M, Laskowski P. Emission from internal combustion engines and battery electric vehicles: case study for Poland. Atmosphere. 2022;13(3):401. https://doi.org/10.3390/atmos13030401

[43] Insurance for you in PZU (in Polish). https://www.pzu.pl/kampania/auto/auto5?mcid=p_sem&gad=1&gclid=EAIaIQobChMI8evhooKMgAMVZIyDBx0f5gOeEAAYASAAEgI2nPD_BwE&gclsrc=aw.d

Michał Lasota, MEng. – Faculty of Transport, Warsaw University of Technology, Poland.
e-mail: *michal.lasota@pw.edu.pl*

Aleksandra Zabielska, MEng. – Faculty of Transport, Warsaw University of Technology, Poland.
e-mail: *aleksandra.zabielska@pw.edu.pl*

Prof. Marianna Jacyna, DSc., DEng. – Faculty of Transport, Warsaw University of Technology, Poland.
e-mail: *marianna.jacyna@pw.edu.pl*

Jolanta Żak, DSc., DEng. – Faculty of Transport, Warsaw University of Technology, Poland.
e-mail: *jolanta.zak@pw.edu.pl*

Article citation info:
Pryciński P, Wawryszczuk R, Korzeb J, Pielecha P, Murawski J. Selected vehicle emission assessment issues in passenger transport services. Combustion Engines. 2023;195(4):14-22. https://doi.org/10.19206/CE-169806

Piotr PRYCIŃSKI
Róża WAWRYSZCZUK
Jarosław KORZEB
Piotr PIELECHA
Jakub MURAWSKI

Combustion Engines
Polish Scientific Society of Combustion Engines

Selected vehicle emission assessment issues in passenger transport services

ARTICLE INFO

Received: 14 June 2023
Revised: 18 July 2023
Accepted: 19 July 2023
Available online: 8 August 2023

The paper presents an analytical method for determining the pollutant emission of transport modes, based on emission indicators for various vehicle types and statistical data. The method developed enables the determination of the emission of various vehicle types without the need to carry out tests on real vehicles. The purpose of this paper is to compare the vehicle emission results obtained using the developed analytical method with the real-world results obtained in RDE tests based on a case study, i.e. an analysis of the emission of passenger transport modes in Warsaw. The paper contains a summary of the results of measurements and calculations, as well as an analysis of potential areas of application for the developed analytical method.

Key words: *vehicle emission, RDE tests, emission analysis, passenger vehicles, emission indicators*

1. Introduction

Poland is one of the more motorised countries in the European Union. According to the data presented by Statistics Poland (GUS), in 2020 as many as 664 passenger vehicles were registered per 1,000 inhabitants, placing Poland third in relation to the other Member States [23]. The statistics compiled by GUS based on the data from the Central Register of Vehicles (CEP) show that the number of passenger vehicles in the country exceeded 25 million, the largest share of which were vehicles registered in the Mazowieckie Voivodeship (just under 4 million). The age structure of the vehicle fleet in 2020 in Poland indicates that most vehicles in use are older than 10 years. These cars accounted for more than 75% of all vehicles [24]. The statistical data, including a detailed breakdown of passenger vehicles by age, are shown in Fig. 1.

Furthermore, a dominant proportion of over 53% of passenger vehicles in 2020 were gasoline engine vehicles and over 32% were diesel engine vehicles as shown in Fig. 2. The low share of vehicles powered by alternative fuels, combined with the rather advanced age of vehicles, is indicative of the potentially high emission of passenger transport modes in Poland, especially in urban areas. Although an upward trend in the number of new vehicles, including electric vehicles, can be observed in recent years, the purchase of this type of vehicle is still unattainable for a large segment of the Polish society. Often, the most convenient choice for vehicle ownership is still buying used vehicles imported from the Western European countries. The above contributes to some of the worst air quality results in Polish cities compared to other centres in the European Union. One of the most polluted agglomerations in Poland is Warsaw, which shows one of the highest vehicle ownership rates in Europe. Warsaw also has one of the highest daily commuter vehicle inflow rates [24]. The development of transport organised via mobile apps or car sharing is also becoming apparent.

In April 2022, a report was published on the actual pollutant emission generated by transport in Warsaw [22]. The report was developed by The Real Urban Emissions Initiative (TRUE), a joint initiative of the International Automobile Federation (FIA) and the International Council on Clean Transportation (ICCT). The document contains a detailed assessment of vehicle pollutant emissions and recommendations for improving the environmental effectiveness of road transport in Warsaw. Air pollution measurements from almost 150,000 vehicles were used in the analyses. The report's main findings are that diesel vehicles significantly exceed the limits for nitrogen oxide emissions. Emissions from diesel vehicles were between 1.6 and 4.3 times higher than permitted, according to the report. For vehicles that meet the higher emission standards, requiring type-approval under real-world driving conditions (RDE tests), their emissions are lower than the highest permitted by the RDE tests, but exceed laboratory air pollutant emission standards. Furthermore, the particulate matter (PM) emissions limit was exceeded by around 1.5% of diesel vehicles. These results apply to vehicles meeting the Euro 4 standard and above. Particularly noteworthy is the fact that as many as 83% of passenger vehicles in Warsaw do not meet the emission durability conditions; a large share of passenger vehicles in Warsaw, i.e. approximately 32%, are vehicles whose average age exceeds 13 years and whose mileage exceeds 223,000 km.

Considering the above, the authors determined the actual emission of the transport modes available to a taxi corporation operating in Warsaw. Due to the high frequency of taxi use and the significant daily mileage of these vehicles, they are a significant source of emissions in urban areas. The cited report [3] presented a comparison of the emission of taxis offering services in Warsaw and Brussels. The report's authors also determined the statistics on the age and average mileage of this type of vehicles in both cities. The average age of taxis in Warsaw is around seven years, while in Brussels it is only four years. It should be noted that this difference is undoubtedly due to the restrictions placed on vehicles intended to carry passengers for a fee in Brussels. The upper age limit for these vehicles is seven years. Despite the lower average age of Warsaw taxis compared to personal vehicles, most have a mileage of over

300,000 km, which undoubtedly translates into the vehicles' higher emission relative to Brussels taxis. The report [22] also indicates, in relation to Warsaw taxis, that nitrogen oxide emissions are nearly twice as high and PM emissions more than four times as high as those of passenger transport vehicles in Brussels. If similar legal restrictions on the operation of taxis were to be adopted in Warsaw, regarding their age and technical condition, nearly 43% of the vehicles currently in use would have to be taken out of service. Replacing existing vehicles with alternatively-fuelled vehicles could reduce pollution in Warsaw by almost 60%. It can therefore be concluded that motorised transport, especially in urban areas, contributes significantly to environmental degradation and affects the comfort of living in the city.

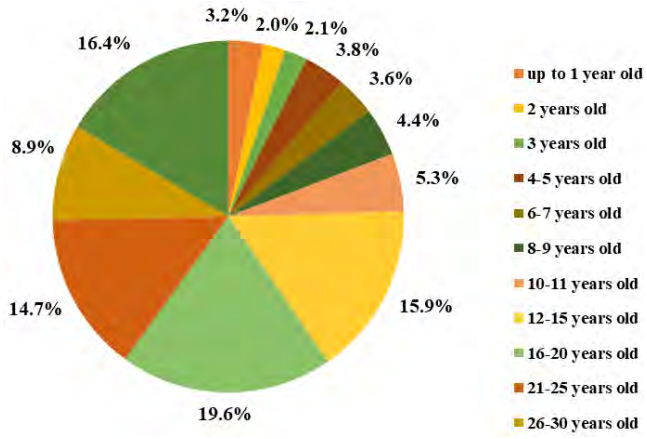

Fig. 1. Age structure of passenger vehicles in Poland in 2020 [24]

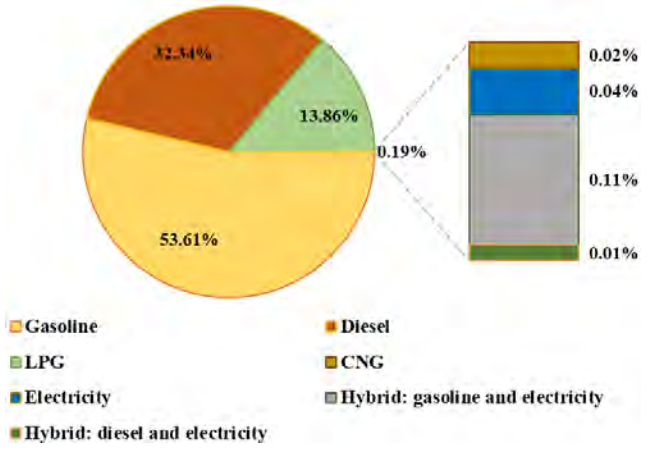

Fig. 2. Fuel type structure of passenger vehicles in Poland in 2020 [24]

The deliberations on pollutant emissions in transport presented in the paper are limited to determining the greenhouse gas emissions, such as carbon dioxide, carbon monoxide and nitrogen oxides. The above assumption is required to compare the emissions determined under the real-world conditions of the RDE road tests with the emission calculations determined by the analytical method, developed using the statistical emission indicators for transport modes defined by the authors.

2. Methodology

In the paper, the authors used the analytical indicator method of calculating the emission of transport modes to determine the emission of vehicles and the environmental impact of individual vehicle types. The diagram presenting the method is shown in Fig. 3. The emissions of main air pollutants were identified based on the report concerning the methodology for estimating air pollutant emissions in Poland, published in 2018 [34]. However, the methodology developed by GUS did not specify the values of unit emission indicators of particular types of air pollutants for selected types of road transport modes. Based on the data published by GUS, the authors of this paper determined the values of the constant emission indicators for particular types of air pollutants for:

– various types of vehicles, i.e. passenger vehicles, light-duty vehicles, heavy-duty vehicles, motorcycles and buses
– various types of fuels, i.e. gasoline, diesel and LPG
– various ranges of engine cubic capacities.

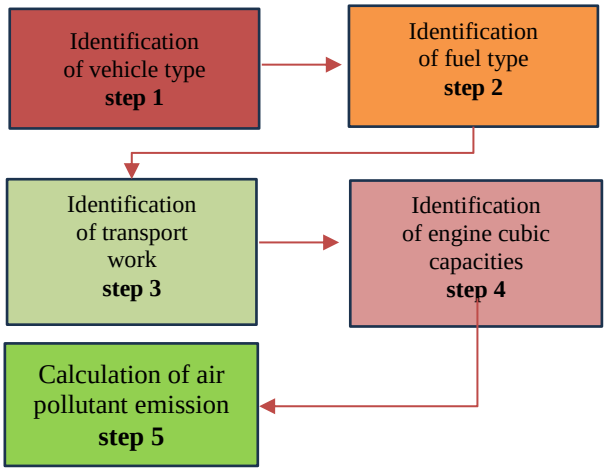

Fig. 3. The diagram of analytical indicator method of calculating the emission of transport modes [21]

In the scope of the present paper, an analysis of the emission of 11 types of passenger vehicles was carried out and their characteristics are presented in Table 1.

The source of the data used to determine the constant and statistical values of the emission indicators was the data derived from the 2015 GPR survey conducted on behalf of the General Directorate for National Roads and Motorways, data from the database of the Ministry of Digital Affairs, based on the odometer readings, among others, collected in CEP. In the analytical index method, the emission of particular vehicle types can be determined for passenger vehicles, light-duty vehicles and heavy-duty vehicles, with different versions of fuels used and engines of different cubic capacities. The indicators define pollutant emission expressed in units [g/km]; the method does not require using a complex mathematical formulation, and has the form of a statistical analysis adequate for the Polish transport organisation conditions. In this method, the emission of transport modes is calculated as the product of the emission indicator and the mileage of the given vehicle type. The emissions of the main air pollutants determined

as a result of the literature review and real-world tests are presented in Table 2.

Table 1. Types of vehicles analysed in terms of pollutant emissions in the case study

Vehicle type (production year)	Vehicle code	Fuel type	Engine capacity [cm^3]	Power [kW]	Emission class
Opel Astra 2017	V1	gaso-line	999	77	Euro 6b
VW Golf 2017	V2	gaso-line	1,498	96	Euro 6c
VW Touran 2018	V3	gaso-line	1,395	110	Euro 6b
Škoda Superb 2018	V4	diesel	1,968	110	Euro 6c
Peugeot 308 2018	V5	diesel	1,499	96	Euro 6d-Temp
Mercedes-Benz C220 2018	V6	diesel	2,143	125	Euro 6b
BMW 530d 2017	V7	diesel	2,993	195	Euro 6b
Toyota Prius 2019	V8	hybrid	1,798	90	Euro 6d-Temp
VW Jetta 2015	V9	diesel	2,000	105	Euro 6b
Hyundai i30 2015	V10	diesel	1,600	96	Euro 6b
Škoda Octavia 2015	V11	diesel	1,900	77	Euro 6b

Calculation of air pollutant emissions for vehicles indicated in Table 1 is carried out using the statistical values of the indicators presented in Table 3, as well as the length of the road connecting the points of dispatch and collection of cargo or passengers covered by the types of vehicles, by the following equation:

$$E_m = l\,(i,j)\ x\ W_{m,k} \tag{1}$$

where E_m – the emission of m-th type air pollutants (NO_x, CO_2, CO) generated by the k-th vehicle type, l (i, j) – the length of connecting the i-th sending point with the j-th receiving point, $W_{m,k}$ – m-th type air emission factor taken from Table 2, for the k-th vehicle type.

Table 3 presents the statistical values of the emission factors of particular transport modes.

Table 2. Results of the vehicles' real-world emission – RDE measurements for various vehicle types [g/km] [1, 18, 20, 31]

Vehicle type	NO_x	CO_2	CO
	RDE	RDE	RDE
V1	0.0910	140.0000	0.9900
V2	0.0110	154.0000	0.3160
V3	0.0200	172.0000	0.1610
V4	0.0130	152.0000	0.0200
V5	0.0600	139.0000	0.0200
V6	0.0780	150.0000	0.0130
V7	0.0330	156.0000	0.0350
V8	0.0840	118.0000	0.0060
V9	0.2200	107.0000	0.0050
V10	0.2500	125.0000	0.0062
V11	0.1350	202.0000	0.0105

Table 3. Emission indicators for various vehicle types [g/km]

Vehicle type	NO_x	CO_2	CO
	IM	IM	IM
V1	0.07241	71.79265	0.50972
V2	0.12731	83.77379	0.50705
V3	0.07241	71.79265	0.50972
V4	0.19522	44.66578	0.01267
V5	0.19522	44.66578	0.01267
V6	0.19968	60.76343	0.01610
V7	0.19968	60.76343	0.01610
V8	–	–	–
V9	0.19968	60.76343	0.01610
V10	0.19522	44.66578	0.01267
V11	0.19522	44.66578	0.01267

Under the analytical indicator method, having the relevant data in the form of:
- the test vehicle's mileage in connection with the transport task in question
- the test vehicle's engine cubic capacity
- the fuel type used

using constant statistical indicators, it is possible to determine the approximate emissions of a given vehicle type with regard to the following air pollutants:
- carbon oxides
- carbon dioxide
- nitrogen oxides
- nitrogen dioxide
- PM2.5 and PM10.

As part of the verification of the developed analytical indicator method intended for the determination of the transport modes' emission, the indicator emission was compared with the results of real-world measurements obtained in RDE tests for the three main types of air pollutants, i.e. nitrogen oxides, carbon oxides and carbon dioxide. The results of real-world vehicle measurements are widely published in the literature [1, 3, 10–12, 17, 19, 20, 29–33, 35]. Reviewing passenger vehicle emissions regulations and comparing laboratory tests with real emission results are also widely published [3, 6]. The transport modes' real-world emissions used in the paper are based on literature data [1, 18, 31] and on real-world tests carried out in the engineering thesis [20]. It should be emphasised that analyses of the emission of vehicle-generated pollutants can vary depending on a number of external factors. The test results are affected by the test conditions, e.g. ambient temperature, topography, road conditions, vehicle characteristics such as age, mileage, and technical condition [2, 16, 25, 31].

The analytical method proposed by the authors, which is based on the determination of a constant emission factor, enables the determination of the approximate pollutant emission values. If a large number of real-world test results is available, it is possible to analyse the impact of other factors on emission and to correct the constant indicators in terms of additional criteria, such as the vehicle's age or technical condition. The analytical method developed does not take these factors into account and this may constitute a further stage of the research work. It should also be pointed out that emission measurement methods based on real-world measurements of the transport modes' emission have

the highest accuracy in determining the vehicle's real-world emissions. Tests of emission can be carried out for various vehicle types, in various traffic conditions, in different natural topographies as well as using various fuels and engines [9, 19, 27, 28, 36]. RDE tests require the use of rather complex test instrumentation and a considerable amount of time to be carried out under various traffic conditions. The research methodology adopted utilised real-world study results published in the literature [1, 18, 31] and results obtained during real-world tests carried out in the Poznan agglomeration in the engineering thesis [20]. The measurements were carried out using the SEMTECH DS exhaust fume analyser. An illustration of the two vehicles tested in terms of real-world emission is presented in Fig. 4 and Fig. 5.

Fig. 4. Vehicle tested in real-world conditions (Toyota Prius) [20]

Fig. 5. Vehicle tested in real-world conditions (VW Golf) [20]

The measuring equipment for the RDE tests (SEMTECH DS exhaust fume analyser) is mounted inside the vehicles; in addition, an independent power generator used to supply the exhaust fume analysers is placed outside on a special platform (Fig. 4). The analytical indicator method does not enable testing the emission of hybrid vehicles, but it does enable the determination of the emission of electric vehicles. New hybrid and electric technologies appear to be the solution to further attempts to decarbonise transport modes [8, 19, 27]. Considering the above, the emission of transport modes is also affected by factors such as:

– traffic congestion as well as adequate road designing and topography [5, 7, 14, 16]
– conventional vehicles' adaptation to enable utilisation of new fuel types [10, 28]
– natural topography, vehicle load [11, 17, 25, 33]
– the engine's operating conditions and its technical condition [3, 36].

The issue of emission will remain relevant until vehicles that emit pollutants from fuel combustion are in use. It should be emphasised that, in addition to the RDE tests, which are considered the most accurate tests for the emission of transport modes, there are other methods for determining the emission of vehicles, including indirectly behind the vehicle [26].

3. Results

The analytical method developed by the authors enables the determination of the emission of transport modes without the need for real-world testing and is based on statistical data showing the given vehicle type's emissions [21]. Based on a case study, emission calculations were carried out for vehicles providing taxi services in the Warsaw agglomeration, using constant air pollutant emission values. The emissions determined by the analytical method based on statistical data were compared with the results of real-world pollutant emissions determined based on data obtained from literature sources (RDE test results) [1, 18, 31] and from results of tests carried out by the authors of the engineering thesis [20]. Passenger vehicles providing taxi services in the Warsaw agglomeration were classified into categories V1 to V11. For each vehicle category, the emission of a representative transport mode was determined and a simplification was adopted, assuming that a given type of vehicle has the same emission values. The authors analysed the emission of transport modes providing passenger transport services in the Warsaw agglomeration. The company providing transport services in Warsaw has more than 250 vehicles, 130 of which are included in the calculation example. The vehicles (11 types) included in the case study individually travel approx. 100 km per day, with the vehicles collectively travelling nearly 3.6 million km per year. Therefore, they transport a minimum of 4 million passengers. For the purposes of the analysis, it was assumed that the vehicle types V1 to V11 have the same technical parameters in terms of exploitation and their emission in the given type group are the same. This assumption resulted from the fact that it was impossible to carry out real-world emission tests on a large population of vehicles travelling around Warsaw. The real vehicle mileage data are presented in Table 4.

Table 4. Transport work performed by vehicles in a month

Vehicle type	Week mileage per vehicle in each type			
	Week 1	Week 2	Week 3	Week 4
V1	622	748	508	846
V2	898	935	679	614
V3	529	650	424	656
V4	453	426	507	646
V5	558	679	682	769
V6	620	705	548	757
V7	509	756	618	745
V8	487	568	605	446
V9	688	543	785	604
V10	653	540	789	599
V11	409	279	505	345
Total km per week	6,426	6,829	6,650	7,027
Average km per week	494	525	512	541
Average km per day	99	105	102	108

The distances travelled by individual vehicles from each vehicle type were multiplied by the number of vehicles in that type. The total distance travelled by the vehicles was obtained as a result. In the case study, the vehicles mainly served service points, hotels as well as railway and airport stations. The company providing the data for the case study ceased to operate in Warsaw during the pandemic due to the limited number of passengers using taxi services in Warsaw in 2019–2020. It would have been very complicated to carry out emission test for 130 vehicles, so a simplification was adopted, which involved reading the emission for one vehicle from a given type (V1–V11), derived from literature results, supported by real-world studies and RDE tests. The emission of all transport modes from types V1 to V2 was then simulated, taking into account the real-world mileage data of 11 vehicles over a period of one month. One month's data was replicated to obtain approximate figures for the total annual mileage of individual representative vehicles. The annual mileage constituted the basis for determining the total distance travelled by all vehicles included in the study, assuming that, in the scope of a given vehicle type, the vehicles travel the same distances as the representative vehicle. The real transport work data are presented in Table 5.

Table 5. Transport work performed by vehicles in a year

Vehicle type	Total km in a month per one vehicle	Total km in a year per one vehicle	Number of vehicles	Total km in a year for all vehicles
V1	2,724	32,688	5	163,440
V2	3,126	37,512	7	262,584
V3	2,259	27,108	15	406,620
V4	2,032	24,384	10	243,840
V5	2,688	32,256	6	193,536
V6	2,630	31,560	18	568,080
V7	2,628	31,536	3	94,608
V8	2,106	25,272	19	480,168
V9	2,620	31,440	11	345,840
V10	2,581	30,972	15	464,580
V11	1,538	18,456	21	387,576
Total	26,932	323,184	130	3,610,872

For the above data, the transport modes' main pollutant emission was determined as part of RDE tests as well as the transport modes' analytical, statistical emission was determined by using the indicator method. The emission was determined for all 130 vehicles of a given type, providing annual transport services in a Warsaw taxi corporation. The vehicles adopted as reference vehicle, representative of the type [V1 to V2], are not older than 8 years. The vehicles correspond to the age structure of the vehicles providing transport services indicated in the report [22]. It should be pointed out, however, that vehicles operating in the Warsaw area have high mileage (over 300,000 km), which may contribute to significantly higher emission of transport modes relative to the results obtained in the study in question.

Figures 6–16 show the results of air pollutant emissions for various types of vehicles in one year period. During analyses taking into account the real emission from RDE tests and results from the analytical method developed by the authors, based on statistical data.

The results of air pollutant emissions in the form of NO_x obtained during one year of operation of the taxi company's vehicles, calculated using the indicator method, are higher than the emission indicators obtained as part of RDE tests (Fig. 6). The exception is the V1 vehicle, for which NO_x emissions in RDE are lower than the emissivity determined by the indicator method. The reason for this may be the low engine capacity of the V1 vehicle, as the analyzed vehicle has a petrol engine capacity of less than 1000 cm^3. Based on statistical data, the NO_x emissions of air pollutants calculated using the indicator method are higher than the results obtained in RDE tests by about 36% on average for V1–V7 vehicles. Regarding V9–V10 vehicles powered by diesel engines, NO_x emissions are higher in the measurements obtained in the RDE tests by nearly 20% on average compared to the indicator method. For the V8 vehicle, which is a hybrid vehicle, it was not possible to determine the values of statistical indicators showing the emissions of the primary air pollutants. Considering the averaged values of RDE emission measurements and calculations of NO_x emissions based on statistical data, it is possible to estimate NO_x emissions without conducting RDE tests. The error scale in such a procedure is relatively small, about 30%. The NO_x emission value obtained using the indicator method was higher than the RDE results by the indicated error.

The total CO_2 emission from the operation of taxi company vehicles over one year, determined using the statistical indicator, is lower for all vehicles on average by nearly 40% (Fig. 7). The most significant differences in the results were recorded for two types of vehicles, i.e., V1 and V9. These vehicles are highly different from others regarding the installed engines' characteristics, capacity, and propellant used. Considering the averaged values of RDE emission measurements and the calculation of CO_2 emissions based on statistical data, it is possible to estimate CO_2 emissions without conducting RDE tests. The error scale in such a procedure is relatively small, about 40%. The CO_2 emission value obtained using the indicator method was lower than the RDE results by the indicated error.

The total CO emission from the operation of taxi company vehicles over one year, determined using the statistical indicator method, is lower than the RDE results for V1, V4, V5, and V7 vehicles by over 50%. For the remaining vehicles, i.e., V2, V3, V6, V9, V10, and V11, CO emissions were, on average, almost twice as high (Fig. 8 and Fig. 9). Considering all the collected results of calculations and measurements, the most significant discrepancies were recorded about CO emissions in terms of the results obtained by the indicator method and the RDE tests. The average absolute value of the difference in emissivity measurements obtained in the RDE and indicator methods was about 130%. The CO emission value obtained using the indicator method was higher by the indicated error.

With the results of global NO_x emissions (Fig. 10) and CO emissions (Fig. 12), it can be concluded that the emission of NO_x and CO pollutants calculated using the indicator method is higher than the results obtained in RDE tests. The situation is different regarding CO_2 emissions (Fig. 11). A summary of the emission of primary air pollutants in a graphical interpretation is shown in Fig. 13–16.

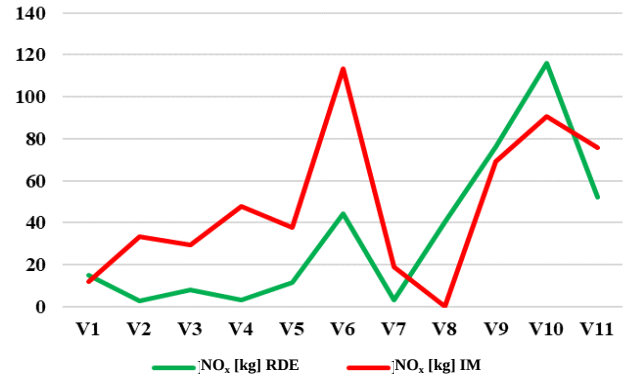

Fig. 6. Total NO_x emissions from transport trips during a one year period per type of vehicle

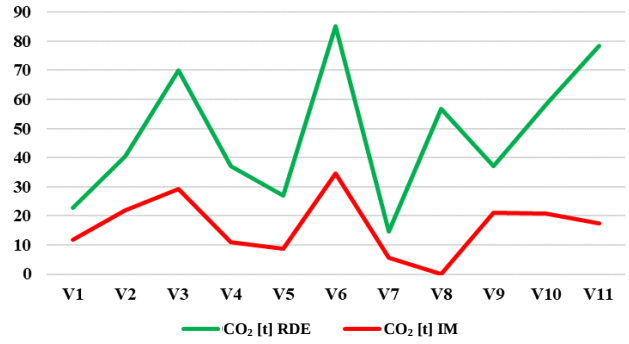

Fig. 7. Total CO_2 emissions from transport trips during a one year period per type of vehicle

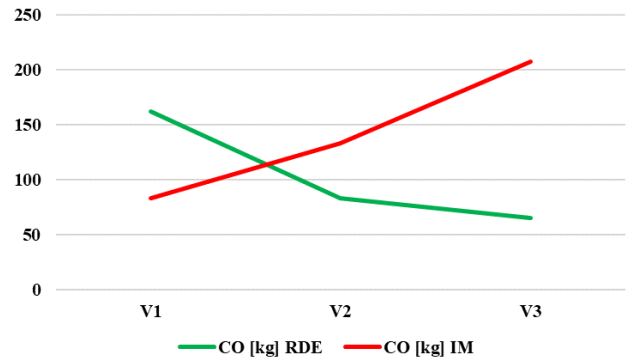

Fig. 8. Total CO emissions from transport trips during a one year period per type of vehicle (V1–V3)

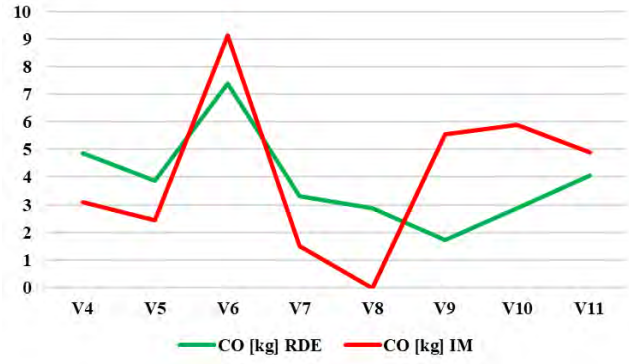

Fig. 9. Total CO emissions from transport trips during a one year period per type of vehicle (V4–V11)

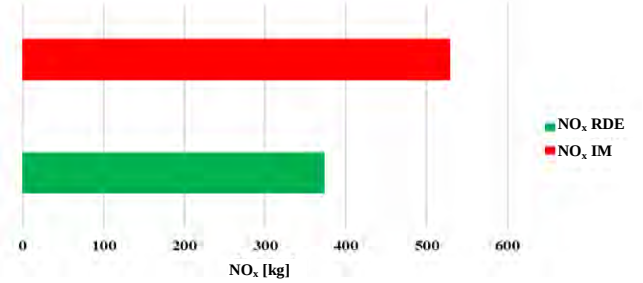

Fig. 10. Total NO_x emissions from transport trips during a one year period

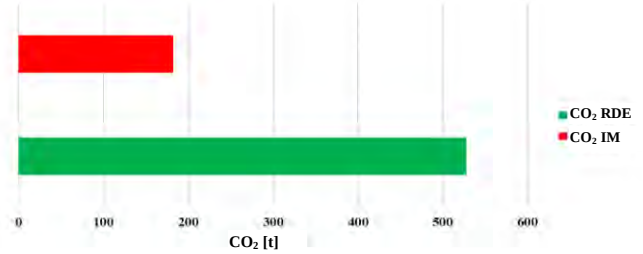

Fig. 11. Total CO_2 emissions from transport trips during a one year period

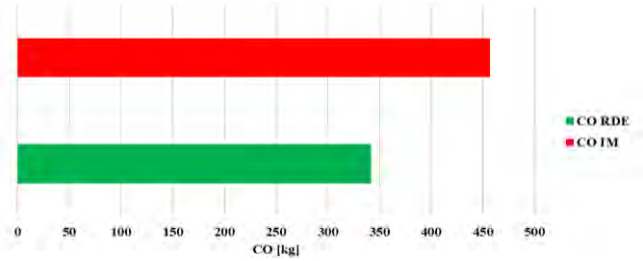

Fig. 12. Total CO emissions from transport trips during a one year period

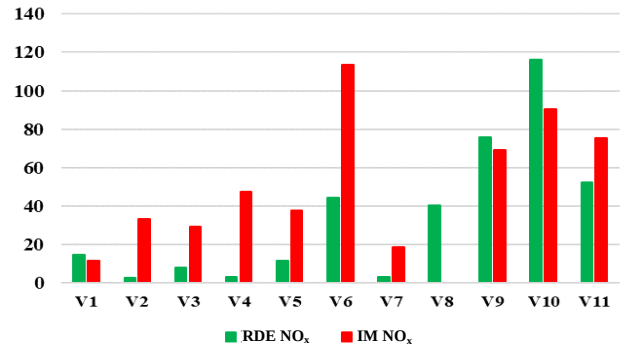

Fig. 13. Total NO_x emissions from transport trips during a one year period by vehicle type [kg]

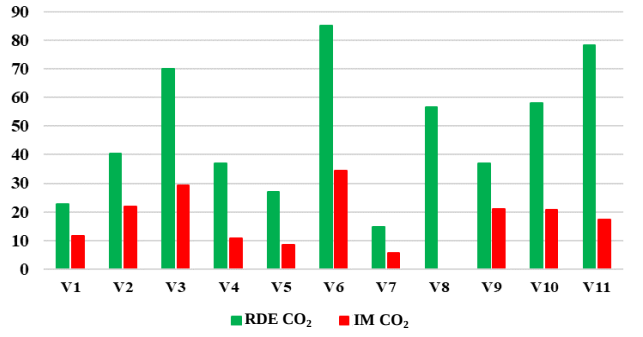

Fig. 14. Total CO_2 emissions from transport trips during a one year period by vehicle type [t]

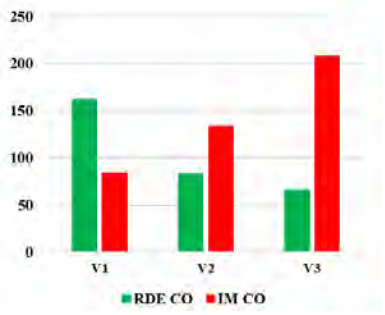

Fig. 15. Total CO emissions [kg] from transport trips during a one year period by vehicle type (V1–V3)

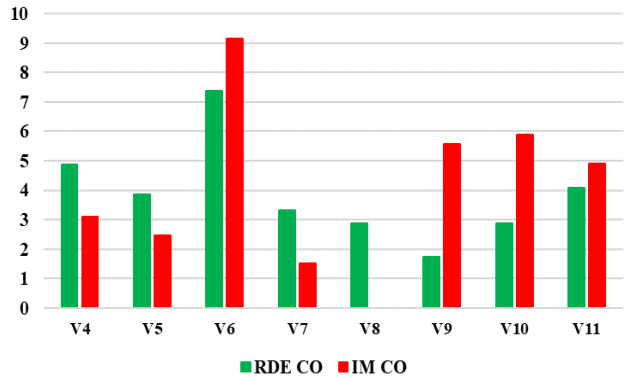

Fig. 16. Total CO emissions [kg] from transport trips during a one year period by vehicle type (V4–V11)

4. Discussion

An analytical indicator method intended for determining the vehicles' main pollutant emission enables the calculation of approximate main pollutant emission generated by various types of transport modes. The method enables the determination of the emission of basic and most commonly used passenger vehicles quickly and in a manner comparable in terms of quantities to the results obtained in RDE tests. In order to better represent the reality, the method should be supplemented with elements correcting the emission in terms of external factors, such as the vehicle's age, technical condition and mileage. These factors are currently not taken into account in the calculation of emission using the indicator method. Nevertheless, the absence of these factors makes it possible to record approximate emission of a given vehicle type, which can be used practice in all kinds of designing and simulation activities when estimating emissions without the need for labour-intensive road tests.

The organisation of passenger transport, e.g. in urban areas, optimising passenger transport routes in terms of cost, can be combined with a calculation of the transport modes' emission and the external costs generated. In this way, passenger transport planning can become more sustainable and the selection of transport modes with lower emission may contribute to a reduction in the transport's negative impact on the environment. The indicator method intended for determining the emission of transport modes presented in this paper allows for quick estimation of the emission of the main transport mode types. The results illustrate the main pollutant emission by the most common road transport modes used for passenger and freight transport.

5. Conclusions

An analysis of the total emissions of the test vehicles, i.e. the annual emissions of, e.g. nitrogen oxides, allowed for obtaining results that demonstrated a higher emission of the vehicles tested in real-world conditions than that obtained in the analytical method calculations, except for vehicle type V9 and V10. However, because the vehicles providing transport services in Warsaw are heavily used, the actual vehicle emission in Warsaw, determined in the RDE tests, may prove to be up to twice as high. In such a case, the emission values obtained in the analytical method will coincide with the real-world measurements of vehicle emission in the RDE tests. The same applies to air pollutant emissions for carbon dioxide and carbon oxides.

In terms of the annual transport plans and the transport work performed by the 130 vehicles analysed, nitrogen oxide and carbon oxide emissions are higher in the analytical method calculations. In terms of the total annual carbon dioxide emissions, the real-world emissions determined by the RDE tests are higher. The vehicles analysed in the calculation example, on an annual basis, collectively emit between 375 kg and 528 kg of nitrogen oxides, from 182 t to 341 t of carbon dioxide and from 341 kg to 456 kg of carbon oxide. Considering the averaged values of RDE air pollutant emission measurements and calculations of emissions based on statistical data in the indicator method, it is possible to estimate air pollutant emission without conducting RDE tests with the indicated above errors (chapter 3).

Acknowledgements

This paper was co-financed under the research grant of the Warsaw University of Technology supporting the scientific activity in the discipline of Civil Engineering, Geodesy and Transport.

Nomenclature

CEP	Central Register of Vehicles
CO	carbon monoxide
CO_2	carbon dioxide
FIA	International Automobile Federation
GPR	General Traffic Measurement 2015
GUS	Statistics Poland
ICCT	International Council on Clean Transportation
IM	indicator method for determining vehicle emission
LPG	liquefied petroleum gas
NO_x	nitric oxides
PM	particulate matter
RDE	Real Driving Emission test
TRUE	The Real Urban Emissions Initiative

Bibliography

[1] Chong HS, Kwon S, Lim Y, Lee J. Real-world fuel consumption, gaseous pollutants, and CO_2 emission of light-duty diesel vehicles. Sustain Cities Soc. 2020;53:101925. https://doi.org/10.1016/j.scs.2019.101925

[2] Costagliola MA, Costabile M, Prati MV. Impact of road grade on real driving emissions from two Euro 5 diesel vehicles. Appl Energ. 2018;231:586-593. https://doi.org/10.1016/j.apenergy.2018.09.108

[3] Fontaras G, Zacharof NG, Ciuffo B. Fuel consumption and CO_2 emissions from passenger cars in Europe–laboratory versus real-world emissions. Prog Energ Combust. 2018;60: 97-131. https://doi.org/10.1016/j.pecs.2016.12.004

[4] Gis W, Pielecha J, Merkisz J, Kruczyński S, Gis M. Determining the route for the purpose light vehicles testing in Real Driving Emissions (RDE) test. Combustion Engines. 2019;178(3):61-66. https://doi.org/10.19206/CE-2019-311

[5] Gołda IJ, Gołębiowski P, Izdebski M, Kłodawski M, Jachimowski R, Szczepański E. The evaluation of the sustainable transport system development with the scenario analyses procedure. J Vibroeng. 2017;19(7):5627-5638. https://doi.org/10.21595/jve.2017.19275

[6] Hooftman N, Messagie M, Van Mierlo J, Coosemans T. A review of the European passenger car regulations – real driving emissions vs local air quality. Renew Sust Energ Rev. 2018;86:1-21. https://doi.org/10.1016/j.rser.2018.01.012

[7] Jacyna M, Wasiak M, Lewczuk K, Kłodawski M. Simulation model of transport system of Poland as a tool for developing sustainable transport. Archives of Transport. 2014; 31(3):23-35. https://doi.org/10.5604/08669546.1146982

[8] Jacyna M, Żochowska R, Sobota A,Wasiak M. Scenario analyses of exhaust emissions reduction through the introduction of electric vehicles into the city. Energies. 2021; 14(7):2030. https://doi.org/10.3390/en14072030

[9] Lee T, Park J, Kwon S, Lee J, Kim J. Variability in operation-based NO_x emission factors with different test routes, and its effects on the real-driving emissions of light diesel vehicles. Sci Total Environ. 2013;461-462:377-385. https://doi.org/10.1016/j.scitotenv.2013.05.015

[10] Lejda K, Jaworski A, Mądziel M, Balawender K, Ustrzycki A, Savostin-Kosiak D. Assessment of petrol and natural gas vehicle carbon oxides emissions in the laboratory and on-road tests. Energies. 2021;14(6):1631. https://doi.org/10.3390/en14061631

[11] Mendoza-Villafuerte P, Suarez-Bertoa R, Giechaskiel B, Riccobono F, Bulgheroni C, Astorga C et al. NO_x, NH_3, N_2O and PN real driving emissions from a Euro VI heavy-duty vehicle. Impact of regulatory on-road test conditions on emissions. Sci Total Environ. 2017;609:546-555. https://doi.org/10.1016/j.scitotenv.2017.07.168

[12] Mera Z, Fonseca N, López JM, Casanova J. Analysis of the high instantaneous NO_x emissions from Euro 6 diesel passenger cars under real driving conditions. Appl Energ. 2019; 242:1074-1089. https://doi.org/10.1016/j.apenergy.2019.03.120

[13] Merkisz J, Pielecha J. Selected remarks about RDE test. Combustion Engines. 2016;166(3):54-61. https://doi.org/10.19206/CE-2016-340

[14] Merkisz J, Pielecha J, Nowak M, Andrzejewski M, Molik P. Pollutant emissions by transport modes when driving on a selected road infrastructure section (in Polish). Logistyka. 2014;3:4302-4310.

[15] Merkisz J, Rymaniak Ł. Determining the environmental indicators for vehicles of different categories in relation to CO_2 emission based on road tests. Combustion Engines. 2017;170(3):66-72. https://doi.org/10.19206/CE-2017-310

[16] Mądziel M, Campisi T, Jaworski A, Tesoriere G. The development of strategies to reduce exhaust emissions from passenger cars in Rzeszow city – Poland, a preliminary assessment of the results produced by the increase of e-fleet. Energies. 2021;14(4):1046. https://doi.org/10.3390/en14041046

[17] Nowak M, Rymaniak Ł, Fuć P, Andrzejewski M, Daszkiewicz P. Testing the emissions of gaseous components and particulate matter by a light-duty commercial vehicle in real operating conditions (in Polish). Autobusy: technika, eksploatacja, systemy transportowe. 2017;18(12):327-331.

[18] Pelkmans L, Debal P. Comparison of on-road emissions with emissions measured on chassis dynamometer test cycles. Transport Res D-Tr E. 2006;11(4):233-241. https://doi.org/10.1016/j.trd.2006.04.001

[19] Pielecha J, Skobiej K, Kurtyka K. Exhaust emissions and energy consumption analysis of conventional, hybrid, and electric vehicles in real driving cycles. Energies. 2020;13(23):6423. https://doi.org/10.3390/en13236423

[20] Pielecha P. Comparative analysis of exhaust fume emissions based on the example of selected passenger vehicles in real road traffic conditions (in Polish). Engineering thesis, Faculty of Transport of the Warsaw University of Technology. 2023.

[21] Pryciński P, Wawryszczuk R, Korzeb J, Pielecha P. Indicator method for determining the emissivity of road transport means from the point of supplied energy. Energies. 2023;16(12):4541. https://doi.org/10.3390/en16124541

[22] Report: Evaluation of real-world vehicle emissions in Warsaw – International Council on Clean Transportation. https://theicct.org/publication/true-warsaw-emissions-apr22/#:~:text=This%20report%20provides%20a%20detailed%20assessment%20of%20the,second-hand%20vehicles%2C%20whose%20use%20is%20widespread%20in%20Poland

[23] Report: Poland on its way towards sustainable development. GUS. 2022. https://raportsdg.stat.gov.pl/Miasta_i_rolnictwo.html.

[24] Report: Transport – activity results in 2020. GUS. https://stat.gov.pl/en/topics/transport-and-communications/

[25] Rosero F, Fonseca N, López JM, Casanova J. Effects of passenger load, road grade, and congestion level on real-world fuel consumption and emissions from compressed natural gas and diesel urban buses. Appl Energ. 2021;282: 116195. https://doi.org/10.1016/j.apenergy.2020.116195

[26] Rymaniak Ł, Kamińska M, Szymlet N, Grzeszczyk R. Analysis of harmful exhaust gas concentrations in cloud behind a vehicle with a spark ignition engine. Energies. 2021;14(6):1769. https://doi.org/10.3390/en14061769

[27] Sitnik LJ, Ivanov ZD, Sroka ZJ. Energy demand assessment for long term operation of hybrid electric vehicles. IOP Conf Ser Mater Sci Eng. 2020;1002(1):012026. https://doi.org/10.1088/1757-899X/1002/1/012026

[28] Sitnik LJ, Sroka ZJ, Andrych-Zalewska M. The Impact on emissions when an engine is run on fuel with a high heavy alcohol content. Energies. 2020;14(1):41. https://doi.org/10.3390/en14010041

[29] Sokolnicka B, Fuć P, Szymlet N, Siedlecki M, Grzeszczyk R. Harmful exhaust components and particles mass and number emission during the actual drive of a passenger car

in accordance with the RDE procedure. Combustion Engines. 2019;178(3):198-202. https://doi.org/10.19206/CE-2019-334
[30] Suarez-Bertoa R, Astorga C, Franco V, Kregar Z, Valverde V, Clairotte M et al. Technical report by the Joint Research Centre (JRC). On-road vehicle emissions beyond RDE conditions. 2019. https://publications.jrc.ec.europa.eu/repository/bitstream/JRC115979/jrc_technical_report_redeem_final_online.pdf
[31] Suarez-Bertoa R, Valverde V, Clairotte M, Pavlovic J, Giechaskiel B, Franco V et al. On-road emissions of passenger cars beyond the boundary conditions of the real-driving emissions test. Environ Res. 2019;176:108572. https://doi.org/10.1016/j.envres.2019.108572
[32] Triantafyllopoulos G, Katsaounis D, Karamitros D, Ntziachristos L, Samaras Z. Experimental assessment of the potential to decrease diesel NO_x emissions beyond minimum requirements for Euro 6 Real Drive Emissions (RDE) compliance. Sci Total Environ. 2018;618:1400-1407. https://doi.org/10.1016/j.scitotenv.2017.09.274
[33] Wang H, Ge Y, Hao L, Xu X, Tan J, Li J et al. The real driving emission characteristics of light-duty diesel vehicle at various altitudes. Atmos Environ. 2018;191:126-131. https://doi.org/10.1016/j.atmosenv.2018.07.060
[34] Wegner M, Andrychowska A, Bawelska A, Bącela K, Brzezińska J, Budny D et al. Establishment of methodology and estimation of the external costs of air pollutant emissions by road transport modes at the national level (in Polish). Statistics Poland's Centre for Statistical Research and Education. GUS. 2018. https://stat.gov.pl/statystyki-eksperymentalne/uslugi-publiczne/opracowanie-metodyki-i-oszacowanie-kosztow-zewnetrznych-emisji-zanieczyszczen-do-powietrza-atmosferycznego-ze-srodkow-transportu-drogowego-na-poziomie-kraju,6,1.html
[35] Yu YS, Chon MS, Cha J. Evaluation of real driving emissions with acting regulations (3rd and 4th RDE packages) in Korea. Alexandria Engineering Journal. 2022; 61(12):9471-9484. https://doi.org/10.1016/j.aej.2022.03.025
[36] Zhai Z, Xu J, Zhang M, Wang A, Hatzopoulou M. Quantifying start emissions and impact of reducing cold and warm starts for gasoline and hybrid vehicles. Atmos Pollut Res. 2023;14(1):101646. https://doi.org/10.1016/j.apr.2022.101646

Piotr Pryciński, DEng. – Faculty of Transport, Warsaw University of Technology, Poland.
e-mail: *piotr.prycinski@pw.edu.pl*

Piotr Pielecha, Eng. – Graduate of the Faculty of Transport, Warsaw University of Technology, Poland.
e-mail: *piotrpielecha@gmail.com*

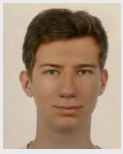

Róża Wawryszczuk, MEng. – Faculty of Transport, Warsaw University of Technology, Poland.
e-mail: *roza.wawryszczuk@pw.edu.pl*

Jakub Murawski, DEng. – Faculty of Transport, Warsaw University of Technology, Poland.
e-mail: *jakub.murawski@pw.edu.pl*

Jarosław Korzeb, DSc., DEng. – Faculty of Transport, Warsaw University of Technology, Poland.
e-mail: *jaroslaw.korzeb@pw.edu.pl*

Article citation info:
Kawakami T, Liu J, Jin M, Eto K. Effect of DMC blend ratio on emission characteristics for diesel engine generator fueled with DMC/diesel blend fuel. Combustion Engines. 2023;195(4):23-27. https://doi.org/10.19206/CE-168386

Tadashige KAWAKAMI
Jinru LIU
Meiling JIN
Kuniyoshi ETO

Combustion Engines
Polish Scientific Society of Combustion Engines

Effect of DMC blend ratio on emission characteristics for diesel engine generator fueled with DMC/diesel blend fuel

ARTICLE INFO

Received: 30 May 2023
Revised: 8 June 2023
Accepted: 15 June 2023
Available online: 16 September 2023

In this study, the DMC/diesel blend with 5%, 10%, 15% DMC by volume are prepared to investigate the emission characteristics. Since the combustion process is strongly influenced by the addition of low boiling point DMC boosts the atomization and liquid fuel mixture, the emissions of hydrocarbons and particulate matter are significantly reduced by the DMC addiction especially on the high-load conditions. Also, the nitrogen oxide emission has reduction on the high-load conditions. The scope for balancing NO_x and HC emissions exists.

Key words: *dimethyl carbonate, oxygenate fuel, diesel engine, emission characteristics, blend fuel*

1. Introduction

Diesel engines are well-known for the high thermal efficiency and extensively utilized in various applications due to their reliability and durability. However, the combustion of fossil fuels in internal combustion engines, including diesel engines, has contributed significantly to the increasingly severe climate issues [2]. It is imperative to seek solutions for reducing consumption of traditional fossil fuel and emission for diesel engines [11]. In response to these challenges, diesel engines have adapted many technical solutions like the innovation of injection method or the application of alcohol fuel to meet both the strict emission regulation and the depletion problems of fossil fuel resources [3, 5], like using higher injection pressure [12], the HEUI fuel injection system [9], the HCCI diesel engines [22], also the adaption of air filter to reduce the HC and CO emission [7]. many efforts about engine with alternative fuel and adaption on engine have been made. The possible attempt of prechambers in hydrogen internal combustion engines is discussed [15]. Research about LPG+DME blend fuel on SI engine is conducted [14]. Previous research indicated the efficiency of oxygenated fuel application on diesel engines can benefit those two purposes as well, such as using the alcohols, ethers, and esters for its good performance on diesel engines and the merits as the renewable fuels [18]. As the mostly investigated oxygenate, the biodiesel is also attracting attention. It is widely accepted for compression ignition (CI) engine for its renewability [19]. Biodiesel has many advantages such as reducing dependence on imported petroleum, mitigating global warming, improving lubrication, and reducing harmful emissions by its oxygen content. However, it can affect in-cylinder parameters like atomization, vaporization, and fuel-air mixing which considered as disadvantages. Insufficient cetane quality in biodiesel can lead to unfavorable starting characteristics, higher fuel consumption, and elevated exhaust emissions [6]. To solve these problems, the use of fuel additives can achieve effective atomization and fuel-air mixing. The cetane number plays an important role. Fuel with higher cetane numbers have shorter ignition delays, completing a shorter duration of the combustion process [1, 21]. Previous studies found that dimethyl carbonate (DMC)-diesel can lead to reduction on smoke and particulate mass with little change in NO_x emission [16].

DMC can be used as an oxygenated additive to blend with diesel fuel to improve combustion and reduce pollutant emission of diesel engines since it has a high oxygen fraction of 53.3% by mass. It is non-toxic and highly miscible with diesel fuel. DMC exists in liquid state at room temperature, which makes storage and transportation convenient. Research suggested that DMC is a suitable oxygenated additive with good blend fuel properties, and there exists a relationship between the amount of soot reduction and the oxygen content of the blended fuel [17]. Others [10, 23] investigated the combustion and emission characteristics of diesel engine fueled with diesel–DMC blends and found that smoke emission can be reduced without sacrificing NO_x emission and thermal efficiency. Dimethyl carbonate (DMC) added into diesel can help fuel atomize and produce a uniform air-fuel mixture due to its favorable evaporation attribute. It is a nontoxic compound and can easily dissolve in diesel at ambient temperature. Previous studies have indicated the potential of DMC in emissions reduction and thermal efficiency enhancement [5, 17, 20].

The emissions of an indirect injection diesel engine were compared while operating on ultra-low sulfur diesel oil blended with up to 30% DMC by volume [4]. Researchers employed a new approach that involved combining internal exhaust gas recirculation with a small injection of diesel fuel to ignite the DMC, which was directly injected into the engine cylinder [13]. The results demonstrated that the engine fueled with DMC exhibited lower NO_x emissions, almost zero smoke levels, and a 2–3% higher effective thermal efficiency compared to the engine fueled with diesel fuel, particularly under moderate and high load conditions. Additionally, the blended fuel showed a reduction in particulate number concentrations, highlighting its potential in mitigating emissions in diesel engines.

In this study, the DMC/diesel blend with 5%, 10%, 15% DMC by volume are prepared to investigate the emission

characteristics of low DMC blend ratio on a diesel engine. Since the combustion process is strongly influenced by the addition of low boiling point, DMC boosts the atomization and liquid fuel mixture, the emissions of hydrocarbons and soot are significantly reduced by the DMC addiction especially on the high-load conditions. Also, the nitrogen oxide emission show reduction on DMC15 with all load conditions, meanwhile the CO emission increased.

2. Experiment and method

2.1. Experiment apparatus

The schematic diagram of the experimental setup is shown in Fig. 1. In this experiment, we used a diesel generator which has a single-cylinder 4-stroke diesel engine (model YDG300VS, by Yanmar Holdings Co., Ltd.) as the test engine. We used the AVL Di-com4000 and an opacity meter (ALTAS-5100D, Yanaco Opacimeter) to measure the exhaust characteristics. The main specifications of the engine shown in Table 1. It should be noted that the engine specifications indicate the conditions under standard atmospheric conditions (ambient temperature of 298 K, atmospheric pressure of 100 kPa, and relative humidity ranges from 20~30%).

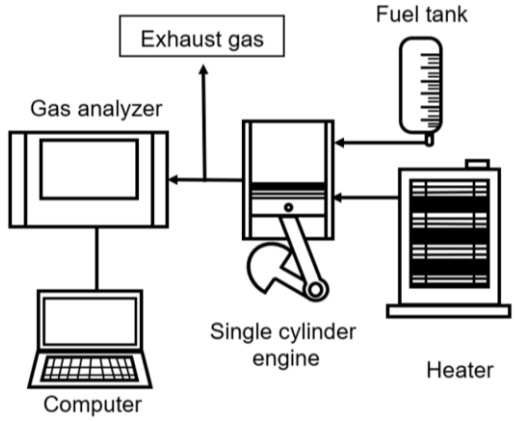

Fig. 1. Experimental apparatus

2.2. Test fuel properties and experiment method

Table 2 show the fuel properties of diesel and DMC. Diesel and DMC (Dimethyl Carbonate) were mixed for 30 minutes at 1500 rpm by using a magnetic stirrer. DMC/diesel blend fuels were prepared with a volumetric ratio at 5vol%, 10vol% and 15% vol% DMC with diesel. These are abbreviated as DMC5, DMC10 and DMC15 in the following. The calculation formula for the blending ratio (W) is shown in Eq. (1) below

$$W = \frac{\text{Volume of DMC}}{\text{Volume of Light oil+Volume of DMC}} \times 100\ [\%] \qquad (1)$$

The DMC/diesel blend fuel was supplied into the test engine. After the engine warm-up stage ended, the exhaust characteristics were measured by the exhaust measurement device (AVL Di-Com 4000). The measurements data for each load condition were averaged using arithmetic mean. Load conditions were set at nine levels by using heaters: 0 W, 300 W, 600 W, 900 W, 1200 W, 1500 W, 1800 W, 2100 W and 2400 W. The experiment environment condition stays same for each load condition. Furthermore, viscosity measurements were conducted using an SV-10 fork-type vibrating viscometer (AND Co., Ltd). Table 3 shows the viscosity of diesel and DMC/diesel blend fuels. With the DMC blend ratio increase, the viscosity of DMC/diesel blend fuel decrease.

Table 1. Engine specifications

Engine type	4 stroke cycle diesel engine
Injection system	Direct injection
Bore × stroke [mm]	ϕ78×67
Rated output [kW/min^{-1}]	4.0/3000
Cooling system	Forced air cooling
Displacement [dm^3]	0.320
Compression ratio [-]	21.1

Table 2. Properties of Diesel and DMC

	Diesel	DMC
Chemical formula	–	$C_3H_6O_3$
Kinematicviscosity @20°C[mm^2/s]	2.77	0.63
Density @20°C [kg/m^3]	822	1079
Boiling point [°C]	160~360	90.1
Oxygen content rate [% by weight]	0.09	53.3
Cetane number	52	36
Laten heat of vaporization [kJ/kg]	280	369
Lower heat value [MJ/kg]	42.50	15.78

Table 3. Viscosities of test fuel

	Viscosity [mPa·s]	Kinematic viscosity [cSt]
Diesel	2.06	2.46
DMC	0.568	0.529
DMC5	1.76	2.07
DMC10	1.26	1.46
DMC15	0.87	1.02

3. Results and discussion

The emission characteristics of diesel fuel and DMC/diesel blend fuel for various blend ratio are examined and discussed in this section.

Effect of DMC on HC emission with load for diesel, DMC/diesel blend fuels shown in Fig. 2. From Fig. 2, with the engine load increased, the HC emission decreased for all fuel conditions. This is attributed to the increased combustion chamber temperature resulting from higher loads, which leads to a decrease in incomplete combustion. Regarding the impact of DMC blending, it shows a general tendency of reducing HC emissions. With the oxygenate additive DMC blended in, it can be observed that the HC emissions reduction exist with the use of DMC5 and DMC10 under all load conditions. However, when the DMC blend ratio raises up to 15%, the HC emission at low load region (from 0 W to 900 W) show substantial increase, but still show the reduction effect on the mid and high load region (from 1200 W to 2400 W). Since the DMC additive has lower viscosity than diesel, with the small amount DMC additive (DMC blend ratio under 10%), the evaporability of DMC improves the mixing process of liquid fuel and boosts the combustion, its oxygen content contributes to the HC emission reduction effect. On the other side, while the DMC blend ratio raises up to 15%, due to the low cetane number of DMC, which has impact on the ignition delay time, also lead to incomplete combustion thus caused higher HC emission at the low-load region. Still, under the high-load region, since the combustion chamber tempera-

ture raised thus accelerate the physical ignition delay, with the high oxygen content and lower kinematic viscosity which forms better liquid fuel mixture and promotes the fuel atomization effect, the DMC15 realized lower HC emission than that of diesel on the high-load area.

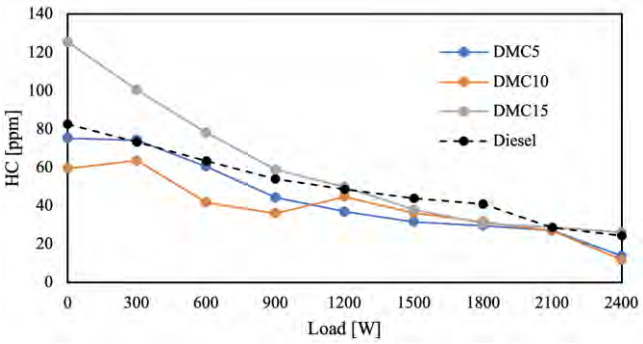

Fig. 2. HC emission

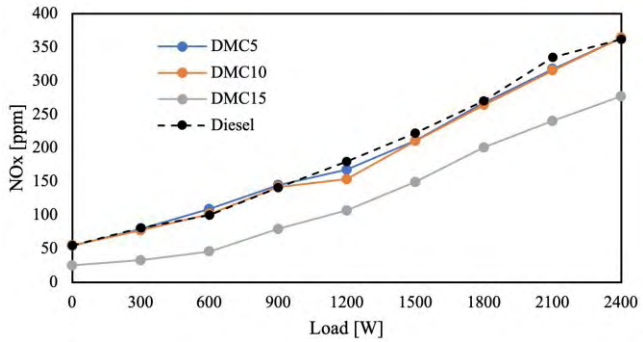

Fig. 3. NO_x emission

Figure 3 shows the nitrogen oxides (NO_x) emission at each load condition with diesel and DMC/diesel blend fuels. From Fig. 3, the NO_x emissions increase with load increase under all fuel conditions. This is because with the load increase, the combustion temperature increase, resulting in increased emissions of NO_x derived from thermal sources.

Focus on the effect of DMC additive, compare to the diesel, with the DMC additive, the NO_x emission reduction effect exists with all DMC/diesel blend fuels. The maximum reduction rate of DMC5 is 6.7%, that of DMC10 is 14.5%, both exist at 1200 W load condition. However, when the DMC blend ratio raises to 15%, the minimum and maximum NO_x reduction ratio of DMC15 is 23.4% and 59.6% at 2400 W and 300 W, respectively. The main reason is that, with the DMC blend ratio increased, the LHV of DMC/diesel blend fuel decreased. Since the fuel injection amount is at same with same engine load condition, under the interact of evaporation laten heat of DMC, the lower LHV of DMC/diesel blend fuel release less heat that improves the thermal NO_x reduction effect. The maximum NO_x emission reduction ratio appears in low load region, which is affected by the combustion temperature. On the other hand, the low cetane value of DMC increases the ignition delay time with the increasing DMC blending ratio, thereby leading to the incomplete combustion as mentioned in Fig. 2, lowering the combustion temperature, and suppressing the formation of thermal NO_x. Furthermore, due to the lower boiling point of DMC compared to diesel, the evaporation enthalpy of DMC reduced the flame temperature, which considered as a factor of the NO_x emission reduction effect.

From Fig. 2 and Fig. 3, due to the high oxygen content, low LHV, low cetane number and kinematic viscosity of DMC, with the use of 15% DMC, it achieved simultaneous reduction of NO_x and HC emission under the high load region (from 1500 W to 2400 W).

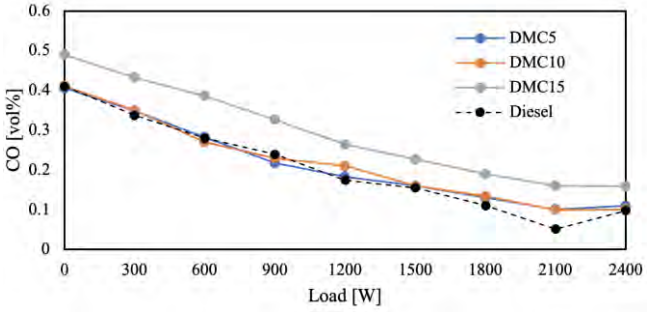

Fig. 4. CO emission

$$CO + OH \Leftrightarrow CO_2 + H$$

$$2OH \Leftrightarrow O_2 + H_2$$
$$2H_2O \Leftrightarrow O_2 + 2H_2$$
$$H_2 \Leftrightarrow 2H$$
$$O_2 \Leftrightarrow 2O$$
$$N_2 \Leftrightarrow 2N$$

Fig. 5. Kinetic oxidation of CO

Figure 4 shows the CO emission at each load condition with diesel and DMC/diesel blend fuels. Figure 5 shows the main reaction pathways of CO oxidation. From Fig. 4, with the use of DMC5 and DMC10, under low load region (from 0 W to 900 W), the CO emission show little decrease. On the 1200 W to 2400 W load region, the CO emission of DMC/diesel fuel show increase compared to that of diesel fuel. The main reason is considered as that, at the low load region, the interaction between the increase of oxygen content and low combustion temperature caused by the DMC additive makes the little CO emission decrease. Meanwhile, on the high load region, the combustion temperature raised up, but the insufficient oxygen content in the rich region at the flame front lead to the CO emission increase [8]. For DMC15, the CO emission is higher than all other fuel conditions under all load regions. Since the DMC15 has more oxygen content, the main reason is considered as that the low LHV of DMC lead to a lower combustion temperature, which has been proved in Fig. 3, the NO_x emission data. The lower combustion temperature didn't satisfy the temperature of CO oxidation condition.

Figure 6 shows the CO_2 emission at each load condition with diesel and DMC/diesel blend fuels. From Fig.6, CO_2 has little increasement with the use of DMC additive on low and mid load region with all DMC/diesel blend fuels. Since DMC15 has highest DMC blend ratio, the higher

oxygen content benefits the CO oxidation process that led to higher CO_2 emission. For high load region, the increase rate of DMC5 and DMC15 decreased, which is considered as the CO oxidation process is suppressed with DMC5 and DMC15. The main reason is considered as the interaction between the oxygen content and the low LHV of different DMC/diesel blend fuel.

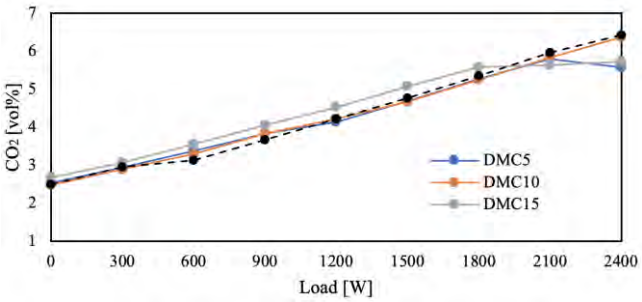

Fig. 6. CO_2 emission

An opacimeter is used to measure the contamination level of exhaust gases caused by particulate matter by passing light through the exhaust gas collected from the exhaust pipe and measuring the transmittance (optical absorption coefficient [m^{-1}]). Figure 7 shows the soot emission at each load condition with diesel and DMC/diesel blend fuels. From Fig. 7, with the use of DMC additive, soot emission significantly decreased at the DMC15 under the low load region (from 0 W to 1200 W), except the mid load region, the soot extremely decreased at 2400 W. However, the DMC blend ratio has great influence on the soot emission decrease tendency. Further studies needed to investigate the influence of DMC blend ratios under different engine load conditions.

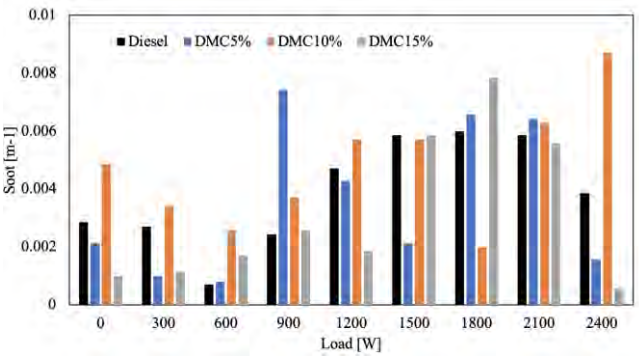

Fig. 7. Soot emission

4. Conclusions

In this study, we observed the effect of DMC blend ratio on emission characteristics with a use of diesel generator. The DMC/diesel blend fuels with three DMC blend ratio are used as test fuel. Through the observation of HC, NO_x, CO, CO_2, and soot, we discussed the influence of DMC's fuel properties on emission characteristics. Further studies about the proper DMC blend ratio are need. The main conclusions show as follows:

(1) The DMC/diesel blend fuel can realize the simultaneous reduction of HC and NO_x emissions under the high load region by the influence of DMC fuel properties.

(2) The HC and CO can not simultaneously reduce with the use of DMC15.

(3) It is possible to realize the soot reduction effect under the low and high load region by using DMC15. The impact of the DMC blend ratio on soot reduction exhibits varying tendencies across different load regions.

Nomenclature

CO	carbon monoxide
CO_2	carbon dioxide
DMC	dimethyl carbonate
DME	dimetyloeter
HC	hydrocarbon
HCCI	homogeneous-charge compression ignition
HEUI	hydraulic electronic unit injector
LPG	liquified petrolum gas
LHV	lower heat value
NO_x	nitrogen oxides
SI	spark ignition

Bibliography

[1] Anderson A, Devarajan Y, Nagappan B. Effect of injection parameters on the reduction of NO_x emission in neat biodiesel fuelled diesel engine. Energ Source Part A. 2017; 40(2):186-192. https://doi.org/10.1080/15567036.2017.1407844

[2] Andrych-Zalewska M. Research of pollutant emissions from automotive internal combustion engines in conditions corresponding to the actual use of vehicles. Combustion Engines. 2023;193(2):64-70. https://doi.org/10.19206/CE-162621

[3] Ayhan V. Effects of emulsified fuel on the performance and emission of direct injection diesel engine. J Energ Eng. 2013;139(2):91-98. https://doi.org/10.1061/(ASCE)EY.1943-7897.0000097

[4] Cheung CS, Liu MA, Lee SC, Pan KY. Experimental study on emission characteristics of diesels with diesel fuel blended with dimethyl carbonate. International Journal of Energy for a Clean Environment. 2005;6:239-253. https://doi.org/10.1615/InterJEnerCleanEnv.v6.i3.30

[5] Cheung CS, Zhu R, Huang Z. Investigation on the gaseous and particulate emissions of a compression ignition engine fueled with diesel-dimethyl carbonate blends. Sci. Total Environ. 2011;409(3):523-529. https://doi.org/10.1016/j.scitotenv.2010.10.027

[6] Devaraj A, Yuvarajan D, Vinoth Kanna I. Study on the outcome of a cetane improver on the emission characteristics of a diesel engine. International Journal of Ambient Energy. 2020;41(7):798-801. https://doi.org/10.1080/01430750.2018.1492452

[7] Dziubak T, Karczewski M, Dziobek I. Empirical study of the effect of the air filter on the performance and exhaust

emissions of a diesel engine. Combustion Engines. 2023; 193(2):94-111. https://doi.org/10.19206/CE-161881

[8] Fuyuto T, Ueda R, Hattori Y, Mizuta J, Akihama K, Aoki H. et al. Analysis of CO emission sources in diesel combustion (third report) – CO reduction techniques and its validation. Transactions of Society of Automotive Engineers of Japan. 2013;44(2):237-243. https://doi.org/10.11351/jsaeronbun.44.237

[9] Glassey SF, Stockner AR, Flinn MA. HEUI – a new direction for diesel engine fuel systems. SAE Technical Paper 930270. 1993. https://doi.org/10.4271/930270

[10] Huang ZH, Jiang DM, Zeng K, Liu B, Yang ZL. Combustion characteristics and heat release analysis of a direct injection compression ignition engine fuelled with diesel-dimethyl carbonate blends. P I Mech. Eng D-J Eng. 2003; 217:595-605. https://doi.org/10.1243/095440703322114979

[11] Jiaqiang E, Zhao X, Qiu L, Wei K, Zhang Z, Deng Y et al. Experimental investigation on performance and economy characteristics of a diesel engine with variable nozzle turbocharger and its application in urban bus. Energ Convers Manage. 2019;93:149-161. https://doi.org/10.1016/j.enconman.2019.04.062

[12] Kato T, Tsujimura K, Shintani M, Minami T, Yamaguchi I. Spray characteristics and combustion improvement of D.I. diesel engine with high pressure fuel injection. SAE Technical Paper 890265. 1989. https://doi.org/10.4271/890265

[13] Li XL, Chen HY, Zhu ZY, Huang Z. Study of combustion and emission characteristics of a diesel engine operated with dimethyl carbonate. Energ Convers Manage. 2006;47(11-12):1438-1448. https://doi.org/10.1016/j.enconman.2005.08.021

[14] Marzec P. Tests of a SI engine powered by gaseous fuels blends of LPG + DME of various proportions with variable load. Combustion Engines. 2022;190(3):23-26. https://doi.org/10.19206/CE-144124

[15] Matla J. Possible applications of prechambers in hydrogen internal combustion engines. Combustion Engines. 2022; 191(4):77-82. https://doi.org/10.19206/CE-148170

[16] Miyamoto N, Ogawa H, Arima T, Miyakawa K. Improvement of diesel combustion and emissions with addition of various oxygenated agents to diesel fuels. SAE Technical Paper 962115. 1996. https://doi.org/10.4271/962115

[17] Murayama T, Zheng M, Chikahisa T, Oh Y, Fujiwara Y, Tosaka S et al. Simultaneous reductions of smoke and NO_x from a DI diesel engine with EGR and dimethyl carbonate. SAE Technical Paper 952518. 1995. https://doi.org/10.4271/952518

[18] Pan M, Qian W, Huang R, Tong C, Huang H, Xu L et al. Effects of dimethyl carbonate and 2-ethylhexyl nitrate on energy distribution, combustion, and emissions in a diesel engine under different load conditions. Energ Convers Manage. 2019;199:111985. https://doi.org/10.1016/j.enconman.2019.111985

[19] Rashedul HK, Masjuki HH, Kalam MA, Ashraful AM, Ashrafur Rahman SM, Shahir SA. The effect of additives on properties, performance and emission of biodiesel fuelled compression ignition engine. Energ Convers Manage. 2014; 88:348-364. https://doi.org/10.1016/j.enconman.2014.08.034

[20] Rounce P, Tsolakis A, Leung P, York APE. A comparison of diesel and biodiesel emissions using dimethyl carbonate as an oxygenated additive. Energy Fuel. 2010;24(9):4812-4819. https://doi.org/10.1021/ef100103z

[21] Shahabuddin M, Liaquat AM, Masjuki HH, Kalam MA, Mofijur M. Ignition delay, combustion and emission characteristics of diesel engine fueled with biodiesel. Renew Sust Energ Rev. 2013;21:623-632. https://doi.org/10.1016/j.rser. 2013.01.019

[22] She J. Experimental study on improvement of diesel combustion and emissions using flash boiling injection. SAE Technical Paper 2010-01-0341. 2010. https://doi.org/10.4271/2010-01-0341

[23] Zhang GD, Liu H, Xia XX, Zhang WG, Fang JH. Effect of dimethyl carbonate fuel additive on diesel engine performance. P I Mech Eng Part D-J Eng. 2005;219(7):897-903. https://doi.org/10.1243/095440705X28358

Prof. Tadashige Kawakami, DEng. – Faculty of Science and Engineering, Hosei University, Japan.
e-mail: *kawakami@hosei.ac.jp*

Jinru Liu, MEng. – PhD Student at Faculty of Science and Engineering, Hosei University, Japan.
e-mail: *jinru.liu.7s@stu.hosei.ac.jp*

Meiling Jin, BEng. – Master's Student at Faculty of Science and Engineering, Hosei University, Japan.
e-mail: *meiling.jin.9i@stu.hosei.ac.jp*

Kuniyoshi Eto – Engineer of Yamabiko Corporation, Japan.
e-mail: *etou@yamabiko-corp.co.jp*

Article citation info:
Kropiwnicki J, Gawłas T. Evaluation of the energy efficiency of electric vehicle drivetrains under urban operating conditions. Combustion Engines. 2023;195(4):28-34. https://doi.org/10.19206/CE-169492

Jacek KROPIWNICKI
Tomasz GAWŁAS

Combustion Engines
Polish Scientific Society of Combustion Engines

Evaluation of the energy efficiency of electric vehicle drivetrains under urban operating conditions

ARTICLE INFO

Received: 4 June 2023
Revised: 7 July 2023
Accepted: 11 July 2023
Available online: 8 August 2023

In electric vehicles, as in hybrids vehicles, a very important factor affecting the energy efficiency of the powertrain is the ability to use the regenerative braking energy. Depending on the settings available in electric vehicles, the driver can choose different modes of operation: switch off the regenerative braking mode altogether, select the intensity of regenerative braking, or leave the control system in automatic mode. The last mode is often the only one available on eclectic vehicles, so the driver cannot decide whether to switch off or increase intensity of the regenerative braking. This paper presents a new method for evaluating the energy efficiency of electric vehicle powertrains under urban operating conditions. The presented method uses a procedure for mapping the operating conditions allowing to determine the reference level of energy consumption in relation to those recorded during the identification tests. Identification tests were carried out in the Tri-City area using electric vehicles of different purposes and operating parameters. Performed tests allowed to evaluate the regenerative braking efficiency of tested vehicle, which varies over a relatively wide range, for vehicle A from 33 to 77%, for vehicle B from 27 to 55% and for vehicle C from 36 to 58%. It can be concluded that one of the main factors determining the regenerative braking efficiency is the level of state of charge of the accumulator and the management algorithm used by the vehicle for controlling this parameter.

Key words: *electric vehicle, urban conditions, regenerative braking, energetic efficiency, drivetrains*

1. Introduction

Electric drive systems have the potential to be much more efficient than conventional ones [6, 19], influenced by the very high efficiency of the electric motor itself, but also by its low variability over the range of typical operating conditions [6, 18]. Taking into account typical urban operating conditions, the efficiency of an eclectic motor can be expected to reach values ranging from 70% for very low loads up to 90% for maximum loads [14].

A very important factor in reducing the energy consumption of electric vehicles in urban conditions is the possibility of using regenerative braking to recharge the battery while driving [16, 21]. The efficiency of the process itself of generating electricity by the generator reaches a very similar level to that obtained in driving mode, but the process of reusing the electricity to drive the vehicle includes converting the energy twice, on the way from the wheels to the battery and back to the drive wheels. This means that the efficiency of the regenerative braking process can reach at most the square of the efficiency of the electric drive system. Control strategies for hybrid and electric vehicles are relatively complex [14, 16, 19] and depend on the state of charge of the batteries [9, 10, 20]. Typically, the efficiency of a regenerative braking process [1, 3, 4] is defined as a regenerative braking energy delivered to the battery and back to a drive system divided by the energy achievable from the braking process [5, 7]. Performed research show varying results, depending on the type of test, the vehicle and the strategy used by the manufacturer: 86% [14], 50% [15] and 31–42% [21].

Evaluation of the efficiency of an electric vehicle's drive system can be carried out under laboratory conditions for strictly defined operating conditions with the assumed repeatability of the tests. However, from a practical point of view, for the users of such vehicles, the results of tests and perform evaluations, which are created on the basis of real operating conditions [2, 8, 17], will be of greater value. It is necessary to use a testing method, which, on the one hand, allows for a simple and quick determination of the expected energy indicators, while on the other hand, the results obtained should be comparable regardless of the types of vehicles tested and the place of operation.

This paper presents a description of an original method of evaluation of the energy efficiency of electric vehicle drivetrains under urban operating conditions. The study uses measurements carried out in regular urban traffic. The presented method uses a procedure for mapping the operating conditions allowing to determine the reference level of energy consumption and compare it to the recorded during the identification tests.

In the first stage of energy efficiency evaluation, the drive system efficiency in a driving mode is determined, and in the second stage in a regenerative braking mode. The method is demonstrated using operating examples of three electric vehicles.

The work supports the evaluation of guidelines for controlling traffic in city centers using mobile applications and on-board navigation systems to reduce the energy consumption of vehicles equipped with regenerative braking systems.

2. Drive system description and parameters defining energy efficiency

Mapping the operating conditions depends on recording position, speed and elevation of the tested vehicles and evaluation of parameters, which map the operating condition for covered route. The first parameter mapping operating condition is a specific energy consumption (SEC) [12, 13]:

$$SEC = \frac{E_t}{m \cdot L} \tag{1}$$

where SEC is the specific energy consumption, E_t is the mechanical energy delivered by drive system to the wheels, L is the distance covered by the car and m is the gross vehicle mass.

Mechanical energy transmitted to the drive wheels (traction energy), can be calculated using the following equation:

$$E_t = \int_{t=0}^{t=t_c} (k_p \cdot F_t \cdot V) dt \tag{2}$$

where k_p is the positive traction force factor:

$$k_p = \begin{cases} 1 & \text{for powered wheels} \\ 0 & \text{for idlling or braking} \end{cases} \tag{3}$$

F_t is the traction force, calculated for recorded speed and altitude change,

$$\begin{aligned} F_t &= m \cdot a \cdot \delta + m \cdot g \cdot \sin(\alpha) \\ &+ \rho_{air} \cdot A_f \cdot C_D \cdot \frac{V^2}{2} + m \cdot g \cdot C_r \cdot \cos(\alpha) \end{aligned} \tag{4}$$

where a is the vehicle acceleration, δ is the rotating mass factor, g is the acceleration due to gravity, α is the road grade, ρ_{air} is the air density, A_f is the vehicle frontal area, C_D is the vehicle aerodynamic drag coefficient, C_r is the vehicle rolling drag coefficient and V is the vehicle speed.

Alternatively, for the data recorded at the uniform time step, traction energy transmitted to the drive wheels may be calculated using the following equation:

$$E_t = \Delta t \cdot \sum_{i=1}^{N} (k_{p_i} \cdot F_{t_i} \cdot V_i) \tag{5}$$

where Δt is the time step.

Total energy that can potentially be delivered to the regenerative braking system (regeneration energy) can be calculated using the following equation:

$$E_{reg} = \Delta t \cdot \sum_{i=1}^{N} (k_{reg_i} \cdot F_{t_i} \cdot V_i) \tag{6}$$

where k_{reg} is the negative traction force factor:

$$k_{reg} = \begin{cases} -1 & \text{for idlling or braking} \\ 0 & \text{for powered wheels} \end{cases} \tag{7}$$

The second parameter mapping operating condition is regenerative braking specific energy (RBSE) for the covered distance can be calculated using the following equation:

$$RBSE = \frac{E_{reg}}{m \cdot L} \tag{8}$$

Some part of the electrical energy is consumed by auxiliary devices. This energy consumption is defined by the parameter P_{AD}, which is electrical power delivered to the auxiliary devices (non traction electricity consumption).

The third parameter mapping operating condition is auxiliary devices specific energy (ADSE).

$$ADSE = \frac{\Delta t \cdot \sum_{i=1}^{N} (P_{AD_i})}{L \cdot m} \tag{9}$$

where P_{AD} is electrical power delivered to the auxiliary devices (non traction electricity consumption).

Figure 1 shows a diagram of the energy flow in the drive system of an electric vehicle with a regenerative braking system and auxiliary devices.

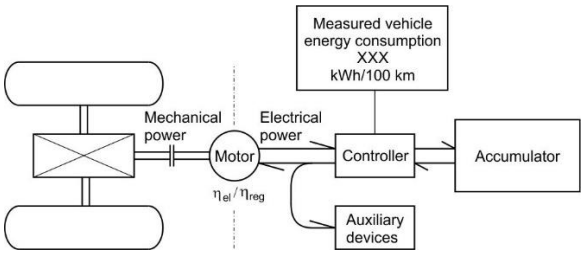

Fig. 1. Diagram of the energy flow in the drive system of an electric vehicle with a regenerative braking system and auxiliary devices

According to the diagram shown in Fig. 1, two operating modes of the drive system can be considered:

a) driving mode, when the electrical energy from the battery is supplied via the controller to the electric motor and then via the driveline to the wheels
b) regenerative braking mode, when the mechanical energy from the wheels is transferred by the driveline to the electric motor, which in this situation acts as an electricity generator and is then transferred to the battery via the controller.

A drive system efficiency is corresponding to the electric energy delivered by the accumulator to the controller and transformed into mechanical energy in the electric motor, then conversed by the drive line into form consumed for traction purposes. It can be defined as follows:

$$\eta_{el} = \frac{E_t}{E_{el}} \cdot 100\% \tag{10}$$

where E_{el} – is the electric energy delivered to the electric motor by the accumulator (used for traction)

$$E_{el} = \Delta t \cdot \sum_{i=1}^{N} (P_{el_i}) \tag{11}$$

P_{el} is the electrical power delivered by the accumulator to the electric motor. The power of the electric motor did not need to be measured directly in the proposed algorithm. According to eq. (10), electrical energy taken from the battery was measured using the on-board system of the vehicle.

A regenerative braking efficiency is corresponding to mechanical energy delivered to the driveline, next to the electric generator and by the controller to the accumulator, then back to the controller, electric motor, and the drive line. It can be defined as follows:

$$\eta_{reg} = \frac{E_{t_{reg}}}{E_{reg}} \cdot 100\% \tag{12}$$

where $E_{t_{reg}}$ – is the traction energy reused from regeneration energy.

The regenerative braking efficiency determines how much of the recoverable energy from the regenerative braking process will be reused to drive the vehicle. The amount of usable energy is determined by mapping the operating conditions.

Calculation of the electric energy consumption, which corresponding to energy measured by the on-board system of the vehicle, can be performed using the following equation:

$$EEC = SEC \cdot m \cdot \frac{1}{\eta_{el}} - RBSE \cdot m \cdot \eta_{reg} + ADSE \cdot m \quad (13)$$

where EEC is the electric energy consumption; SEC is the specific energy consumption; RBSE is the regenerative braking specific energy; ADSE is auxiliary devices specific energy; η_{el} is the drive system efficiency; η_{reg} is the regenerative braking efficiency; m is the mass of the vehicle.

3. Evaluation of the energy efficiency of electric vehicle drivetrains

3.1. Evaluation of the drive system efficiency in driving mode

Performed evaluation of the drive system efficiency in driving mode depended on making drive tests in regular city traffic in the Tri-City area. Global Positioning System (GPS) was used for recording position, speed and altitude of the car with phenomenological correction of the altitude signal [11] at a frequency of 10 Hz using a VBOX GPS Racelogic recorder.

All tests were performed with the cooling or heating system turned off, and the energy consumption of other comfort systems (radio, displays, and ventilation) was reduced to a minimum. It was assumed that electrical power delivered to the auxiliary devices is constant and equal to 0.3 kW, which is a typical value for electric cars with cooling and heating systems switched off [14]. Electric energy consumption was measured using the on-board system of the vehicle, according to the layout shown in Fig. 1. The reading was taken once, at the end of the test. During the tests, 3 vehicles were tested of different purposes and operating parameters. Drive system parameters of the tested vehicles have been shown in Table 1.

Table 1. Drive system parameters of the tested vehicles

No.	Vehicle	Mass [kg]	Power [kW]	Battery capacity [kWh]
A	Mercedes EQE 500	2575	375	90.6
B	Mercedes EQB 300	2275	168	66.5
C	Mazda MX-30	1745	107	35.0

In the first stage of energy efficiency evaluation, the drive system efficiency is determined. For this purpose, the best way is make test, when the regeneration system is switched off. Unfortunately most of electric cars have this function unachievable, in several models driver can regulate the intensity of regenerative braking, which enable to achieve similar effect.

The evaluation tests of the drive system efficiency were performed for all three tested vehicles. Formula (13) was used to determine the drive system efficiency. For vehicle A and B, it was not possible to disable regenerative braking entirely, but to minimise the impact of the error in the estimation of the regenerative braking efficiency, tests with the highest possible ratio of traction energy (5) to regenerative braking energy (6) were used. In this case, the efficiency of regenerative braking system was assumed to be equal to the square of the drive system efficiency. For vehicle C, it was possible to disable regenerative braking entirely. Figures 2–4 show the courses of speed, altitude and power delivered to the driveline (positive) or potentially useful for regenerative braking (negative) vs. time. When determining the drive system efficiency of vehicle A and B, a route with gradually increasing altitude was used, allowing high traction energy to be achieved during the test, with relatively low level of regenerative braking energy (Fig. 2 and 3). For vehicle C test, the relation of traction energy to regenerative braking energy was not relevant, as it was technically possible to switch off regenerative braking entirely.

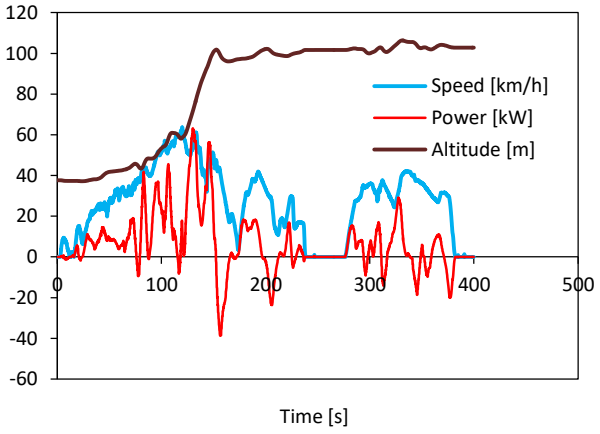

Fig. 2. Speed, power and altitude while evaluating the drive system efficiency of vehicle A

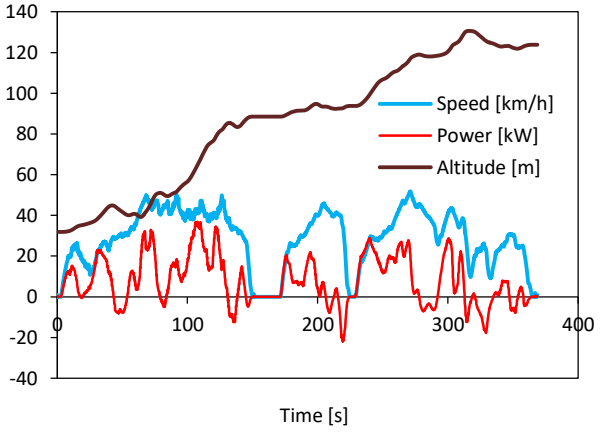

Fig. 3. Speed, power and altitude while evaluating the drive system efficiency of vehicle B

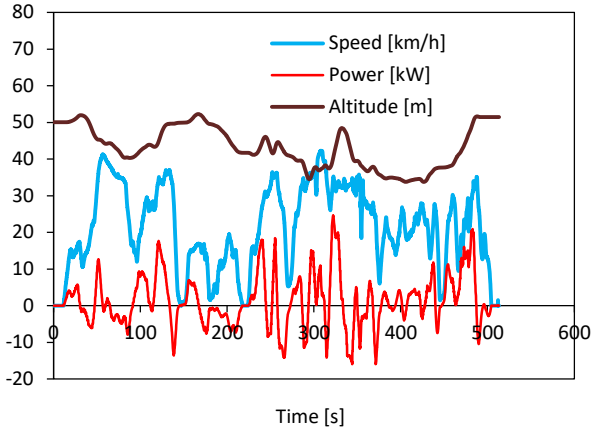

Fig. 4. Speed, power and altitude while evaluating the drive system efficiency of vehicle C

Table 2 shows the test results of the evaluated drive system efficiency and the assumed regenerative braking efficiency.

Table 2. Results of the evaluation tests of the drive system efficiency

Vehicle	E_t/E_{reg}	η_{reg}	η_{el}
A	4.24	$\eta_{reg} = (\eta_{el})^2$	83%
B	6.35	$\eta_{reg} = (\eta_{el})^2$	82%
C	1.66	0%	85%

The drive system efficiency for the vehicles analysed reaches a similar level of 82–85%, and the results are in line with literature data [14, 15, 21]. The values obtained will be used when testing the regenerative braking efficiency.

3.2. Evaluation of the regenerative braking efficiency

Evaluation of the regenerative braking efficiency was carried out using the vehicles whose data are shown in Table 1. On the basis of the test performed, the values of traction energy, regenerative braking energy were calculated. It was assumed that electrical power delivered to the auxiliary devices is constant and equal 0.3 kW. Using the previously determined values of the drive system efficiency, the regenerative braking efficiency for analysed vehicles was determined based on equation (13). The results of the evaluation are shown in Fig. 5.

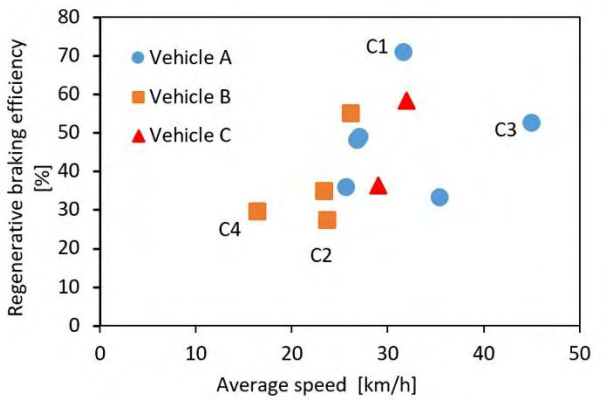

Fig. 5. Influence of average speed on regenerative braking efficiency

It can be conclude that the regenerative braking efficiency varies over a relatively wide range, for vehicle A from 33% to 77%, for vehicle B from 27% to 55% and for vehicle C (2 tests only) from 36% to 58%. In order to identify more closely the factors influencing the observed distribution of the regenerative braking efficiency, four case studies were selected, which are analysed below:
C1 – maximum regenerative braking efficiency
C2 – minimum regenerative braking efficiency
C3 – maximum average speed
C4 – minimum average speed.

The coordinates of the case studies are shown in Fig. 5. In Fig. 6–9 courses of speed, power and altitude of tested vehicles for analysed case studies C1-C4 have been presented. Those courses enable to evaluate the parameters mapping operating condition (SEC and RBSE), the third mapping operating parameter, related to the auxiliary devices (ADSE), must be evaluated separately. In Table 3 parameters mapping operating conditions for analysed case studies have been presented. The results shown in Table 3 are averages for the entire test, without distinguishing between acceleration, braking and constant-speed driving phases. The results obtained are consistent with the data of the manufacturers of these vehicles, but it should be noted that the results given in Table 3 are related to the weight of the vehicle expressed in Mg (1000 kg), hence a direct comparison is possible after multiplying the result by the weight of the vehicle.

Table 3. Parameters mapping operating conditions for case studies C1–C4

Case study	SEC [kWh/(Mg·100 km]	RBSE [kWh/(Mg·100 km)]	ADSE [kWh/(Mg·100 km)]	Average speed [km/h]	η_{reg}
C1	8.60	2.49	0.37	32	71%
C2	6.02	2.41	0.56	24	27%
C3	5.51	3.87	0.26	45	53%
C4	9.56	6.00	0.80	16	30%

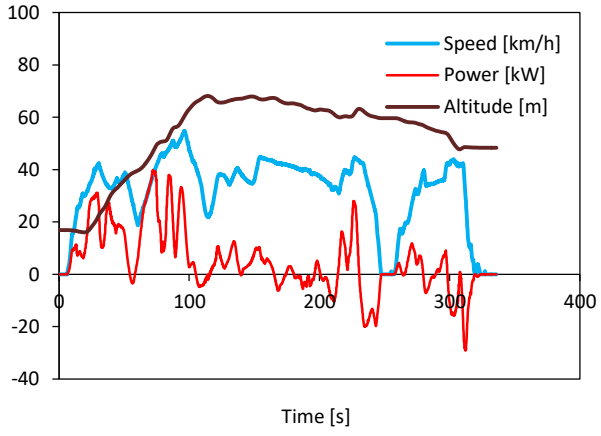

Fig. 6. Speed, power and altitude for case study C1 (maximum regenerative braking efficiency)

Case study C1 corresponds to uphill driving, with relatively small share of regenerative braking. It can be assumed that state of charge (SOC) of the accumulator, just after intensive driving mode is at an adequate level to ab-

sorb all regenerative braking energy. Additionally, higher initial speed of the braking process corresponds to higher speed of the electric generator, which also corresponds to higher efficiency of the regenerative braking process.

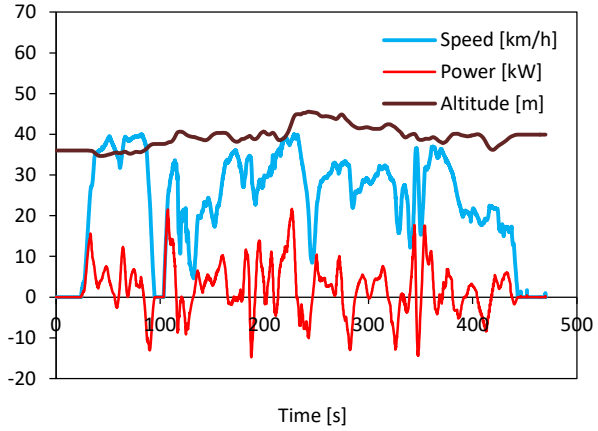

Fig. 7. Speed, power and altitude for case study C2 (minimum regenerative braking efficiency)

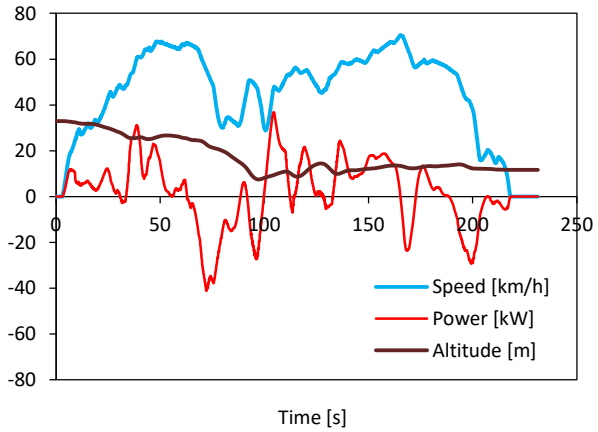

Fig. 8. Speed, power and altitude for case study C3 (maximum average speed)

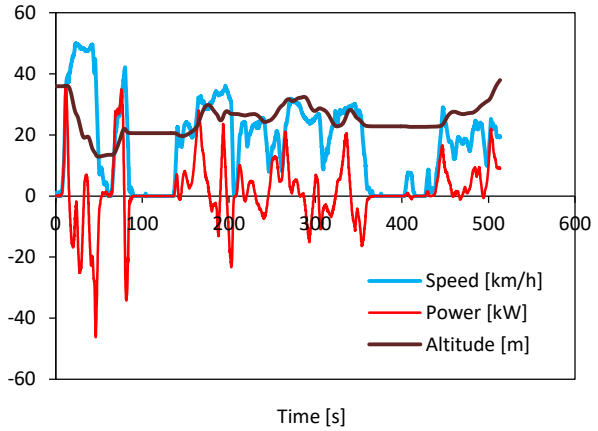

Fig. 9. Speed, power and altitude for case study C4 (minimum average speed)

Case study C2 corresponds to low average speed route, with relatively small elevation change and non-intensive regenerative braking. I can be assumed that SOC of the accumulator is all the time in relatively high lever, which limits absorption of the achievable regenerative braking energy. Additionally, the lower initial speed of the braking process corresponds to a lower speed of the electric generator, which also corresponds to the lower efficiency of the regenerative braking process.

Case study C3 corresponds to high average speed route, with down-hill driving and long-time intensive regenerative braking. It can be assumed that high level of state of charge (SOC) of accumulator is reached relatively quickly during intensive regenerative braking, after that energy cannot be used any longer. The energy recovery process, when applicable is performed with high efficiency due to the relatively high rotational speed of the generator during the initial braking phase, which corresponds to high efficiency of the regenerative braking process.

Case study C4 corresponds to low average speed route, with small elevation change and long-time regenerative braking. It can be assumed that SOC of the accumulator is all the time at high level, which limits absorption of the achievable regenerative braking energy. Additionally, lower initial speed of the braking process corresponds to a lower speed of the electric generator, which corresponds to lower efficiency of the regenerative braking process.

4. Conclusions

This paper presents a description of an original method of evaluation of the energy efficiency of electric vehicle drivetrains under urban operating conditions. The method uses universal measuring devices to collect the data for the following analyses. The method can be widely used and results can be implemented in applications that support drivers in energy-efficient driving. A novelty of this method is the use of a procedure for mapping the operating conditions allowing to determine the reference level of energy consumption and compare it to the electric energy consumption recorded during the identification tests. In the paper, the full calculation algorithm was presented using equations (1)–(10), for example, traction energy was evaluated using eq. (5), traction force was calculated based on the vehicle's resistance to motion (4) using design data provided by vehicle manufacturers. The power of the electric motor did not need to be measured directly in the proposed algorithm. According to eq. (10), electrical energy taken from the battery was measured using the on-board system of the vehicle.

In the first stage of the electric vehicle drivetrain efficiency evaluation, the drive system efficiency (in driving mode) is determined, and in the second stage in the regenerative braking mode. In this study, a new method of mapping operating conditions was used, based on recorded vehicle speed, position and latitude. Performed tests enabled to determine the drive system efficiency. In vehicles, where regenerative braking cannot be switched off, this evaluation stage requires a special approach. It has been proposed to use testing routes with a sufficiently high ratio of the specific energy consumption to the regenerative braking specific energy. This minimise the impact of the unknown value of the regenerative

braking efficiency. At the same time, it was necessary to assume a certain value for this efficiency, which was defined as the square of the drive system efficiency. Based on the known value of the electric energy consumption (on-board recording system) and the other components of equation (13), the drive system efficiency was determined.

The drive system efficiency for the vehicles analysed reaches a similar level of 82–85%, and the results are in line with literature data [15, 16]. The values obtained were then used to test the regenerative braking efficiency. The parameters mapping operating conditions and the equation (13) were consequently used for this purpose.

To conclude, the regenerative braking efficiency varies over a relatively wide range, for vehicle A from 33% to 77%, for vehicle B from 27% to 55% and for vehicle C (2 tests only) from 36% to 58%, which is in line with literature data [14, 21]. To identify more closely the factors influencing the observed distribution of the regenerative braking efficiency, four case studies were analysed (C1–C4). Based on the case studies, it can be concluded that one of the main factors determining the regenerative braking efficiency is the level of state of charge (SOC) of the accumulator and the management algorithm used by the vehicle for controlling this parameter. If the regenerative braking distances are long then the controller managing the SOC is limiting absorption of energy from regenerative braking process. On the other hand, low driving speeds at the start of the regenerative braking process, i.e. typical for urban conditions, corresponds to low generator speeds, which does not guarantee high operating efficiency of the generator.

Nomenclature

a	vehicle acceleration
ADSE	auxiliary devices specific energy
A_f	vehicle frontal area
C_D	vehicle aerodynamic drag coefficient
C_r	vehicle rolling drag coefficient
EEC	electric energy consumption
E_{el}	electric energy delivered to the electric motor by the accumulator
E_t	mechanical energy delivered by drive system to the wheels
$E_{t_{reg}}$	traction energy reused from regeneration energy
g	acceleration due to gravity
GPS	Global Positioning System
k_p	positive traction force factor
k_{reg}	negative traction force factor
L	distance covered by the vehicle
m	gross vehicle mass
P_{AD}	electrical power delivered to the auxiliary devices
RBSE	regenerative braking specific energy
SEC	specific energy consumption
V	vehicle speed
α	road grade
δ	rotating mass factor
η_{el}	drive system efficiency
η_{reg}	regenerative braking efficiency
ρ_{air}	air density
Δt	time step

Bibliography

[1] Alves J, Baptista PC, Gonçalves GA, Duarte GO. Indirect methodologies to estimate energy use in vehicles: application to battery electric vehicles. Energy Convers Manage. 2016; 124:116-129. https://doi.org/10.1016/j.enconman.2016.07.014

[2] Andrych-Zalewska M, Chłopek Z, Merkisz J, Pielecha J. Analysis of the operation states of internal combustion engine in the Real Driving Emissions test. Archives of Transport. 2022;61(1):71-88. https://doi.org/10.5604/01.3001.0015.8162

[3] Berzi L, Delogu M, Pierini M. Development of driving cycles for electric vehicles in the context of the city of Florence. Transport Res D-Tr E. 2016;47:299-322. https://doi.org/10.1016/j.trd.2016.05.010

[4] Brady J, O'Mahony M. Development of a driving cycle to evaluate the energy economy of electric vehicles in urban areas. Appl Energ. 2016;177:165-178. https://doi.org/10.1016/j.apenergy.2016.05.094

[5] Cieslik W, Zawartowski J, Fuc P. The Impact of the drive mode of a hybrid drive system on the share of electric mode in the RDC test. SAE Technical Paper 2020-01-2249. 2020. https://doi.org/10.4271/2020-01-2249

[6] Damiani L, Repetto M, Prato AP. Improvement of powertrain efficiency through energy breakdown analysis. Appl Energ. 2014;121:252-263. https://doi.org/10.1016/j.apenergy.2013.12.067

[7] Fiori C, Ahn K, Rakha HA. Power-based electric vehicle energy consumption model: model development and validation. Appl Energ. 2016;168:257-268. https://doi.org/10.1016/j.apenergy.2016.01.097

[8] Fiori C, Arcidiacono V, Fontaras G, Makridis M, Mattas K, Marzano V et al. The effect of electrified mobility on the relationship between traffic conditions and energy consumption. Transport Res D-Tr E. 2019;67:275-290. https://doi.org/10.1016/j.trd.2018.11.018

[9] Galvin R. Energy consumption effects of speed and acceleration in electric vehicles: laboratory case studies and implications for drivers and policymakers. Transport Res D-Tr E. 2017;53:234-248. https://doi.org/10.1016/j.trd.2017.04.020

[10] Huang J, Qin D, Peng Z. Effect of energy-regenerative braking on electric vehicle battery thermal management and control method based on simulation investigation. Energy Convers Manage. 2015;105:1157-1165. https://doi.org/10.1016/j.enconman.2015.08.080

[11] Kropiwnicki J, Gawłas T. Estimation of the regenerative braking process efficiency in electric vehicles. Acta Mechanica et Automatica. 2023;17(2):303-310. https://doi.org/10.2478/ama-2023-0035

[12] Kropiwnicki J, Kneba Z, Ziółkowski M. Test for assessing the energy efficiency of vehicles with internal combustion engines. Int J Automot Technol. 2013;14(3):479-487. https://doi.org/10.1007/s12239-013-0052-9

[13] Kropiwnicki J. A unified approach to the analysis of electric energy and fuel consumption of cars in city traffic. Energy. 2019;182:1045-1057. https://doi.org/10.1016/j.energy.2019.06.114

[14] Li L, Li X, Wang X, Song J, He K, Li C. Analysis of downshift's improvement to energy efficiency of an electric vehicle

during regenerative braking. Appl Energ. 2016;176:125-137. https://doi.org/10.1016/j.apenergy.2016.05.042
[15] Li L, You S, Yang C, Yan B, Song J, Chen Z. Driving-behavior-aware stochastic model predictive control for plug-in hybrid electric buses. Appl Energ. 2016;162:868-879. https://doi.org/10.1016/j.apenergy.2015.10.152
[16] Liu W, Qi H, Liu X, Wang Y. Evaluation of regenerative braking based on single-pedal control for electric vehicles. Front Mech Eng. 2020;15(1):166-179. https://doi.org/10.1007/s11465-019-0546-x
[17] Mamala J, Śmieja M, Prażnowski K. Analysis of the total unit energy consumption of a car with a hybrid drive system in real operating conditions. Energies. 2021;14:3966. https://doi.org/10.3390/en14133966
[18] Pielecha I, Cieślik W, Fluder K. Analysis of energy management strategies for hybrid electric vehicles in urban driving conditions. Combustion Engines. 2018;173(2):14-18. https://doi.org/10.19206/CE-2018-203
[19] Pielecha I, Cieślik W, Szałek A. The use of electric drive in urban driving conditions using a hydrogen powered vehicle – Toyota Mirai. Combustion Engines. 2018;172(1):51-58. https://doi.org/10.19206/CE-2018-106
[20] Qian KF, Liu XT. Hybrid optimization strategy for lithium-ion battery's state of charge/health using joint of dual Kalman filter and modified sine-cosine algorithm. J Energy Storage. 2021;44:103319. https://doi.org/10.1016/j.est.2021.103319
[21] Qiu C, Wang G. New evaluation methodology of regenerative braking contribution to energy efficiency improvement of electric vehicles. Energy Convers Manage. 2016;119:389-398. https://doi.org/10.1016/j.enconman.2016.04.044

Jacek Kropiwnicki, DSc., DEng. – Faculty of Mechanical Engineering, Gdańsk University of Technology, Poland.
e-mail: *jkropiwn@pg.gda.pl*

Tomasz Gawłas, MEng. – BMG Goworowski, Gdynia, Poland.
e-mail: *tomasz.gawlas@mazdagdynia.pl*

Article citation info:
Longwic R, Tatarynow D, Kuszneruk M, Wozniak-Borawska G. Preliminary tests of a Diesel engine powered by diesel and hydrogen. Combustion Engines. 2023;195(4):35-39. https://doi.org/10.19206/CE-169485

Rafal LONGWIC
Dawid TATARYNOW
Michal KUSZNERUK
Gracjana WOZNIAK-BORAWSKA

Combustion Engines
Polish Scientific Society of Combustion Engines

Preliminary tests of a Diesel engine powered by diesel and hydrogen

ARTICLE INFO

Received: 1 June 2023
Revised: 10 July 2023
Accepted: 11 July 2023
Available online: 22 July 2023

This article discusses the possibilities of powering a commonly used diesel engine with renewable fuels. It analyses scientific studies that clearly indicate that the use of hydrogen is a potentially future-proof option due to its potential to reduce specific fuel consumption and improve performance and increase thermal efficiency. The research was carried out on a laboratory bench designed to test a diesel engine fueled by different fuels. A proprietary hydrogen injection system with dedicated control software was used. Hydrogen injection pressures of 0.15, 0.18, 0.20 MPa and hydrogen injector opening times of 2.5, 3.0, 3.5 ms, respectively, were set as control parameters. The rapidly varying engine operating parameters were recorded and the parameters calculated from them were analysed.

Key words: *hydrogen, combustion, diesel engine, indication, test stand, fuel*

1. Introduction

The well-known effects of excessive pollutant emissions such as global warming, higher sea levels, smog or a health crisis are driving the drive towards climate neutrality [1]. This goal can be achieved, among other things, through the use of alternative fuels. This is why engines powered by renewable energy sources are currently gaining more and more interest. These include hydrogen, which is an environmentally friendly fuel with a zero carbon footprint that contributes to cleaner combustion. There is a huge dynamic of interest in hydrogen on a global scale. In the report 'Geopolitics of the Energy Transformation The Hydrogen Factor', according to Francesco La Camera Director-General International Renewable Energy Agency, hydrogen sources are expected to cover up to 12 per cent of global energy consumption by 2050 [14].

According to the European Automobile Manufacturers Association (ACEA), the European Union has 560 passenger cars and 81 commercial vehicles per 1000 inhabitants. Diesel-powered light commercial vehicles continue to dominate in most EU countries, with as much as 91.2% of the commercial vehicle fleet in the EU running on diesel. A similar situation (96.3%) applies to heavy goods vehicles. In the second quarter of 2022, the market share of passenger cars powered by both petrol and oil was still 55.8% despite the declines [12, 13].

It is, therefore important that conventional diesel engines can eventually be adapted to run on hydrogen, e.g. while leaving the pilot diesel injection in place. A great deal of research work is being carried out in this area. The use of hydrogen as a fuel for diesel engines is a complex issue. Ceraat et al. [2] carried out experimental studies in which they showed that increasing the amount of hydrogen improves the combustion process and reduces the carbon content in the fuel-air mixture, leading to lower CO_2 and CO emissions. It has been noted that soot content decreases with an increase in hydrogen by up to 20%.

Similarly, Juknelevičius et al. [5] showed that the introduction of hydrogen fuel has a positive effect on exhaust emissions, smoke and CO emissions. Combustion becomes smoother, smoke and CO emissions decrease, while HC emissions increase. In [15], it was found that with the enrichment of the mixture with hydrogen, there is a significant reduction in specific CO_2 emissions (the maximum reduction in emissions is observed at 62% in the presence of 46% hydrogen). It was noted that soot emissions decrease significantly with the addition of hydrogen and are 0.28 g/kWh, 0.20 g/kWh and 0.16 g/kWh at 16% H_2, 36% H_2 and 46% H_2, respectively. In contrast, the amount of soot emitted without hydrogen addition was 0.66 g/kWh. According to Santoso et al. [16], at constant load and engine speed, the addition of hydrogen to the intake manifold results in a reduction in diesel consumption.

Work has shown that hydrogen is a potentially future-proof option because it reduces specific fuel consumption [3, 4, 6, 7], increases engine performance, improves efficiency and thermal efficiency [8–10]. It has also been found that, by increasing the dosage of diesel, more hydrogen can be supplied without adversely affecting the working process [11, 17–19].

2. Materials and Methods

2.1. Test stand

The tests were carried out in the Laboratory of the Department of Motor Vehicles of the Lublin University of Technology. The test object was a 1.3 MultiJet compression-ignition engine installed in a Fiat Qubo car. Parameters and technical data of the engine are presented in Table 1. The test environment is shown in Fig. 1.

Table 1. Main characteristics of Fiat Qubo vehicle used for the tests

Parameter	Unit
Engine capacity	1248 cm^3
Cylinder diameter	69.6 mm
Piston stroke	82 mm
Compression ratio	16.8:1
Max power	55 kW CEE/75 KM CEE
Max torque	190 Nm CEE/kg m CEE
Idle speed	850 ±20 rpm
Rotational speed at maximum torque	1500 rpm
Injection system/fuel supply	Common Rail/diesel

Fig. 1. Test bench: 1 – 1.3 Multijet engine, 2 – Fiat Qubo, 3 – Dynorace DF4FS-HLS chassis dynamometer, 4 – computer with software: AVL Indicom, MultiEcuScan and dedicated gas control software, 5 – MAHA MET 6.3 exhaust gas analyzer, 6 – MultiCon CMC-99 data logger, 7 – AVL IndiMicro 602 measuring system, 8 – ZPR 1-B/S fuel consumption meter

During the tests, the engine was fueled with diesel and hydrogen, the dosage of which was adjusted using dedicated control software. Traction tests were carried out using a Dynorace DF4FS-HLS chassis dynamometer. The test rig is shown in detail in the block diagram (Fig. 2). The test vehicle can be supplied with diesel fuel from the vehicle's main tank and other liquid fuel mixtures from an installed auxiliary tank, which allows rapid replacement of the test fuel. The entire process is managed by ECU1 (Electronic Control Unit 1). Fuel consumption was then measured using a flow meter which took into account the return overflow from the injectors and high-pressure pump. Fuel was then fed sequentially to the high-pressure pump, the fuel tank and the injectors. In addition, the stand was adapted to supply the engine with hydrogen gas. The hydrogen fuel supply line originates in a hydrogen storage tank, and the flow pressure can then be set via the I-regulator. The pressurized hydrogen then enters the flow meter with the possibility of recording it in real time. Reducer II has the task of stabilizing the hydrogen operating pressure (this is a control parameter). From this point, two options are possible for feeding the engine. The first is to feed the fuel to the main rail, from which the hydrogen is distributed to four injectors. Each one assigned to a specific cylinder. In the second option, fuel is fed directly from the reducer II via two injectors mounted between the turbocharger and the air cooler. The block diagram shows the electrical signal measurement paths through which the hydrogen injection controller (ECU2) receives information from the sensors on the temperature, hydrogen pressure, and temperature of the reducer II and then controls the gas injectors.

The control and measurement track allows the recording of parameters of engine operation under dynamic conditions, measurement of fuel consumption and environmental and energy parameters. The AVL IndiMicro 602 measurement system, together with the AVL IndiCom software, allows the recording of rapidly changing in-cylinder pressures and the analysis of injection parameters. Ecological measurements are made using the MAHA MET 6.3 exhaust-gas analyzer, the measuring probe of which is installed upstream of the catalytic converter. The analyzer measures HC, CO, CO_2, O_2, NO_x, λ, PM and smoke opacity. Other actual engine operating values were recorded using the Multiecuscan OBD II (On Board Diagnostics) diagnostic interface.

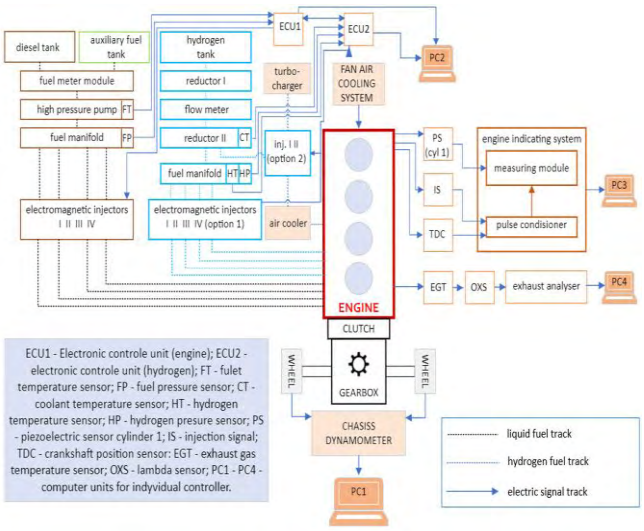

Fig. 2. Block diagram of the test bench

2.2. Course of tests

Tests were carried out with the vehicle running on a chassis dynamometer in fourth gear (closest to direct ratio) at a constant speed of 2600 rpm. The vehicle was subjected to rolling movement resistance. Measurements were carried out for two variants of engine fueling, i.e. diesel and diesel with hydrogen injection into the intake manifold. Hydrogen was injected sequentially according to the ignition sequence 1-3-4-2 (first option shown in Fig. 2) at the opening of the intake valves on successive cylinders. The operating pressures of the hydrogen addition were determined experimentally, based on preliminary tests described in [9], and were set successively at – 0.15 MPa, 0.18 MPa and 0.20 MPa. In addition, the hydrogen injection time was changed for each pressure value; it was 2.5 ms, 3.0 ms and 3.5 ms, respectively.

3. Results

The graphs show the values of the average indicating pressure, maximum combustion pressure, and maximum combustion pressure build-up rate. Also highlighted are the values for the position of the accelerator lever, amount of fuel injected, air flow, hydrogen flow and amount of fuel consumed.

During the combustion of diesel with hydrogen, the recorded values of the average index pressure increased. The observed increase had a linear trend and depended mainly on the set pressure on the operating regulator. The highest values were reached at 0.20 MPa. Hydrogen injection with an injector opening time of 2.5 ms and an injection pressure of 0.20 MPa resulted in a higher average index pressure of 13.7% than diesel combustion. The exact results are included in the table below the graph (Fig. 3). In the case of maximum combustion pressure, higher values were recorded with increasing hydrogen pressure and increasing the opening time of the hydrogen injectors, as shown in Fig. 4. Un-

der the set test conditions, the maximum value of 7.51 MPa achieved gave an 11.2% increase compared to the combustion of diesel alone. Parallels were noted in the case of the maximum combustion pressure rate. At the maximum set hydrogen injection rate, a 20% increase was recorded compared to the combustion of diesel alone (Fig. 5).

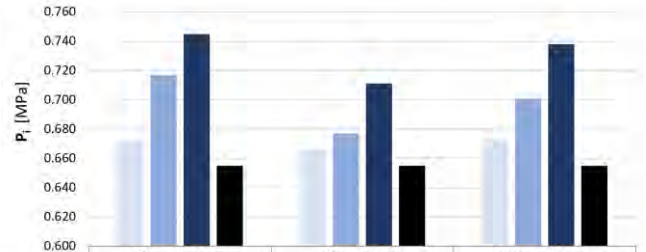

	ON + H 2.5 ms	ON + H 3 ms	ON + H 3.5 ms
0.15 MPa	0.672	0.666	0.673
0.18 MPa	0.717	0.677	0.701
0.20 MPa	0.745	0.711	0.738
ON	0.655	0.655	0.655

Fig. 3. Indicative mean effective pressure – diesel-hydrogen co-combustion for selected hydrogen pressures and hydrogen injector opening times

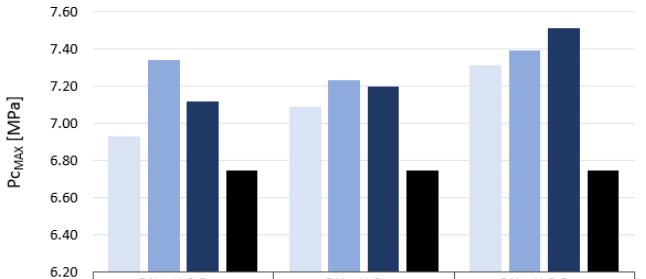

	ON + H 2.5 ms	ON + H 3 ms	ON + H 3.5 ms
0.15 MPa	6.93	7.09	7.31
0.18 MPa	7.34	7.23	7.39
0.20 Mpa	7.12	7.20	7.51
ON	6.75	6.75	6.75

Fig. 4. Maximum combustion pressure – diesel-hydrogen co-combustion for selected hydrogen pressures and hydrogen injector opening times

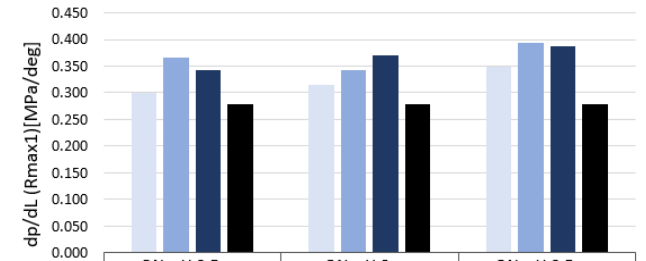

	ON + H 2.5 ms	ON + H 3 ms	ON + H 3.5 ms
0.15 MPa	0.301	0.315	0.349
0.18 MPa	0.365	0.342	0.393
0.20 Mpa	0.343	0.370	0.387
ON	0.279	0.279	0.279

Fig. 5. Maximum build-up rate of combustion pressure – diesel-hydrogen co-combustion for selected hydrogen pressures and hydrogen injector opening times

An analysis was carried out of the recorded values of hydrogen flow when co-combustion it with diesel fuel. By setting the hydrogen injection control map to an opening time of 2.5 ms, the observed increase in hydrogen flow with respect to pressures of 0.15 and 0.18 MPa was up to 1.7 dm^3/min. On the other hand, each time the injector opening time increased by 0.5 ms, the hydrogen flow increased by an average of about 8 dm^3/min (Fig. 6). As the hydrogen flow increased, the average diesel fuel consumption decreased. The largest reduction in diesel fuel consumption was recorded at the hydrogen injector opening setting of 3.5 ms and a pressure of 0.18 MPa and was 3.31 dm^3/h. This was compared with a value of 4.22 dm^3/h of average diesel consumption alone. At this static test measurement point, this is 0.91 dm^3/h less diesel consumption (Fig. 7).

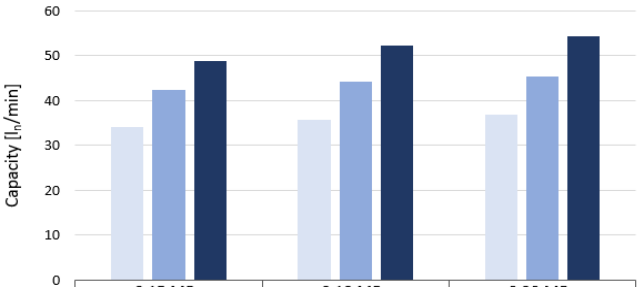

	0.15 MPa	0.18 MPa	0.20 MPa
2.5ms	34	35.7	36.9
3.0ms	42.5	44.3	45.3
3.5ms	48.9	52.2	54.4

Fig. 6. Hydrogen flow – diesel-hydrogen co-combustion for selected hydrogen pressures and hydrogen injector opening times

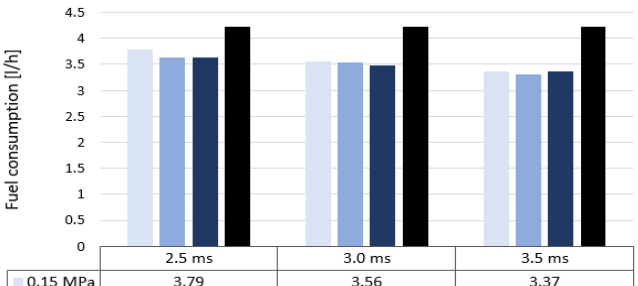

	2.5 ms	3.0 ms	3.5 ms
0.15 MPa	3.79	3.56	3.37
0.18 Mpa	3.63	3.54	3.31
0.20 MPa	3.63	3.48	3.37
ON	4.22	4.22	4.22

Fig. 7. Fuel consumption – diesel/hydrogen co-combustion for selected hydrogen pressures and hydrogen injector opening times

It was observed that the addition of hydrogen had an effect on the set angle of the accelerator lever (Fig. 8), where, when driving in fourth gear at 2600 rpm, the value of the accelerator lever swing decreased as the hydrogen injection pressure increased. At a setting of 3.5 ms and a pressure of 0.20 MPa, the difference with the diesel test was 11%. It was also noted that there was an increase in air mass demand to burn the diesel-hydrogen mixture. During one duty cycle, the test engine required on average 6% more air to burn the fuel mixture (Fig. 9). The average amount of diesel fuel injected during one duty cycle of the combustion engine under test was 13.1 mm^3/stroke. Re-estimating this value in ECU1 (Fig. 2) in parallel with ECU2 (Fig. 2) by adding hydrogen to the combustion process, a decrease of 2 mm^3/w on average was observed, as shown in Fig. 10.

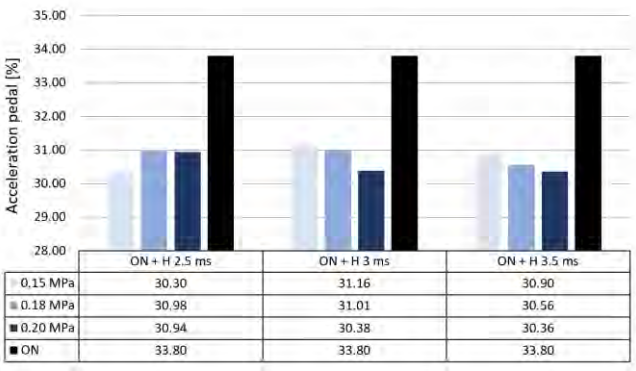

	ON + H 2.5 ms	ON + H 3 ms	ON + H 3.5 ms
0.15 MPa	30.30	31.16	30.90
0.18 MPa	30.98	31.01	30.56
0.20 MPa	30.94	30.38	30.36
ON	33.80	33.80	33.80

Fig. 8. Acceleration pedal position – diesel-hydrogen co-combustion for selected hydrogen pressures and hydrogen injector opening times

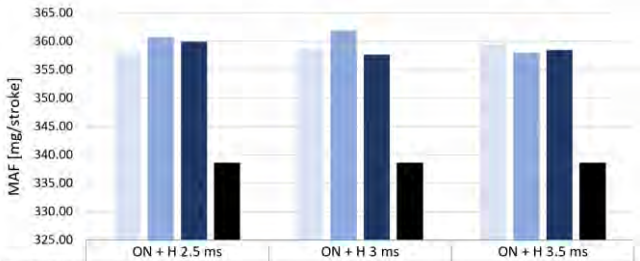

	ON + H 2.5 ms	ON + H 3 ms	ON + H 3.5 ms
0.15 MPa	358.13	358.66	359.51
0.18 MPa	360.73	361.90	358.01
0.20 MPa	359.95	357.69	358.46
ON	338.60	338.60	338.60

Fig. 9. Mass air intake (MAF) for three injector opening times and three hydrogen injection pressures – diesel-hydrogen co-combustion

4. Conclusions

Indicating the engine tested for diesel-hydrogen co-combustion clearly shows that the rapidly varying in-cylinder combustion parameters analyses are improving. The recorded real values indicated that, as the hydrogen injection time and pressure increase, the air requirement for the correct combustion process increases. In addition, it was observed that the ECU1 reacts by decreasing the set amount of diesel fuel injected during a single duty cycle for each additional fuel injection. The control parameters determined were injection time and hydrogen pressure. Their control range was so small that the correction of the amount of diesel injected by ECU1 over their entire range was practically unchanged. Correct adjustment of the amount of diesel to hydrogen is crucial for stabilizing the working processes of the combustion engine under power.

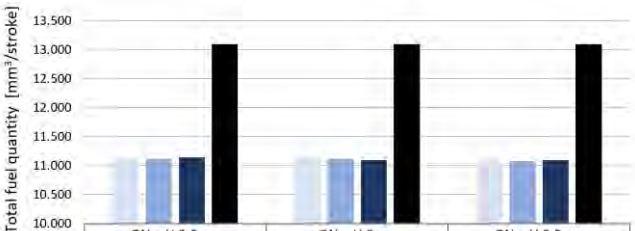

	ON + H 2.5 ms	ON + H 3 ms	ON + H 3.5 ms
0.15 MPa	11.110	11.165	11.126
0.18 MPa	11.119	11.120	11.075
0.20 MPa	11.146	11.100	11.100
ON	13.100	13.100	13.100

Fig. 10. Amount of diesel fuel injected during one cycle of the diesel-hydrogen co-combustion engine for selected hydrogen pressures and hydrogen injector opening times

A study of a diesel engine fueled with hydrogen allowed the control parameters for the addition of renewable fuel to be determined so as to reduce the consumption of fossil fuel, i.e. diesel. When driving the test vehicle in 4th gear at an engine speed of 2600 rpm, the best fast-variable in-cylinder parameters were achieved when the injector was opened for 3.5ms at 0.20 MPa. Adjusted in this way, ECU2 reduced diesel consumption by an average of 21.5%. Analysis of the results indicates that the search for alternative power sources for existing and technologically refined internal combustion engines is in the right direction. Further research will focus on the search for further control parameters that will directly translate into improvements in the energy and environmental values of the engine studied.

Nomenclature

ACEA	European Automobile Manufacturers' Association
CO	carbon monoxide
CO_2	carbon dioxide
ECU	engine control unit
H	hydrogen
HC	hydrocarbons
MAF	mas air flow
NO_x	nitrogen oxides
OBD	on board diagnostics
O_2	oxygen
PM	solid particles
λ	excess air factor

Bibliography

[1] Bruyninckx H. Health in focus: moving towards zero emissions means healthier lives in Europe. Bulletin EEA, 2022. https://www.eea.europa.eu/en/newsroom/editorial/health-in-focus-moving-towards-zero-pollution-means-healthier-lives-in-europe

[2] Ceraat A, Pana C, Negurescu N, Nutu C, Mirica I, Fuiorescu D. Effect of hydrogen use on diesel engine performance. IOP Conf Ser Mater Sci Eng. 2016;161:012075. https://doi.org/10.1088/1757-899X/161/1/012075

[3] Chojnowski J, Karczewski M. Analysis of the market structure of long-distance transport vehicles in the context of retrofitting diesel engines with modern dual-fuel systems. Combustion Engines. 2022;188(1):13-17. https://doi.org/10.19206/CE-142167

[4] Das S, Kanth S, Das B, Debbarma S. Experimental evaluation of hydrogen enrichment in a dual-fueled CRDI diesel engine. Int J Hydrogen Energ. 2022;47(20):11039-11051. https://doi:10.1016/j.ijhydene.2022.01.125

[5] Juknelevičius R, Rimkus A, Pukalskas S, Matijošius J. Research of performance and emission indicators of the compression-ignition engine powered by hydrogen – Diesel

mixtures. Int J Hydrogen Energ. 2019;44(20):10129-10138. https://doi.org/10.1016/j.ijhydene.2018.11.185
[6] Koten H. Hydrogen effects on the diesel engine performance and emissions. Int J Hydrogen Energ. 2018;43(22):10511-10519. https://doi:10.1016/j.ijhydene.2018.04.146
[7] Köse H, Ciniviz M. An experimental investigation of effect on diesel engine performance and exhaust emissions of addition at dual fuel mode of hydrogen. Fuel Process Technol. 2013;114:26-34. https://doi:10.1016/j.fuproc.2013.03.023
[8] Kumar CB, Lata DB. Effect of di-tert butyl peroxide (DTBP) on combustion parameters and NO_x in dual fuel diesel engine with hydrogen as a secondary fuel. Int J Hydrogen Energ. 2021;46(5):4507-4525. https://doi.org/10.1016/j.ijhydene.2020.10.235
[9] Longwic R, Borawska GW, Tatarynow D, Sander P, Gita A. Analysis of the combustion process of a diesel engine fuelled by diesel and hydrogen. Laribi MA, Carbone G, Jiang Z. (eds). Advances in Automation, Mechanical and Design Engineering. SAMDE 2021. Mechanisms and Machine Science. 2021;121. Springer, Cham. https://doi.org/10.1007/978-3-031-09909-0_9
[10] Longwic R, Woźniak G, Sander P. Compression-ignition engine fuelled with diesel and hydrogen engine acceleration process. Combustion Engines. 2020;180(1):47-51. https://doi.org/10.19206/CE-2020-108
[11] Mickevicius T, Labeckas G, Slavinskas S. Experimental investigation of biodiesel-n-butanol fuels blends on performance and emissions in a diesel engine. Combustion Engines. 2022;188(1):90-95. https://doi.org/10.19206/CE-142030
[12] Report ACEA. New car registrations by fuel type. European Union. 06.2022.
[13] Report ACEA. Vehicles in use, Europe 2022. 01.2022.
[14] Report „Geopolitics of the Energy Transformation The Hydrogen Factor" IRENA, Geopolitics of the Energy Transformation: The Hydrogen Factor, International Renewable Energy Agency. Abu Dhabi 2022.
[15] Sandalci T, Karagöz Y. Experimental investigation of the combustion characteristics, emissions and performance of hydrogen port fuel injection in a diesel engine. Int J Hydrogen Energ. 2014;39(32):18480-18489. https://doi.org/10.1016/j.ijhydene.2014.09.044
[16] Santoso WB, Bakar RA, Nur A. Combustion characteristics of diesel-hydrogen dual fuel engine at low load. Energy Proced. 2013;32:3-10. https://doi.org/10.1016/J.EGYPRO.2013.05.002
[17] Siadkowska K, Barański G, Sochaczewski R, Wendeker M. Experimental investigation on indicated pressure and heat release for direct hydrogen injection in a dual fuel diesel engine. Adv Sci Tech. 2022;16(3):54-66. https://doi.org/10.12913/22998624/149300
[18] Stelmasiak, Z., Larisch, J., Pietras, D., Issues related to naturally aspirated and supercharged CI engines fueled with diesel oil and CNG gas. Combustion Engines. 2017;169(2): 24-31. https://doi.org/10.19206/CE-2017-205
[19] Zhou JH, Cheung CS, Leung CW. Combustion, performance, regulated and unregulated emissions of a diesel engine with hydrogen addition. Appl Energ. 2014;126:1-12. https://doi.org/10.1016/j.apenergY.2014.03.089

Rafał Longwic, DSc., DEng. – Faculty of Mechanical Engineering, Lublin University of Technology, Poland.
e-mail: *r.longwic@pollub.pl*

Dawid Tatarynow, MEng. – Faculty of Mechanical Engineering, Lublin University of Technology, Poland.
e-mail: *d.tatarynow@pollub.pl*

Michał Kuszneruk, MEng. – Faculty of Mechanical Engineering, Lublin University of Technology, Poland.
e-mail: *m.kuszneruk@pollub.pl*

Gracjana Woźniak-Borawska, MEng. – Faculty of Mechanical Engineering, Lublin University of Technology, Poland.
e-mail: *g.wozniak@pollub.pl*

Article citation info:
Zacharewicz M, Socik P, Wirkowski P, Zadrąg R, Bogdanowicz A. Evaluation of the impact of supplying a marine diesel engine with a mixture of diesel oil and n-butanol on its efficiency and emission of toxic compounds. Combustion Engines. 2023;195(4):40-47. https://doi.org/10.19206/CE-169484

Marcin ZACHAREWICZ
Paweł SOCIK
Paweł WIRKOWSKI
Ryszard ZADRĄG
Artur BOGDANOWICZ

Combustion Engines
Polish Scientific Society of Combustion Engines

Evaluation of the impact of supplying a marine diesel engine with a mixture of diesel oil and n-butanol on its efficiency and emission of toxic compounds

ARTICLE INFO

Received: 30 May 2023
Revised: 7 July 2023
Accepted: 11 July 2023
Available online: 8 August 2023

The article presents the results of research on the impact of feeding marine reciprocating internal combustion engines with blends of diesel fuel and n-butanol on their performance parameters. The study includes a research plan and empirical results, in which the engine efficiency and emissions of harmful compounds in the exhaust gases were determined. A promising aspect is also the decrease in the concentration of NO_x, which has a positive impact on reducing the toxicity of exhaust gases. An important aspect of the passive defence of a vessel is the reduction of exhaust gas temperature under nominal loads.

Key words: *marine diesel combustion engine, engine efficiency, n-butanol, Box-Behnken plan, NO_x*

1. Introduction

Fuel can be simply defined as a substance (solid, gas, liquid) that releases a large amount of heat energy during the combustion process [16]. This energy can be utilized for heating purposes or technological applications. One of the main applications of fuels is in internal combustion engines, where they convert chemical energy into mechanical energy.

One of the major users of fuels is maritime transport. It is estimated that maritime transport accounts for 3.5–4% of greenhouse gas emissions, primarily carbon dioxide. In terms of total global air pollution emissions, shipping "produces" 18–30% of nitrogen oxides and 9% of sulphur oxides. In the context of European transportation, maritime and inland waterway shipping account for 13.5% of greenhouse gas emissions (including approximately 18% of total CO_2 emissions and around 24% of total NO_x emissions – data referring to global maritime transport in 2018) – according to the report by the European Environment Agency and the European Maritime Safety Agency [4, 15]. In April 2018, the IMO (International Maritime Organization) established a strategy to reduce total greenhouse gas emissions from shipping by at least 50% compared to 2008 [5].

Due to the unstable geopolitical situation (including the armed conflict in Ukraine) and the global trend towards minimizing (eliminating) toxic compounds in exhaust gases, alternative solutions to fossil fuels are being sought. Alternative solutions include harnessing energy from wind, solar power, geothermal sources, nuclear reactions, fuel cells, and alternative fuels.

One of the most forward-thinking ways to reduce pollution and improve engine efficiency is to use alternative fuels. Over the years, extensive research has been conducted on alternative fuels such as alcohols, methyl tert-butyl ether (MTBE), and n-butanol [1, 8].

Alcohol-based fuels, which can be combined with conventional fuels, have the potential as alternative transportation fuels. Previous interest has focused on the use of simple alcohol-gasoline blends in internal combustion engines. Alcohols have a higher octane rating, making them suitable for spark-ignition engines. The combustion properties of alcohols in spark-ignition engines are better than gasoline. However, due to the different physical and chemical properties of alcohols compared to gasoline and diesel fuels, their use may require modifications to engines and fuel systems. On the other hand, blends of up to about twenty percent usually do not require any changes [1, 14, 17].

The idea of using n-butanol and its isomers to create fuel blends is not new, but it has not been sufficiently explored in the case of powering marine reciprocating internal combustion engines.

Iso-butanol has been used as a surfactant to increase the stability of methanol/gasoline and ethanol/gasoline blends [10, 18]. In the past, it was used in a 1:2 ratio with methanol as a co-solvent to eliminate phase separation issues that occur when mixing methanol with gasoline [8]. Bata and his team found that when testing an engine with a 20% iso-butanol blend, there was only a 2.5% reduction in thermal efficiency. They was also a 6.5% increase in specific fuel consumption compared to gasoline under the same experimental conditions. They showed that butanol is superior to methanol and ethanol in terms of thermal efficiency and lower specific fuel consumption. They also found that iso-butanol has a higher stoichiometric air-to-fuel ratio than lighter alcohols, which allows for higher proportions of iso-butanol in blends as an additive without requiring significant engine modifications [1, 17].

The primary economic advantage of butanol is the fact that it is a renewable fuel. An additional benefit is its physicochemical properties, including its ability to blend with hydrocarbon fuels. Research studies on fuel blends with n-butanol have been conducted in various research fields [6].

Labeckas et al. [9] studied the effects of n-butanol-oil fuel blends on engine performance and exhaust emissions. They compared engine performance using a traditional diesel fuel and mixtures with n-butanol. This allowed them, based on the interpretation of various quantities such as

ignition delay angle, torque, and emissions of NO_x and CO, to determine potential trends in the utilization of the tested fuel blends [6, 9].

Pielecha et al. [13] applied a non-conventional system for creating gasoline blends with ethanol, n-butanol, or n-heptane using dual direct injection. The interpretation of combustion process indicators led to the conclusion that the fuel blend with n-butanol was the most efficient and resulted in a 6.1% increase in efficiency compared to pure gasoline combustion [6].

Elfasakhany and Mahrous [2] investigated the impact of two-component blends (fuel with n-butanol) and three-component blends (fuel, n-butanol, methanol) at various concentrations on the efficiency and exhaust emissions of spark-ignition engines. The key finding of the research was the unfavourable effect of using the three-component blend compared to the two-component blend (both with low alcohol content) on engine efficiency and the emission of toxic compounds. However, for three-component blends with higher alcohol content (> 10%), the engine efficiency and emission of toxic compounds were found to be more favourable compared to the two-component blend (n-butanol > 10%).

Otaka et al. [12] conducted a research study using a blend of biobutanol with marine fuel on a single-cylinder compression ignition engine. The results of the study showed an extended ignition delay for the used blend and an increase in hydrocarbon and CO emissions, primarily in the low engine load range.

Wang et al. [20] investigated the impact of alternative fuel blends used in two-stroke slow-speed marine diesel engines on their performance. They discovered that by introducing a certain amount of n-butanol into the fuel, it is possible to reduce NO_x emissions, and increasing the concentration of n-butanol leads to a decrease in CO_2 emissions.

Kniaziewicz et al. [10] conducted research on a marine internal combustion engine fuelled with a blend of F–75 marine fuel and n-butanol. They demonstrated that n-butanol improves combustion conditions and has a beneficial impact on the emission of toxic compounds. The empirical research was supported by a mathematical model analysed using artificial neural networks.

The results of Zhang et al. [22] demonstrated that blends of diesel fuel and methanol and n-butanol had a key effect on fuel dispersion and combustion. Fuel containing methanol and n-butanol had a longer ignition delay, higher maximum heat and higher in-cylinder pressure release rate compared to diesel fuel. The authors concluded that the optimal fuel mixture ratio was 70% diesel + 20% methanol + 10% n-butanol. According to the above, the mixture of diesel fuel with methanol and n-butanol allows to improve the combustion and emission parameters of the engine.

Tipanluisa et al. [19] conducted a study on the application of a single-zone combustion model along with Wiebe triple functions to analyze the effects of blends of diesel and n-butanol as drop-in fuel in a four-cylinder heavy-duty diesel engine (HDDE). Blends of 5%, 10% and 20% n-butanol were used at varying speed and load conditions. All n-butanol blends reduced CO and particulate emissions, regardless of operating conditions, while NO_x emissions increased primarily at full load.

The article continues the work of previous researchers to find the optimal blend of marine fuel with n-butanol and its application in marine reciprocating internal combustion engines. The authors decided to conduct empirical and modeling research on a single-cylinder research engine to analyse the obtained efficiency and emission levels of toxic compounds for marine fuel and its blend with n-butanol.

During laboratory tests, a single-cylinder engine test rig was used, which was driven by a planetary gearbox and equipped with an electric dynamometer brake. The engine, gearbox, and brake were equipped with the necessary measurement equipment for analysing torque, crankshaft speed, fuel and oil temperature, gravimetric fuel consumption measurement, exhaust gas analysis, and cylinder pressure indication.

2. Research plan and research object

2.1. Research plan

Following the methodology of conducting research, a research plan was developed that included the research object, the measurement apparatus used, and the measured parameters of the research object, i.e., in the case of the examined engine, the crankshaft rotational speed, engine load by torque, fuel consumption, and indicated pressure, the content of toxic compounds in exhaust gases and their temperature.

Design of experiments (DoE) is often used to create empirical models. It reduces the number of necessary measurements, which translates into reduced consumption of the tested object, and ultimately – cost reduction. It systematically and structurally explains cause-and-effect relationships in the processes being studied, which allows this method to be the most effective in solving problems. A properly selected research plan allows for obtaining precise and validated results, i.e., mathematical relationships describing selected process variables [3, 21].

One of the strategies used in experimental design is the response surface methodology (RSM). The Box-Behnken design, chosen by the authors of the article, is based on this method. It is used for modeling and analysing phenomena in which multiple variables interact with the output variable [3]. The chosen experimental design is suitable for the assumption that the engine is a non-linear object due to the emission of exhaust gases. A non-linear object is best described by a non-linear equation with at least three input values [6].

One of the stages of experimental planning is determining a set of characteristic quantities for the object under study (Fig. 1), which was selected by introducing the following simplifications:

1. Constant values, due to their invariable effect on output values, are not taken into account
2. The disturbing factors are omitted due to conducting tests under identical external conditions
3. The set of input variables was defined as follows:
   - crankshaft rotational speed n = 800–1200 rpm
   - concentration of n-butanol as a percentage by weight C_b = 0–35%
   - rated brake power (input power to the engine measured at the output shaft) N_z = 0–6 kW.

4. The output quantities are limited to the quantities:
   - mean induced torque T_i [Nm]
   - average fuel consumption b_s [g/s]
   - fuel rail setting [%]
   - ignition angle α_{ign} [°OWK]
   - maximum indicated pressure angle α_{pmax} [°OWK]
   - exhaust gas temperature $t_{exh.}$ [°C]
   - nitrogen oxides concentration in the exhaust gas NO_x [ppm]
   - nitrogen oxide concentration in the exhaust gas NO [ppm]
   - nitrogen dioxide concentration in the exhaust gas NO_2 [ppm]
   - carbon monoxide concentration in the exhaust gas CO [ppm]
   - carbon dioxide concentration in the exhaust gas CO_2 [%].

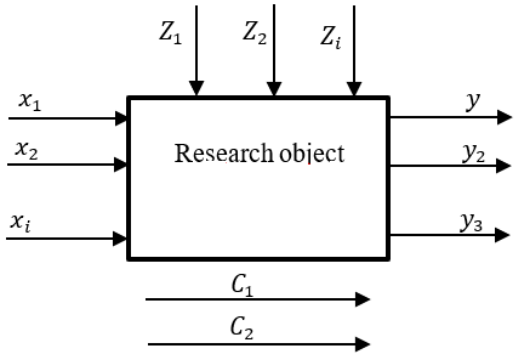

Fig. 1. Research object – structure. x-input quantities, y – output quantities, Z – disturbing quantities, C – constant values

Input parameters (k in number) within the specified ranges during the experiments took on three levels of variability, allowing for the construction of a mathematical model of the studied process in the form of a second-order polynomial [7]:

$$y = b_0 + \sum b_k x_k + \sum b_{kk} x_k^2 + \sum b_{kj} x_k x_j \qquad (1)$$

where: y – dependent output factor, x – j-th independent input factor, b – regression function coefficient.

To determine the efficiency of the studied system for the applied mixtures, the calorific value of the mixture was determined for each mass percentage concentration of n-butanol using the KL-11 calorimeter (Fig. 2).

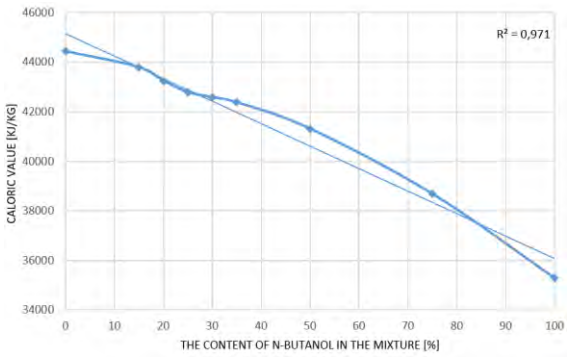

Fig. 2. The calorific value of marine fuel mixture with n-butanol

By analyzing the course of the calorific value curve, the most favorable concentrations of n-butanol in the mixture were chosen, i.e. 15% and 35%. The area between 15% and 35% has a fault, which can affect efficiency as well as of toxic compounds.

The experiment was carried out according to the appropriate set of input parameter values for the selected experimental plan (Table 1).

Table 1. The experimental plan

The Box-Behnken Plan 3**(3–1)						
TEST	A	B	C	crankshaft rotational speed [rpm]	concentration of n-butanol [%]	rated brake power [kW]
1	–1	–1	–1	800.0	0.0	0.0
2	–1	0	1	800.0	15.0	6.0
3	–1	1	0	800.0	35.0	3.0
4	0	–1	1	1000.0	0.0	6.0
5	0	0	0	1000.0	15.0	3.0
6	0	1	–1	1000.0	35.0	0.0
7	1	–1	0	1200.0	0.0	3.0
8	1	0	–1	1200.0	15.0	0.0
9	1	1	1	1200.0	35.0	6.0

The Box-Behnken plan was used because it is very economical and therefore particularly useful when taking measurements is expensive and their number should be limited to the really necessary. The researcher were able to perform as few as nine tests, which made it possible to satisfactorily analyze the results obtained. In this plan:

- A is crankshaft rotational speed
- B is concentration of n-butanol
- C is rated brake power.

Number –1, 0 and 1 means lowest, middle and highest value of parameters A, B and C.

2.2. Research object

Empirical and model studies were carried out for the same engine operating parameters (requested power, fuel mixture and crankshaft speed).

The research object was a laboratory single-cylinder engine installed on a stand at the Institute of Naval Architecture and Marine Engineering of the Polish Naval Academy. The basic data of the engine are grouped in Table 2, while the laboratory setup is shown in Fig. 3. The control panel of the single-cylinder engine setup is presented in Fig. 4.

Table 2. Technical data of the engine used in the tests

Cylinder arrangement and quantity	single-cylinder, vertical
Piston stroke	160 mm
Cylinder bore	135 mm
Cylinder displacement	2290 cm^3
Compression ratio	16:1
Specific fuel consumption	215 g/kWh
Rated torque at rated power	127 Nm
Injection pressure	17.17 MPa
Rated power	20 kW at 1500 rpm

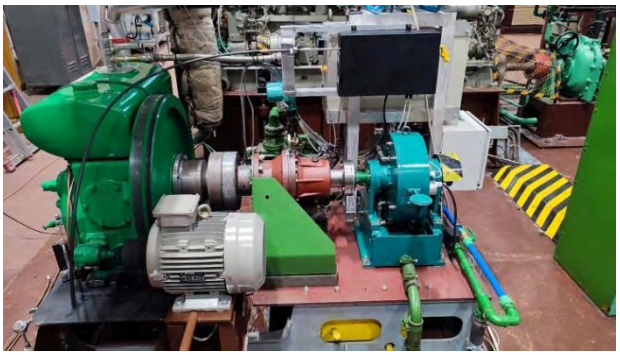

Fig. 3. Laboratory engine stand

Fig. 4. Single-cylinder engine stand control panel

3. Results

3.1. The significance of input parameter influence

Following the established research plan, all listed engine operating parameters were measured and recorded for specified rotational speeds, n-butanol concentrations, and loads (brake power).

After the tests, the obtained output values were analysed using STATISTICA software. A modified quadratic model was selected for fitting, containing only statistically significant elements. The significance of the effect of each input parameter and its interaction was determined by analysis of variance (ANOVA). The next step was to determine the level of fit of the obtained models to the measured values for a specific experimental design, which was defined based on the coefficients of determination R^2 and the standard deviation of the residual component s [3, 7, 11].

The approximated polynomials (1) allowed for determining the relationships between individual variables, including the calculation and evaluation of the influence of n-butanol concentration in the fuel mixture on engine performance indicators (correlation determination). It can be assumed that this method allows for optimizing the selection of n-butanol concentration in the fuel mixture to achieve better engine performance and reduce exhaust toxicity, as indicated by Pareto charts [9, 20].

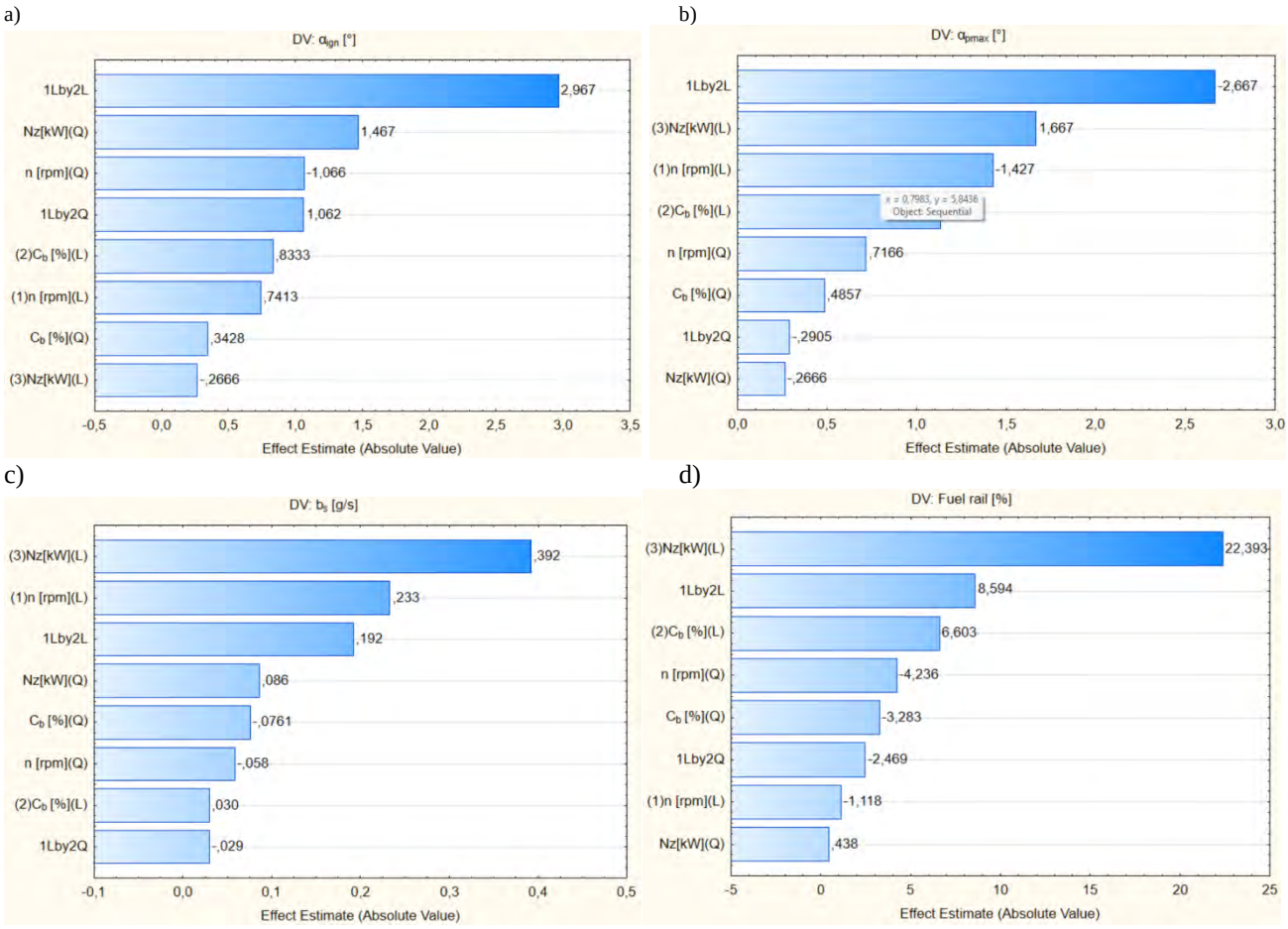

Fig. 5. Pareto charts of concentration of a) ignition angle, b) maximum indicate pressure angle, c) average fuel consumption, d) fuel rail

Pareto analysis (charts) is a technique that helps to visually present and rank individual independent variables affecting the output variable [18].

Figure 5 shows the influence of individual independent factors and their interactions on engine performance indicators (including those related to combustion quality). The input variables are represented on the vertical axis of the graph. Number 1 is crankshaft rotational speed, 2 – concentration of n-butanol in the blend fuel, 3 – rated brake power. The notation "L" indicates that the coefficient value is assigned to the linear term of the polynomial, "Q" – to the quadratic term, and "by" – in relation to a reference value. The main influence is seen from the linear relationship of rotational speed n to n-butanol concentration C_b.

Figure 6 shows the influence of individual independent factors and their interactions on the content of toxic compounds in engine exhaust. The obtained main results and interactions demonstrate the existing relationship between the concentration of n-butanol in the fuel and the concentration of toxic compounds in the engine exhaust.

3.2. Evaluation of the influence of n-butanol concentration on engine performance indicators

Based on the obtained data, surface plots were created and changes in the investigated parameters were presented as functions of n-butanol concentration in the fuel and rotational speed for the specified brake power $N_z = 3$ kW. Due to the repeatability of the function course for $N_z \in \langle 0,6 \rangle$ kW surface plots were not presented for $N_z = \{0,6\}$ kW.

a)

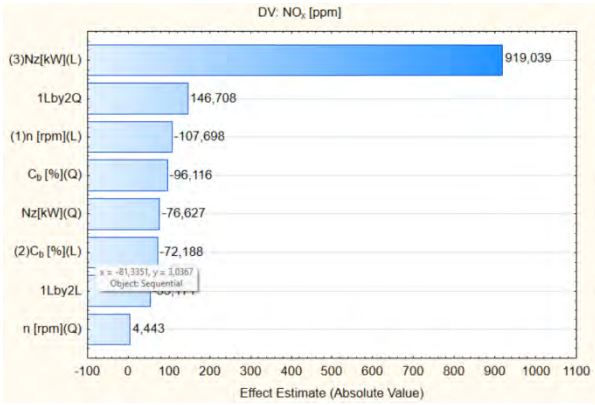

b)

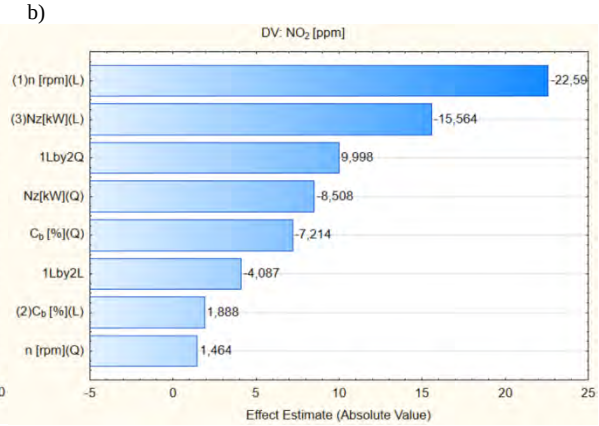

c)

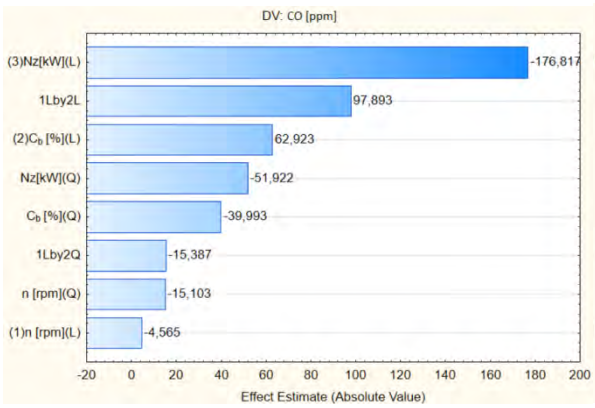

d)

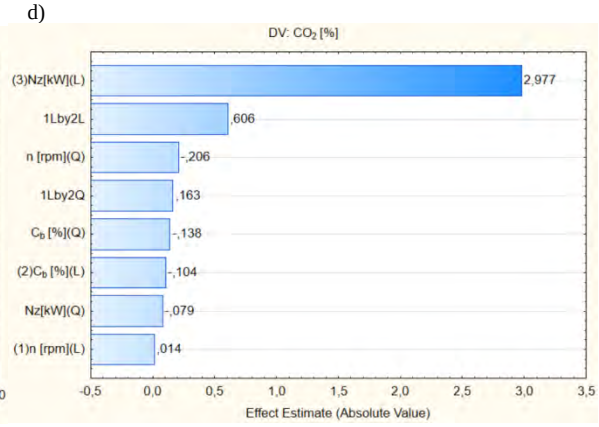

e)

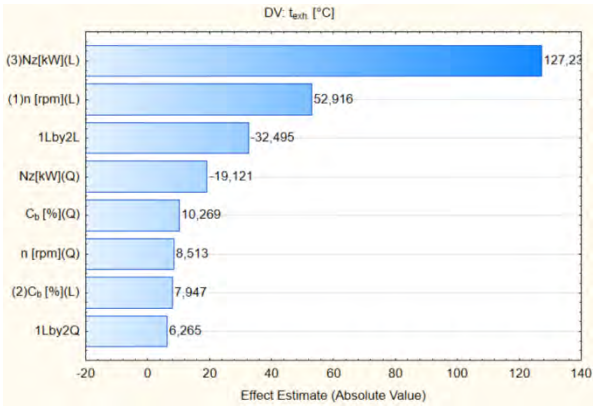

Fig. 6. Pareto charts of concentration of a) nitrogen oxide, b)) nitrogen dioxides, c) carbon monoxide, d) carbon dioxides, e) exhaust temperature

The ignition angle α_{ign} (Fig. 7) for an n-butanol-rich mixture decreases with increasing engine speed. It reaches a minimum in the range of $C_b \in \langle 25,35 \rangle$. Similarly, the maximum indicated pressure angle α_{pmax} (Fig. 8) for the same range of n-butanol concentration C_b decrease.

It follows that regardless of the set load, the ignition angles and maximum indicated pressure angle approached the TDC, which has a positive effect on the combustion process, efficiency (Fig. 9c), and reducing the level of toxic exhaust components (Fig. 10a–d).

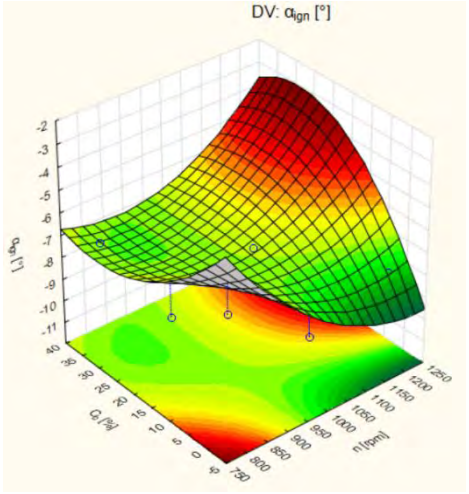

Fig. 7. Dependence of ignition angle on concentration of n-butanol and crankshaft rotational speed

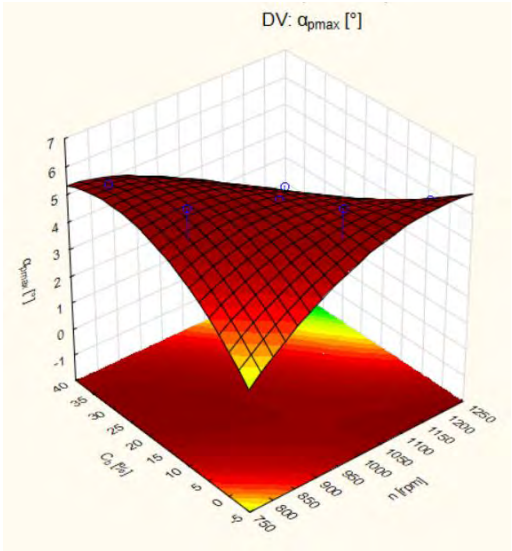

Fig. 8. Dependence of maximum indicate pressure angle on concentration of n-butanol and crankshaft rotational speed

The study showed that in the tested range of load and rotational speed, an increase in n-butanol concentration in the fuel mixture results in an increase in the load index, and thus greater fuel consumption (Fig. 9a–b). This means that the calorific value of the fuel mixture is lower compared to the marine fuel used, which is confirmed by the study of calorific values of the used mixtures (Fig. 2). However, it should be noted that the use of an n-butanol mixture resulted in an increase in engine efficiency (Fig. 9c).

a)

b)

c)

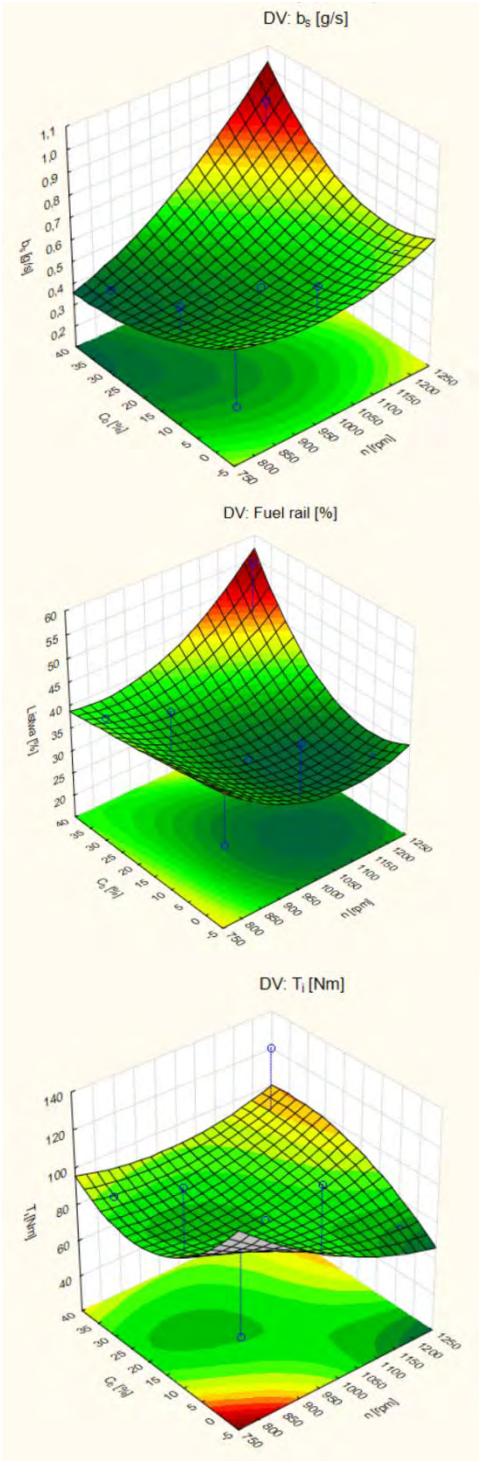

Fig. 9. Dependence of a) average fuel consumption, b) load indicator, c) indicated torque on concentration of n-butanol and crankshaft rotational speed

In the load and speed range studied, it was observed that raising the rotational speed resulted in a decrease in the concentration of both NO and NO_2 (Fig. 10a–b). This effect was particularly noticeable for NO_2. It should be noted that at low rotational speeds, the content of NO_x significantly increases for high C_b concentrations, which is related to the values of the ignition and maximum indicated pressure angles (Fig. 7, 8).

The influence of n-butanol content is visible for CO emissions (a significant increase for upper input limits) and CO_2 – the gradient of the increase takes smaller values (Fig. 10c–d). The increase in CO concentration may be caused by the individual influence of specific carbon, hydrogen, and oxygen atoms in the structure of n-butanol and its mixture with the ship fuel [6].

The analysis of the research results also revealed the influence of the percentage concentration of n-butanol C_b on the oxygen content in the exhaust gases O_2 and on the exhaust gas temperature $t_{spal.}$. The decrease in exhaust gas temperature for $C_b > 15\,\%$ at high rotational speeds is a desirable effect in military applications due to the limitation of thermal fields of tanks, vehicles, ships, and aircrafts.

3. Conclusion

Both empirical and model-based research indicates that it is reasonable to use fuel blends containing n-butanol. N-butanol positively affects the combustion conditions (α_{ign} and α_{pmax} angles approach TDC) and efficiency, which shows Fig. 9c. A promising aspect is also the decrease in the concentration of NO_x, which has a positive impact on reducing the toxicity of exhaust gases. An important aspect of the passive defence of a vessel is the reduction of exhaust gas temperature under nominal loads.

The prospective results encourages to continue and expand the research. The focus will be put on optimizing the selection of n-butanol concentration in the fuel blend, introducing an additional component to the blend to minimize the concentration of toxic compounds in exhaust gases and confirming the use of fuel blends in military applications (minimizing the physical fields of ships, including the thermal field).

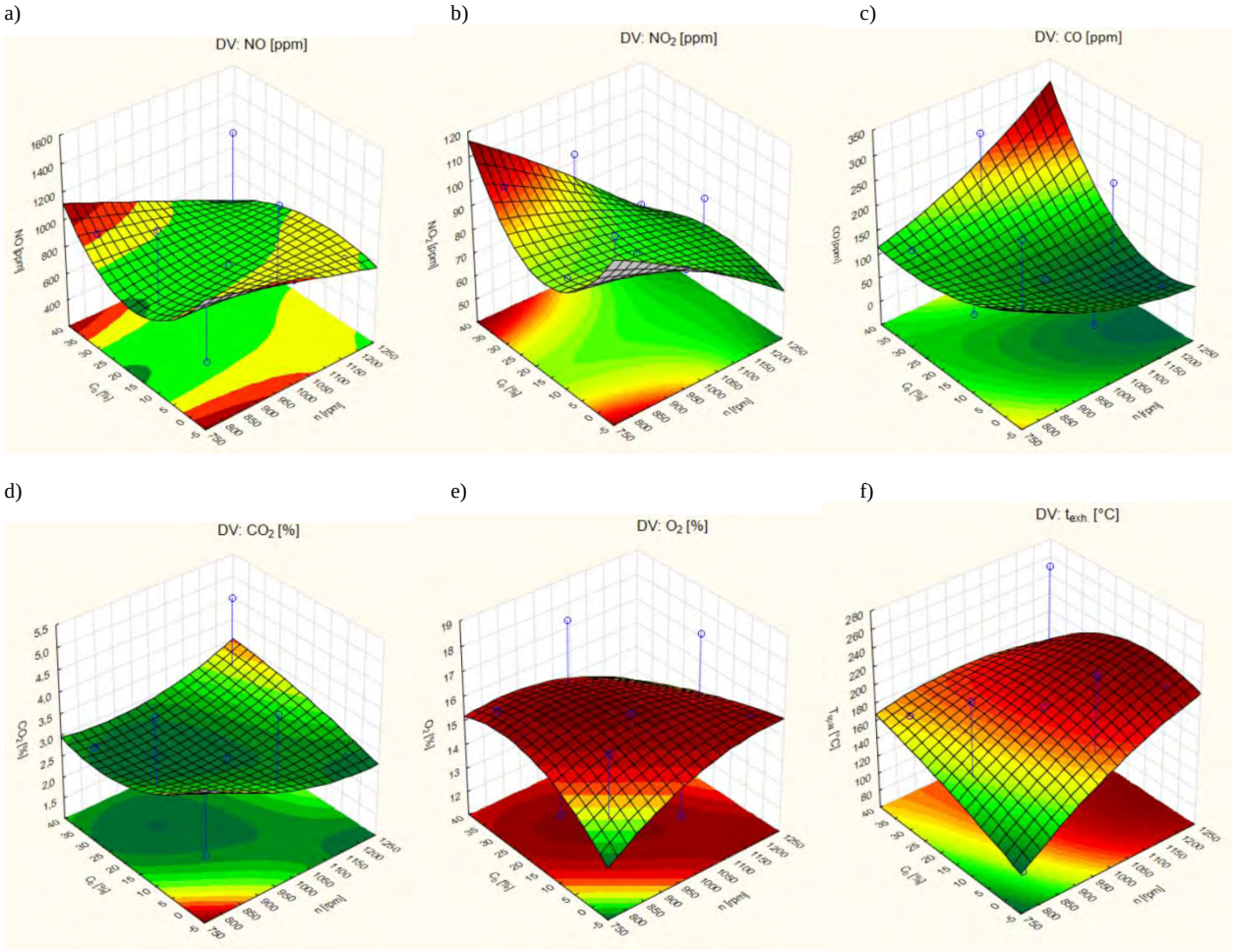

Fig. 10. Dependence of a) nitrogen monoxide, b) nitrogen dioxides, c) carbon monoxide, d) carbon dioxides, e) oxygen, f) exhaust temperature on concentration of n-butanol and crankshaft rotational speed

Nomenclature

ANOVA	analysis of variance
DV	dependent variable
DoE	design of experiments
IMO	International Maritime Organization
MTBE	methyl tert-butyl ether
TDC	top dead centre
RSM	response surface methodology

Bibliography

[1] Bata RM, Elrod AC, Rice RW. Emissions from IC engines fueled with alcohol-gasoline blends: a literature review, engine emissions, J Eng Gas Turbines Power. 1989;111(3):424-431. https://doi.org/10.1115/1.3240271

[2] Elfasakhany A, Mahrous A-F. Performance and emissions assessment of n-butanol–methanol–gasoline blends as a fuel in spark-ignition engines. Alexandria Engineering Journal. 2016;55(3):3015-3024. https://doi.org/10.1016/j.aej.2016.05.016

[3] Habrat W, Żółkoś M, Świder J, Socha E. Forces modeling in a surface peripheral grinding process with the use of various design of experiment (DoE). Mechanik. 2018;91(10):929-931. https://doi.org/10.17814/mechanik.2018.10.165

[4] Hydrogen bulk carrier, battery container ship. https://mlodytechnik.pl/technika/29907-masowiec-na-wodor-kontenerowiec-na-baterie

[5] Initial IMO Strategy on the Reduction of GHG Emissions From Ships. Resolution MEPC.304(72), 2018.

[6] Kniaziewicz T, Zadrąg R, Bogdanowicz A. Environmental characteristics of marine diesel engine fueled by butanol. Renewable Energy. 2022;182:887-899. https://doi.org/10.1016/j.renene.2021.10.068

[7] Korzyński M. Experiment methodology. Planning, implementation and statistical elaboration of the results of technical experiments (in Polish). Wydawnictwo WNT, Warsaw 2017.

[8] Kozak M. Exhaust emissions from a diesel passenger car fuelled with a diesel fuel-butanol blend. SAE Technical Paper 2011-28-0017. 2011. https://doi.org/10.4271/2011-28-0017

[9] Labeckas G, Slavinskas S, Rudnicki J, Zadrąg R. The effect of oxygenated diesel-n-butanol fuel blends on combustion, performance, and exhaust emissions of a turbocharged CRDI diesel engine. Pol Marit Res. 2015;25:108-120. https://doi.org/10.2478/pomr-2018-0013

[10] Lee RC. Effect of compression ratio, mixture strength, spark timing, and coolant temperature upon exhaust emissions and power. SAE Technical Paper 710832. 1971. https://doi.org/10.4271/710832

[11] Online Statistics Handbook. https://www.statsoft.pl/textbook/stathome_stat.html

[12] Otaka T, Kukisaki M, Fushimi K, Kinoshita E, Yoshimoto Y. Combustion characteristics of DI diesel engine fueled with marine diesel oil and 1-butanol blends. J Japan Inst Mar Eng. 2015;50(6):135-141. https://doi.org/10.5988/jime.50.840

[13] Pielecha I, Wierzbicki S, Sidorowicz M, Pietras D. Combustion thermodynamics of ethanol, n-heptane, and n-butanol in a rapid compression machine with a dual direct injection (DDI) supply system. Energies. 2021;14:2729. https://doi.org/10.3390/en14092729

[14] Puzdrowska P. Evaluation of the influence of the opening pressure of a marine diesel engine injector on the results of numerical simulation of the working cycle and their comparison with the results of the laboratory experiment. Combustion Engines. 2023;193(2):9-14. https://doi.org/10.19206/CE-155873

[15] Report: shipping accounted for 13.5 percent of greenhouse gas emissions from transport in the EU. https://www.cire.pl/artykuly/serwis-informacyjny-cire-24/raport-zegluga-odpowiadala-za-135-proc-emisji-gazow-cieplarnianych-z-transportu-w-ue

[16] Rychter W. Dzieje samochodu. WKiŁ, Warszawa 1983.

[17] Sriram SSP, Bata RM. A performance study of iso-butanol-, methanol-, and ethanol-gasoline blends using a single cylinder engine. SAE Technical Paper 932953. 1993. https://doi.org/10.4271/932953

[18] Sriram SSP, Bata RM. A technical assessment of alcohol fuels – alternate fuels Committee of the Engine Manufacturers Association. SAE Technical Paper 820261. 1982, https://doi.org/10.4271/820261

[19] Tipanluisa L, Thakkar K, Fonseca N, Lopez J-M. Investigation of diesel/n-butanol blends as drop-in fuel for heavy-duty diesel engines: Combustion, performance, and emissions. Energ Convers Manage. 2022;255:115334. https://doi.org/10.1016/j.enconman.2022.115334

[20] Wang SY, Yao L, Zhang JD. Homogeneous charge compression ignition combustion and emissions of methyl decanoate and n-butanol in low-speed diesel engine. Tuijin Jishu/Journal Propuls Technol. 2020;11:2558-2565. https://doi.org/10.13675/j.cnki.tjjs.200367

[21] What is a planned experiment and can almost anything be improved with it? https://sigmavalue.blog/planowany-eksperyment-doe/

[22] Zhang Z, Tian J, Xie G, Li J, Xu W, Jiang F et al. Investigation on the combustion and emission characteristics of diesel engine fueled with diesel/methanol/n-butanol blends. Fuel. 2022;314:123088. https://doi.org/10.1016/j.fuel.2021.123088

Marcin Zacharewicz, DSc., DEng. – Faculty of Mechanical and Electrical Engineering, Polish Naval Academy, Poland.
e-mail: *m.zacharewicz@amw.gdynia.pl*

Paweł Socik, MEng. – Faculty of Mechanical and Electrical Engineering, Polish Naval Academy, Poland.
e-mail: *p.socik@amw.gdynia.pl*

Paweł Wirkowski, DEng. – Faculty of Mechanical and Electrical Engineering, Polish Naval Academy, Poland.
e-mail: *p.wirkowski@amw.gdynia.pl*

Ryszard Zadrąg, DSc., DEng. – Faculty of Mechanical and Electrical Engineering, Polish Naval Academy, Poland.
e-mail: r.zadrag@amw.gdynia.pl

Artur Bogdanowicz, DEng. – Faculty of Mechanical and Electrical Engineering, Polish Naval Academy, Poland.
e-mail: *a.bogdanowicz@amw.gdynia.pl*

Article citation info:
Skuza A, Szumska E, Jurecki R. Fuel consumption and CO_2 emission analysis of hybrid and conventional vehicles in urban driving conditions. Combustion Engines. 2023;195(4):48-55. https://doi.org/10.19206/CE-169569

Adriana SKUZA
Emilia SZUMSKA
Rafał JURECKI

Combustion Engines
Polish Scientific Society of Combustion Engines

Fuel consumption and CO_2 emission analysis of hybrid and conventional vehicles in urban driving conditions

ARTICLE INFO

Received: 29 May 2023
Revised: 12 July 2023
Accepted: 13 July 2023
Available online: 10 August 2023

Hybrid vehicles are a good solution for a smooth transition towards electromobility. The aim of this paper is to examine the relationship between route parameters and fuel consumption and emissions of harmful exhaust components of vehicles with a conventional and hybrid drive system. As a result of simulation tests, values for fuel consumption and CO_2 emissions for HEV and ICEV vehicles were obtained in 28 trips in urban conditions. The average fuel consumption achieved by the hybrid was 53% lower than that of a conventional vehicle. When analysing the average value of CO_2 emissions, the hybrid showed a 54% lower value than a conventional vehicle. Using statistical methods, the relationship between the route parameters and the operational parameters of the vehicle was determined. It has been shown that the route parameters strongly correlate with the fuel consumption and CO_2 emissions of a conventional vehicle. In the case of hybrid vehicles, there was a weaker relationship between these parameters.

Key words: *hybrid vehicle, conventional vehicle, emission, fuel consumption, CO_2*

1. Introduction

Hybrid vehicles are competitive with conventional vehicles. They are becoming an increasingly popular choice among drivers due to their lower fuel consumption and lower emissions. The European Automobile Manufacturers' Association (ACEA) has prepared a report on the number of newly registered hybrid vehicles in the European Union. In 2022, the number of registered HEVs (Hybrid Electric Vehicles) amounted to 2,089,653 units, which is 8.6% more than in the previous year. In Poland, the number of newly registered HEVs increased by 5.1% [46].

The dynamic growth of the market of vehicles with alternative drives is observed. The reason is the tightening of exhaust emission standards. Since 1992, the European emission standard has regulated the emission levels of nitrogen oxides (NO_x), hydrocarbons (HC), carbon oxides (CO) and particulate matter (PM) for most vehicles, passenger cars, trucks and buses. Vehicles that do not meet emission requirements cannot be sold in the EU.

The standard in force since 2015 is Euro 6 (referred to as Euro 6b) [10]. It assumes the emission level that cannot be exceeded by motor vehicles sold after 2015 (Table 1). This standard has been amended several times. The change to the Euro 6c standard was related to the introduction of the WLTP (Worldwide Harmonized Light-duty Test Procedure) replacing the outdated NEDC (New European Driving Cycle). The Euro 6d-temp standard was a transitional variant, preparing for the new method of measuring exhaust emissions in the Euro 6d standard. Its introduction was intended to reduce the differences in exhaust emissions between laboratory and road tests.

Table 1. Euro 6 emissions standards

	Emissions, g/km							
Type of vehicle	CO	THC	NMHC	NH_3	NO_x	HC+NO_x	PM	Brake PM_{10}
Diesel	0.50	–	–	–	0.80	0.170	0.0045	–
Petrol	1.0	0.10	0.068	–	0.06	–	0.0045	–

Currently, the introduction of the Euro 7 has been announced [9]. The new emission standard aims to unify the restrictions related to the emission of harmful exhaust components. The proposed emission values of individual exhaust gas components are presented in Table 2. The Euro 7 standard additionally defines the values of pollutants that were not regulated before, e.g. nitrous oxide.

Table 2. Euro 7 emissions standards

	Emissions, g/km							
Type of vehicle	CO	THC	NMHC	NH_3	NO_x	HC+NO_x	PM	Brake PM_{10}
Diesel	0.50	0.10	0.068	0.02	0.060	–	0.0045	0.007
Petrol								

The authors of the paper [33] presented the methodology related to the preparation of vehicles to meet the emission values set out in Euro 7. It was shown that driving conditions have a large impact on emissions and can reduce the efficiency of some filtering devices. The methods of reducing the emission of harmful exhaust components include: modification of exhaust gas treatment devices, optimization of the engine operating temperature, and modifications in the field of vehicle electronic systems.

A number of studies provide examples of implemented construction modifications to passenger car powertrains that have resulted in reduced vehicle emissions. For example, the study [7] investigated the effect of a three-way catalyst on exhaust emissions. So far, unregulated components, e.g. NH_3 or N_2O, and presented in the Euro 7 standard, have also been included. It has been shown that the emission level of these components is related to the temperature of the catalyst. A way to control the emission of these components may be to optimize the temperature of the catalytic converter after starting the engine. In paper [8], the authors decided to create a control model for an electrically heated catalyst. Appropriate adjustment of the exhaust aftertreatment system can reduce the amount of NO_x emit-

ted. The proposed strategy of predictive catalyst control allowed them to reduce their average emissions by 50% and in exceptional situations – even by 70%. This allows it to meet the expected Euro 7 standards.

Another method that will significantly reduce emissions is the cooperation of the internal combustion engine with the electric drive system [24, 45]. This solution is otherwise called a hybrid drive system. The paper [22] presents a model of a passenger car (segment C), in which a 1.6 Euro 6d-temp diesel engine cooperated with an electric drive system. The results of the simulation tests confirmed that both in the standard WLTP and in the RDE (real-life drive cycle) the hybrid achieved lower fuel consumption and CO_2 emissions, up to 50% in urban conditions. The authors of papers [14, 17, 22] indicate that hybridization in diesel vehicles is necessary to achieve the level of CO_2 emissions assumed in the new standards.

Vehicles with a hybrid drive system, unlike electric cars, do not have a limited range. Thanks to the electric drive that supports the internal combustion engine, hybrids achieve lower fuel consumption and lower emissions.

The adoption of hybrid vehicles by customers is the subject of many research studies [1, 18, 26]. According to the authors of the paper [44], the most important factor in the adoption of hybrid vehicles is the sense of control over one's own resources. The study found that the most influential determinant of the intention to buy hybrid cars is the feeling that people have better control over their financial assets. Environmental awareness turned out to be the second most important factor influencing the intention to buy a hybrid car. This finding confirms that people's knowledge of the environmental impact of transport carbon emissions will strengthen their intention to buy a hybrid car. Government incentives can significantly increase the acceptance of hybrid vehicles by potential buyers. The study [21] showed that the impact of the purchase price, operating costs, and environmental impact has an impact on the willingness to purchase HEVs by the surveyed group. About 37% of the 150 surveyed people declare their willingness to buy a vehicle with a hybrid drive in the future.

Hybrid vehicles have become the subject of many scientific studies. Especially often the authors decide to compare the level of operational parameters of HEV and ICEV (Internal Combustion Engine Vehicle). For example, in the paper [31], the authors examined the impact of vehicle load and its power on fuel consumption and emission of harmful exhaust components. A 100 kg increase in vehicle weight has been shown to increase fuel consumption by 0.4 dm^3/100 km for HEV and 0.7 dm^3/100 km for ICEV. The use of a linear regression model made it possible to compare the same vehicle models with different drives. The difference in fuel consumption ranged from 2.7 to 3.25 dm^3/100 km.

The authors [2] studied the emission of a conventional vehicle and two models of hybrid vehicles. The results indicate that Euro 3 hybrid vehicles achieved lower emission values than a Euro 4 conventional vehicle. In [16] it was shown that two different hybrids emit significantly less CO_2 than conventional vehicles. HEVs also reported lower fuel consumption, ranging from 40 to 60%. In a study [28], HEV and ICEV vehicle emissions were compared in real road conditions. In the test runs in urban conditions, the vehicles were equipped with exhaust gas analysers. It has been shown that the CO and NO_x emissions of a hybrid vehicle are several times lower than those of a conventional vehicle. The inverse relation concerned the emission of particulate matter. The HEV vehicle, as a result of intermittent operation of the internal combustion engine, emitted more than two times more PMx. The research results presented in [11, 13, 42] also confirm that hybrids have lower fuel consumption and lower emission levels than conventional vehicles in various driving conditions.

In many papers, comparisons can be found between vehicles with different powertrain variants in terms of emissions or fuel consumption [23, 25]. In paper [27], fuel consumption was compared between an ICEV vehicle and two hybrid vehicles (Toyota Yaris Hybrid and Toyota Prius). The results showed that the higher the vehicle speed, the lower the fuel economy. A comparison of the two HEV versions showed that the Toyota Prius consumes 17% less fuel thanks to a more efficient electrical energy recovery system. In the publication [40], the emissions of a full hybrid and a plug-in hybrid were compared. It has been shown that low temperature increases exhaust emissions. However, there were no differences in the emission of regulated exhaust gas components of both vehicles when using a different fuel mixture. On the other hand, the lower SOC value increased the differences in the case of a PHEV (Plug-in Hybrid Electric Vehicle). The authors [41] analysed the operation of the hybrid drive in terms of energy consumption and braking strategy. It has been shown that energy recovery is approx. 2.3 kWh, which contributes to significant fuel savings. In addition, the use of methods to optimize the operation of the internal combustion engine and the electric machine may contribute to meeting the assumptions of the Euro 7 standard.

A comparison of emission values recorded under real traffic conditions and in relation to standardised driving cycles can be found in various studies. In papers [35, 36], the emission of a vehicle with a hybrid drive that met the Euro 6d standard was examined. The vehicle's emissions complied with the applicable exhaust emission standard. Tests in laboratory conditions showed lower values of CO and NO_x emissions than in real tests. Of the unregulated components, only N_2O met the required level. In [12], a Euro 6 hybrid vehicle was examined in the context of CO_2 emission in the NEDC and WLTP cycles at different levels and engine start temperatures. It was shown that in WLTP, the vehicle's energy consumption increased by 50% and CO_2 emissions by 30%. In addition, the difference between cold and warm start in WLTP is 4%, while for NEDC, it is 10%.

The publication [19] presents comparisons of the emission of harmful exhaust gas components and the HEV and ICEV fuel consumption in the RDE and laboratory cycles. The results showed that HEV has lower fuel consumption in the range of 23–49% compared to ICEV, and its efficiency is the highest in the city. In addition, the analysis also showed that the vehicles emitted less harmful exhaust components than the Euro 6 standard. The start-stop hybrid

generated higher HC or CO values as a result of frequent stops and low exhaust gas temperatures.

Many papers show the level of CO_2 emission in real-world driving conditions. The results of tests carried out in real traffic conditions confirm that driving conditions effect the level of emissions for both HEV and ICEV [3, 6, 43]. The paper [36] compared the carbon dioxide emissions of hybrid and conventional vehicles on different types of roads. It has been shown that the highest CO_2 emission occurs in urban traffic for both vehicle types. The lowest emission value occurs on suburban and highway roads. On all types of roads hybrids emit less CO_2 than conventional vehicles, the difference can be up to 50% [29]. As the results of research presented in [31] show, the use of hybrid vehicles may increase by 3% per 1 km.

As mentioned before, driving conditions are crucial for both conventional and hybrid vehicle efficiency. In [39], the impact of ambient temperature on the emission of vehicles meeting the Euro 6 standard was examined. It was revealed that the emission values of THC, CO, NO_x, SPN and NH_3 were higher at –7ºC than at 23ºC. CO_2 and N_2O emission values were higher at temperatures below 0°C. The results of the study [15] show that the use of a plug-in hybrid vehicle on the motorway generates high emission values, which may even exceed the limit in the Euro 6 standard. The problem of increased emissions is also the cold start of the engine. The implemented route has a large impact on the fuel consumption and emissions of vehicles equipped with an internal combustion engine. The intensity of traffic and the location of road infrastructure elements (i.e. traffic lights, intersections, roundabouts) force frequent acceleration, braking and stopping, and thus affect the smoothness of driving.

The purpose of this paper is to compare the values of fuel consumption and CO_2 emissions of passenger cars equipped with a conventional drive and a hybrid drive. For simulation tests, speed profiles from 28 trips recorded in real conditions were used. The relationship between travel time and average travel speed and the values of fuel consumption and CO_2 emissions were analysed.

2. Methodology

2.1. Logging of vehicle movement parameters under real conditions

First, velocity profiles were recorded for trips in urban conditions. It was assumed that the length of each run was 5 km. The registration was carried out twice a day: at noon and during the afternoon rush hour. The measurements were carried out using the Kistler Data Logger GPS sensor, the measurement vehicle was a Hyundai Kona (Fig. 1). The SOC (State of Charge) value of each trip was the same and amounted to 95%. The following parameters were recorded: time, instantaneous speed, instantaneous acceleration, distance traveled and instantaneous geographic location.

Data from each run was logged in separate files. The data was then verified and edited appropriately so that it could be entered as input into the simulation program. The collected vehicle dynamic parameters from each run were subjected to further statistical analysis.

Fig. 1. Measurement apparatus and test vehicle

2.2. Simulation tests

Simulation tests were carried out in the AVL Cruise program. The collected speed profiles were used as input data, reflecting the parameters of the route and the driving style of the driver. The program adapts models of vehicles with conventional drive (ICEV) and hybrid drive (HEV). Table 3 presents a summary of selected technical parameters of the analysed vehicles.

Table 3. Selected technical parameters of the analysed vehicles

		ICEV	HEV
Vehicle	Mass, kg	1600	1600
	Frontal area, m^2	1.72	1.75
	Drag coefficient	0.33	0.33
Internal combustion engine	Engine displacement, cm^3	1200	1497
	Number of cylinders	4	4
	Max speed, 1/min	6000	4700
	Idle speed, 1/min	850	945
	Maximum torque, Nm	90	–
	Inertia moment, $kg \cdot m^2$	0.1055	0.18
PSM Electric motor	Maximum power, kW	–	50
	Max speed, 1/min	–	6000
NiMH Battery	Battery capacity, kWh	–	1.31
	Initial state of charge, %	–	60
	Nominal voltage, V	–	7.2

As a result of the simulation, CO_2 emissions and vehicle fuel consumption values were obtained for each trip. The results were then subjected to further statistical analysis.

2.3. Data analysis

The aim of the study was to assess the impact of the route on the operational parameters of the vehicle. In the measurements of real traffic conditions, velocity profiles as a function of time were obtained. On their basis, the parameters reflecting the driving conditions were selected. The following were used for further analysis: travel time, average velocity during the trip, and the share of stopping time in the travel time. Two parameters were selected to assess vehicle efficiency: fuel consumption and CO_2 emissions. The impact of route parameters on fuel consumption and CO_2 emissions of hybrid and conventional vehicles was examined using correlation analysis.

3. Results

3.1. Analysis of vehicle movement parameters during trips

During the tests in real driving conditions, 28 trips were made. Each of the trips ran in the city, measuring about 5 km. The velocity profile of one randomly selected trip is shown in Fig. 2. The time of travel, the average velocity in each trip and the percentage of stopping time during each trip were statistically analysed.

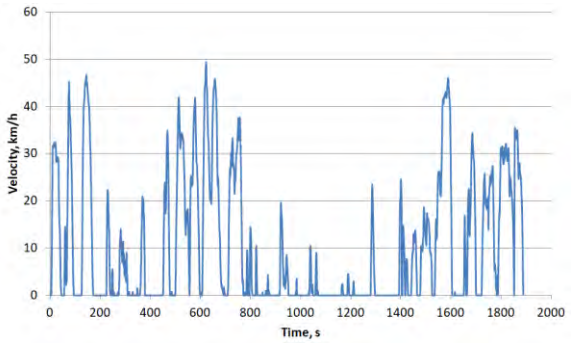

Fig. 2. Recorded velocity profile of a randomly selected trip

Selected statistical parameters of the analysed trips are shown in Table 4. The shortest of the recorded trips was 574 s (about 10 min), while the longest was 1890 s (31.5 min). The mean travel time of the analysed 5 km sections under urban conditions was 962 s (about 16 min). On average, the travel time values deviate from the arithmetic mean by ±346 s (about 6 min).

Table 4. Summary of selected statistical parameters of trips

	Mean	SD	Median	Min	Max
Travel time, s	962	346	881	574	1890
Average velocity, km/h	21.19	6.13	21	10	31.80
Share of stopping time in the travel time, %	25.01	11.97	22.90	7.14	48.54

Another parameter is the average velocity of the trip. This parameter reflects the movement smoothness. The lower the average velocity, the higher the traffic density for the duration of the trip, resulting in a higher share of stopping time. Among the analysed trips, the highest average speed was 31.8 km/h and the lowest was 10 km/h. The mean value of this parameter was 21.19 km/h. The standard deviation (SD) was 6.13 km/h. Figure 3 shows box plots of travel time, average speed, and the share of stopping time in total travel time.

The parameter reflecting the smoothness of the trip is also the share of stops during the drive. On average, the share of stops during the trip was 25%. In one of the analysed trips, the vehicle spent more than half of the duration of the entire run at a standstill due to heavy traffic.

3.2. Analysis of vehicle movement parameters during trips

On the basis of the recorded speed profiles, simulation tests of vehicles with conventional and hybrid drives were carried out. A summary of selected statistical measures of fuel consumption of the analysed vehicles is presented in Table 5. Figure 4 shows box plots of fuel consumption

Table 5. Selected statistical measures of fuel consumption (kg)

Vehicle	Mean	SD	Median	Min	Max
ICEV	0.37	0.11	0.35	0.25	0.67
HEV	0.17	0.04	0.16	0.13	0.24

The lowest vehicle fuel consumption recorded in the runs was 0.25 kg, and the highest was 0.67 kg. The mean value of fuel consumption was 0.37 kg. The fuel consumption values of a vehicle with a conventional drive in the analysed trips are strongly differentiated, as evidenced by the high value of the standard deviation – 0.11 kg.

On selected trips, the difference between the maximum and minimum fuel consumption recorded by the hybrid vehicle was 0.11 kg. The mean fuel consumption of this vehicle in the analysed journeys was 0.17 kg, the SD was 0.04 kg.

Then, the fuel consumption values were analysed in detail for the following stages of motion: idling, acceleration phase, driving at constant speed and deceleration. Table 6 and Table 7 present statistical measures of fuel consumption at the indicated stages of movement by the analysed vehicles. Figure 5 shows box plots of the fuel consumption values of the analysed vehicles

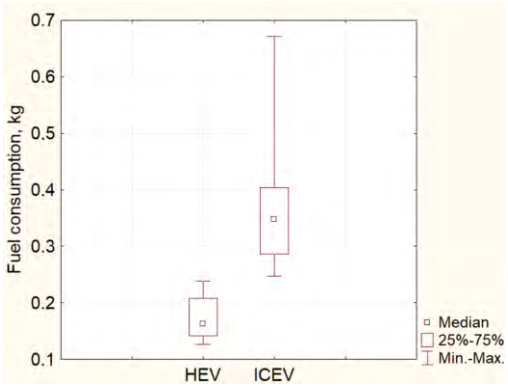

Fig. 4. Box plots of fuel consumption

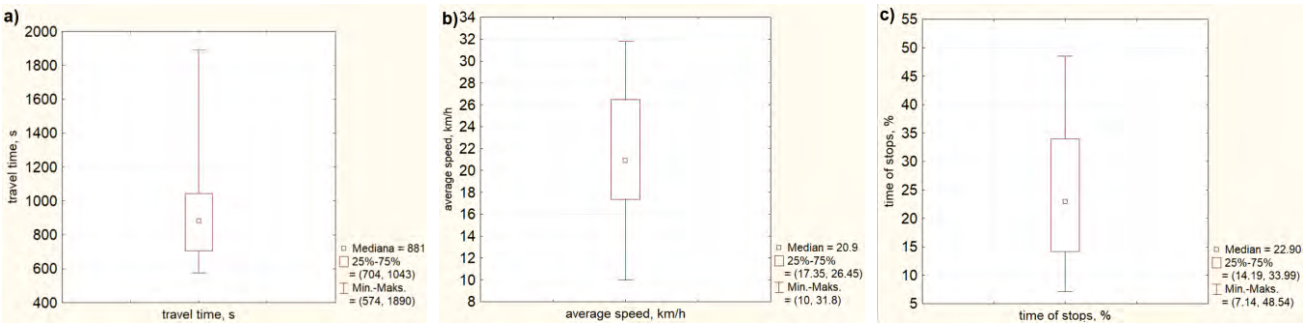

Fig. 3. Box plots of (a) travel time, (b) average speed of the analysed trips, (c) share of stopping time

Table 6. Selected statistical measures of fuel consumption (kg) of the conventional vehicle at various stages of movement

Movement stage	Mean	SD	Median	Min	Max
Idling	0.10	0.08	0.07	0.01	0.31
Acceleration	0.20	0.03	0.19	0.15	0.27
Driving with constant speed	0.03	0.01	0.03	0.02	0.04
Deceleration	0.05	0.01	0.05	0.03	0.09

Table 7. Selected statistical measures of fuel consumption (kg) of the hybrid vehicle at various stages of movement

Movement stage	Mean	SD	Median	Min	Max
Idling	0.00	0.00	0.00	0.00	0.00
Acceleration	0.13	0.02	0.12	0.09	0.17
Driving with constant speed	0.01	0.00	0.01	0.01	0.02
Deceleration	0.03	0.01	0.03	0.02	0.08

Taking into account fuel consumption in particular stages of motion, it can be seen that both for the hybrid and the conventional vehicle, the highest values were noted during acceleration. The lowest fuel consumption was recorded while driving at a constant speed. For a conventionally powered vehicle, high levels of fuel consumption occur when idling. The hybrid vehicle recorded no fuel consumption while idling. The highest fuel consumption occurred during acceleration. The mean fuel consumption for acceleration is 0.13 kg.

Comparing the fuel consumption of both vehicles in each of the movement phases, it can be seen that the conventional vehicle shows higher values in each driving phase. The fuel consumption level recorded by the conventional vehicle was higher than that of the hybrid by 35% during acceleration, 67% during steady speed and 0.4% during braking, respectively.

Table 8 presents a summary of selected statistical measures of CO_2 emissions of the analysed vehicles.

Table 8. Selected statistical measures of CO_2 emission (kg)

Vehicle	Mean	SD	Median	Min	Max
ICEV	1.18	0.34	1.10	0.78	2.12
HEV	0.54	0.11	0.51	0.40	0.75

The difference between the maximum and minimum CO_2 emissions recorded by a conventional vehicle in the analysed trips was 1.34 kg. The average CO_2 emission was 1.18 kg. The CO_2 emission values obtained in the analysed runs are strongly differentiated, which is expressed by the value of the standard deviation. The mean CO_2 emission of the hybrid in the analysed trips amounted to 0.54 kg. The spread of recorded emission values was 0.35 kg. On average, CO_2 emissions deviate from the arithmetic mean by ±0.11 kg. The box plots of CO_2 emissions for both vehicles is shown in Fig. 6.

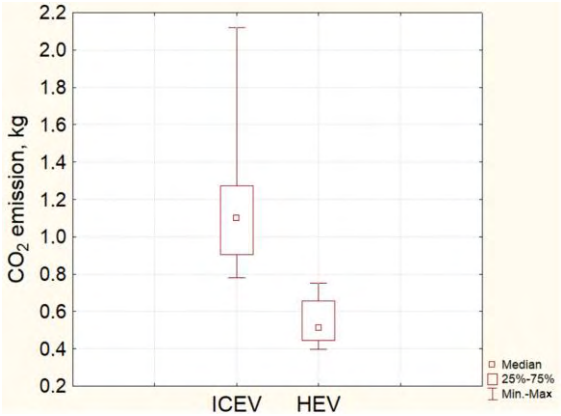

Fig. 6. Box plots of CO_2 emission

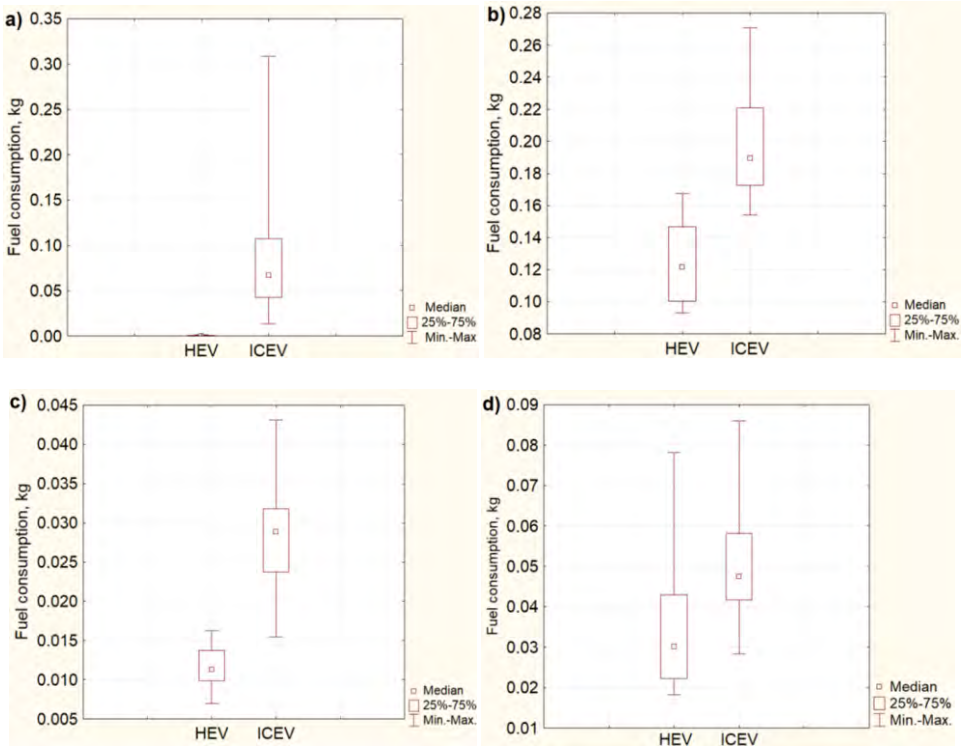

Fig. 5. Box plots of ICEV and HEV fuel consumption in various stages of motion: (a) idling, (b) acceleration, (c) constant speed driving, (d) deceleration

3.3. Evaluation of the impact of route parameters on the fuel consumption and CO_2 emissions of the analysed vehicles

Next, the relationships between the route parameters and the operational parameters of the conventional vehicle were studied. It can be seen that there are strong correlations between fuel consumption and CO_2 emissions and travel time. Similarly, there is a strong correlation between fuel consumption and CO_2 emissions and average speed during the trip (Table 9 and Table 10). A strong correlation was noted for the time share of a stop versus the values of fuel consumption and CO_2 emissions.

Table 9. Correlation coefficients of route parameters and fuel consumption of the analysed vehicles ($p < 0.05$)

	Travel time, s	Average velocity, km/h	Stopping time, %
ICEV	0.94	–0.85	0.73
HEV	0.55	–0.59	0.21

Table 10. Correlation coefficients of route parameters and CO_2 emissions of the analysed vehicles ($p < 0.05$)

	Travel time, s	Average velocity, km/h	Stopping time, %
ICEV	0.94	–0.85	0.73
HEV	0.55	–0.59	0.21

Considering the operational parameters of the hybrid, a moderate relationship was observed between the parameters selected for the route and the level of fuel consumption and CO_2 emissions trip (Table 9 and Table 10). A weak relationship exists between the share of stopping time in the total trip and the values of fuel consumption and CO_2 emissions.

4. Discussion

Based on the results of the simulation tests, it can be concluded that the hybrid has lower fuel consumption and lower CO_2 emissions than a conventional vehicle. The analysed values of nitrogen dioxide emissions and fuel consumption were obtained on the basis of real velocity profiles of 28 trips made in urban conditions. The mean fuel consumption achieved by the hybrid was 53% lower compared to a conventional vehicle. The maximum value noted in by ICEV was 64% higher than that obtained by HEV. The hybrid vehicle also showed the lowest carbon dioxide emissions in selected trips. When analysing the average value of CO_2 emissions, the hybrid showed 54% lower than the conventional vehicle.

The results of simulation tests presented in the paper confirm that the use of a hybrid drive system in vehicles can significantly reduce the level of CO_2 emissions and fuel consumption. The papers cited in the Introduction section confirm that hybrids have lower emissions and lower fuel consumption levels not only in urban conditions, but also in highway and suburban driving conditions.

Based on the results of the correlation analysis, it can be seen that the operating parameters of a conventional vehicle are fully affected by the analysed route. Correlation studies have confirmed a strong relationship between travel time and average travel speed on fuel consumption and CO_2 emissions. Urban driving at different times of the day has different traffic flows, so it affects the vehicle's fuel consumption and, thus its emissions. The longer the travel time, the higher the values of these parameters. Lower traffic density, reducing average driving speed, results in higher fuel consumption and emissions. This is confirmed by the results of tests conducted in real world traffic conditions, which can be found in publications [4, 5, 37].

Operational parameters of hybrid vehicles are less dependent on the performed route. The correlation analyses showed a moderate impact of travel time and average travel speed on fuel consumption and CO_2 emissions. The results of real-world studies presented in papers [20, 30, 34] confirm the effectiveness of hybrid propulsion especially in urban conditions. The internal combustion engine, supported by the electric drive, works in its optimal operating range, so its operation is not significantly affected by the conditions of the route. This results in lower emissions and fuel consumption.

5. Conclusions

The purpose of this study was to examine the values of CO_2 emissions and fuel consumption for vehicles with conventional and hybrid drives. In the first part, speed profiles were collected during 28 trips in urban conditions. The recorded speed profiles were used as input data for the simulation program, reflecting the route profile. As a result of simulation tests, the values of fuel consumption and CO_2 emissions of a hybrid and a conventional vehicle were obtained. Based on the simulation results, it can be concluded that the hybrid vehicle showed the lowest fuel consumption and CO_2 emissions. Then, the impact of the route on the operating parameters of the analyzed vehicles was analyzed.

The results of the correlation study showed that the route has a strong impact on the fuel consumption and CO_2 emissions of a conventional vehicle. Studies have shown a correlation of 0.94 for driving time – 0.85 for average speed and 0.73 for stopping time.

In the case of a hybrid vehicle, these dependencies are much smaller (less than 0.60). A moderate relationship was demonstrated.

Fuel consumption at various stages of vehicle movement was also analyzed. The results showed that a conventional vehicle consumes more fuel at each stage of motion. During acceleration alone, the ICEV recorded an average of 67% higher fuel consumption than the HEV. When idling, no fuel consumption was recorded for the hybrid vehicle.

This paper shows a comparison of fuel consumption and CO_2 emissions of vehicles with conventional and hybrid drive in urban driving conditions. It is evident that hybrid drive vehicles indisputably have lower fuel consumption values, which also translates into economic benefits as well as a reduction of harmful impact on the environment. Hybrid vehicles may therefore compete with conventional vehicles in the future. However, it is necessary to reduce the cost of its purchase.

Nomenclature

ACEA	European Automobile Manufacturers' Association
CO	carbon oxide
CO_2	carbon dioxide
HEV	hybrid electric vehicle
ICEV	internal combustion engine vehicle
NEDC	New European Driving Cycle
NO_x	nitrogen oxide
PM	particulate matter
RDE	Real Driving Emissions
WLTP	Worldwide Harmonized Light-duty Test Procedure

Bibliography

[1] Adnan N, Vasant PM, Rahman I, Noor A. Adoption of plug-in hybrid electric vehicle among Malaysian consumers. Industrial Engineering & Management. 2016;5(2):1000185. https://doi.org/10.4172/2169-0316.1000185

[2] Alessandrini A, Orecchini F, Ortenzi F, Campbell FV. Drive-style emissions testing on the latest two Honda hybrid technologies. Eur Transp Res Rev. 2009;1:57-66. https://doi.org/10.1007/s12544-009-0008-3

[3] Alvarez R, Weilenmann M. Effect of low ambient temperature on fuel consumption and pollutant and CO_2 emissions of hybrid electric vehicles in real-world conditions. Fuel. 2012;97:119-124. https://doi.org/10.1016/j.fuel.2012.01.022

[4] Anttila P, Nummelin T, Väätäinen K, Laitila J, Ala-Ilomäki J, Kilpeläinen A. Effect of vehicle properties and driving environment on fuel consumption and CO_2 emissions of timber trucking based on data from fleet management system. Transport Research Interdisciplinary Perspectives. 2022;15:100671. https://doi.org/10.1016/j.trip.2022.100671

[5] Bartholomeu DB, Filho JVC. Quantification of the environmental impacts of road conditions in Brazil. Ecol Econ. 2009;68(6):1778-1786. https://doi.org/10.1016/j.ecolecon.2008.11.009

[6] Bielaczyc P, Merkisz J, Pielecha J, Woodburn J. A comparison of gaseous emissions from hybrid vehicle and a non-hybrid vehicle under real driving conditions. SAE Technical Paper 2018-01-1272. 2018. https://doi.org/10.4271/2018-01-1272

[7] Brinklow G, Herreros JM, Rezaei SZ, Doustdar O, Tsolakis A, Kolpin A et al. Non-carbon greenhouse gas emissions for hybrid electric vehicles: three-way catalyst nitrous oxide and ammonia trade-off. Int J Environ Sci Technol. 2023. https://doi.org/10.1007/s13762-023-04848-2

[8] Cane S, Brunelli L, Gallian S, Perazzo A, Brusa A, Cavina N. Performance assessment of a predictive pre-heating strategy for hybrid electric vehicle equipped with an electrically heated catalyst. Appl Therm Eng. 2023;219(A):119341. https://doi.org/10.1016/j.applthermaleng.2022.119341

[9] Commission proposes new Euro 7 standards to reduce pollutant emissions from vehicles and improve air quality. European Commission. 10 November 2022. https://ec.europa.eu/commission/presscorner/detail/en/ip_22_6495

10] Commission Regulation (EU) No 459/2012 of 29 May 2012 amending Regulation (EC) No 715/2007 of the European Parliament and of the Council and Commission Regulation (EC) No 692/2008 as regards emissions from light passenger and commercial vehicles (Euro 6) Text with EEA relevance.

[11] Costagliola MA, Prati MV, Mariani A, Unich A, Morrone B. Gaseous and particulate exhaust emissions of hybrid and conventional cars over legislative and real driving cycles. Energy and Power Engineering. 2015;7(5):181-192. https://doi.org/10.4236/epe.2015.75018

[12] Cubito C, Millo F, Boccardo G, Di Pierro G, Ciuffo B, Fontaras G et. al. Impact of different driving cycles and operating conditions on CO_2 emissions and energy management strategies of a Euro-6 hybrid electric vehicle. Energies. 2017;10(10):1590. https://doi.org/10.3390/en10101590

[13] De Robbio R, Cameretti MC, Mancaruso E. Investigation by modeling of a plug-in hybrid electric commercial vehicle with diesel engine on WLTC. Fuel. 2022;317:123519. https://doi.org/10.1016/j.fuel.2022.123519

[14] Eifler G. Are hybrid powertrains the right solution to meet EU-Emission-Targets in 2030. 21. Internationales Stuttgarter Symposium. Proceedings Springer Vieweg, Wiesbaden 2021:181-203. https://doi.org/10.1007/978-3-658-33466-6_13

[15] Feinauer M, Ehrenberger S, Epple F, Schripp T, Grein T. Investigating particulate and nitrogen oxides emissions of a plug-in hybrid electric vehicle for a real-world driving scenario. Appl Sci. 2022;12(3):1404. https://doi.org/10.3390/app12031404

[16] Fontaras G, Pistikopoulos P, Samaras Z. Experimental evaluation of hybrid vehicle fuel economy and pollutant emissions over real-world simulation driving cycles. Atmos Environ. 2008;42(18):4023-4035. https://doi.org/10.1016/j.atmosenv.2008.01.053

[17] Franco V, Zacharopoulou T, Hammer J, Schmidt H, Mock P, Weiss M et al. Evaluation of exhaust emissions from three diesel-hybrid cars and simulation of after-treatment systems for ultralow real world NO_x emissions. Environ Sci Technol. 2016;50(23):13151-13159. https://doi.org/10.1021/acs.est.6b03585

[18] Hamzah MI, Tanwir NS. Do pro-environmental factors lead to purchase intention of hybrid vehicles? The moderating effects of environmental knowledge. J Clean Prod. 2021;279:123643. https://doi.org/10.1016/j.clepro.2020.123643

[19] Huang Y, Surawski NC, Organ B, Zhou JL, Tang OHH, Chan EFC. Fuel consumption and emissions performance under real driving: comparison between hybrid and conventional vehicles. Sci Total Environ. 2019;659:275-282. https://doi.org/10.1016/j.scitotenv.2018.12.349

[20] Ivanov Y, Ivanov R, Kaadikyanov G, Staneva G, Danilov I. A study of the fuel consumption of hybrid Toyota Yaris. Transport Problems. 2019;14(1):155-167. https://doi.org/10.20858/tp.2019.14.1.14

[21] Karunanayake TRK, Wanninayake WMCB. Impact of key purchasing determinats on purchase intention of hybrid vehicle brands in Sri Lanka, an empirical study. Journal of Marketing Management. 2015;3(1):40-52. https://doi.org/10.15640/jmm.v3n1a4

[22] Kulikov I, Kozlov A, Terenchenko A, Karpukhin K. Comparative study of powertrain hybridization for heavy-duty vehicles equipped with diesel and gas engines. Energies. 2020;13:2072. https://doi.org/10.3390/en13082072

[23] Lasocki J, Gis M. The influence of driving pattern on pollutant emission and fuel consumption of hybrid electric vehicle. Combustion Engines. 2019;177(2):145-150. https://doi.org/10.19206/CE-2019-226

[24] Luján JM, Garcia A, Monsalve-Serrano J, Martinez-Boggio S. Effectiveness of hybrid powertrains to reduce the fuel

consumption and NO_x emissions of a Euro 6d-temp diesel engine under real-life driving conditions. Energ Convers Manage. 2019;199,:111987. https://doi.org/10.1016/j.enconman.2019.111987
[25] Melas A, Selleri T, Franzetti J, Ferrarese C, Suarez-Bertoa R, Giechaskiel B. On-road and laboratory emissions from three gasoline plug-in hybrid vehicles-part 2: solid particle number emissions. Energies. 2022;15(14):5266. https://doi.org/10.3390/en15145266
[26] Narayan JJ, Rai K, Naidu S, Greig T. A factor structure for adoption of hybrid vehicles: differing impact on males, females and different age groups. Research in Transportation Bussines & Management. 2022;45:100897. https://doi.org/10.1016/j.rtbm.2022.100897
[27] Orecchini F, Santiangeli A, Zuccari F, Ortenzi F, Genovese A, Spazzafumo G et al. Energy consumption of a last generation full hybrid vehicle compared with conventional vehicle in real drive conditions. Energy Proced. 2018;148:289-296. https://doi.org/10.1016/j.egypro.2018.08.080
[28] Pielecha J, Skobiej K, Kurtyka K. Exhaust emissions and energy consumption analysis of conventional, hybrid and electric vehicles in real driving cycles. Energies. 2020; 13(23):6423. https://doi.org/10.3390/en13236423
[29] Pignatta G, Balazadeh N. Hybrid vehicles as a transition for full e-mobility achievement in positive energy districts: a comparative assessment of real-driving emissions. Energies. 2022;15(8):2760. https://doi.org/10.3390/en15082760
[30] Pitanuwat S, Srripakagorn A. An investigation of fuel economy potential of hybrid vehicles under real-world driving conditions in Bangkok. Energy Proced. 2015;79:1046-1053. https://doi.org/10.1016/j.egypro.2015.11.607
[31] Plötz P, Funke SA, Jochem P. Empirical fuel consumption and CO_2 emissions of plug-in hybrid electric vehicles. J Ind Ecol. 2017;22(4):773-784. https://doi.org/10.1111/jiec.1262
[32] Reynolds C, Kandlikar M. How hybrid-electric vehicles are fiferent from conventional vehicles: the effect of weight and Power on fuel consumption. Environ Res Lett. 2007;2: 014003. https://doi.org/10.1088/1748-9326/2/1/014003
[33] Samras ZC, Kontses A, Dimaratos A, Kontses D, Balazs A, Hausberger S et al. A European regulatory perspective towards a Euro 7 proposal. SAE Technical Paper 2022-37-0032. 2022. https://doi.org/10.4271/2022-37-0032
[34] Šarkan B, Gnap J, Kiktová M. The importance of hybrid vehicles in urban traffic in terms of environmental impact. The Archives of Automotive Engineering – Archiwum Motoryzacji. 2019;85(3):115-122. https://doi.org/10.14669/AM.VOL85.ART8
[35] Selleri T, Melas AD, Franzetti J, Ferrarese C, Giechaskiel B, Suarez-Bertoa R. On-road and laboratory emissions from three gasoline plug-in hybrid vehicles – part 1: regulated and unregulated gaseous pollutants and greenhouse gases. Energies. 2022;15(7):2401. https://doi.org/10.3390/en15072401
[36] Selleri T, Melas A, Farrarese C, Franzetti J, Giechaskiel B, Suarez-Bertoa R. Emissions from a modern Euro 6d diesel plug-in hybrid. Atmosphere. 2022;13(8):1175. https://doi.org/10.3390/atmos13081175
[37] Shahariar HGM, Bodisco TA, Zare A, Sajjad M, Jahirul MI, Van TC et al. Impact of driving style and traffic condition on emissions and fuel consumption during real-world transient operation. Fuel. 2022;319:123874. https://doi.org/10.1016/j.fuel.2022.123874
[38] Skuza A, Jurecki R, Szumska E. Analysis of the operating parameters of electric, hybrid and conventional vehicles on different types of roads. Open Engineering. 2023;13(1): 20220443. https://doi.org/10.1515/eng-2022-0443
[39] Suarez-Bertoa R, Astorga C. Impact of cold temperature on Euro 6 passenger car emissions. Environ Pollut. 2018;234: 318-329. https://doi.org/10.1016/j.envpol.2017.10.096
[40] Suarez-Bertoa R, Astorga C. Unregulated emissions from light-duty hybrid electric vehicles. Atmos Environ. 2016; 136:134-143. https://doi.org/10.1016/j.atmosenv.2016.04.021
[41] Szramowiat M, Szałek A. Analysis of the operation of the hybrid drive system in the light of the proposed Euro 7 standard. Combustion Engines. 2021;187(4):65-68. https://doi.org/10.19206/CE-141263
[42] Szumska E, Jurecki R, Pawełczyk M. Evaluation of the use of hybrid electric powertrain system in urban traffic conditions. Eksploat Niezawodn. 2019;22(1):154-160. https://doi.org/10.17531/ein.2020.1.18
[43] Tansini A, Pavlovic J, Fontaras G. Quantyfying the real-world CO_2 emissions and energy consumption of modern plug-in hybrid vehicles. J Clean Prod. 2022;362:132191. https://doi.org/10.1016/j.clepro.2022.132191
[44] Tanwir NS, Hamzah MI. Predicting purchase intention of hybrid electric vehicles: evidence from an emerging economy. World Electric Vehicle Journal. 2020;11(2):35. https://doi.org/10.3390/wevj11020035
[45] Wang Y, Biswas A, Rodriguez R, Keshavarz-Motamed Z, Emadi A. Hybrid electric vehicle specific engines: state-of-the-art review. Energy Report. 2022;8:832-851. https://doi.org/10.1016/j.egyr.2021.11.265
[46] www.acea.auto/fuel-pc/fuel-types-of-new-cars-battery-electric-12-1-hybrid-22-6-and-petrol-36-4-market-share-full-year-2022/ (accessed on 25.04.2023).

Adriana Skuza, MEng. – Faculty of Mechatronics and Mechanical Engineering, Kielce University of Technology, Poland.
e-mail: *askuza@tu.kielce.pl*

Emilia Szumska, DSc., DEng. – Faculty of Mechatronics and Mechanical Engineering, Kielce University of Technology, Poland.
e-mail: *eszumska@tu.kielce.pl*

Prof. Rafał Jurecki, DSc., DEng. – Faculty of Mechatronics and Mechanical Engineering, Kielce University of Technology, Poland.
e-mail: *rjurecki@tu.kielce.pl*

Article citation info:
Kaźmierczak AR. Research on the wear of novel sets of piston rings in a diesel locomotive engine. Combustion Engines. 2023;195(4):56-62. https://doi.org/10.19206/CE-168518

Andrzej R. KAŹMIERCZAK

Combustion Engines
Polish Scientific Society of Combustion Engines

Research on the wear of novel sets of piston rings in a diesel locomotive engine

ARTICLE INFO

Received: 28 April 2023
Revised: 5 June 2023
Accepted: 19 June 2023
Available online: 25 August 2023

The paper describes the results of the wear test of innovative sets of piston rings intended, among others, to drive diesel locomotives operated in North America, including the USA. The main subject of research is an innovative set of piston rings, the first sealing ring containing a synthetic diamond embedded in a porous chrome coating. The developed multilayer coating is designed to reduce the wear of the piston rings and the combustion engine cylinder. This technology has been implemented at Piston Rings Manufactory "Prima" S.A. in Łódź. The tests were carried out using a two-stroke diesel engine of the EMD 645 type. This engine is manufactured by General Motors Corporation in the United States. The described research was carried out in the United States in San Antonio, Texas, at the Southwest Research Institute. The EMD 645 engine is widely used in power units of heavy diesel locomotives and inland waterway barges in the United States of America, India, and South Africa.

Key words: *piston ring, cylinder, combustion engines, research, simulation*

1. Introduction

The EMD 12-645-E two-stroke internal combustion engine was tested [24]. This engine is the main source of propulsion for diesel locomotives in the United States. Depending on the type, it has a power of 750 to 1500 kW. The number of locomotives operated in the USA powered by the EMD 12-645-E engine is approximately 3,000. The tests carried out at the Southwest Research Institute were carried out using a two-stroke diesel engine with direct fuel injection and a turbocharger power system [22], of which the data are given in Table 1. The engine piston with a diameter of 9 inches has 6 rings; 4 sealing w mounted on the annular part of the piston and two wipers mounted on the piston skirt (Fig. 1).

Fig. 1. EMD 645-E power assembly and GP38-2 locomotive [6]

Table 1. EMD 12-645-E engine data [2]

EMD 12-645-E	
Number of cylinders	V-12
Bore of the cylinder	230 mm
Stroke of the piston	254 mm
Cylinder displacement	10.6 dm^3
Compression Ratio	16:1
Rated power	1100 kW
Specific fuel consumption	254 g/kWh

2. The durability engine test

The main purpose of the research was to check the durability and determine the wear value of the steel piston rings installed in a two-stroke diesel engine. Rings tested with anti-wear coating were mounted in the first groove of the piston [11]. This coating, which consists of 22 layers [10], was created as a result of a porosity galvanic chrome plating, during which, after the polarity was reversed, diamond dust was deposited in the pores [1]. The chrome coating is multi-layered. Due to the diamond content in the coating, it is characterized by high hardness [17, 18] and good tribological properties [9, 13]. This technology is a development of a similar porous chrome plating technology with aluminum oxide deposited in the pores. Its disadvantage was that under boundary friction conditions, it was possible to cooperate with the peaks of surface roughness of the ring and the cylinder in the presence of hard alumina particles, which caused the intensification of the wear process of the upper part of the cylinder, especially at high temperature [4, 16]. The multilayer coating tested does not have this defect [19, 21], because the diamond at a temperature of 873 K (600°C) and higher changes its crystal lattice, becoming graphite. Graphite is a kind of solid lubricant that significantly reduces the coefficient of friction in rubbing pairs and reduces their wear [8].

The main purpose of the tests carried out was to determine the wear value of the radial thickness of the piston rings with the multilayer coating under test. The tests were carried out as comparative tests with standard rings. Before assembly in the EMD 645-E engine, the rings were geometrically measured by measuring their axial height and radial thickness. The test stand at the Southwest Research Institute is mounted on a Union Pacific 3450 diesel locomotive, equipped with additional resistance devices and cooling sets. After checking the correct operation of the engine, multistage durability tests were carried out during 85 hours of engine operation. This test was carried out at a rotational speed of 550 rpm and a power of 650 kW.

3. Measurement before and after the test and the wear of the tested piston rings

In addition to geometric measurements of the axial height and radial thickness of the piston rings, the diameters of the cylinders were also measured and their surface was described in detail [23]. Geometric measurements of the rings were carried out at 10 points in their circumference according to the measurement scheme shown in Fig. 2.

The ring number consists of a number followed by the letter "b" (Fig. 2) in the case of a test ring with a diamond coating. The number in the nomenclature means the cylinder number from 1 to 12. The numbering of the cylinders is in accordance with the standards, and looking from the front of the engine (the side opposite to the output power), the left row of cylinders is numbers 1 to 6, and the right row of cylinders is numbers 7 to 12. The absence of the letter "b" in the ring designation indicates measurements for an uncoated ring. The test rings on one crank worked with standard comparative rings. The test rings were installed in the left row in the odd-numbered cylinders, and in the right row in the even-numbered cylinders.

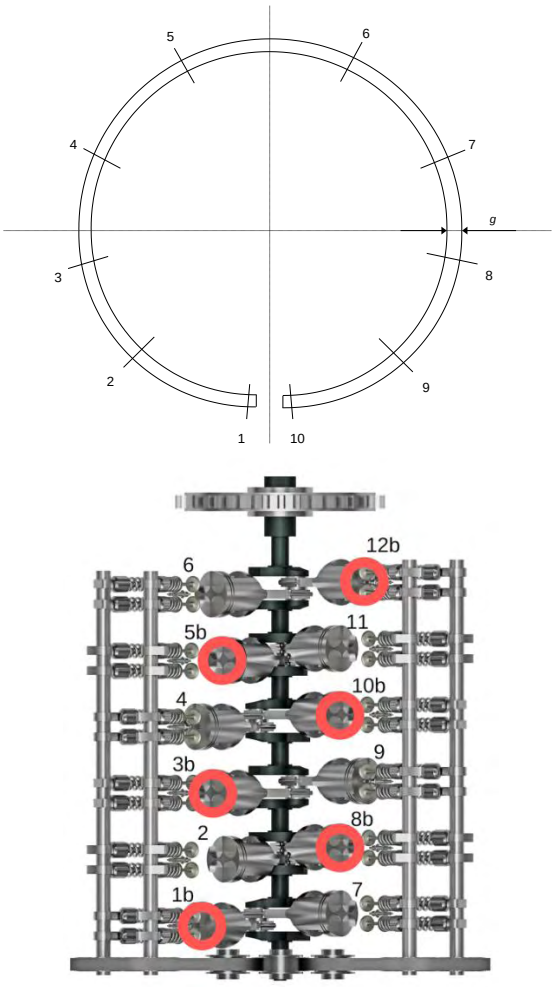

Fig. 2. The measurement scheme of axial high, radial thickness, and the ring number of the EMD 645 engine

The internal combustion engine team durability tests were carried out by implementing the 85-hour test, called the team durability. Such a test is used, among others, by the Federal Mogul. During the test, the engine runs at the rotational speed of the maximum torque value on the external characteristics. This causes an increase in wear as a result of maximising thermal and mechanical loads. The ring-piston assembly is exposed to particularly intensive wear in these conditions. The tests were carried out using the EMD 645-E engine, which has a cylinder diameter of 9.065 inches (230.2 mm). The displacement of one cylinder is equal to 10.35 litres. EMD 645 engines are made in six-cylinder to twenty-cylinder versions with powers ranging from 0.6 MW to 3.1 MW, respectively. whereas a six-cylinder engine is filled with a Roots compressor, and engines with twelve and more cylinders are filled with a turbocharger. The tests were carried out on a turbocharged EMD645-E engine with a rated power of 1200 kW and a maximum torque of 12000 Nm. The cubic capacity of this engine is 124.2 litres [11]. Despite the relatively short duration of the test (85 h), as a result of the intensification of its loads, measurable wear values of the piston rings were found, both in their axial height and radial thickness. To calculate the wear value of the piston rings, the difference in the measurements of their radial thickness and axial height before and after the verification test, lasting 85 hours, was calculated. The results of these calculations are presented in Fig. 3. They are the results of measuring the wear of the axial height and radial thickness, which is the result of the wear process of the diamond-based coating.

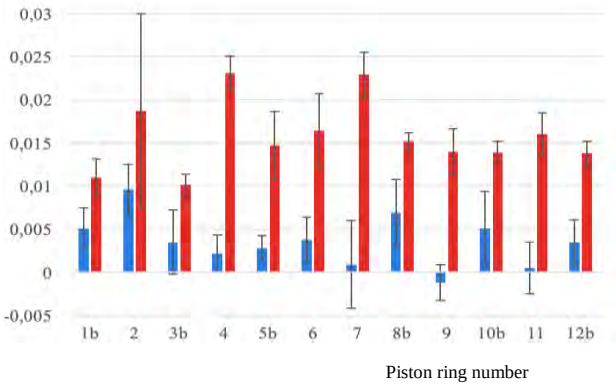

Fig. 3. Average wear of the wear of the ring at axial height (blue) and radial thickness (red)

In cooperation in the piston-cylinder combination, the rings coated with a diamond-based coating were characterised by much lower wear compared to rings that did not have this coating, especially for the wear of the radial width, which is the most heavily loaded working surface of the ring (Fig. 10). The smallest wear of the radial width is about 0.01 mm for the ring with designation 3b with a diamond coating, while the wear of the axial height is low.

The geometric measurements performed showed that the average wear value of the radial thickness of the multilayer porous chrome coating with diamond grit is equal to 0.013 mm. Wear measurements of the radial thickness of the comparative standard rings showed an average wear value of 0.019 mm. The measurement accuracy was 0.001 mm. This means that the differences demonstrated in the average value of the test and standard rings may be signifi-

cant. Appropriate statistical tests were performed to determine the significance of the differences.

3.1. Statistical analysis

Due to the high variability of the wear values of the rings in their circumference, both in axial height and in radial thickness, the Grubbs test was carried out to determine the existence of outliers. The rejection level of the hypothesis about the lack of outliers was chosen as p = 0.05 ("p" values below this value indicate the existence of outliers in the sample population). The test was performed on all 12 rings. In the Table 3 and 4, exemplary results of the test of the wear values of rings 3b and 4 are presented [3].

The test result with a value lower than the assumed significance level of p = 0.05 was marked in red [5, 6]. All outliers of the 12 piston rings were identified and removed.

Table 3. Grubbs test for piston ring 3b

Variable	Piston ring 3b Statistics						
	N value	Average	Grubbs-statistic	p-value	Minimum	Maximum	Std. deviation
High-wear axial axis	10	0.004	2.422	0.017	–0.012	0.010	0.0064
Radial thickness wear	10	0.010	1.836	0.440	0.006	0.013	0.0022

Table 4. Grubbs test for piston ring 4

Variable	Piston ring 4 statistics						
	N value	Average	Grubbs-statistic	p-value	Minimum	Maximum	Std. deviation
High-wear axial axis	10	0.002	1.943	0.296	–0.005	0.008	0.0037
Radial thickness wear	10	0.023	1.480	1.000	0.018	0.028	0.0034

Next, using the Shapiro-Wilk test, the normality of the distribution of variables in individual groups (wear of the axial high and radial thickness) was verified for both variables: "axial height wear" and "radial thickness wear". The assumptions for the analysis of variance (ANOVA), i.e. the normality of the distribution for individual ring wear values, were checked. As in the previous test, Fig. 4 and Fig. 5 present the results in the form of histogram plots and fitted normal distributions for rings 3b and 4 regarding the radial thickness.

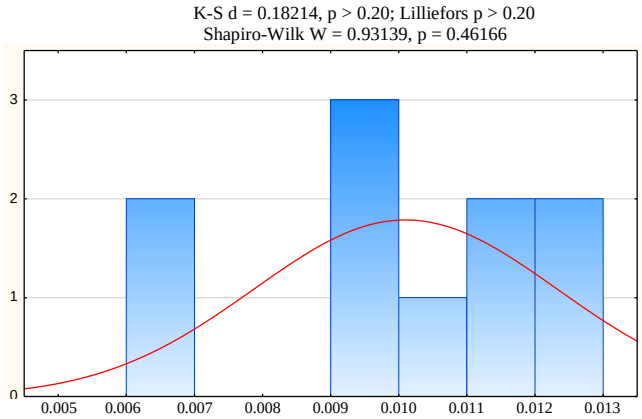

Fig. 4. The histogram of the radial thickness wear of the piston ring 3b [3]

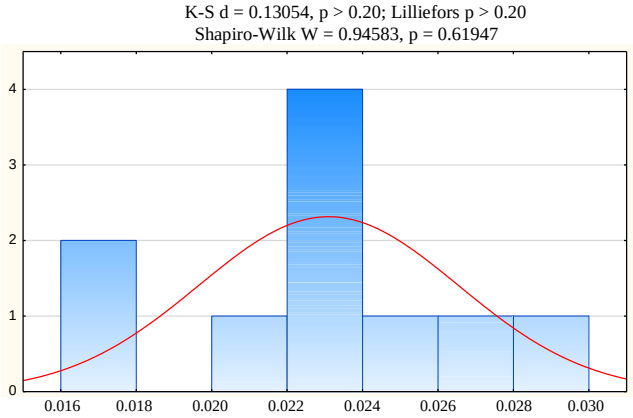

Fig. 5. The histogram of radial thickness wear of the piston ring 4 [3]

Eliminating outliers significantly improved the normality of distribution in individual research groups (wear). With the exception of one study group (ring 6 – "radial thickness wear"), for all others, the value of the Shapiro-Wilk test does not give grounds to reject the null hypothesis about the normality of the distribution.

The assumptions for the analysis of variance (ANOVA), i.e. homogeneity of variance (Levene's test) were also checked, Table 5.

Table 5. Levene's test for all piston rings

Variable	Levene's test, i.e. an analysis of homogeneity of variance Marked effects in red are significant with p < 0.05							
	SS effect	Df effect	MS effect	SS misstatement	Df misstatement	MS misstatement	F	p
High-wear axial axis	0.0003	11	0.000029	0.0008	104	0.000008	3.821	0.000126
Radial thickness wear	0.0002	11	0.000022	0.0004	106	0.000004	5.966	0.000000

For both variables, the homogeneity of variance was challenged in Levene's test. Therefore, analysis of variance (ANOVA) with Welch correction was performed. In addition, the results of the analysis will be confirmed by the nonparametric equivalent of ANOVA, the Kruskal-Wallis test.

An analysis of variance (ANOVA) was also performed; see Table 6.

The calculated significance level "p" indicates the rejection of the hypothesis of equal mean values in the groups for both examined variables. In other words, the tested groups (rings) are significantly differentiated in terms of height wear and thickness wear. The "p" value indicates greater variation in thickness wear (lower value – sixth decimal place still 0).

Table 6. Variance analysis with Welch correction

Variable	Variance Analysis with Welch correction Marked effects in red are significant with p < 0.05											
	SS Effect	df Effect	MS Effect	SS Misstatement	df Misstatement	MS Misstatement	F	p	df WelchEffect	df WelchMis-statement	F Welch	p Welch
High-wear axial axis	0.001025	11	0.000093	0.002594	104	0.00003	3.735	0.000165	11	40.837	4.891	0.000086
Radial thick-ness wear	0.001841	11	0.000167	0.001595	106	0.00002	11.1194	0.000000	11	41.480	12.227	0.000000

Due to the undermined homogeneity of variance in the study groups, the nonparametric Kruskal-Wallis test was used to confirm the ANOVA results. The level of rejection of the hypothesis was maintained as for the above tests, i.e. p = 0.05 (Table 7 and 8).

Table 7. The Kruskal-Wallis test for variable: axial high of the piston rings

Dependent variable: axial high	ANOVA rang Kruskal-Wallis; axial high wear Grouping independent variable: Kruskal-Wallis piston-ring test: H (11, N = 116) = 33.29436, p = 0.0005		
	N important value's	Summ Rang	Averange Ranga
1b	9	728.00	80.889
2	10	932.00	93.200
3b	9	649.00	72.111
4	10	513.50	51.350
5b	10	547.50	54.750
6	9	490.50	54.500
7	10	414.00	41.400
8b	10	748.50	74.850
9	10	271.50	27.150
10b	10	609.50	60.950
11	10	429.50	42.950
12b	9	452.50	50.278

Table 8. The Kruskal-Wallis test for variable: radial thickness of the piston rings

Dependent variable: radial thick-ness	ANOVA rang Kruskal-Wallis; radial thickness wear Grouping independent variable: Kruskal-Wallis test of the piston ring: H (11, N = 118) = 56.70718, p = 0.0000		
	N important value's	Summ Rang	Average Rang
1b	10	325.50	32.550
2	9	383.00	42.556
3b	10	218.50	21.850
4	10	1034.00	103.400
5b	9	405.00	45.000
6	10	587.50	58.750
7	10	1023.00	102.300
8b	10	707.00	70.700
9	10	538.50	53.850
10b	10	561.00	56.100
11	10	684.00	68.400
12b	10	554.00	55.400

The results of the Kruskal-Wallis test for both verified variables unequivocally confirmed the ANOVA results: wear on the axial height and radial thickness of the tested piston rings are significantly different. This means that the rings wear unevenly around the circumference. At the same time, there is no strictly preferred wear direction.

3.2. Analysis of test results

The engine was found to have consumed 22,400 dm^3 of diesel oil and 45.42 dm^3 of lubricating oil during the 85-hour verification test. Considering the size of this drive unit and comparing it with the results of other studies conducted at the Southwest Research Institute, it was found that these were the correct sizes. The consumption of lubricating oil was small and was 0.2% of the fuel consumption [9]. Whereas, based on the available source data, oil consumption in relation to fuel consumption for a turbocharged EMD 645 engine is equal to 0.5 ±0.2%. This means significant savings in lubricating oil consumption resulting from the use of an innovative piston ring solution with a diamond-based coating [9].

Based on Tables 2 and 3, pie charts were prepared showing the wear of the radial thickness at each of the 10 measurement points on the circumference of the rings for rings coated with and without a diamond-based coating (Fig. 6, 7).

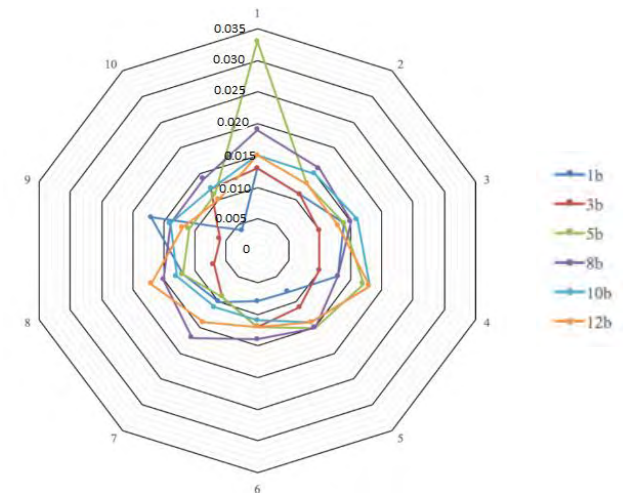

Fig. 6. Wear of the radial thickness of the diamond-coated rings at each of the 10 measurement points [3]

Figure 6 shows the wear of rings at the radial thickness with a diamond coating. The highest wear value was at the measurement point no. 1 on the circumference of the ring marked 5b and was 0.033 mm. The smallest wear value was observed at the measurement point no. 9 at the circumference of the ring marked 1b, which was 0.004 mm. The distribution of wear on the radial width was even, and for all measurement points the wear value did not exceed 0.02 mm, except for measurement point No. 1 on the circumference of the ring marked 5b, which could have been a measurement error.

Figure 7 shows the wear of the rings on the radial width without the diamond coating. The highest wear value was at the measurement point no. 3 on the circumference of the

ring marked 2 and amounted to 0.073 mm. This point was outside the area in Fig. 6, due to the adopted scale, which was introduced to maintain similarity to Fig. 5. The smallest wear value was observed at the measurement point no. 7 in the circumference of the ring marked 6, which was 0.008 mm [7].

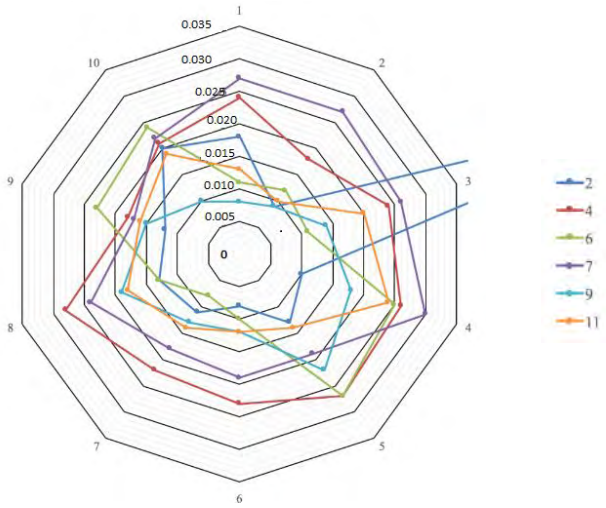

Fig. 7. Wear of the radial thickness of the rings without the diamond coating at each of the 10 measurement points [3]

Cylinder wear values were determined on the basis of completed diameter measurements. Measurements were made at three measurement levels:

– in the Top Dead Centre (TDC) of the first sealing ring (including diamond-coated),
– in the middle of the piston stroke (corresponding to the stroke of the first sealing ring),
– and in the Bottom Dead Centre (BDC) of the first sealing ring.

Measurements were made in two measuring directions: along the longitudinal axis of the engine and across this axis [5]. Due to the fact that the engine is made as a V-shaped arrangement, this is along and across the rows of cylinders. The numbering of the cylinders is in accordance with the Polish standard. Cylinder numbers 1 through 6 apply to the left row cylinders when looking at the engine along the axis opposite the power output side, and cylinder numbers 7 to 12 apply to the right row also when viewed opposite the power output side. If the diamond-based coating in question was made incorrectly, then the indicated measurement accuracy was sufficient to determine such a fact during the tests described in the previous point. The measurement results discussed are presented in Table 9, where the measuring height "0" (measured in mm) is the ZZ of the first sealing ring, the measuring height "127" is the centre of the piston stroke of the first sealing ring, and the measuring height "254" is the ZW of the first sealing ring.

The measured cylinder wear values were within the measurement error range of the bore gauge used for testing, which was 10 micrometres. The bore gauge measurement was a control. If there was excessive wear to the cylinder, a bore gauge with a measuring accuracy of 10 micrometres would show excessive wear. This meant the correct cooperation of the piston rings with the cylinders. The confirmation of the correct cooperation of the developed piston rings with the cylinders is the photograph of the ZZ area of the cylinders No. 3, 5 and 9 in Fig. 8, in which the sealing ring with a diamond coating worked. The honing scratches visible in the photo show little or even no wear of the cylinders.

Table 9. EMD 645 engine cylinder wear values after the verification test

Cylinder No.	Measurement height, mm	Cylinder wear in the longitudinal axis of the engine, mm	Cylinder wear in the cross section of the engine, mm
1	0	0.01	0.00
	127	0.00	0.00
	254	0.00	0.00
2	0	0.00	0.01
	127	0.01	0.00
	254	0.00	0.00
3	0	0.01	0.00
	127	0.00	0.01
	254	0.00	0.00
4	0	0.00	0.01
	127	0.00	0.00
	254	0.00	0.00
5	0	0.00	0.01
	127	0.01	0.00
	254	0.00	0.00
6	0	0.01	0.00
	127	0.00	0.00
	254	0.00	0.01
7	0	0.01	0.01
	127	0.00	0.00
	254	0.00	0.00
8	0	0.01	0.01
	127	0.01	0.00
	254	0.00	0.01
9	0	0.01	0.01
	127	0.01	0.00
	254	0.00	0.01
10	0	0.01	0.00
	127	0.00	0.00
	254	0.01	0.01
11	0	0.01	0.00
	127	0.00	0.00
	254	0.00	0.00
12	0	0.01	0.00
	127	0,00	0,01
	254	0,00	0,00

Fig. 8. Photograph of the surface of cylinders no. 3, 5 and 8 after the engine verification test

During the implementation of the 85-hour team durability test, the concentrations of harmful components of the exhaust gases and the emissions of selected components were also measured. These tests were performed at the beginning of the trial and after its completion. Sulphur dioxide (SO_2), particulate matter, hydrocarbon content in exhaust gases (HC) and nitrogen oxides (NO_x) measurements were performed. The results of the measurement of these components are presented in the form of concentrations per 1 litre of fuel consumed. The sulphur dioxide

concentration was also measured, even though sulphur-free fuel was used. It is normal for a two-stroke engine to consume significant amounts of lubricating oil. For this reason, the presence of sulphur dioxide is found in the exhaust gases, despite the use of sulphur-free fuel. In this case, the results are given in ppm.

Table 10. The value of the emission and concentration of the toxic exhaust components of the EMD 645 engine before and after the verification test

Chemical to be measured	Before test	After test
Sulphur dioxide, SO_2, ppm	0.15	0.18
Solid particles, g/dm^3	2.16	2.15
Carbon monoxide, CO, g/dm^3	9.46	9.85
Hydrocarbons, HC, g/dm^3	4.32	4.55
Nitrogen oxides, NO_x, g/dm^3	81.02	90.5

The concentration limits for harmful compounds in the United States are given in grammes per gallon of used fuel. Therefore, in order to reference these standards, the described measurement of the concentration per litre of fuel was used. The measured concentrations of harmful compounds in the exhaust gases are within the standards applicable in the USA for EMD 645 series engines, introduced by the Environmental Protection Agency (EPA), according to the NSPS standard for the engine category with the designation 1/2 (for ships and locomotives), updated in 2008, which dates back to 1999.

During the 85-hour test, a number of engine performance indicators were discreetly measured. The engine worked at parameters close to the maximum torque value. Measurements of the engine operation indicators were performed every 3 seconds, thanks to which a significant database was obtained, that is, 102,000 records stored in the form of 16 gears corresponding to the engine starts during the test. The analysis of the collected material allowed us to draw conclusions of a utilitarian nature. Figures 9 and 10 show power and hourly fuel consumption curves as examples.

Figure 9 shows the changes in power in particular hours of the verification test. There were no visible differences in the values in the individual hours of the 85-hour test and in the settings. This value was on average at the level of 650 kW–700 kW. Only a change was noticeable at the very beginning of engine operation, but this is caused by the running-in of the TPC unit and the associated load reduction.

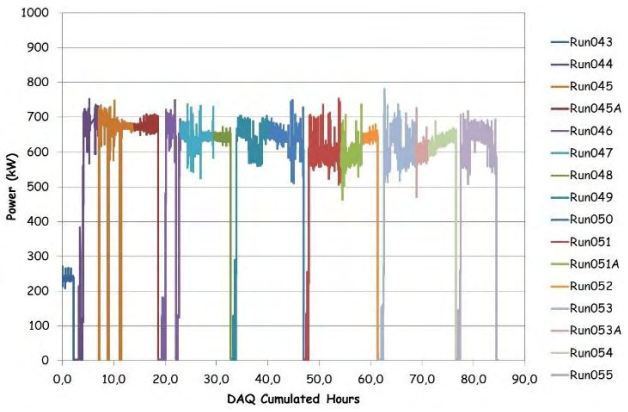

Fig. 9. Power as a function of time during the 85-hour verification test

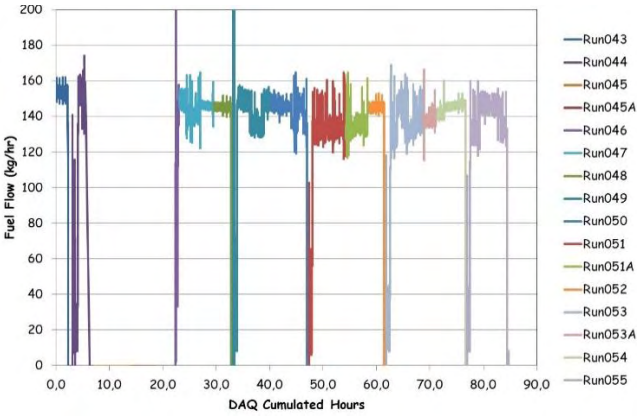

Fig. 10. Hourly fuel consumption as a function of time during the 85-hour verification test

Figure 10 shows changes in the hourly fuel consumption in individual hours of the verification test for each of the controller settings. From about 34.00 hours, the wear showed no signs of disturbance and remained at an even level. However, at 34:00, jumps in these values were observed; they may have been caused by the engine running. Two characteristic peaks were also observed: one to the value of 200 kg/h around the 22nd hour and the other to the value of 200 kg/h around the 32nd hour of the test. Also very characteristic was the moment of lack of fuel consumption measurement between the 6th and 22nd hour of the test, which was caused by a failure of the measuring device.

4. Summary and conclusion

Based on research, among others, presented in [21], it was found that the coefficient of friction of an element with a coating made in a technology based on diamond-containing layers is lower, especially in cooperation with steel and cast iron surfaces. Another extremely important feature of these coatings is wear resistance, manifested by its lower value, which was also found based on the presented research [14]. The use of these coatings becomes particularly important in the event of an intensification of loads, which is, for example, the case in the drive engines of diesel locomotives and inland waterway vessels. They are subjected to extreme loads and are most often operated with maximum torque settings [15]. The tests carried out confirm the desirability of using coatings containing synthetic diamond in their composition. This may be a new direction of research on their wider use for components of internal combustion engines, especially for sealing piston rings [25–27]. The wear values obtained of the radial thickness of the rings tested with coatings containing synthetic diamonds allow us to conclude that their use in highly loaded two-stroke diesel engines is justified [10]. The developed and tested diamond coatings show high adhesion to the steel piston ring substrate despite being subjected to a complex load condition, which is a characteristic feature of the operation of piston rings while ensuring very good tribological properties. Diamond-containing coatings are also characterised by high hardness, even up to 70 GPa [12]. They also have a high electrical resistance value and a low specific mass [20, 28].

Bibliography

[1] Aldwell B, Trimble D, Yin S, Lupoi R. Enabling diamond deposition with cold spray through the coated particle method. Material Science Forum. 2017;879:1194-1199. https://doi.org/10.4028/www.scientific.net/MSF.879.1194

[2] Asaulyak AA, Rozhdestvenskii YV, Gavrilov KV. Elasto-hydrodynamic lubrication (EHL) of piston rings in the internal combustion engine. Procedia Engineer. 2016;150: 536-540. https://doi.org/10.1016/j.proeng.2016.07.037

[3] Borkowska J. The impact of the surface energetic state in frictional pairs on friction and wear in combustion engine, doctoral dissertation. Wroclaw University of Science and Technology. Wroclaw 2019.

[4] Buckmaster J, Clavin P, Linan A, Matalon M, Peters N, Sivashinsky G et al. Combustion theory and modelling. P Combust Inst. 2005;30:1-19. https://doi.org/10.1016/j.proci.2004.08.280

[5] Corcione FE, Vaglieco BM, Consales S, Costa M, Formisano G, Merola SS. Temporal and spatial evolution of radical species in the experimental and numerical characterisation of diesel auto-ignition. Proceedings of The Fifth International Symposium on Diagnostics and Modelling of Combustion in Internal Combustion Engines (COMODIA 2001). 2001:355-363. Nagoya 2001.

[6] Froelund K, Fritz S, Smith B. Ranking lubricating oil consumption of different power assemblies on an EMD16-645-e locomotive diesel. CIMAC Congress 2004. Kyoto 2004.

[7] Heywood JB. Internal combustion engines fundamental. McGraw-Hill Inc., New York 1988.

[8] Hryniewicz T. Surface and coating technology (in Polish). Koszalin University Press. Koszalin 2004.

[9] Joshi DS, Shah AV, Gosai D. Importance of tribology in internal combustion engine: a review. International Research Journal of Engineering and Technology. 2015;2(7):803-809. https://www.irjet.net/archives/V2/i7/IRJET-V2I7124.pdf

[10] Kaźmierczak A. The influence of the energy state of the surface layer of internal combustion engine elements on the wear and friction of rubbing pairs (in Polish). Wroclaw University of Science and Technology Press. Wroclaw 2013.

[11] Kaźmierczak A, Borkowska J. Diamond derivating coating impact on wearing in combustion engine International Automotive Conference (KONMOT2018). Conference Series – Materials Science and Engineering, IOP Publishing, 2018;032005:1-10.

[12] Kim Y, Park H, An J, Kan T, Park J. Development of nano diamond polymer coating on piston skirt for fuel efficiency. SAE Int J Engines. 2011;4(1):2080-2086. https://doi.org/10.4271/2011-01-1401

[13] Love CA, Cook RB, Harvey TY, Dearnley PA, Wood RJK. Diamond like carbon coatings for potential application in biological implants-a review. Tribol Int. 2013;63:141-150. https://doi.org/10.1016/j.triboint.2012.09.006

[14] Madej M. Properties of tribological systems with diamond-based coatings (in Polish). Kielce University Press. Kielce 2013.

[15] Makhlof ASN. High performance coatings for automotive and aerospace industries. B Nova Science Publishers. New York 2010.

[16] Matla J. Possible applications of prechambers in hydrogen internal combustion engines. Combustion Engines. 2022; 191(4):77-82. https://doi.org/10.19206/CE-148170

[17] Mellor BG.(ed.) Surface coatings for protection against wear. Woodhead Publishing Series in Metals and Surface Engineering. Woodhead Publishing. 2009. https://doi.org/10.1016/B978-1-85573-767-9.50014-7.

[18] Moseler M, Gumbsch P, Casiraghi C, Ferrari AC, Robertson J. The ultrasmoothness of diamond-like carbon surfaces. Science. 2005;309(5740):1545-1548. https://doi.org/10.1126/science.1114577

[19] Moulin D, Raymond O, Chevrier P, Lipinski P, Barre T. CVD diamond coatings for machining. Material Science Forum. 2006;526:55-60. https://doi.org/10.4028/www.scientific.net/MSF.526.55

[20] Nakashima K, Uchiyama Y. Influence of piston surface treatment on piston assembly friction in an eco-mileage vehicle engine. Combustion Engines. 2022;188(1):18-23. https://doi.org/10.19206/CE-142552

[21] Ping L, Xingcheng X, Lukitsch M, Chou K. Micro-scratch testing and simulations for adhesion characterization of diamond-coated tools. Proceedings of NAMRI/SME. 2011; 39.

[22] Pischinger S. The combustion process in diesel engines. Intern. Combust. Engines II Lect. Notes. RWTH-Aachen University. 2017;171-177.

[23] Poulon-Quintin A, Faure C, Teule-Gay L, Manaud JP. Microstructure coating influence for optimized diamond deposition. Material Science Forum. 2012;706-709:2898-2903. 2012. https://doi.org/10.4028/www.scientific.net/MSF.706-709.2898

[24] Reif K, Dietsche KH. Automotive Handbook. Robert Bosch GmbH. Karlsruhe 2014.

[25] Rusiński E. Principles of designing load-bearing structures of motor vehicles. Wroclaw University of Science and Technology Press. Wroclaw 2002.

[26] Rusiński E, Czmochowski J, Smolnicki T. Advanced finite element method in load-bearing structures. Wroclaw University of Science and Technology Press, Wroclaw 2000.

[27] Tormos B, Martin J, Blanco-Cavero B, Jimenes-Reyes AS. One-dimensional modeling of mechanical and frictional lossse distribution in a four-stroke internal combustion engine. J Tribol. 2020;142(1):011703. https://doi.org/10.1115/1.4044856

[28] Uzumaki ET, Lambert CS, Belangero WD, Zavaglia CAC. Biocompatibility of titanium based implants with diamond-like carbon coatings produced by plasma immersion ion implantation and deposition. Key Eng Mat. 2017;361-363: 677-680. https://doi.org/10.4028/www.scientific.net/KEM.361-363.677

Prof. Andrzej R. Kaźmierczak, DSc., DEng. – Faculty of Mechanical Engineering, Wroclaw University of Science and Technology, Poland.
e-mail: *andrzej.kazmierczak@pwr.edu.pl*

Article citation info:
Borucka A, Kozłowski E. Modeling the dynamics of changes in CO_2 emissions from Polish road transport in the context of COVID-19 and decarbonization requirements. Combustion Engines. 2023;195(4):63-70. https://doi.org/10.19206/CE-169697

Anna BORUCKA
Edward KOZŁOWSKI

Combustion Engines
Polish Scientific Society of Combustion Engines

Modeling the dynamics of changes in CO_2 emissions from Polish road transport in the context of COVID-19 and decarbonization requirements

ARTICLE INFO

Received: 13 May 2023
Revised: 8 July 2023
Accepted: 17 July 2023
Available online: 22 July 2023

Emissions from transport account for 20–25% of anthropogenic global carbon dioxide emissions [17, 37], with more than 70% coming from road transport, making it an extremely important topic in the context of decarbonization. The aim of the article is to analyze the trend of CO_2 generated from road transport, taking into account various sources, and also to examine how reduced mobility during the pandemic affected the emissions at the time. For this purpose, a time series containing observations up to the pandemic outbreak and a time series containing additional observations from the pandemic period were analyzed. For each time series, a trend was determined and described by a polynomial and then verified to see if the pandemic phenomenon significantly affects a parameter of the proposed model, using appropriate statistical tests.

Key words: *transport decarbonization, CO_2 emissions, road transport, COVID-19 pandemic, polynomial model*

1. Introduction

Global warming, the main cause of which is the growing emission of carbon dioxide, causes drastic consequences for many ecosystems, bringing about irreversible changes in them [27, 36, 38]. The use of petroleum fuels in transport determines its significant share in greenhouse gas emissions, which is why this sector faces the greatest demands [5, 12, 23]. Meanwhile, the progressing globalization, population growth, increasing demand for goods, as well as the dynamic development of the tourism industry and the number of people travelling do not make this task easier, especially since it is estimated that by the 2050, the EU economy will more than double [10].

Emissions from transport account for 20–25% of anthropogenic global carbon dioxide emissions [17, 37], of which 71.7% are from road transport, but taking into account the production of cars and the construction of road infrastructure, this number increases to 37% of all emissions [7, 14, 16, 24]. Transport uses 30% of the world' energy. Although only 7% of the population owns cars, this translates into 40% of the world's petrol production.

Cars are considered the most polluting means of transport and at the same time the most unsafe [3, 4, 18]. They are also the largest emitter of toxic chemical compounds not subject to legal regulation, such as butadiene, benzene and others [22, 25]. The area necessary to build a road (30 to 40 m on average) is much larger than the requirements for railway traction (10 to 14 m) [25]. What's more, 30% of car journeys in the European Union do not exceed 3 km, and 50% – 6 km [39], so they could be successfully replaced by environmentally friendly natural forms of transport, such as bicycles.

The share of Polish road transport in the total emissions of the European Union is significant. Poland has been occupying leading positions for years [9]. Moreover, due to the intensive increase in passenger and transport activity, CO_2 emissions are constantly growing, increasing in 2020 by almost 150% compared to 2000, while emissions throughout the EU remain relatively constant [2].

The transport sector is therefore a challenge on the way to achieving climate neutrality, related to the reduction of greenhouse gases emissions, which is the result of the European climate policy. Currently, the European Parliament requires a 40% reduction in greenhouse gas emissions by EU countries by the 2030, compared to the level of 2005 [29]. This is a recent change (March 2023). The previous target was 30%.

Therefore, the article analyses the current dynamics of changes in CO_2 emissions from road transport, including various types of transport means. Mathematical identification of the examined time series and determination of the forecast was aimed at relating the current level of CO_2 emissions to the requirements imposed by the EU in this regard.

In addition, the article features an analysis of the impact of the COVID-19 pandemic on CO_2 emissions. Global movement restrictions, limited travel options and remote work, as well as fear of contagion, have strongly influenced changes in people's preferences in their choice of transport and travel in general. More people staying indoors or using safer forms of transport like cycling or walking may have reduced these emissions, as confirmed by studies by a number of authors [11, 13, 20, 32, 42]. On the other hand, the fear of coming into contact with an infected person has fostered a switch from public to private transport [1,6], and a number of authors believe that the decrease in emissions was too short-lived to have a relative effect [31, 33]. Therefore, the article also features an attempt to answer the question of how the COVID-19 pandemic in Poland affected the trend in CO_2 emissions, taking into account different modes of transport.

For this purpose, time series of CO_2 emissions from transport, published by the European Environment Agency, expressed in Gg [8], were analyzed. Time series with observations up to the outbreak of the pandemic and time series with additional observations from the pandemic period were analyzed.

For each time series, a trend was determined and described by a polynomial and then verified to see if the pandemic phenomenon significantly affects a parameter of the

proposed model, using appropriate statistical tests. A detailed survey procedure is presented in Chapter 2. The lack of confirmation of the significance of the impact of the pandemic on the model coefficients means that the hazard did not significantly affect CO_2 emissions.

2. Materials and methods

2.1. Determining the trend in a time series

The trend in the time series $\{x_{t_i}\}_{1\le i\le n}$ is identified as a polynomial [15, 41]

$$x_{\tau_i} = \beta_0 + \beta_1\tau_i + \cdots + \beta_k\tau_i^k + \varepsilon_{\tau_i} \tag{1}$$

where $\{\varepsilon_i\}_{1\le i\le n}$ is a sequence of independent random variables with a normal distribution $N(0,\sigma^2)$ and $x_{\tau_i} \overset{def}{=} x_{t_i}$. The trend occurring in the series is identified using a k degree polynomial. The dependence (1) between the endogenous variable and the predictors (transformations of the variable τ) is linear. At the beginning we define objects:

$$X = \begin{bmatrix} 1 & \tau_1 & \dots & \tau_1^k \\ 1 & \tau_2 & \dots & \tau_2^k \\ \vdots & \vdots & & \vdots \\ 1 & \tau_n & \dots & \tau_n^k \end{bmatrix}, \quad Y = \begin{bmatrix} x_{\tau_1} \\ x_{\tau_2} \\ \vdots \\ x_{\tau_n} \end{bmatrix},$$

$$\varepsilon = \begin{bmatrix} \varepsilon_0 \\ \varepsilon_1 \\ \vdots \\ \varepsilon_n \end{bmatrix}, \quad \beta = \begin{bmatrix} \beta_0 \\ \beta_1 \\ \vdots \\ \beta_k \end{bmatrix}$$

therefore, the dependence (1) can be presented in linear form [21,24]:

$$Y = X\beta + \varepsilon \tag{2}$$

Using the Least Squares Method (LSM) [41] the values of the model parameters can be estimated using the formula

$$\hat{\beta} = (X^TX)^{-1}X^TY \tag{3}$$

The vector of residuals $\varepsilon \in \mathbb{R}^n$ can be presented as $\varepsilon = Y - X\hat{\beta}$. Coefficient of determination [41] is determined as follows

$$R^2 = 1 - \frac{\sum_{j=1}^n \varepsilon_j^2}{\sum_{j=1}^n \left(x_{\tau_i} - \bar{x}\right)^2}, \tag{4}$$

where $\bar{x} = \frac{1}{n}\sum_{j=1}^n x_{\tau_i}$ and the estimator of the variance of the residuals is equal

$$\hat{\sigma}^2 = \frac{1}{n-k-1}\sum_{j=1}^n \varepsilon_j^2$$

Values of variance of structural parameters [41] are determined as follows

$$S^2 = (S_0^2, S_1^2, \dots, S_k^2) = \operatorname{diag}(\hat{\sigma}^2(X^TX)^{-1}).$$

Thus, each of the structural parameters β_j has a normal distribution $N\left(\hat{\beta}_j, S_j^2\right)$ for $0 \le j \le k$. For each parameter β_j the significance of the influence of component τ_i^j on the realizations of the series according to model (1) is tested. At the significance level $0 < \alpha < 1$ for each structural parameter β_j we create a null hypothesis

H_0: $\beta_j = 0$

against an alternative hypothesis

H_0: $\beta_j \neq 0$.

The test statistic

$$t = \frac{\hat{\beta}_j}{\sqrt{S_j^2}} \tag{5}$$

has t – distribution with $n-k-1$ degrees of freedom [15,34,40]. The test probability is equal:

$$p.\,val_j = 2\left(1 - \Psi(|t|)\right)$$

where $\Psi(\cdot)$ is t – distribution function with $n-k-1$ degrees of freedom. If $p.\,val_j < \alpha$ then for the parameter β_j the null hypothesis H_0 is rejected in favor of the alternative hypothesis H_1. Therefore, the component τ_i^j significantly affects the realization of the time series defined by formula (1).

The key in the analyzed mathematical equation is the choice of the degree of the polynomial. To select the appropriate polynomial, the Ramsey RESET test (linearity test) [21, 28] was used in the research. The degree of the polynomial is chosen as the lowest natural number for which the coefficient of determination is at a sufficiently high level and there are no grounds to reject the null hypothesis for the linearity test.

2.2. Study of the impact of COVID-19 on CO_2 emissions

First, a time series of CO_2 emissions is considered for pre-pandemic data, i.e., data covering the years up to and including 2019. Thus, for the series $\{x_{\tau_i}\}_{1\le i\le n-1}$ the model (1) is identified and, taking into account the linearity test of the models, the degree of the polynomial $k \in \mathbb{N}$ is determined. Using LSM the structural parameters of the model and the variances of these structural parameters are determined, therefore $\beta_i^{2019} \sim N\left(\hat{\beta}_i^{2019}, S_i^{2019}\right)$ for $0 \le i \le k$.

Next, the time series of CO_2 emissions for data that includes the COVID-19 pandemic are analyzed, i.e., for data including the year 2020. Thus, for the series $\{x_{\tau_i}\}_{1\le i\le n}$ the model (1) for the degree of the polynomial $k \in \mathbb{N}$ is identified. Using LSM the structural parameters of the model and the variances of these structural parameters are determined, therefore $\beta_i^{2020} \sim N\left(\hat{\beta}_i^{2020}, S_i^{2020}\right)$ for $0 \le i \le k$.

In the next step, for each j indices, $0 \le j \le k$ at significance level $\alpha = 0.05$ the null hypothesis is created:

H_0: $\beta_j^{2019} = \beta_j^{2020}$ (no impact of pandemic on parameter β_j)

against an alternative hypothesis:

H_1: $\beta_j^{2019} \neq \beta_j^{2020}$ (significant impact of pandemic on parameter β_j)

The test statistic

$$T = \frac{\hat{\beta}_j^{2019} - \hat{\beta}_j^{2020}}{\sqrt{\frac{S_j^{2019}}{n-k-2} + \frac{S_j^{2020}}{n-k-1}}} \tag{6}$$

has a normal distribution $N(0,1)$ [15, 41]. The test probability is equal:

$$p.\,val_j = 2\left(1 - \Phi(|T|)\right)$$

where $\Phi(\cdot)$ denotes the standard normal distribution $N(0,1)$. If $p.val_j < \alpha$ then the null hypothesis H_0 is rejected in favor of H_1.

If there is such j index, $1 \leq k$ for which $p.val_j < \alpha$, it is considered that the estimator of β_j parameter determined from observations up to the pandemic and observations with the onset of the pandemic are significantly different, and therefore the pandemic had a significant impact on the trend of CO_2 emissions. If for each j indices, $1 \leq k$ the condition $p.val_j \geq \alpha$ is satisfied, then for each structural parameter, the estimators obtained from observations up to the pandemic and observations with the start of the pandemic are not significantly different from each other, therefore the pandemic did not have a significant impact on CO_2 emissions.

3. Evaluation of the trend of CO_2 emissions in road transport

3.1. Road transport

First, CO_2 emissions from road transport as a whole were evaluated without breaking them down by mode of transport. Figure 1 presents the time series under study (black curve).

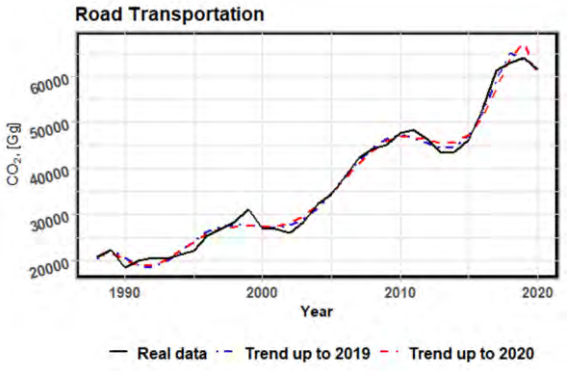

Fig. 1. CO_2 Emission for Road Transportation [8]

Then, for the time series presented, a model built only for the pre-pandemic period was proposed (blue line in Fig. 1). The estimators of structural parameters, standard deviations, t-statistic values and p-values are presented in Table 1.

Table 1. Structural parameters, standard errors, values of t-statistic and p-values for the trend to the pre-pandemic period

	Estimate	Std. error	t value	p-value
β_0	7115.71935	5166.94560	1.37716	0.18172
β_1	22985.07637	6162.91969	3.72958	0.00110
β_2	–12041.9597	2495.18762	–4.82607	0.00007
β_3	2769.26980	479.62213	5.77386	0.00001
β_4	–327.12113	50.15569	–6.52211	< 1e–5
β_5	21.43286	3.01362	7.11200	< 1e–5
β_6	–0.78550	0.10381	–7.56667	< 1e–5
β_7	0.01505	0.00190	7.90711	<1e–5
β_8	–0.00012	0.00001	–8.15249	<1e–5

The coefficient of determination is equal to 0.9907, and the standard deviation of the residuals is equal to 1524.28. At the significance level $\alpha = 0.05$, the H_0 hypothesis was rejected in favor of H_1 for the structural parameters of $\beta_1, \beta_2, \beta_3, \beta_4, \beta_5, \beta_6, \beta_7, \beta_8$, therefore the predictors of these parameters significantly affect the polynomial trend in the time series. The value of the statistic for the Ramsey RESET test is 1.6778, while the p-value is 0.2496.

In the next step, a model was built for data covering the period of the pandemic (red line in Fig. 1). Table 2 presents the estimators of structural parameters, standard deviations, values of t-statistics and p-values for the entire period.

Table 2. Structural parameters, standard errors, values of t-statistic and p-value for the trend to the entire period

	Estimate	Std. error	t value	p-value
β_0	12173.08505	5969.19873	2.03932	0.05258
β_1	15486.44602	6946.95856	2.22924	0.03542
β_2	–8500.03179	2739.16084	–3.10315	0.00485
β_3	2003.84146	512.08133	3.91313	0.00066
β_4	–239.32353	52.03960	–4.59887	0.00012
β_5	15.74571	3.03706	5.18452	0.00003
β_6	–0.57695	0.10158	–5.67979	0.00001
β_7	0.01102	0.00181	6.09446	< 1e–5
β_8	–0.00009	0.00001	–6.43854	< 1e–5

The coefficient of determination is equally high at 0.9873. The standard deviation of the residuals is equal to 1836.77. At the significance level $\alpha = 0.05$, the hypothesis H_0 was rejected in favor of H_1 for the parameters $\beta_1, \beta_2, \beta_3, \beta_4, \beta_5, \beta_6, \beta_7, \beta_8$. Thus, predictors at these parameters significantly affect the polynomial trend in the time series.

For the polynomials constructed above, their parameters were compared. Table 3 presents the calculated values of statistics (6) and p-values for the test of differences of structural parameters.

Table 3. T-statistic values and p-value for the tests of differences in structural parameters

	T	p-value
β_0	–3.10942	0.00187
β_1	3.91841	0.00009
β_2	–4.63753	< 1e–5
β_3	5.29107	< 1e–5
β_4	–5.88978	< 1e–5
β_5	6.44278	< 1e–5
β_6	–6.95724	< 1e–5
β_7	7.43869	< 1e–5
β_8	–7.89137	< 1e–5

At the significance level $\alpha = 0.05$, the H_0 hypothesis was rejected in favor of H_1 for all structural parameters. Thus, the parameters are significantly different for the polynomial trend determined for the CO_2 emission series up to the time of the pandemic outbreak and the polynomial trend determined for the CO_2 emission series containing the first year of the pandemic. Thus, the COVID-19 pandemic significantly affected the CO_2 emissions trend analyzed for road transport in Poland, as a whole.

In the next stage of the study, an analogous analysis was made, however, taking into account the different modes of transport. Passenger cars, light duty trucks, heavy duty trucks and motorcycles were studied.

3.2. Passenger cars

Passenger cars make up the majority of the vehicle market in Poland (more than 60% of the market). The latest available data shows that at the end of 2022, 26.675 million passenger cars were registered in the database of the Central Register of Vehicles and Drivers (CEPiK), 577,000 more than a year earlier [35]. In Fig. 2 CO_2 emissions (black line) are also on an upward trend.

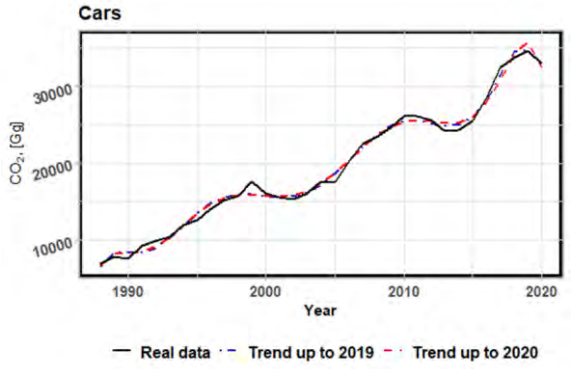

Fig. 2. CO_2 emissions for cars [8]

According to the adopted algorithm, the model was first built for the pre-pandemic period only (blue line in Fig. 2). Its structural parameters, standard deviations, t-statistic values and p-values are presented in Table 4.

Table 4. Structural parameters, standard errors, values of t-statistic and p-value for the trend to the pre-pandemic period

	Estimate	Std. error	t value	p-value
β_0	–902.69310	2570.25660	–0.35121	0.72863
β_1	12031.29715	3065.69611	3.92449	0.00068
β_2	–5793.93596	1241.21153	–4.66797	0.00011
β_3	1326.84643	238.58427	5.56133	0.00001
β_4	–156.72823	24.94956	–6.28180	< 1e–5
β_5	10.23508	1.49910	6.82748	< 1e–5
β_6	–0.37295	0.05164	–7.22225	< 1e–5
β_7	0.00710	0.00095	7.49445	< 1e–5
β_8	–0.00005	0.00001	–7.66937	< 1e–5

The coefficient of determination equals 0.993, and the standard deviation of the residuals equals 758.24. At the significance level $\alpha = 0.05$, the H_0 hypothesis was rejected in favor of H_1 for the structural parameters of $\beta_1, \beta_2, \beta_3, \beta_4, \beta_5, \beta_6, \beta_7, \beta_8$, therefore the predictors of these parameters significantly affect the polynomial trend in the time series. The value of the statistic for the Ramsey RESET test is 0.9118, while the p-value is 0.5895.

Consistently, in a further step, a model was built for data covering the time of the pandemic (red line in Fig. 2). Table 5 presents structural parameters, standard deviations of parameters, values of t-statistics and p-values for the entire period.

The coefficient of determination is equal to 0.9921, and the standard deviation of the residuals is 825.34. At the significance level $\alpha = 0.05$, the H_0 hypothesis was rejected in favor of H_1 for the $\beta_1, \beta_2, \beta_3, \beta_4, \beta_5, \beta_6, \beta_7, \beta_8$. parameters. Thus, also in this case, the predictors at these parameters significantly affect the polynomial trend in the time series.

Table 5. Structural parameters, standard errors, values of t-statistic and p-value for the trend to the entire period

	Estimate	Std. Error	t value	p-value
β_0	801.28414	2682.23759	0.29874	0.76771
β_1	9504.78508	3121.59039	3.04485	0.00558
β_2	–4600.55486	1230.83189	–3.73776	0.00102
β_3	1068.95081	230.10187	4.64555	0.00010
β_4	–127.14660	23.38380	–5.43738	0.00001
β_5	8.31891	1.36469	6.09581	< 1e–5
β_6	–0.30269	0.04564	–6.63143	< 1e–5
β_7	0.00574	0.00081	7.06237	< 1e–5
β_8	–0.00004	0.00001	–7.40639	< 1e–5

For polynomials constructed for CO_2 emitted from passenger vehicles, their parameters were similarly compared. Table 6 presents the estimated values of statistics (6) and p-values for the test of differences of structural parameters.

Table 6. T-statistic values and p-value for the tests of differences of structural parameters

	T	p-value
β_0	–2.22406	0.02614
β_1	2.79922	0.00512
β_2	–3.30850	0.00094
β_3	3.76942	0.00016
β_4	–4.18986	0.00003
β_5	4.57649	< 1e–5
β_6	–4.93458	< 1e–5
β_7	5.26820	< 1e–5
β_8	–5.58048	< 1e–5

At the significance level $\alpha = 0.05$, the H_0 hypothesis was rejected in favor of H_1 for all structural parameters. The parameters are significantly different for the polynomial trend determined for the CO_2 emission series up to the pandemic and the polynomial trend determined for the CO_2 emission series containing the first year of the pandemic. Thus, in the case of passenger cars, the COVID-19 pandemic has significantly affected the trend in CO_2 emissions.

3.3. Light and heavy duty trucks

Trucks, which are the second largest group of vehicles registered in Poland [19, 26, 35] were then examined. As of the end of 2021, the number of registered trucks (including goods and passenger carrying vehicles) will reach 3.6 million [30], 3.0% more than a year ago. CO_2 emissions from light duty tracks (black line in Fig. 3) and heavy duty trucks (black line in Fig. 4) were analyzed.

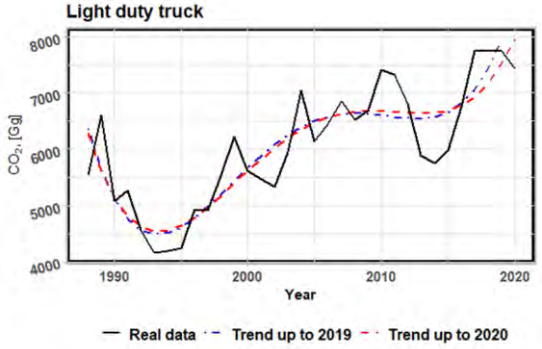

Fig. 3. CO_2 emissions for light duty truck [8]

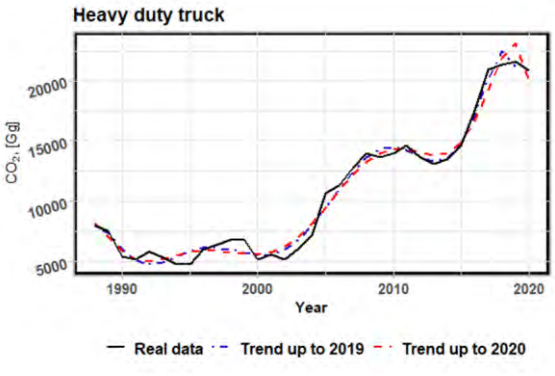

Fig. 4. CO_2 emissions for heavy duty trucks [8]

The models built for the pre-pandemic period (blue line in Fig. 3 and 4), their structural parameters, standard deviations of the parameters, values of the t-statistic and p-values are presented in Table 7.

Table 7. Structural parameters, standard errors, values of t-statistic and p-value for the trend to the pre-pandemic period

	Estimate	Std. error	t value	p-value
	Light duty truck			
β_0	7347.38426	585.58715	12.54704	< 1e–5
β_1	–1103.45576	237.77329	–4.64079	0.00008
β_2	136.30530	28.67462	4.75352	0.00006
β_3	–5.78733	1.29616	–4.46498	0.00013
β_4	0.08198	0.01950	4.20497	0.00026
	Heavy duty truck			
β_0	5669.98087	2480.91621	2.28544	0.03183
β_1	4898.82097	2959.13457	1.65549	0.11141
β_2	–3354.68039	1198.06785	–2.80008	0.01017
β_3	850.59185	230.29124	3.69355	0.00120
β_4	–106.96717	24.08233	–4.44173	0.00019
β_5	7.34736	1.44699	5.07767	0.00004
β_6	–0.27943	0.04984	–5.60608	0.00001
β_7	0.00552	0.00091	6.03490	< 1e–5
β_8	–0.00004	0.00001	–6.37530	< 1e–5

For CO_2 emissions from light duty trucks, the coefficient of determination is equal to 0.7679 and the standard deviation of the residuals is 542.63. At the significance level $\alpha = 0.05$, it was found that the structural parameters $\beta_0, \beta_1, \beta_2, \beta_3, \beta_4$ are significantly different from zero (Table 7), thus, the predictors of these parameters significantly affect the polynomial trend in the time series. The value of the statistic for the Ramsey RESET test is 2.1032, while the p-value is 0.0877.

At the significance level $\alpha = 0.05$ for heavy duty trucks, it was found that parameters $\beta_0, \beta_2, \beta_3, \beta_4, \beta_5, \beta_6, \beta_7, \beta_8$ are significantly different from zero (Tab. 7), thus predictors at these parameters significantly affect the trend of CO_2 emissions. The value of the statistic for the Ramsey test is 1.4937, while the p-value is 0.305. The coefficient of determination is higher and equal to 0.9856. The standard deviation of the residuals, meanwhile, is 731.88.

The models built for the entire study period (red line in Fig. 3 and 4), their structural parameters, standard deviations, t-statistic values and p-values are presented in Table 8.

Table 8. Structural parameters, standard errors, values of t-statistic and p-value for the trend for the entire period

	Estimate	Std. error	t value	p-value
	Light duty truck			
β_0	7166.73855	585.40978	12.24226	< 1e–5
β_1	–993.26539	230.94782	–4.30082	0.00019
β_2	119.85381	27.04951	4.43091	0.00013
β_3	–4.92894	1.18699	–4.15246	0.00028
β_4	0.06762	0.01733	3.90227	0.00055
	Heavy duty truck			
β_0	8345.93187	2968.73528	2.81128	0.00967
β_1	931.14915	3455.01664	0.26951	0.78984
β_2	–1480.57710	1362.30067	–1.08682	0.28791
β_3	445.58876	254.67973	1.74960	0.09296
β_4	–60.51175	25.88150	–2.33803	0.02805
β_5	4.33818	1.51046	2.87209	0.00839
β_6	–0.16909	0.05052	–3.34697	0.00269
β_7	0.00338	0.00090	3.76141	0.00096
β_8	–0.00003	0.00001	–4.11824	0.00039

For CO_2 emissions from light duty trucks, the coefficient of determination for the entire study period is 0.7621 and the standard deviation of the residuals is 554.42. At the significance level $\alpha = 0.05$, thus all parameters of the model are significantly different from zero. For the trend model of CO_2 emissions generated by heavy duty trucks, the coefficient of determination is 0.9792, and the standard deviation of the residuals is 913.5. At the significance level $\alpha = 0.05$, it was found that the structural parameters $\beta_0, \beta_4, \beta_5, \beta_6, \beta_7, \beta_8$ significant are different from zero, thus the predictors at these parameters significantly affect the trend occurring in the time series.

Comparing the two models with each other for each of the modes of transport analyzed, it can be seen again that the COVID-19 pandemic also affected the trend of CO_2 emissions from trucks. Table 9 presents the values of statistic (6) and p-values for the test of differences in the structural parameters. For light duty trucks at the significance level $\alpha = 0.05$, the H_0 hypothesis was rejected in favor of H_1 for the structural parameters β_2, β_3, β_4, while for heavy duty trucks the parameters β_0, β_1, β_2, β_3, β_4, β_5, β_6, β_7, β_8 are significantly different for the polynomial trend determined for the CO_2 emission series up to the pandemic and the polynomial trend determined for the CO_2 emission series containing the first year of the pandemic.

Table 9. T-statistic values and p-value for the tests of differences of structural parameters

	T	p-value		T	p-value
	Light duty truck			Heavy duty truck	
β_0	1.14388	0.25267	β_0	–3.35853	0.00078
β_1	–1.74252	0.08142	β_1	4.23413	0.00002
β_2	2.18704	0.02874	β_2	–5.01350	< 1e–5
β_3	–2.55875	0.01051	β_3	5.72280	< 1e–5
β_4	2.88339	0.00393	β_4	–6.37357	< 1e–5
			β_5	6.97556	< 1e–5
			β_6	–7.53647	< 1e–5
			β_7	8.06220	< 1e–5
			β_8	–8.55730	< 1e–5

3.4. Motorcycles

The analyses conducted ended with a study of motorcycles. Despite their growing popularity — 23,910 new motor-

cycles were registered in 2022, 10.8% more than in the previous year [30, 35]. It is clear that CO_2 emissions have been on a downward trend over the years (black line Fig. 5).

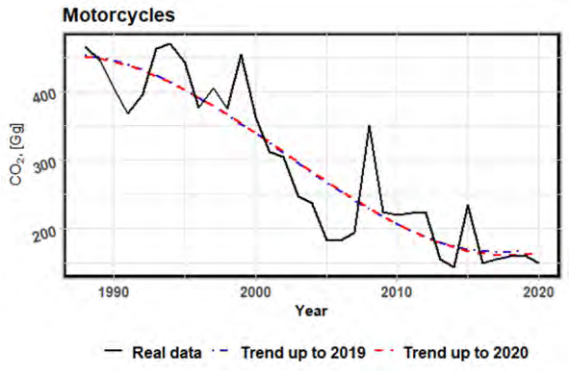

Fig. 5. CO_2 Emission for Motorcycles [8]

The estimators of parameters of the model constructed for the pre-pandemic period (blue line in Fig. 5), standard deviations of parameters, t-statistics and p-values are presented in Table 10.

Table 10. Structural parameters, standard errors, values of t-statistic and p-value for the trend to the pre-pandemic period

	Estimate	Std. error	t value	p-value
β_0	452.59779	17.62924	25.67313	< 1e–5
β_2	–0.94515	0.16588	–5.69780	< 1e–5
β_3	0.02087	0.00535	3.90082	0.00052

The coefficient of determination is 0.8293 and the standard deviation of the residuals is 48.66. At the significance level $\alpha = 0.05$, the H_0 hypothesis was rejected in favor of H_1 for the structural parameters β_0, β_2, β_3, thus the predictors of these parameters significantly affect the polynomial trend in the time series. The value of the statistic for the Ramsey RESET test is 1.3867, while the p-value is 0.2638.

The estimator of model parameters for the entire study period (red line in Fig. 5), standard deviations of parameters, t-statistics and p-values are presented in Table 11.

Table 11. Structural parameters, standard errors, values of t-statistic and p-value for the trend to the entire period

	Estimate	Std. error	t value	p-value
β_0	451.31832	17.10369	26.38718	< 1e–5
β_2	–0.91973	0.15152	–6.07003	< 1e–5
β_3	0.01992	0.00474	4.20027	0.00022

The coefficient of determination is 0.8368, and the standard deviation of the residuals is 47.97. At the significance level $\alpha = 0.05$, the H_0 hypothesis was rejected in favor of H_1 for the structural parameters β_0, β_2, β_3, thus the predictors at these parameters significantly affect the polynomial trend in the time series.

Comparing the parameters of the models for each period this time led to different conclusions. At the significance level $\alpha = 0.05$, there is no basis to reject the H_0 hypothesis for all structural parameters. Thus, the parameters are not significantly different for the polynomial trend determined for the CO_2 emission series up to the pandemic and the polynomial trend determined for the CO_2 emission series containing the first year of the pandemic. The trend parameters of the period up to the pandemic and the period with the onset of the pandemic are not significantly different, thus there was no significant effect on the trend. Table 12 presents the values of statistic (6) and p-values for the structural parameter difference test.

Table 12. T-statistic values and p-value for the tests of differences of structural parameters

	T	p-value
β_0	0.28281	0.77732
β_2	–0.61391	0.53927
β_3	0.72418	0.46895

This result of the study of CO_2 emissions from motorcycles is probably due to the fact that traveling on a motorcycle was not associated with an increased risk of danger, as all single-track vehicles were a safe means of transport from the point of view of virus infection. This is why the result is so different from other modes of transport.

4. Conclusion

The primary objective of the study was to assess whether the COVID-19 pandemic significantly affected CO_2 emissions from road transport. A general analysis was made first, without distinguishing between different modes of transport, and then passenger cars, light and heavy-duty trucks and motorcycles were examined. It turned out that only in the case of motorcycles was the impact of the pandemic not significant. Thus, global mobility restrictions and probably the fear of becoming infected have influenced public behavior. Despite the woeful pandemic period, meaningful conclusions can also be drawn. The study shows that changes are possible regarding CO_2 emissions from transport, but they require comprehensive, systemic solutions.

The obtained results clearly prove that it is possible to implement mechanisms for controlling society on a global scale and to achieve the desired results in terms of harmful emissions. The solutions implemented in this area require the use of appropriate analysis methods that will allow for a reliable assessment of whether the implemented changes bring the expected results and whether the obtained effect is statistically significant. The method proposed in the article can be successfully used for such analyses. The algorithm proposed in the methodological chapter is universal and can also be applied to factors other than the COVID-19 pandemic. This is an additional advantage of the article.

In early 2023, the European Parliament approved new targets to reduce CO_2 emissions produced by new passenger and goods carrying vehicles by 100 percent by 2035 compared to 2021. With regard to the results presented, these assumptions seem difficult to implement. Over the entire period studied, for every mode of transport except motorcycles, the research presented shows an upward trend. Only the COVID-19 pandemic caused small declines but only for passenger cars and heavy duty trucks. Thus, changes in this area are necessary. Given the short time left for Poland and the European Union as a whole to achieve climate neutrali-

ty, it is necessary to introduce the principles of sustainable development and take a holistic view of the environmental impact of individual modes of transport.

In the article, the study was conducted at a general level, observing global trends and considering whether they are possible to change. This provides the basis for more detailed analyzes and the search for relationships between specific solutions and CO_2 emissions.

In addition, due to the fact that the publication of emissions data is delayed, so the authors have not had the opportunity to make a study based on complete historical data, it is necessary to continue research and analyze trends. However, this will be the direction of further research planned in this area.

Bibliography

[1] Advani M, Sharma N, Dhyani R. Mobility change in Delhi due to COVID and its' immediate and long term impact on demand with intervened non motorized transport friendly infrastructural policies. Transport Policy. 2021;111:28-37. https://doi.org/10.1016/j.tranpol.2021.07.008

[2] Antosiewicz M, Gorzałczyński A, Rabiega W. The role of public transport in Poland in the pursuit of climate neutrality (in Polish). 2023. https://managerplus.pl/rola-transportu-publicznego-w-polsce-w-dazeniu-do-neutralnosci-klimatycznej-54351 (accessed on 30.04.2023).

[3] Borucka A, Kozłowski E, Oleszczuk P, Świderski A. Predictive analysis of the impact of the time of day on road accidents in Poland. Open Engineering. 2021;11(1):142-150. https://doi.org/10.1515/eng-2021-0017

[4] Borucka A, Pyza D. Influence of meteorological conditions on road accidents. A model indexed by: for observations with excess zeros. Eksploat Niezawodn. 2021;23(3):586-592. https://doi.org/10.17531/ein.2021.3.20

[5] de Blas I, Mediavilla M, Capellán-Pérez I, Duce C. The limits of transport decarbonization under the current growth paradigm. Energy Strateg Rev. 2020;32:100543. https://doi.org/10.1016/j.esr.2020.100543

[6] Eisenmann C, Nobis C, Kolarova V, Lenz B, Winkler C. Transport mode use during the COVID-19 lockdown period in Germany: The car became more important, public transport lost ground. Transp Policy. 2021;103:60-67. https://doi.org/10.1016/j.tranpol.2021.01.012

[7] European Environment Agency, Air quality in Europe 2022. https://www.eea.europa.eu/publications/air-quality-in-europe-2022

[8] European Environment Agency. National emissions reported to the UNFCCC and to the EU Greenhouse Gas Monitoring Mechanism. https://www.eea.europa.eu/en/datahub/datahubitem-view/3b7fe76c-524a-439a-bfd2-a6e4046302a2

[9] Global Carbon Atlas. CO_2 Emissions |Global Carbon Atlas. Globalcarbonatlas.org. 2020. http://www.globalcarbonatlas.org/en/CO2-emissions

[10] Going climate-neutral by 2050. A strategic long-term vision for a prosperous, modern, competitive and climate-neutral EU economy. 2050 long-term strategy (europa.eu)

[11] Gössling S, Humpe A, Fichert F, Creutzig F. COVID-19 and pathways to low-carbon air transport until 2050. Environ Res Lett. 2021;16(3):034063. https://doi.org/10.1088/1748-9326/abe90b

[12] Graba M, Bieniek A, Prażnowski K, Hennek K, Mamala J, Burdzik R et al. Analysis of energy efficiency and dynamics during car acceleration. Eksploat Niezawodn. 2023;25(1): 17. https://doi.org/10.17531/ein.2023.1.17

[13] Griffiths S, Furszyfer Del Rio D, Sovacool B. Policy mixes to achieve sustainable mobility after the COVID-19 crisis. Renew Sust Energ Rev. 2021;143:110919. https://doi.org/10.1016/j.rser.2021.110919

[14] Groll W, Sowiński B, Konowrocki R. Study of transitional phenomena in rail vehicle dynamics in relation to the reliability and operational state of the continuous welded rail track in terms of rail joints. Eksploat Niezawodn. 2023; 25(1):7. https://doi.org/10.17531/ein.2023.1.7

[15] Hamilton JD. Time series analysis, Princeton University Press. 1994. https://doi.org/10.1515/9780691218632

[16] IEA. Net Zero by 2050 – Analysis. IEA. 2021. https://www.iea.org/reports/net-zero-by-2050

[17] International Energy Agency. CO_2 Emissions in 2022. https://iea.blob.core.windows.net/assets/3c8fa115-35c4-4474-b237-1b00424c8844/CO2Emissionsin2022.pdf

[18] Kozłowski E, Borucka A, Świderski A, Skoczyński P. Classification trees in the assessment of the road–railway accidents mortality. Energies. 2021;14(12):3462. https://doi.org/10.3390/en14123462

[19] Kukulski J, Lewczuk K, Góra I, Wasiak M. Methodological aspects of risk mapping in multimode transport systems. Eksploat Niezawodn. 2023;25(1):19. https://doi.org/10.17531/ein.2023.1.19

[20] Le Quéré C, Jackson RB, Jones MW, Smith AJP, Abernethy S, Andrew RM et al. Temporary reduction in daily global CO_2 emissions during the COVID-19 forced confinement. Nat Clim Change. 2020;10(10):1-7. https://www.nature.com/articles/s41558-020-0797-x

[21] Lee TH, White H, Granger CWJ. Testing for neglected nonlinearity in time series models. J Econometrics. 1993; 56(3):269-290. https://doi.org/10.1016/0304-4076(93)90122-L

[22] Li B, Wang J, Wang J, Zhang L, Zhang Q. A comprehensive study on emission of volatile organic compounds for light duty gasoline passenger vehicles in China: Illustration of impact factors and renewal emissions of major compounds. Environ Res. 2021;193:110461. https://doi.org/10.1016/j.envres.2020.110461

[23] Mączak J, Więcławski K, Szczurowski K. New approach of model based detection of early stages of fuel injector failures. Eksploat Niezawodn. 2023;25(1):6. https://doi.org/10.17531/ein.2023.1.6

[24] Melnik R, Koziak S, Dižo J, Kuźmierowski T, Piotrowska E. Feasibility study of a rail vehicle damper fault detection by artificial neural networks. Eksploat Niezawodn. 2023; 25(1):5. https://doi.org/10.17531/ein.2023.1.5

[25] National Cluster of Innovative Enterprises, Poland 3.0 – A response to modern transport needs (in Polish: Ogólnopolski Klaster Innowacyjnych Przedsiębiorstw, Polska 3.0 – Odpowiedź na współczesne potrzeby transportu). 2016. http://klasterip.pl/polska-3-0-odpowiedz-na-wspolczesne-potrzeby-transportu-jedyny-spojny-projekt-infrastrukturalny-w-polsce/

[26] Oszczypała M, Ziółkowski J, Małachowski J. Semi-Markov approach for reliability modelling of light utility vehicles. Eksploat Niezawodn. 2023;1:25(2). https://doi.org/10.17531/ein/161859

[27] Papalexiou SM, Montanari A. Global and regional increase of precipitation extremes under global warming. Water Resour Res. 2019;55(6):4901-4914. https://doi.org/10.1029/2018WR024067
[28] Ramsey JB. Tests for specification errors in classical linear least-squares regression analysis. J Roy Stat Soc B Met. 1969;31(2):350-371. https://www.jstor.org/stable/2984219
[29] Regulation of the European Parliament and of the Council amending Regulation (EU) 2018/842 on binding annual greenhouse gas emission reductions by Member States from 2021 to 2030 contributing to climate action to meet commitments under the Paris Agreement. https://eur-lex.europa.eu/legal-content/PL/TXT/?uri=CELEX:52021PC0555
[30] Road transport in Poland in the years 2020 and 2021 (in Polish), Główny Urząd Statystyczny Warszawa, Szczecin 2023.
[31] Rojas C, Muñiz I, Quintana M, Simon F, Castillo B, de la Fuente H et al. Short run "rebound effect" of COVID on the transport carbon footprint. Cities. 2022;131:104039. https://www.sciencedirect.com/science/article/pii/S0264275122004784.
[32] Rojas-Rueda D, Morales-Zamora E. Built environment, transport, and COVID-19: a review. Current Environmental Health Reports. 20215;8(2):138-145. https://doi.org/10.1007/s40572-021-00307-7
[33] Schulte-Fischedick M, Shan Y, Hubacek K. Implications of COVID-19 lockdowns on surface passenger mobility and related CO_2 emission changes in Europe. Appl Energ. 2021; 300:117396. https://doi.org/10.1016/j.apenergy.2021.117396
[34] Shumway RH, Stoffer DS. Time series analysis and its applications, Springer International Publishing. 2017.
[35] Statistics | Information Portal of the Central Register of Vehicles and Drivers (in Polish). www.cepik.gov.pl. http://www.cepik.gov.pl/statystyki
[36] Thompson JR, Gosling SN, Zaherpour J, Laizé CLR. Increasing risk of ecological change to major rivers of the world with global warming. earth's future. Earth's Future. 2021;9(11):1-20. https://doi.org/10.1029/2021EF002048
[37] United Nations. Fact Sheet Climate Change. https://www.un.org/sites/un2.un.org/files/media_gstc/FACT_SHEET_Climate_Change.pdf
[38] Wang J, Guan Y, Wu L, Guan X, Cai W, Huang J et al. Changing lengths of the four seasons by global warming. Geophys Res Lett. 2021;22:48(6). https://doi.org/10.1029/2020GL091753
[39] Weiss M, Paffumi E, Clairott M, Drossinos Y, Vlachos T, Bonnel P et al. Including cold-start emissions in the Real-Driving Emissions (RDE) test procedure. Publications Office of the European Union. 2017. https://publications.jrc.ec.europa.eu/repository/bitstream/JRC105595/kjna28472enn.pdf
[40] Woodward WA, Gray HL, Elliott AC. Applied time series analysis with R, CRC Press. 2017. https://doi.org/10.1201/9781315161143
[41] Wooldridge JM. Introductory econometrics: a modern approach, South Western Educ Pub. 2019.
[42] Zhang R, Zhang J. Long-term pathways to deep decarbonization of the transport sector in the post-COVID world. Transp Policy. 2021;110:28-36. https://doi.org/10.1016/j.tranpol.2021.05.018

Anna Borucka, DSc., DEng. – Faculty of Security, Logistics and Management, Military University of Technology, Poland.
e-mail: *anna.borucka@wat.edu.pl*

Edward Kozłowski, DSc., DEng. – Faculty of Management, Lublin University of Technology, Poland.
e-mail: *e.kozlovski@pollub.pl*

Article citation info:
Chijioke EG, Teodorczyk A. CFD simulation of a vortex-controlled diffuser for a jet engine burner. Combustion Engines. 2023;195(4): 71-82. https://doi.org/10.19206/CE-171522

Emeka Gaius CHIJIOKE
Andrzej TEODORCZYK

Combustion Engines
Polish Scientific Society of Combustion Engines

CFD simulation of a vortex-controlled diffuser for a jet engine burner

ARTICLE INFO

Received: 11 April 2023
Revised: 10 July 2023
Accepted: 23 August 2023
Available online: 11 September 2023

A computational flow analysis of an ideal vortex-controlled diffuser (VCD) was carried out. The simulation model used is the compressible Reynolds averaged Navier-Stokes equations(RANS), with the application of the RNG based k-ε turbulence model. The effects of important parameters like static pressure recovery, bleed fraction, position of bleed slot, have been studied and comparisons were made with respect to VCD without the bleed configuration and the following features were revealed: radial profiles of velocity at inlet, mid-planes and exit planes, including diffuser effectiveness (i.e. static pressure recovery), diffuser efficiency, reattachment length and diffuser total pressure loss. Results obtained by applying the RNG turbulence model show an instantaneous improvement in the diffuser efficiency that happen at reasonably minimal suction rates. From the calculations, it has been verified and shown in the analysis that the effect of the bleed positioning offers advantages in relation to where it is located.

Key words: *vortex-controlled diffuser, bleed slot, modelling, static pressure recovery, reattachment length*

1. Introduction

Huge advancements, in recent years, in the technology of different components of aircraft turbines have increased the focus on the need for the design and manufacture of short, effective diffusers suitable to be installed between the compressor and combustor and having the main goal of reducing air velocity to guarantee efficient combustion with a minimal pressure loss.

When a compressor exit velocity increases, the diffuser then needs to compensate by having higher ratio of cross sectional area as to achieve proper mixing and flow conditions for good performance and the use of annular combustors results in lower pressure losses due to their design features, with that said, it's very important to ensure adequate mixing at the diffuser outlet to maintain optimal performance characteristics.

A vortex controlled diffuser allows for precise adjustment of the pressure within specific regions of rapidly expanding fluid flows using small gaps. Heskestad is credited with originating this idea [9]. In his work, the incorporation of edge suction that was fitted at the edge of the curved surface helped to channel the flow to a border in a way that considerably shorten the length of the recirculation zone. Heskestad [8] also did an investigation on edge suction at the step expansion of a circular pipe, analyzing the usefulness of the structure for a short diffuser. Here, he applied a consistent inlet profile with a fine boundary layer. He indicated that the structural design of the suction slot in addition to the suction rate, affected the flow expansion. He emphasized that suction power should be taken in to factor while evaluating the diffuser's effectiveness.

The need for the manufacture of efficient diffuser to be placed between the compressor and combustor was the driving force behind the continued evolution of the vortex controlled diffuser (VCD) design.

Adkins [2] collected data using a variety of tubular and annular research diffusers with inflow to outflow cross sectional area ratios between 1.9:1 to 3.2:1 and with diffuser inlet Mach numbers and velocity-profile displacement levels that were similar to those found in engine systems. He discovered that, for modest bleed rates, diffuser lengths just 1/3 of those needed for conventional conical diffusers may be used to reach efficiencies of more than 80%. Later, Adkins studied a hybrid diffuser, which combines a VCD with
a traditional diffuser [1]. According to his findings, bleed rates were lower than those needed for the step VCD setups that had previously been researched.

The VCD's mode of operation is yet unknown. A possible theory suggests that the bleed gap creates a zone of high shear, which causes a layer of strong turbulence to condense downstream and prevent flow separation along the outer wall [2]. Others have asserted that the principal impact of suction is to merely bend or redirect the mean flow around the acute corner, shortening the recirculation region [10]. In a fluid diffusion system, the fluid naturally has the propensity to detach off the walls of the widening tunnel, change course, and stream backward toward the direction of the negative pressure [7].

In this current paper, the performance of an ideal VCD was carried out numerically. The geometry and mesh was structured using Gambit software and ANSYS FLUENT 14 used for the flow simulation. The flow simulation used the compressible Reynolds averaged Navier-Stokes equations (RANS), with application of the renormalization group (RNG) based k-ε turbulence model. The presented results describes the effects of the bleed rates applied, ranging from 0%, 1%, 1.2%, and 2%.

The findings from the diffuser with no suction configuration were provided for purposes of comparison. The velocity profiles, plots of velocity contours, static pressure rise, and pressure recovery coefficient were used to illustrate and analyze the flow structure in detail.

Chakrabarti et al. [4, 13] performed a computational simulation of a diffuser sudden expansion with fence for low Reynolds number regime and concluded that, at the

point of the neck region, a wall incorporated in a sudden expansion design affects how the flow diffuses and that a quick fence enlargement does not necessarily result in more benefits at a lower fence subtended angle (FSA) when Reynolds numbers are smaller. Aside from being reliant on Reynolds number, the average static pressure rise normally relies on the fence's location relative to the throat as well as its defined angle.

The application of multistep configuration of a sudden expansion diffuser at low Reynolds numbers provides important advantages, although there's no significant improvement in its efficiency at larger Reynolds number flow [14].

There are two primary styles of annular diffusers utilized in gas turbine combustion engines to reduce the speed of fluids, a faired and dump diffuser, both diffusers have long been a common component of aero-engine combustion. Dump diffusers have become commonly adopted due to their greater resilience to fluctuations in inflow velocity patterns and component dimensions [11, 12].

The investigation done on a dump diffuser [19], explained that, since the airspeed dispersion at the diffuser exit is inconsistent, the bleed flow through the dump location helps the dump diffuser work better and the ideal bleed rate is between 0.4 and 0.7 percent. It has been discovered that the ideal inlet vortex level and prediffuser angles are required to get an optimum static pressure recovery. Particularly for a little prediffuser angles, the dump gap prove to have a substantial impact on the static pressure recovery [6].

2. Research objectives

The objectives of this research are listed as follows:

- to give more information on the physical processes that accounts for the efficiency attained by the VCD
- to observe and analyze how the design of the vortex chamber affected diffuser effectiveness while changing the radial and axial positioning of the bleed slot X and Y respectively (see Fig. 1)
- to see how the RNG-based k-ε – model outperforms the traditional k-ε model at predicting difficult flow recirculation of this nature
- to collect and analyze the flow characteristics and properties derived from the computations.

Computational viewpoints of the present work

The computational analysis of a vortex-controlled diffuser (VCD) was performed in this paper. The calculations were done with RNG based k-ε model with enhanced wall functions. Bleed gap effects and the vortex chamber on the diffuser performance was investigated numerically. The following are the lists of certain characteristics and criteria that were taken into account:

- reattachment length, L_R
- separation of the flow within the diffuser
- pressure recovery coefficient.

3. Numerical methodology

The computational approach adopted for this research work is the compressible RANS equations suitable for motion calculation and explanation inside a traditional axisymmetric VCD setup. The mathematical model for instantaneous continuity (1), momentum (2) and energy (3) for compressible fluid are as follows:

$$\frac{\partial \bar{\rho}}{\partial t} + \frac{\partial}{\partial x_i}\left(\bar{\rho}\hat{u}_j\right) = 0 \tag{1}$$

$$\frac{\partial}{\partial t}(\bar{\rho}\hat{u}_i) + \frac{\partial}{\partial x_j}\left(\bar{\rho}\hat{u}_j\hat{u}_i\right) = -\frac{\partial p}{\partial x_i} + \frac{\partial \bar{\sigma}_{ji}}{\partial x_j} + \frac{\partial \tau_{ji}}{\partial x_j} \tag{2}$$

$$\frac{\partial}{\partial t}\left(\bar{\rho}\widehat{E}\right) + \frac{\partial}{\partial x_j}\left(\bar{\rho}\hat{u}_j\widehat{H}\right) = \frac{\partial}{\partial x_j}\left(\bar{\sigma}_{ji}\hat{u}_i + \overline{\sigma_{ji}u_i''}\right)$$
$$-\frac{\partial}{\partial x_j}\left(\bar{q}_j + c_p\overline{\rho u_j'' T''} - \hat{u}_i\tau_{ji} + \frac{1}{2}\overline{\rho u_j'' u_i'' u_i''}\right) \tag{3}$$

where u_i and x_i represents velocity components, p stands for pressure, ρ is the fluid density and τ_{ji} is the viscous stress tensor, $\bar{q}_j$ is the heat flux vector, $\widehat{E}$ is the total energy per unit mass, and $\widehat{H}$ is the total enthalpy per unit mass. Specifically,

$$\widehat{E} = \hat{e} + \frac{1}{2}\hat{u}_i\hat{u}_i \tag{4}$$

$$\widehat{H} = \hat{h} + \frac{1}{2}\hat{u}_i\hat{u}_i - \hat{e} + \frac{\bar{p}}{\bar{\rho}} + \frac{1}{2}\hat{u}_i\hat{u}_i \tag{5}$$

$$\bar{q}_j = -\overline{k_T\,\partial T/\partial x_j} \approx -\frac{c_p\hat{\mu}}{Pr}\frac{\partial \hat{T}}{\partial x_j} \tag{6}$$

where $\hat{e}$ and $\hat{h}$, represents internal energy and enthalpy per unit mass respectively.

The viscous stress term is:

$$\bar{\sigma}_{ji} \approx 2\hat{\mu}\left(\hat{S}_{ji} - \frac{1}{3}\frac{\partial \hat{u}_k}{\partial x_k}\delta_{ji}\right) \tag{7}$$

The Reynolds stress term $\tau_{ji} \equiv -\overline{\rho u_j'' u_i''}$, has a negative sign and the density can occasionally be omitted from the formulation, however, it is irrelevant if the terms are used differently as long as the expression is consistent all through the derivation. The term c_p is the heat capacity at constant pressure, and Pr is the Prandtl number which for air is approximately 0.72. The overline represents the standard average mean time, the averaging time scale is long for turbulent fluctuations, and short for unsteady mean flow. Using Sutherland's Law will help to compute the dynamic viscosity $\hat{\mu}$, which gives a relationship between the dynamic viscosity and the temperature of an ideal gas [17]. By entering the local value of temperature (T) into equation (8), Sutherland's Law can be used to calculate the local value of dynamic viscosity:

$$\mu = \mu_0\left(\frac{T}{T_0}\right)^{3/2}\left(\frac{T_0+S}{T+S}\right) \tag{8}$$

where T, is the temperature and μ_0, T_0,and S are constants, $\mu_0 = 1.716 \times 10^{-5}$ kg/(ms), $T_0 = 491.6$ Rankine (°R), and $S = 198.6$ Rankine (°R).

To close this system, its necessary to specify equation of state:

$$\bar{p} = (\gamma - 1)\left[\bar{\rho}\widehat{E} - \frac{1}{2}\bar{\rho}(\hat{u}^2 + \hat{v}^2 + \hat{w}^2) - \bar{\rho}k\right] \tag{9}$$

where k represents local turbulent kinetic energy:

$$k = \frac{1}{2}[(\hat{u}_i'')^2 + (\hat{v}_i'')^2 + (\hat{w}_i'')^2].$$

Below Favre-averaged mathematical terms need to be approximated: τ_{ji}; $c_p\overline{\rho u_j'' T''}$; $\overline{\sigma_{ji} u_i''}$; and $\frac{1}{2}\overline{\rho u_j'' u_i'' u_i''}$.

Reynolds stress terms (τ_{ji}) are the main subject in most turbulence calculations. The Reynolds-stress tensor is a symmetric tensor ($\tau_{ji} = \tau_{ij}$), and thus it has six independent components that have to be modelled. Therefore to solve Eq. (2), it is necessary to find enough equations to close the system.

The tensor is modelled using the Boussinesq approximation [18], thus the Reynolds stress tensor is given by:

$$\tau_{ji} = 2\hat{\mu}_t\left(\hat{S}_{ji} - \frac{1}{3}\frac{\partial \hat{u}_k}{\partial x_k}\delta_{ji}\right) - \frac{2}{3}\bar{\rho}k\delta_{ij} \tag{10}$$

$$\hat{S}_{ji} = \frac{1}{2}\left(\frac{\partial u_i}{\partial x_j} + \frac{\partial u_j}{\partial x_i}\right) \tag{11}$$

where $\hat{\mu}_t$ – represents eddy viscosity, $\hat{S}_{ji}$ – represents strain-rate tensor, k – represents the specific kinetic energy, ρ – the density, the operator δ_{ij} – is the Kronecker delta.

Equation (12) describes the turbulent heat flux model:

$$c_p\overline{\rho u_j'' T''} \approx -\frac{c_p\hat{\mu}_t}{Pr_t}\frac{\partial \hat{T}}{\partial x_j} \tag{12}$$

where Pr_t stands for turbulent Prandtl number, having a constant number around 0.9 for air. Different models are used to represent the terms associated with turbulent transport and molecular diffusion in the energy equation. For instance:

$$\overline{\sigma_{ji} u_i''} - \frac{1}{2}\overline{\rho u_j'' u_i'' u_i''} \approx \left(\hat{\mu} + \frac{\hat{\mu}_t}{\sigma_k}\right)\frac{\partial k}{\partial x_j} \tag{13}$$

where σ_k is a coefficient associated with the modeling equation for k.

3.1. Turbulence model

Unsteady velocity fields are a defining characteristic of turbulent flows. The unsteady flow would combine with transported quantities such as momentum, energy, and species concentration, causing the transported quantities to fluctuate as well. The Reynolds stress turbulence model is implemented in the program. The choice of the k-ε model is dictated by the calculation time and the recommendations of the k-ε model for the analyzed class of flows.

3.2. The RNG k-ε model

Previous experiments have pointed out that the RNG based models does yield results that are preferable to those of the conventional k-ε model in relation to boundary layer, extreme strained, separated and high laminar bending flows [16].

The instantaneous Navier-Stokes equations are used to develop the RNG-based k-ε turbulence model by employing the RNG computational method. The RNG model has an extra component in its ε calculation that considerably increases the reliability for unsteady shear flows. Only turbulent areas along a radial plane that are not closed to the wall are suitable for the k-ε models. High Reynolds number turbulent flow requires a separate wall modeling to connect the 100% turbulent state and the close to the wall frictional zone. In order to depict flow characteristics like separation effectively, the near wall region must be adequately structured.

4. Computational investigation of the vortex-controlled diffuser (VCD)

The fundamental objectives of this work was to clarify the governing flow mechanics of a VCD by altering the values of the radial and axial distance Y, X respectively (see Fig. 1). The examination initially focuses on the bleed effectiveness and the reattachment mechanism. In order to compare and achieve these objectives, flow simulations were conducted for a basic, 2D VCD without a bleed configuration (Fig. 2). When performing such CFD calculation, it's crucial to make sure the result is realistic within the parameters of the model assumptions employed and grid independent. The basic 2D VCD study would help to:

- develop a grid-based solution
- evaluate the effectiveness of the turbulent model
- apply and check for suitable boundary conditions
- achieve grid independence.

After the study, the concluded methodology was then maintained throughout the CFD analysis, and covering its findings reported in the subsequent chapters.

4.1. Flow domain arrangement

The structure of the VCD with and without the bleed configuration were created using "GAMBIT" modeling software (see Fig. 1 and 2), the inlet diameter is 0.031 m, the overall area ratio is 1.612 and a non-dimensional length. Only half of the geometry is taken into account (an axisymmetric flow calculation). The two-dimensionality allows an axisymmetric boundary condition at mid inlet duct height, where by reducing both the computing effort and the number of grid cells in half.

Referring to Fig. 1, is a primary duct positioned in a secondary duct, with a structured vortex fence placed in the secondary duct downhill of the primary duct's outlet, a bleed duct used for the air pressure regulation is located within the secondary duct. when a little passage of air is allowed using the bleed duct, it enables the incoming stream of air from the primary duct to diffuse quickly, receiving substantially smaller amounts of air in the secondary duct. The velocity of the inflow air is changed by altering the rate of bleed flow, which changes the quantity of air that travels down the secondary duct.

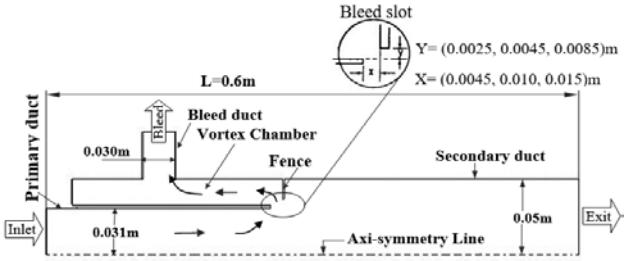

Fig. 1. Vortex-controlled diffuser (VCD) computational domain, with the bleed configuration

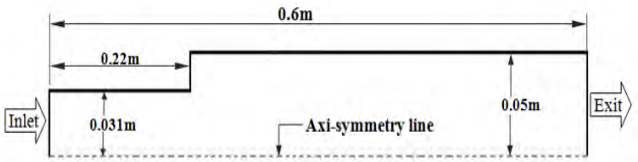

Fig. 2. Fluid domain of the VCD with no bleed configuration

4.2. Computational grid

The fluid flow area was meshed after the VCD models were generated. A multi-block structural mesh was created with a boundary layer close to the recirculation region from the step as shown in Fig. 3 and 4, boundary layer meshing was applied in order to handle the strong velocity fluctuations and for better visualization of fluid characteristics around this region.

4.3. Grid sensitivity study

A detailed grid-independent investigations have been conducted with the goal to choose the appropriate grid size by adjusting the node spacing on the edges and utilizing the standard mesh law approach. The first order discretization methods, the RNG k-ε model, and enhanced wall functions were used to study the grid-independence employing three different sizes of grids. As the mesh size decreases, the more fine mesh is obtained, providing best results and the length of recirculation increases as the mesh size is increased. Table 1 shows the three tested mesh sizes.

Table 1. Three tested mesh sizes

Grid No.	Mesh	Element Type	No. of Cells	No. of Face	No. of Nodes
1.	Coarse mesh (No boundary layer)	**Quad.**	**1985**	**4149**	**2165**
2.	Fine mesh	**Quad.**	**3064**	**6333**	**3270**
3.	Finer mesh	**Quad.**	**4782**	**9846**	**5065**

Grid independence was checked on the static pressure recovery as depicted in Fig. 5, we can observe that the calculation with grid number 2 indicates little change in the static pressure rise compared to the result from grid number 3. Hence, further grid refinement seems unnecessary. Grid number 2 was used for the present analysis.

Streamline plots of velocity magnitude for every grid generated are depicted in Fig. 6, it illustrates the variations in the recirculation flow development and flow reattachment lengths, L_R.

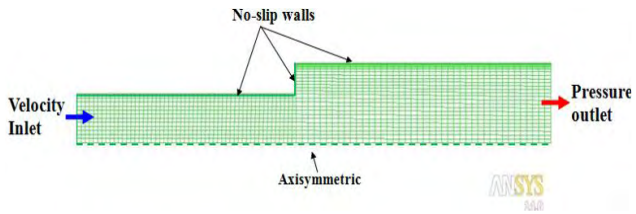

Fig. 3. VCD computational grid, with no bleed configuration

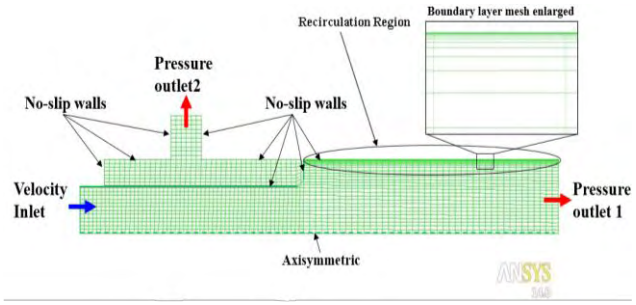

Fig. 4. VCD computational grid, with the bleed configuration (boundary layer near the recirculation region)

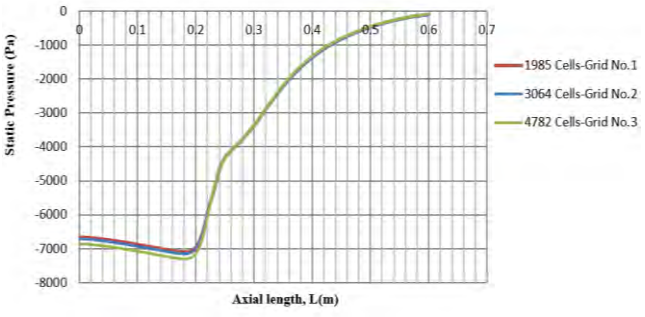

Fig. 5. Static pressure recovery for different set of grids

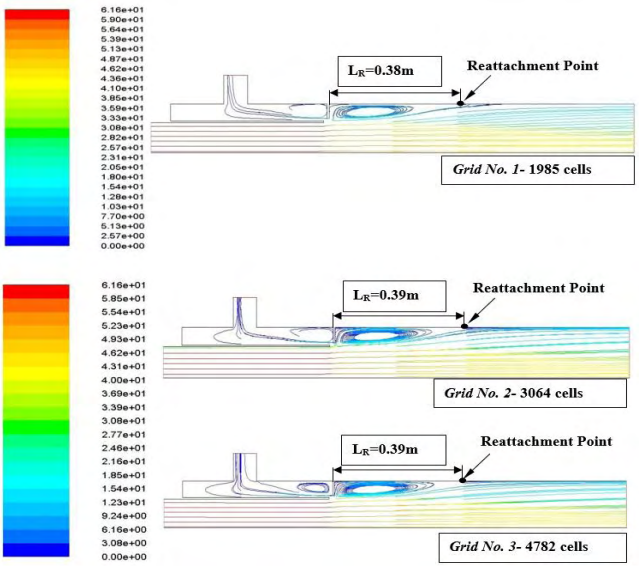

Fig. 6. Velocity streamlines at reattachment length, L_R for all set of grids in grid independence study (RNG k-ε model, Enhanced wall function, First order discretization schemes, for 1% Bleed)

A thorough understanding of the turbulent flow behavior, particularly fluctuations of the principal recirculation zone's reattachment length was offered by Schäfer [15], it was explained that the erratic shear layers separating the principal flow and the recirculation waves contain vertical patterns that cause the immediate reattachment and the secondary separation line to flutter.

4.4. Boundary conditions

Table 2 shows summary of the boundary conditions and the numerical method implemented for RNG k-ε model. Five types of boundary conditions were specified during the flow setup, which includes Inlet, Outlet, Bleed duct, Wall and Axi-symmetry constraints.

Inlet: In the current computation, velocity was set at 60 m/s as the inflow constraint with a flat profile, this value was applied in the two configured diffusers, the hydraulic diameter at the inlet is given as 0.0589 m. A predetermined level of turbulence or 1% of the corresponding flow diameter was used, therefore the turbulent intensity was set at, $I = 0.16(Re_{DH})^{-1/8}$, where Re_{DH} is the Reynolds number based on the hydraulic diameter.

Outlet: A pressure outlet having a zero pressure gauge has been selected as the outlet boundary constraint.

Bleed duct: Pressure outlet boundary constraints is specified at the bleed duct. This duct is in vertical position, therefore a negative uniform pressure was applied. The bleed rates are equal to 0%, 1%, 1.2% and 2% of the operating pressure (1 MPa).

Wall: The entire wall were applied a non-slip surface criteria. To avoid the effects of wall friction, a default friction constant, 0.5 was applied which represents a uniform sand grain roughness.

Axi-Symmetry: The computation solely addresses the top half of the geometry, an axi-symmetric boundary constraints were assigned to both generated models on the symmetry plane, and a higher-order scheme was used. The residuals of all parameters were kept in the order of 10^{-6} in the convergence solution.

The motion of fluids on each side of the mirror plane border condition is subject to restrictions known as "mirroring" conditions, i.e. the normal velocity vector is zero at the border of the symmetry axis [3].

Table 2. The list of applied flow constraints, including numerical method implemented for RNG k-ε model

CASE	**RNG**
Model	Steady, two dimensional compressible
Turbulence model	RNG k-**ε** (2 equation)
MATERIALS	
Density	Ideal-gas
Viscosity	$\mu = 1.7894 * 10^{-5}$ kg/ms
DISCRETIZATION	**Turbulent case**
Pressure	Standard
Pressure-velocity coupling	SIMPLE
Momentum	First order upwind
Turbulent kinetic energy	First order upwind
Turbulent dissipation rate	First order upwind
Energy	First order upwind

BOUNDARY CONDITIONS

Inlet	**RNG**
Velocity components, (method- magnitude and direction)	Assumed velocity 60 m/s and temperature 500 K
Turbulence intensity	Tu = 1%
Hydraulic diameter	D_H = 0.0589 m
Outlet	
Outlet pressure	Gauge pressure (Pascal) = 0
Backflow turbulent intensity	Tu = 1%
Backflow turbulent length scales	D_H = 0.0923 m
Bleed duct	
Outlet pressure	Gauge pressure (Pascal) = (0, 1, 1.2, 2)% of the operating pressure = 1 MPa
Backflow turbulent intensity	Tu = 1%
Backflow turbulent length scales	D_H = 0.057 m
STATIONARY WALL	
Shear condition	No slip

4.5. Computational flow steps

- **First step,** flow domain was generated using Gambit, then meshed with quadratic-mesh. Mesh was refined with elements from 1985–4782. Velocity and pressure criteria was set at the inlet and outlets respectively, axi-symmetry and no-slip wall conditions were applied. The fluid is an air type specification, the mesh was later exported to Fluent for simulation and analysis.
- **Second step,** further analysis was done in Fluent, the grid was resized and tested. A 2-D axi-symmetric technique, pressure based solving approach and, fluid flow parameter for air were selected. RNG k-ε model was applied. The inlet velocity of 60 m/s at temperature 500 K was applied.

Turbulence intensity of 1%, 3% and 5% based on inlet flow diameter were applied and atmospheric pressure type was specified at the outlet. First order upwind scheme was chosen. Convergence requirement was set at 10^{-6} and iterated.

5. Results and discussion

This section provides an overview of the conclusions drawn from the CFD analysis of the two dimensional VCD. To improve the diffuser's efficiency, various alterations on the geometry were made and experimented. Bleed rates for the VCD have been found to be between 0%, 1%, 1.2% and 2%.

5.1. Screening test results

The effectiveness of the VCD with the bleed configuration was checked using the following parameters, radial flow speed profiles at the inlet, middle and exit planes, static pressure recovery, diffuser efficiency, and diffuser total pressure loss.

Identifying the vortex fence placement and dimension that would produce the best diffuser effectiveness and the lowest pressure loss at practical suction rates was the first phase of the test process. Following this, the geometry that passed these tests was then assessed in light of the stated performance criteria. The values of Y and X shown in Fig. 1 above was altered in order to assess the impact of the bleed configuration on the diffuser performance. Table 3 includes the diffuser static pressure rise and reattachment length, L_R at 1% bleed rate, and it provides the conclusion of the investigation performed. The rise in static pressure along the center line for different axial gaps X with constant radial gaps Y is shown in Fig. 7–9.

The behavior or the change in static pressure along the center line may be described as follows: It begins with a fall of the static pressure across the inlet length, later the fluid at the diffuser neck begins to experience a rise in pressure caused by the abrupt expansion of the VCD's outflow space. Figure 10 shows the static pressure rise for different values of the distance, Y with fixed values of distance, X at tested maximum value, X = 0.015 m, we can observe that the static pressure increases as the radial gap Y decreases with increase in axial gap X. The pressure recovery improves as a result of this rise in static pressure, which is vital when designing a VCD. For values of X = 0.015 m and Y = 0.0025 m, the VCD performed well in the static pressure rise and reattachment length, L_R compared to other models values. The symbol (*) in Table 3 confirms the dimensions that were selected for the overall VCD design and were used for further analysis and the report discussed in this paper.

Table 3. Effect of suction chamber geometry on diffuser performance (exit rake position L = 0.4 m)

Model	Axial gap, X [m]	Radial gap, Y [m]	Inlet Mach number, M	Static pressure rise [Pa]	Reattachment length, L_R [m]	Bleed rate [%]
1	0.0045	*0.0025	0.133	–1283	0.3875	1.0
2	0.010	↓	0.133	–1035	0.3840	↓
3	*0.015	↓	*0.133	*–750	*0.3650	↓
4	0.0045	0.0045	0.133	–1204	0.4000	1.0
5	0.010	↓	0.133	–1002	0.3850	↓
6	0.015	↓	0.133	–772	0.3740	↓
7	0.0045	0.0085	0.133	–1049	0.4000	1.0
8	0.010	↓	0.133	–853	0.3863	↓
9	0.015	↓	0.133	–850	0.3862	↓
* – Final geometry chosen						

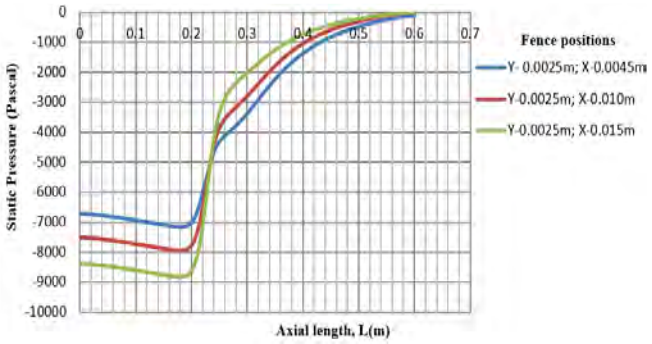

Fig. 7. Difference in static pressure rise for different values of axial gap X for fixed radial gap Y = 0.0025 m

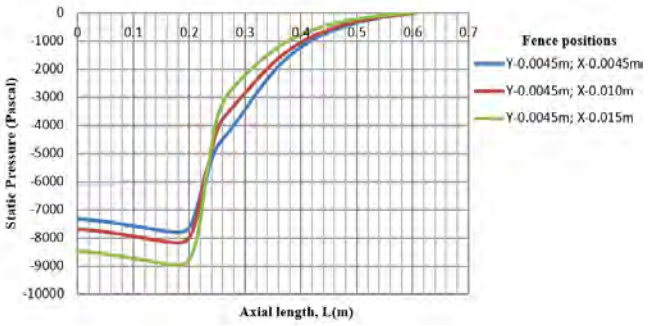

Fig. 8. Difference in static pressure rise for different values of axial gap X at fixed radial gap Y = 0.0045 m

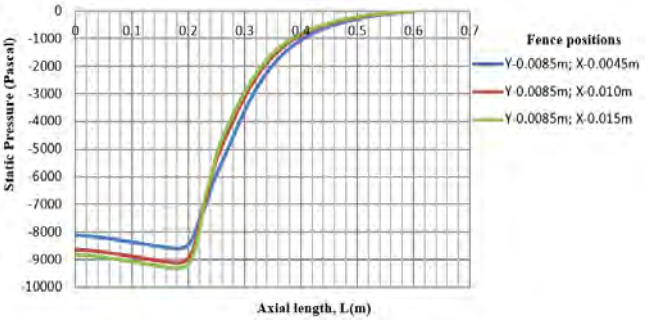

Fig. 9. Difference in static pressure rise for different values of axial gap X at fixed radial gap Y = 0.0085 m

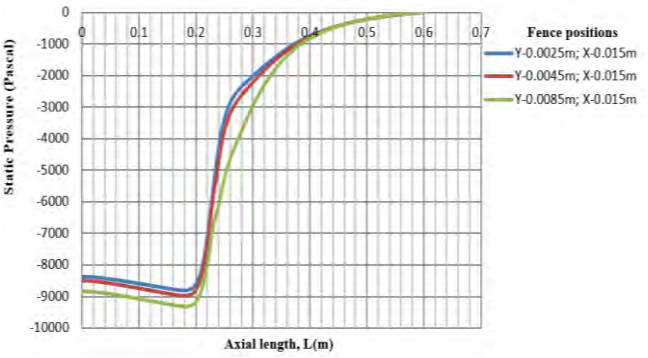

Fig. 10. Difference in static pressure rise for different values of radial gap Y for fixed axial gap X (for maximum axial gap tested X = 0.015 m)

5.2. Graphical representation of re-attachment length

The graphical reattachment length, L_R is described in Fig. 11–14. The reattachment length is determined by plotting the x-wall shear stress along the line lying close to the wall from the step. The reattachment length corresponds to the axial length at which the shear stress changes sign from negative to positive.

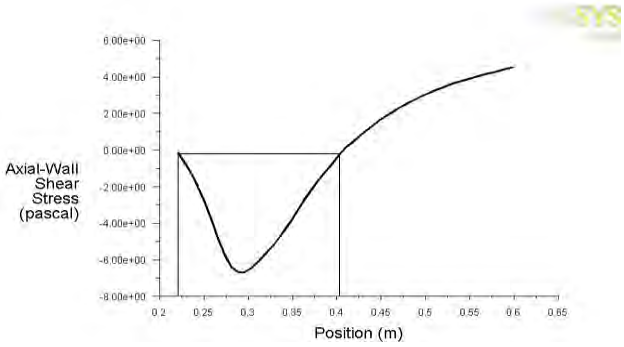

Fig. 11. Graphical representation of Re-attachment length for VCD without bleed configuration

Note that Fig. 11 is direct plot by the ANSYS software while the plots shown in Fig. 12–14 were generated using excel after exporting the corresponding result data from ANSYS, this way it was possible to plot and compare for different positions of the bleed slot and that is why in Fig. 12–14 axis starts from 0.0 and not from 0.2 as in 11.

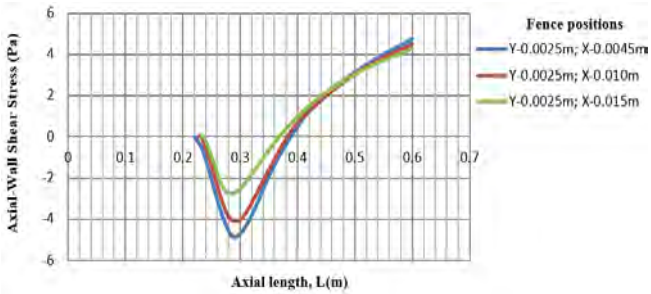

Fig. 12. Graphical representation of Re-attachment length, L_R at varying axial distance values of X at fixed radial distance Y = 0.0025 m

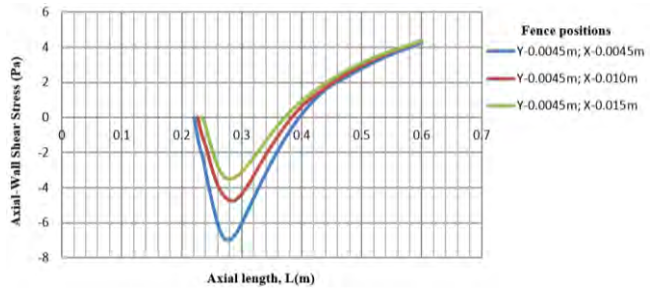

Fig. 13. Graphical representation of Re-attachment length, L_R at varying axial distance values of X at fixed radial distance Y = 0.0045 m

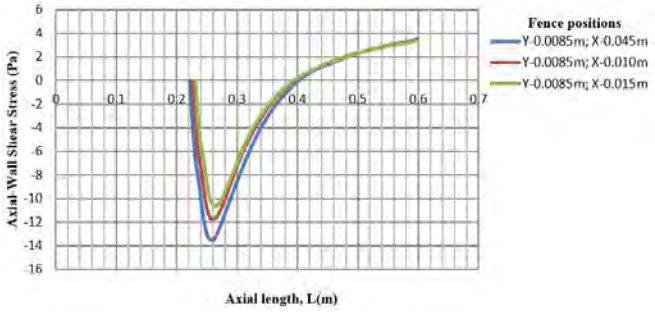

Fig. 14. Graphical representation of Re-attachment length, L_R at varying axial distance values of X at fixed radial distance Y = 0.0085 m

5.3. Conclusions drawn from the finalized vortex chamber design

This chapter presents the performance obtained with the final vortex chamber configuration. The factors listed below were additionally used to evaluate the VCD effectiveness:

- Pressure recovery coefficient:

$$C_p = \frac{P - P_1}{\frac{1}{2}\rho V_1^2} \tag{14}$$

where, P_1 and V_1 are pressure and average velocity inlet reference section.

P represents the static pressure at the location where the pressure coefficient is calculated.

- Ideal pressure recovery coefficient

$$C_{pi} = 1 - \left(\frac{1-B}{AR}\right)^2 \tag{15}$$

$$B = \frac{\dot{m}_b}{\dot{m}_1} \tag{16}$$

where B represents the bleed fraction, AR is the aspect ratio, $\dot{m}_b$ and $\dot{m}_1$ is the mass flow rate at the bleed duct and inlet respectively

- Diffuser efficiency:

$$\eta = \frac{C_p}{C_{pi}} \tag{17}$$

- Pressure loss coefficient:

$$K = C_{pi} - C_p \tag{18}$$

5.4. Static pressure gradients across the VCD's center line

The outcome of the VCD experiments with no bleed configuration and that of 0%, 1%, 1.2%, and 2% bleed is shown in Fig. 15. In this figure we can observe the initial decrease of static pressure across the primary duct (region a to b), there after the fluid starts to experience static pressure rise because of an abrupt expansion of the flow area (region b to c), the plot illustrates that when the bleed percentage rise, the static pressure rises as well. The part c to d is the vortex stabilization expression and at this stage, more increase in bleed would not have a significant effect on the VCD effectiveness. The situation associated with point c is known as the point of lowest bleed required, therefore the conclusion is that, for this particular VCD geometry the minimum bleed required for its proper performance is at bleed rate 2% at axial length, L = 0.3 m.

5.5. Pressure coefficient (Cp)

In fluid dynamics, a dimensionless number called the pressure coefficient is used to characterize the range of pressure present inside a flow field. Any location in a field of fluid motion has a different pressure coefficient. Figure 16 depicts an illustration of the pressure coefficient across the VCD center line for various bleed rates (0%, 1%, 1.2%, and 2%). As the fluid travels, the pressure coefficient rises, although at the beginning it is nearly constant.

The wall pressure coefficient (Cp), near the step corner, is negative, low, and relatively constant. It increases steadily downstream to a favorable level close to the point of reattachment. The conclusion is that the pressure coefficient rises as the bleed rates is increased.

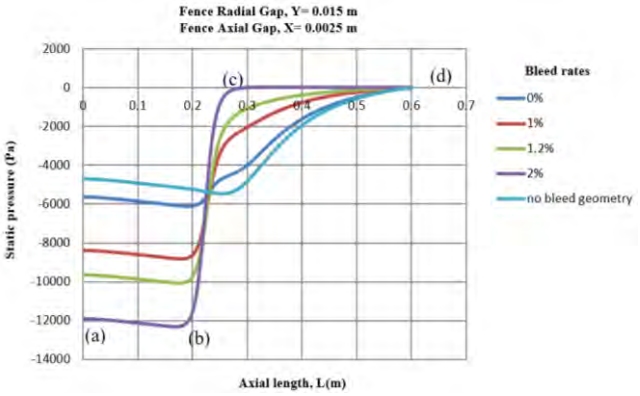

Fig. 15. Variation of static pressure rise for various bleed rates

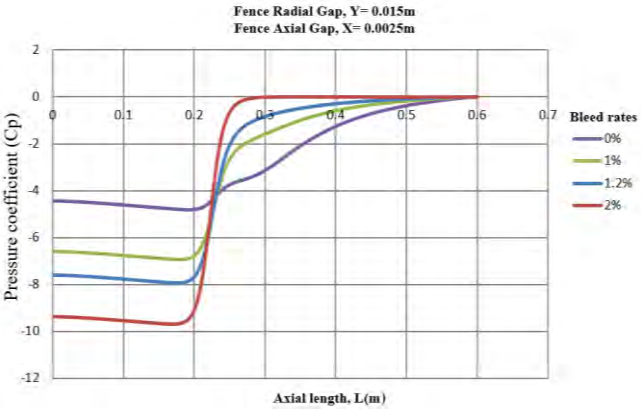

Fig. 16. Variation of pressure coefficient along the center line for various bleed rate

5.6. Static pressure contours at different bleed values

In general the static pressure varies along the length of both diffusers. Static pressure recovery is an important characteristics of an expansion diffuser. The flow pattern of static pressure for VCD with no bleed configuration and for various bleed rates are described in Fig. 17–21 respectively. For VCD without bleed configuration, Fig. 17, we can observe the gradual increase of static pressure and the region of highest static pressure recovered is at the exit of the diffuser. For the VCD with bleed rates, we can observe the region of lowest static pressure recovered mostly in the vortex chambers. In conclusion, the static pressure increases with increase in bleed rates.

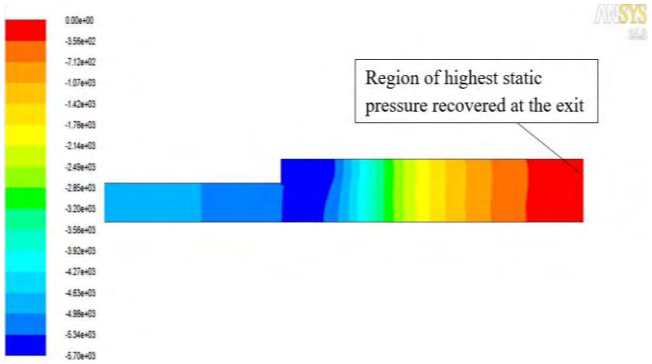

Fig. 17. Visual colors of static pressure (pascal), for VCD with no bleed configuration

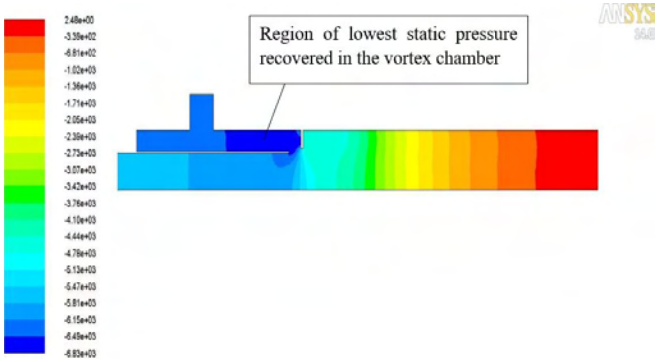

Fig. 18. Visual colors of static pressure (pascal) at 0% bleed

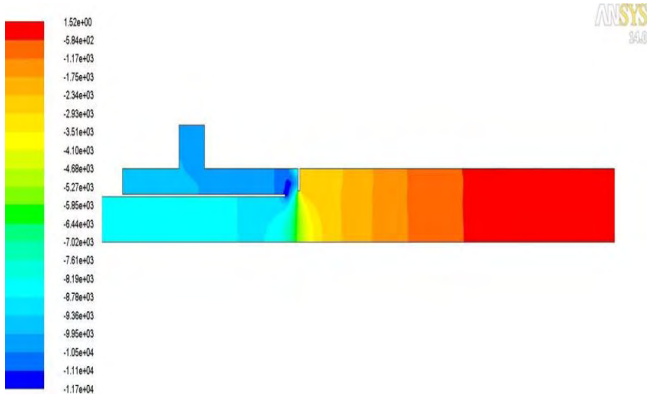

Fig. 19. Visual colors of static pressure (pascal) at 1% bleed

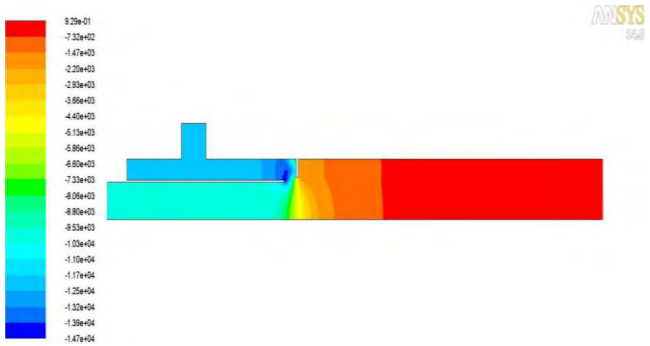

Fig. 20. Visual colors of static pressure (pascal) at 1.2% bleed

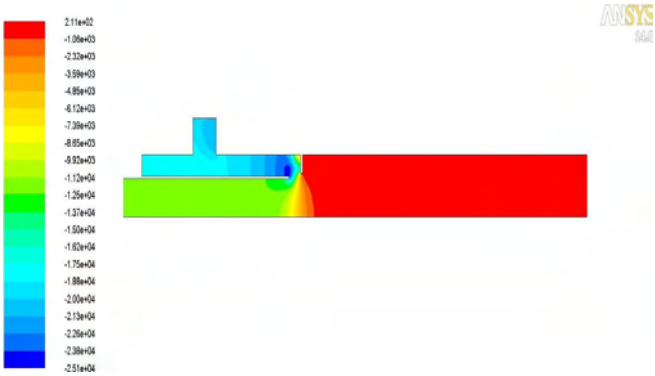

Fig. 21. Visual colors of static pressure (pascal) at 2% bleed

5.7. Streamlines of velocity magnitude

Observations were made on the recirculation and separation region. It was observed that flow separation occurred below the step boundary and free shear layer formed behind the flow separation zone as described by the streamlines of velocity magnitude in Fig. 22–25 for VCD without bleed configuration and with a bleed of 1%, 1.2% and 2% respectively. Included are the reattachment lengths, L_R, we can observe from the streamlines that the reattachment length, L_R decreases with increase in bleed rates. The more the separation reduces the more pressure is recovered.

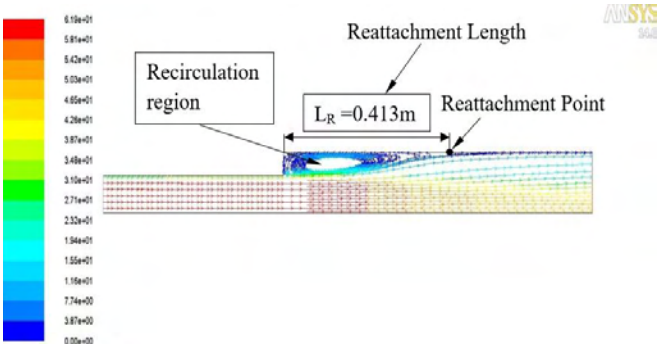

Fig. 22. Velocity magnitude (m/s) streamlines, for VCD with no bleed configuration

Rectangular region is characteristic of stationary flow. In the real flow, this vortex changes its shape and can periodically disappear, run down the stream, generating again in the corner.

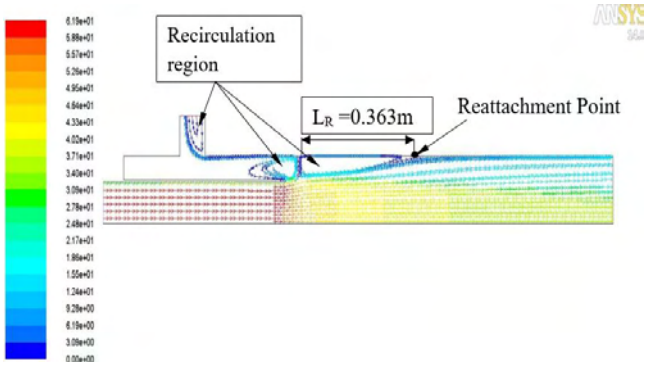

Fig. 23. Velocity magnitude (m/s) streamlines at 1% bleed

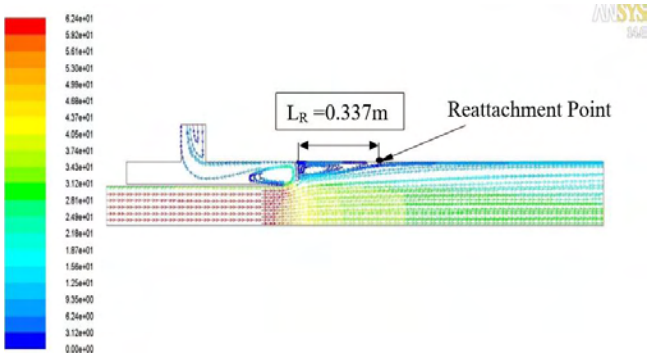

Fig. 24. velocity magnitude (m/s) streamlines at 1.2% Bleed

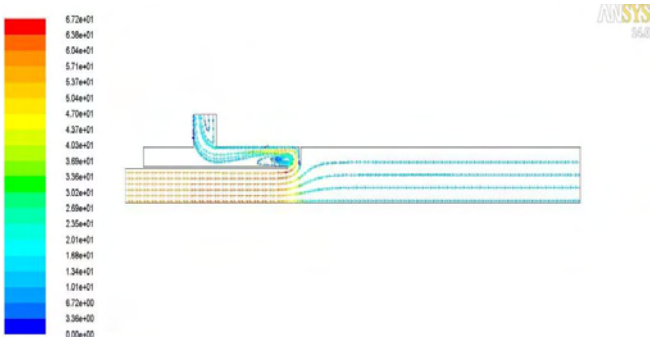

Fig. 25. Velocity magnitude (m/s) streamlines at 2% bleed, no boundary layer separation. Flow entered the vortex chamber mostly from the main stream

5.8. Variation of velocity magnitude along the center line of the VCD

Figure 26 describes the result of variation of velocity along the center line with a bleed of 0%, 1%, 1.2% and 2%, applied at the step corner. The flow behavior here can be characterized as follows: First was the acceleration of velocity along the inlet length, and later the fluid at the throat starts to display a decrease in velocity due to sudden enlargement of flow area of the VCD resulting in the formation of wall recirculation zone (see Fig. 22). In Fig. 26 we can observe that the higher the bleed the lower it is the velocity magnitude.

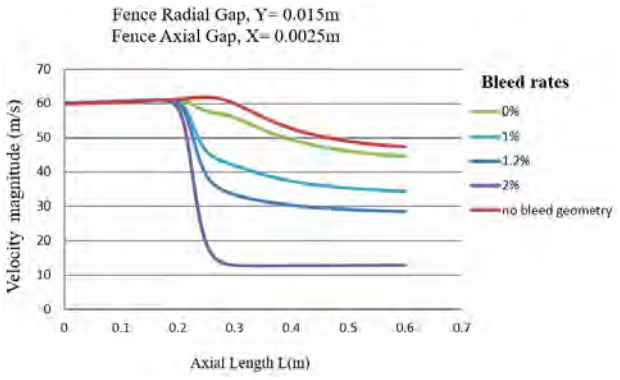

Fig. 26. Variation of velocity along the center line for different bleed rates

5.9. Radial profiles of velocity at inlet, intermediate and outlet planes

Figure 27 depicts the distribution of radial velocity at the inlet plane for different bleed levels, we can observe that at the inlet plane the bleed rates did not affect the flow velocity, the flow is uniform and fully turbulent for all bleed rates and inside the wall there is a favorable gradient i.e dU/dx > 0, dp/dx < 0 and no separation. At the mid plane, radial length, L = 0.03 m we can observe in Fig. 28 that the flow separated from the wall for all bleed rates except for bleed rate 2% which is the minimum percentage bleed rate required. The separation is an indication of unfavorable pressure slope, or dp/dx > 0. At the exit plane we can observe in Fig. 29 that the flow is fully reattached to the wall for all bleed rates indicating that there is a zero pressure gradient at the wall i.e. dU/dx = 0, dp/dx = 0 and no separation.

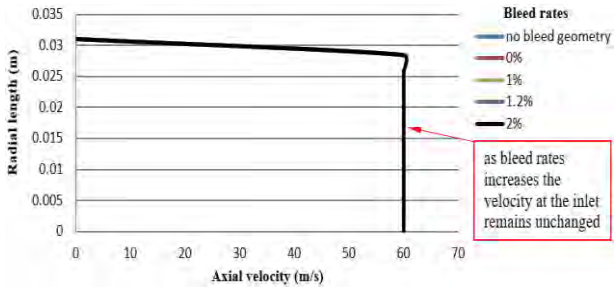

Fig. 27. Turbulent flow, radial velocity plot at the inlet plane with different bleed rates

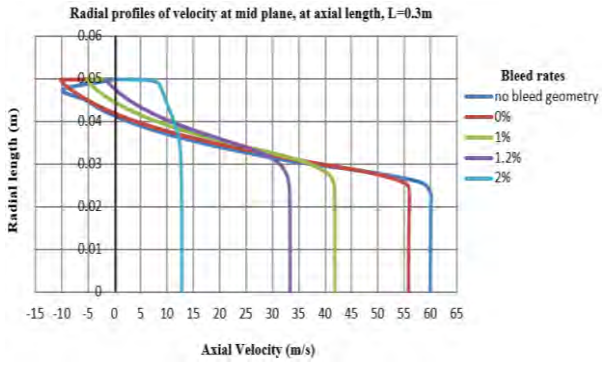

Fig. 28. Velocity radial profiles with different bleed rates at the midplane

Separation occurred except for the bleed rate 2%, which is the minimum percentage bleed rate required for this particular VCD geometry.

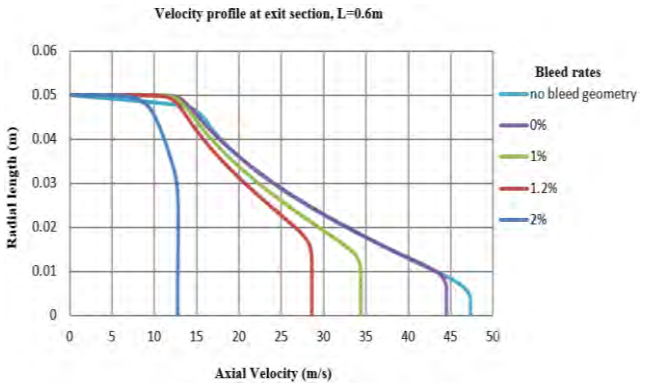

Fig. 29. Outlet plane radial velocity plot for different bleed rates

5.10. Velocity magnitude flow patterns at various bleed rates

Figures 30–34 depict the contour patterns of velocity magnitude for VCD with no bleed configuration and with a bleed of 0%, 1%, 1.2% and 2% respectively.

The contours show the weight of gradual decrease of velocity, from red (the highest value) to blue the lowest value.

In Fig. 30 the blue color close to the step corner tells the extent of boundary layer separation. The flow decreases gradually as it passes the throat due to sudden enlargement of flow area of the VCD resulting in the formation of wall recirculation region.

In Fig. 31–34 we can observe the rapid flow of air through the bleed slot as the bleed rates increases respectively. The highest rapid fluid flow through the bleed slot is observed at bleed rate 2% (see Fig. 34), this is the minimum bleed rate required for this particular VCD geometry, further increase in bleed rate greater than 2% may affect the VCD's effectiveness in terms of static pressure recovery.

In summary, observation made is that, the diffuser incorporating the bleed geometry performed better in reducing the velocity at the exit. Due to this decrease in velocity the pressure recovery at the exit improves which is important when designing a vortex controlled diffuser.

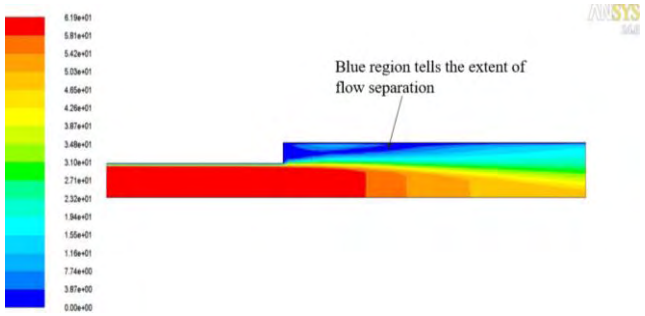

Fig. 30. Velocity magnitude (m/s) patterns with respect to the vortex controlled diffuser with no bleed configuration

5.11. Static temperature flow patterns

In the flowing figures static temperature rise for the VCD without bleed geometry and with a bleed of 1% and 1.2% are presented respectively. Generally the temperature in both geometries did not increase significantly, their orders of magnitude ranges from 500 K (initial condition) to 502 K which is not very high, it is suitable for the considered geometries.

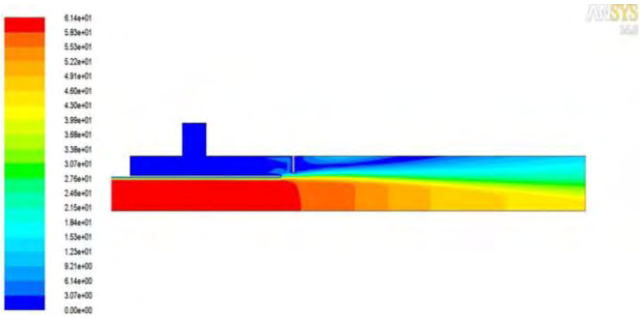

Fig. 31. Velocity magnitude (m/s) patterns at 0% Bleed

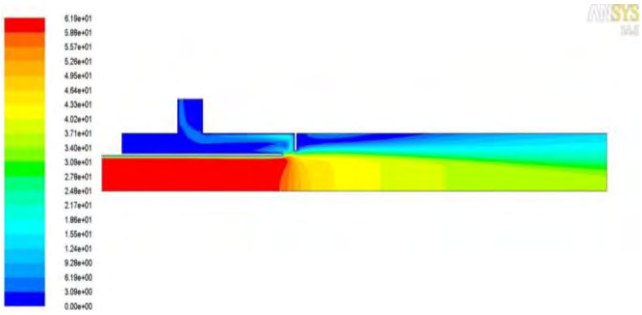

Fig. 32. Velocity magnitude (m/s) patterns at 1% bleed

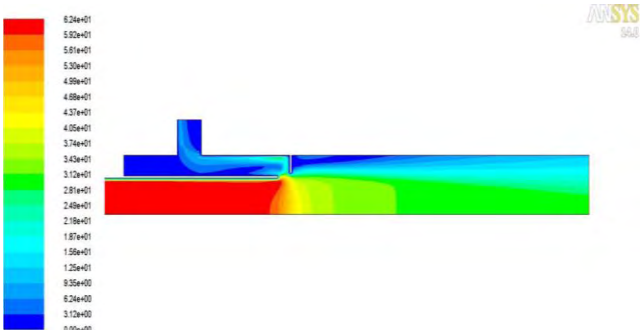

Fig. 33. Velocity magnitude (m/s) patterns at 1.2% bleed

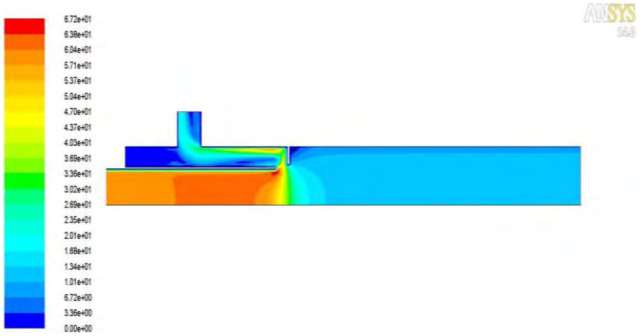

Fig. 34. Velocity magnitude (m/s) patterns at 2% bleed

In Fig. 35 the temperature rises gradually after it passes the throat, the order of magnitude is greater close to the step corner and the diffusing wall. In Fig. 36 and 37 we can observe the highest order of temperature magnitude in the vor-

tex chamber and close to the recirculation region where it is observed to be low velocity region (Bernoulli's principle).

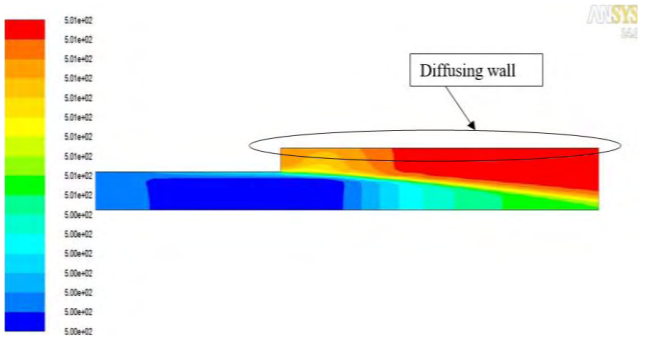

Fig. 35. Static temperature (k) patterns, with respect to the vortex controlled diffuser with no bleed configuration

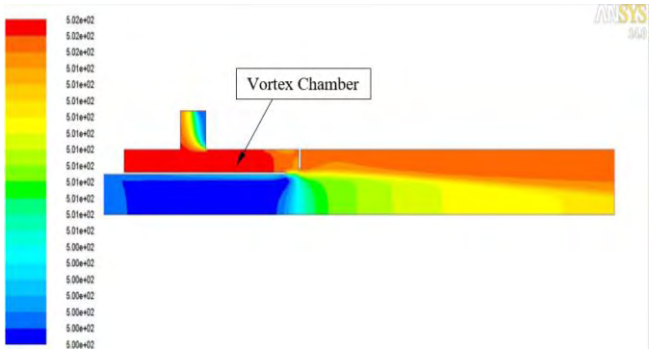

Fig. 36. Static temperature (k) patterns at 1% bleed

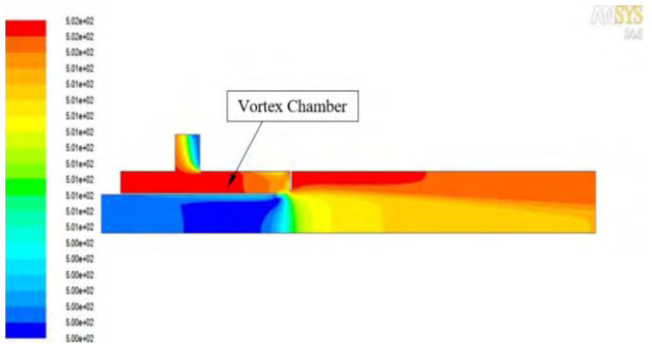

Fig. 37. Static temperature (k) patterns at 1.2% bleed

6. Summary and conclusions

A 2-D VCD effectiveness modeling has been conducted in the present study. The dimensions of Y and X shown in Fig. 1 were altered to check the efficiency of the VCD with bleed configuration. The final goal was to increase the pressure recovery inside the VCD by relieving pressure through the bleed slot.

Gambit software was used for the flow domain and mesh generation, and ANSYS FLUENT for flow modeling, applying the compressible RANS model, and RNG based k-ε for vortex flow.

Parameters like static pressure recovery, bleed fraction, position of bleed slot were observed and compared to VCD with no bleed configuration and below characteristics were found:

- When bleed is applied, the VCD acts differently from the VCD with no bleed configuration in relation to changes in total pressure inside fluid domain.
- With fixed velocity 60 m/s and specified aspect ratio, the static pressure rise improves as the bleed rates gets higher.
- The favorable dimension for the bleed fence for this particular VCD geometry is at distance, X = 0.015 m and Y = 0.0025 m close to the step corner of the VCD.
- The VCD without bleed configuration did not reduce the velocity magnitude at its exit, but the chosen geometry for the VCD with the bleed configuration performed better by decreasing the exit velocity from 60 m/s (assumed inlet velocity) to 41 m/s at 1% bleed and 10.5 m/s at 2% bleed.
- When air is delivered to the combustion chamber, the air bleed regulates the strength of the vortex that is created in the vortex chamber, which in turn regulates the pace at which air diffuses.

Nomenclature

VCD	vortex-controlled diffuser
RANS	Reynolds averaged Navier-Stokes
AR	aspect ratio
L_R	reattachment length
RNG	Re-Normalisation Group (turbulence flow model)
CFD	computational fluid dynamics
Cp	pressure coefficient

Bibliography

[1] Adkins RC, Matharu DS, Yost JO. The hybrid diffuser. ASME Technical Paper 1980;80-GT-136. https://doi.org/10.1115/80-GT-136

[2] Adkins RC. A short diffuser with low pressure loss. J Fluids Eng.1975;97(3):297-302. https://doi.org/10.1115/1.3447306

[3] ANSYS CFX solver theory guide. Release 14. ANSYS Inc. Canonsburg 2011.

[4] Chakrabarti S, Rao S, Mandal DK. Numerical simulation of the performance of a sudden expansion with fence viewed as a diffuser in low Reynolds number regime. J Eng Gas Turbines Power. 2010;132(11):114502. https://doi.org/10.1115/1.4000800

[5] Cockrell DJ, Markland E. A review of incompressible diffuser flow: a reappraisal of an article by G. N. Patterson entitled 'Modern diffuser design' which was published in this

journal twenty-five years ago. Aircr Eng Aerosp Tec. 1963; 35(10):286-292. https://doi.org/10.1108/eb033790
[6] Ghose P, Datta A, Mukhopadhyay A. Effect of prediffuser angle on static pressure recovery in flow through casing-liner annulus of a gas turbine combustor at various swirl levels. J Thermal Sci Eng. Appl. 2016;8(1):1-7. https://doi.org/10.1115/1.4030734
[7] Gorla RSR, Khan AA, Turbomachinery: Design and theory. 1st ed. CRC Press, Taylor and Francis Group. Boca Raton 2003. https://doi.org/10.1201/9780203911600
[8] Heskestad G. A suction scheme applied to flow through sudden enlargement. J Basic Eng. 1968;90(4):541-552. https://doi.org/10.1115/1.3605188
[9] Heskestad G. An edge suction effect. AIAA J. 1965; 3(10):1958-1961. https://doi.org/10.2514/3.3294
[10] Heskestad G. Further experiments with suction at a sudden enlargement in a pipe. J Basic Eng. 1970;92(3):437-447. https://doi.org/10.1115/1.3425025
[11] Klein A. Characteristics of combustor diffusers. Prog Aerosp Sci. 1995;31(3):171-271. https://doi.org/10.1016/0376-0421(95)00006-K
[12] Lefebvre AH, Ballal DR. Gas turbine combustion. Alternative fuels and emissions. 3rd ed. CRC Press, Taylor and Francis Group. New York 2010. https://doi.org/10.1201/9781420086058
[13] Mandal DK, Bandyopadhyay, Chakrabarti S. A numerical study on the flow through a plane symmetric sudden expansion with a fence viewed as a diffuser. Int J Eng Sci Tech. 2011;3(8):210-233. https://www.ajol.info/index.php/ijest/article/view/80186
[14] Mandal DK, Manna NK, Bandyopadhyay S, Biswas BP, Chakrabarti S. A numerical study on the performance of a sudden expansion with multisteps as a diffuser. Int J Appl Mech. 2011;3(4):779-802. https://doi.org/10.1142/S1758825111001238
[15] Schäfer F, Breuer M, Durst F. The dynamics of the transitional flow over a backward-facing step. J Fluid Mech. 2009; 6233:85-119. https://doi.org/10.1017/S0022112008005235
[16] Versteeg HK, Malalasekera W. An introduction to computational fluid dynamics. 2nd ed. Pearson. Prentice Hall, Glasgow 1995. http://ftp.demec.ufpr.br/disciplinas/TM701/Versteeg_Malalasekera_2ed.pdf
[17] White FM. Viscous fluid flow. 3rd ed. McGraw Hill. New York 1974. http://paginapessoal.utfpr.edu.br/fandrade/teaching/files/Viscous_Fluid_Flow_3rd_White.pdf
[18] Wilcox DC. Turbulence modelling for CFD. 3rd ed. DCW Industries. California 2006. https://cfd.spbstu.ru/agarbaruk/doc/2006_Wilcox_Turbulence-modeling-for-CFD.pdf
[19] Xing F, Su H, Chan S, Xu L, Yu X. Optimization study of the dump diffuser in gas turbine to reduce pressure loss. Int J Aerospace Eng. 2018;1-14. https://doi.org/10.1155/2018/6070782

Emeka Gaius Chijioke, DEng. – Faculty of Power and Aeronautical Engineering, Warsaw University of Technology, Poland.
e-mail: *emekachijioke9@gmail.com*

Prof. Andrzej Teodorczyk, DSc., DEng. – Faculty of Power and Aeronautical Engineering, Warsaw University of Technology, Poland.
e-mail: *andrzej.teodorczyk@pw.edu.pl*

Article citation info:
Mamala J, Graba M, Mitrovic J, Prażnowski K, Stasiak P. Analysis of speed limit and energy consumption in electric vehicles. Combustion Engines. 2023;195(4):83-89. https://doi.org/10.19206/CE-169370

Jarosław MAMALA
Mariusz GRABA
Jovan MITROVIC
Krzysztof PRAŻNOWSKI
Patryk STASIAK

Combustion Engines
Polish Scientific Society of Combustion Engines

Analysis of speed limit and energy consumption in electric vehicles

ARTICLE INFO

Received: 30 May 2023
Revised: 3 July 2023
Accepted: 7 July 2023
Available online: 19 August 2023

This paper presents an analysis of the mileage energy consumption for an electric passenger vehicle in terms of introducing numerous speed limits. Regulations concerning the limiting of vehicle speed to30 km/h in cities or residential areas are particularly common. This restriction is intended to increase traffic safety, but at the same time introduces increased mileage fuel or energy consumption in electric drivetrain. Regardless of the energy carrier, any increase in energy causes negative effects for the environment. The analysis was focused on the mileage energy consumption of electric passenger cars for a constant speed under real traffic conditions. During the tests, the tested vehicles' speed on a specially designated road section was changed gradually by 10 km/h, simultaneously recording the car's traction parameters and mileage energy consumption. An analysis of the mileage energy consumption was then carried out for the assumed fleet of cars travelling one after another (in a so-called traffic jam), while maintaining a safe distance. This allowed for the calculation of the environment's energy burden caused by a fleet of vehicles travelling on a given road section, indicating that a reduction in vehicle speed causes an increase in the vehicles' energy consumption. Both total and mileage energy consumption of electric vehicles were analysed during the tests.

Key words: *energy consumption, constant speed, safe driving distance*

1. Introduction

The reduction of carbon dioxide (CO_2) emissions and other components resulting from the combustion of hydrocarbon fuels to power vehicles and machinery is a global issue for the 21st century's civilization. It derives not only from global norms, but also due to the passenger vehicles sector, where the mobility of society has become a common phenomenon. For this reason, the passenger vehicles manufacturing sector is one of the most growing areas of the economy, and in many countries the passenger car saturation rate per 1,000 inhabitants exceeds the magic number of 700 units. This value represents a high degree of mobility in society, meaning that there are more cars on the market than opportunities for people to use them on the road at any one time. Powering these passenger cars requires an energy carrier in the form of fossil fuels, gaseous fuels, alternative fuels [3, 5] or electric energy in the case of electric drive units. Electric drive units are equipped with energy storages known as traction batteries, powered by the mains electricity supply or supplemented by energy recovered during the car's deceleration process. In Poland, electricity is produced [6] mostly from fossil fuels. This makes passenger vehicles neutral in terms of emissions on the road, but their environmental burden is transferred to the location of electricity production. This is beneficial for urbanised areas, but in terms of supplying energy to the wheels in the so-called "Well-to-Wheels" system, the final efficiencies are comparable (Table 1).

The final efficiency of electric drive units depends less on the drive unit itself, which is an electric machine with a high specific field efficiency, but more on the traffic conditions in which the vehicle operates. It is the driver's speed profile that has a significant impact on the electric drive unit's performance. At the same time, under real traffic conditions, the performance deviates from that measured in the WLTP cycle, similarly as in the case of internal combustion drive systems of passenger cars [1]. Hence, the range in real traffic conditions is shorter by several to over a dozen percent in the case of many electric vehicles as the range declared by the manufacturer [12]. This paper includes an analysis of the performance of an electric drive unit, achieved while driving at a constant speed under road conditions.

Table 1. Well-to-Wheel efficiency for battery electric vehicles (BEV) and internal combustion engine vehicles (ICEV)

	Well	**T**ank	Tank to **W**heel	
Drive unit	Production	Transport	Energy Conversion efficiency	**WTW Efficiency**
BEV	**35–60%** Depends on different methods of electricity production	**81–85%** Power transmission + charging efficiency	**65–82%** Losses during energy conversion, motion, friction of the drive unit	**18–42%**
ICEV	**82–87%** Extraction of fossil fuels and refining processes	**99%** Low energy losses during transport as a result of evaporation or sticking to tanks	**19–25%** Most of the energy is lost as heat. included efficiency of a drive unit featuring a combustion engine	**16–20%**

2. Mileage energy consumption and vehicle speed

A direct manner of improving the safety of road traffic and also the safety of other road users is usually a speed limit introduced by traffic regulations. This is implemented through signs or the introduction of speed-limit zones on city streets, with the speed limit being 30 km/h. Such regulations work well in terms of safety and this is not disputed by the authors in terms of energy, however consumption varies over a wide range. The simulated mileage energy consumption under different traffic conditions for an electric passenger vehicle is presented in paper [7], which shows a large spread of mileage energy consumption (Fig. 1).

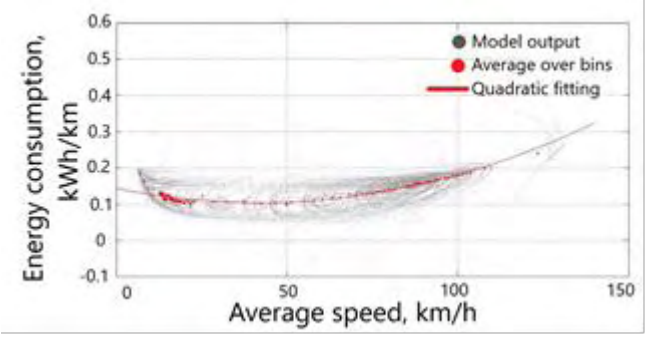

Fig. 1. Mileage energy consumption of an electric passenger vehicle [7]

The electric energy consumption shown varies for an average speed of 50 km/h from 5 kWh/100 km to 18 kWh/100 km with an average consumption of 10.5 kWh/100 km. This variation is caused by the simulated traffic conditions on different road sections when travelling at different speeds [16, 17]. The points highlighted in grey are the unit values and those in red correspond to the average mileage energy consumption. The average values shown for the mileage energy consumption indicate minimum consumption at speeds in the range of 30 to 45 km/h. In the same work, the authors compared the mileage fuel consumption for an internal combustion drive unit, as shown in Fig. 2.

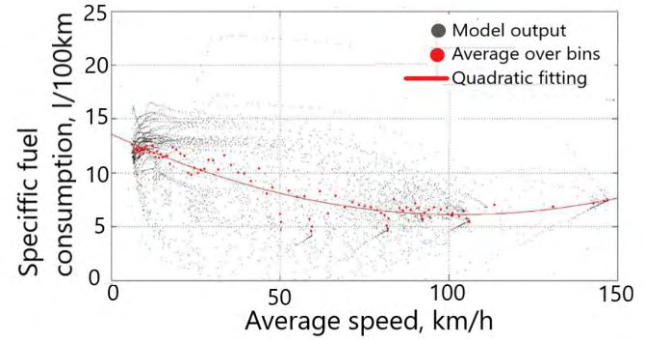

Fig. 2. Mileage fuel consumption of combustion drive units [7]

Internal combustion vehicles have a significantly greater spread of fuel consumption and their average value is in the range of 90 to 100 km/h. It is interesting that the different drive unit designs (BEV and ICE) feature minimum mileage fuel and energy consumptions that occur at a given speed. Attention should be paid to identical vehicle parameters related to weight, tire type, drag coefficient c_x or frontal surface area. It is not correct to directly compare the presented mileage fuel and energy consumption. Therefore, in paper [8], the authors compared the electricity consumption and fuel consumption per unit of electricity for travels made under real road conditions.

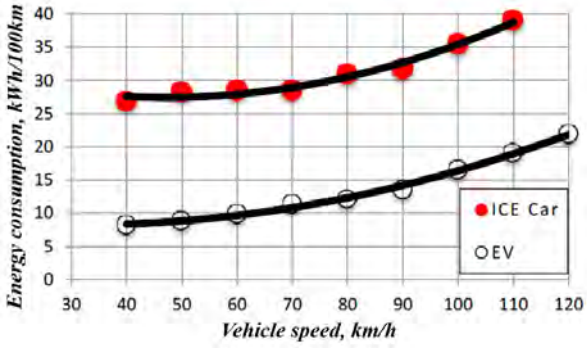

Fig. 3. Mileage energy consumption for various passenger vehicle drive units [13]

A similar comparison can be found in paper [8, 10], where the difference in the mileage energy consumption of an internal combustion engine and an electric engine is substantial. However, the authors of this paper compared the variation in the aforementioned drive units' energy carrier consumption depending on the driver. The results of energy carrier consumption for a random selection of 10 vehicles over a period of at least one year are presented in Fig. 4.

a)

b)

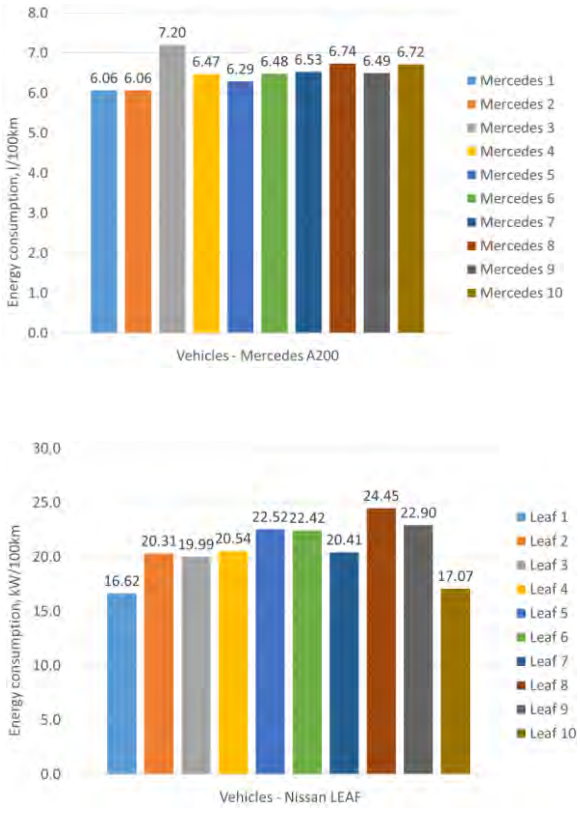

Fig. 4. Differences in energy carrier consumption for different drive units: a) internal combustion, b) electric

The reason for these differences is the operation period of over 12 months, in which the vehicles covered a maximum distance of 31,000 km for the electric drive unit and 34,000 km for the internal combustion drive unit. The spread of results is significantly greater for electric drive units for which the standard deviation is in the range of 1.5 to 12.8 (Fig. 5), while for the internal combustion drive unit, this value does not exceed 0.7.

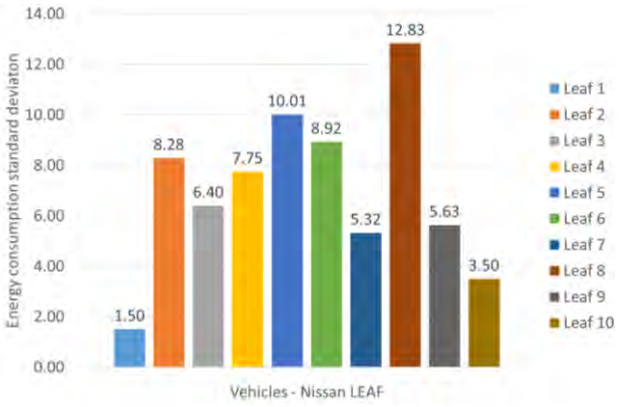

Fig. 5. Standard deviation of an electric drive unit

Therefore, the internal combustion engine's consumption is characterised by a significantly smaller spread in the average mileage fuel consumption. In the case of the electric drive system, the driver's driving style is important in terms of the ability to recover energy from the deceleration process and in terms of the average vehicle speed [11]. In paper [10], the authors presented the energy consumption at an average speed of an electric engine. The differences are significant and amount from 135 to 420 Wh/km.

3. Mileage energy consumption and constant vehicle speed

The electric drive unit's mileage energy consumption is measure of the energy expended on a given road section at a given speed. Due to the fact that vehicle speed depends on the driver's will and on the environmental conditions (road topography, weather conditions, other road users' manoeuvres) or the legal conditions that regulate traffic in a given area. The regulations introduced to limit the speed to 30 km/h result in an increased fuel consumption, according to the information shown in Fig. 7a. From the information presented, it is possible to conclude that the minimum mileage energy consumption occurs at a well-defined electric vehicle speed. In Mitrović's paper [14], it is possible to find confirmation of the above information for an internal combustion vehicle with an assumed speed limit on a limited length road section. Under these assumptions, a vehicle moving at a very low speed $V \rightarrow 0$ will have a fuel consumption rising to infinity (Fig. 6) due to the internal combustion engine's operation in its low-efficiency range resulting from idling Q_0 and under such traffic conditions the travel time also increases to $\tau \rightarrow \infty$. This shows that the time τ [h] and fuel consumption Q [l] are very high for a very low vehicle speed, Eq. (1).

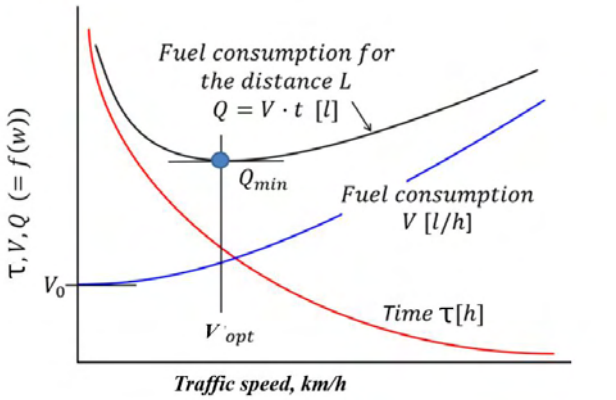

Fig. 6. Analysis of the vehicle's traction variables in road traffic at limited speeds

Low vehicle speed:

$$V \rightarrow 0\ \{(\ Q_p\ [l/h] = Q_0;\ \tau \rightarrow \infty)\}: Q\ [l] \rightarrow \infty, \text{large} \quad (1)$$

High vehicle speed:

$$V \rightarrow \text{large}\{(Qp\ [l/h] = \text{large};\ \tau \rightarrow \text{small})\}: Q\ [l] \rightarrow \text{finite} \quad (2)$$

In the second extreme position for high speeds, the fuel consumption increases, but the travel time decreases greatly (2). In this case, the fuel consumption, treated as the product of high-intensity fuel flow Q_τ [l/h] and short travel time τ [h], will provide a finite fuel value in Q [l] (3).

$$Q\ [l] = Q_\tau\ [l/h] \cdot \tau\ [h] \quad (3)$$

It was assumed that similar dependencies apply to electric vehicles. Hence, energy consumption was measured for selected vehicle models under traffic conditions. The difference in mileage energy consumption derives from the differences in the drive units.

4. Mileage energy consumption under road conditions

The energy consumption of an electric passenger vehicle was analysed on a selected road section of 2.5 km with a good bituminous road surface, sheltered from the wind and the road slope was close to zero. The tests were carried out at similar temperatures of 5°C.

The traction and energy parameters were monitored using a measurement platform developed at the Department of Vehicles of the Opole University of Technology [9]. The platform enables the measurement of traction parameters from several data sources simultaneously including, among others, the on-board diagnostic (OBD) network or the on-board CAN Bus data transmission network. In addition, for Mercedes-Benz vehicles, the authors used the company's software that enabled a continuous preview of the following data: energy storage capacity, total distance travelled, travel time, average speed and energy expenditure as the mileage electricity consumption. The aforementioned data were systematically recorded in the database and then analysed.

The technical data of the analysed electric vehicles is presented in Table 2.

Table 2. Tested vehicle parameters

Manufacturer	Renault	Mercedes-Benz	Mercedes-Benz
Type	ZOE	CLA	A250e
Electric engine's output	68 kW	75 kW	75 kW
Electric engine's max. torque	220 Nm	330 Nm	300 Nm
Engine assembly	Front, transverse	Front, transverse	Front, transverse
Engine system type	EV	PHEV	PHEV
Transmission system	1 gear	Automatic – 8 gears	Automatic – 8 gears
Battery capacity	41.1 kWh	–	15.6 kWh
Vehicle mass	1445 kg	1325 kg	1817 kg
Vehicle travel range	255 km	80 km	75 km
Vehicle energy consumption	165 Wh/km	190 Wh/km	209 Wh/km

The energy consumption was analysed for the vehicle's real operating conditions at a preset constant speed from 30 km/h to 130 km/h, with the speed being changed gradually by 10 km/h once the energy consumption had stabilised. It should be noted that two hybrid vehicles equipped with an additional combustion engine were among the analysed drive units. However, in the case of both aforementioned vehicles, the analysis was carried out solely on the basis of a forced electric drive. For the Renault ZOE, tests were carried out for two drive unit control modes ("Normal" and "ECO"). The "ECO" mode limits the drive unit's available output to 38 kW, maximum vehicle speed to 96 km/h and cockpit temperature to 21°C.

Figure 7 shows the mileage energy consumption as a function of the vehicle's speed. The results shown are the averaged values recorded at the measurement points (constant speed). For each recorded mileage energy consumption, its minimum values can be determined for a given constant vehicle speed. In the case of the analysed vehicles, these values were as follows:

- Renault ZOE, ECO mode; V – 37 km/h → 12.2 kW/100 km
- Renault ZOE, normal mode; V – 50 km/h → 14.50 kW/100 km
- Mercedes-Benz CLA; V – 40 km/h → 11.5 kW/100 km
- Mercedes-Benz A250e; V – 60 km/h → 15.7 kW/100 km.

There is a noticeable effect of speed on energy consumption, which increases below and above the set speed. The Mercedes-Benz CLA has the lowest energy consumption, but the drive unit's output required to drive the analysed vehicles is similar, as shown in Fig. 8. These values are in line with the research presented in another paper [4] on the analysis of fuel consumption in an internal combustion drive unit. Despite the significant differences in the vehicles' drive units, its output at a constant speed is similar and is approximately 20 kW for the 100 km/h vehicle speed. In contrast, significant differences were registered in torque. Regardless of its operating mode, Renault ZOE has a similar torque as both Mercedes-Benz, which share the same drive unit (Fig. 9). The drive unit of the Mercedes-Benz vehicles uses an eight-speed transmission, which affects its torque, unlike the ZOE, which has a fixed transmission ratio in its drive units.

a)

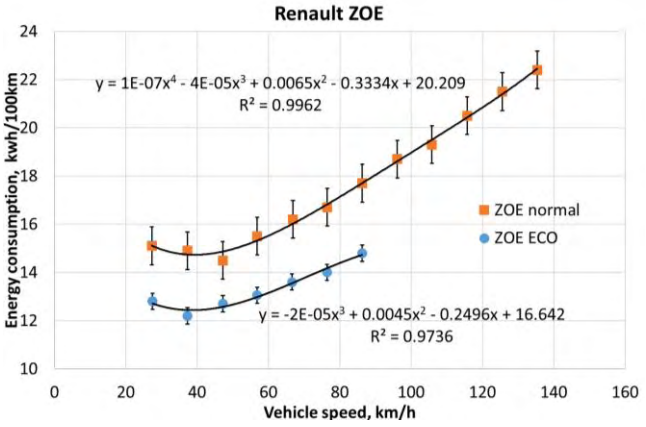

b)

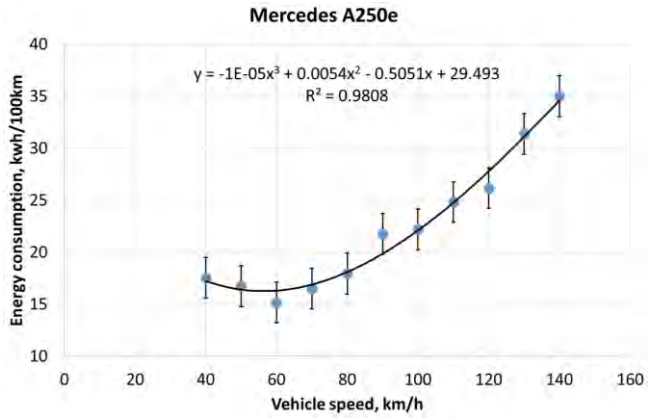

c)

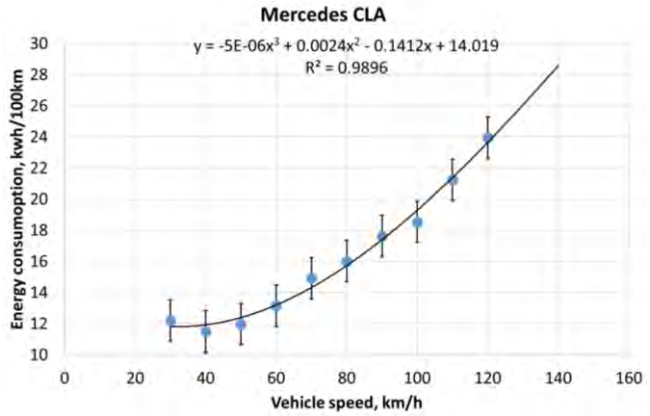

Fig. 7. Mileage energy consumption for the analysed electric vehicles: a) Renault ZOE, b) Mercedes-Benz A250e, c) Mercedes-Benz CLA

The values shown above for the vehicle's electric drive unit are determined empirically for a constant vehicle speed. The values are similar in terms of mileage and characteristics for internal combustion drive units widely reported in the literature, but also presented in Chapter 2.

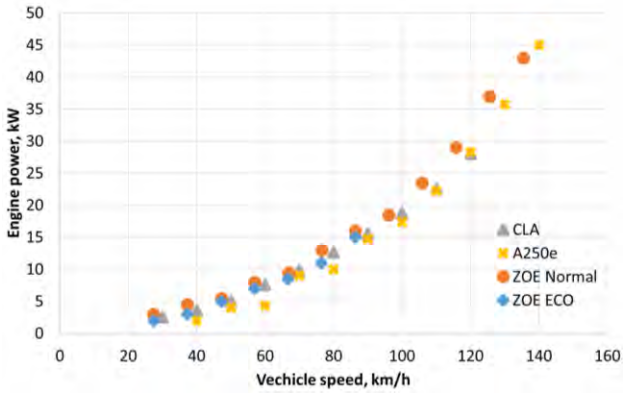

Fig. 8. Drive unit output at constant vehicle speed

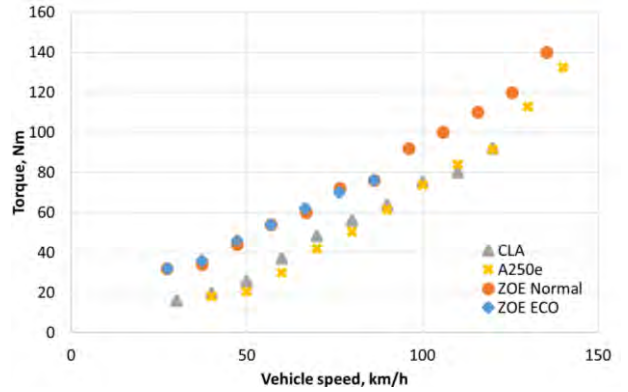

Fig. 9. Drive unit torque at the constant vehicle speed

5. Energy consumption for the vehicle fleet

The electric energy consumption Q_e [kWh] was analysed for the following vehicle movement pattern on the road at a constant speed. The pattern refers to the vehicles' travel on road section L [km] from points A to B, while maintaining a safe distance between the vehicles. The safe distance is not a fixed value and is not precisely defined. It is generally acknowledged that this distance ensures the driver's safety in the event of emergency braking, both in front of and behind the vehicle. The term is not precise due to the use of the words "safe distance" in the context of two conditions related to braking distance and the driver's reaction time. The braking distance depends on many conditions, such as the road type, the vehicle's condition and even its type, brand or weather conditions. Reaction time is the driver's subjective ability to respond to an occurring traffic event and refers to the driver's psychomotor properties, experience and even the force with which the driver presses on the brake pedal. In practice, the driver's reaction time is between 0.5 and 1.5 seconds and can therefore be three times as long. For safety reasons, the response time is assumed to be 3 seconds and is preferred by the Polish road manager, i.e. the General Directorate for National Roads and Motorways. The Road Traffic Law defines the safe distance in Article 19, paragraph 3a as "the minimum distance between the driver's vehicle and the vehicle in front of him in the same lane. This distance, expressed in meters, shall be defined as not less than half the number representing the driver's vehicle's speed, expressed in kilometers per hour". The minimum safe distance at 30 km/h is therefore 15 m and at 100 km/h – 50 m.

Therefore, the number of vehicles is variable for a queue of vehicles moving one after the other, without interruption, on the same road section at a constant speed. This is important in terms of minimising the vehicle fleet's energy consumption, which requires determining the grid energy demand for minimum values at the recommended speed in terms of energy consumption and that resulting from legal regulations. Each energy consumption $Q > Q_{min}$ increases the intake of grid energy and is adverse for the environment. It is therefore important to estimate the difference $\Delta Q = Q - Q_{min}$, and for the analysed vehicle, e.g. Renault ZOE, the difference is presented in Fig. 10.

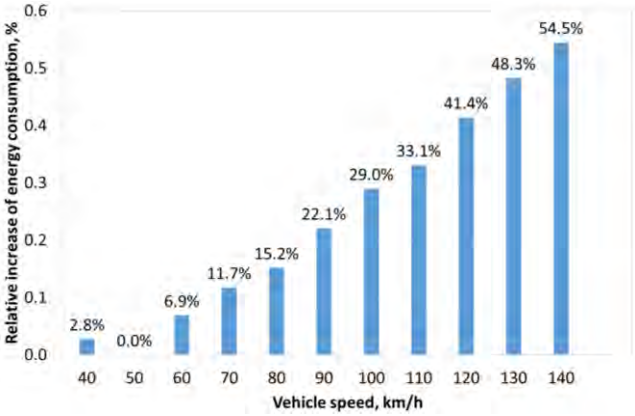

Fig. 10. Relative energy gain compared to its minimum value for Renault ZOE

Each travel at a speed V that differs from V_{opt} ($V \neq V_{opt}$), featuring a minimum energy consumption, increases energy consumption. A plot describing the dependency between consumption and travel time over a 10 km distance for the selected electric vehicle (Renault ZOE) is shown in Fig. 11. It corresponds to Fig. 6, presented in Mitrović's paper [14] for the internal combustion drive unit.

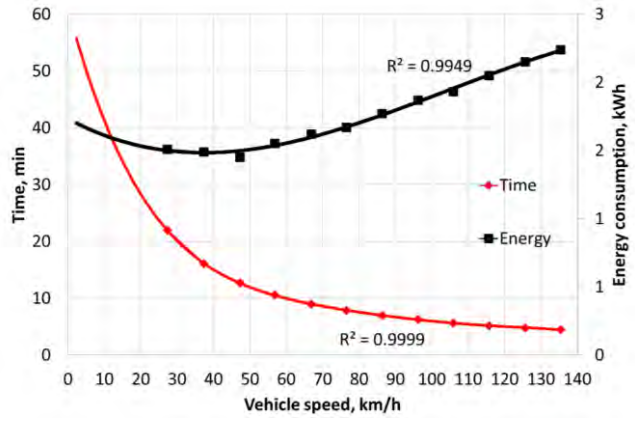

Fig. 11. Approximate energy consumption and time values for the analysed road section of 10 km

The energy consumption determined this way was used to calculate the energy consumption of a fleet of electric vehicles travelling at a constant speed, assuming a safe distance between them is maintained as required by traffic regulations, as shown in Fig. 12.

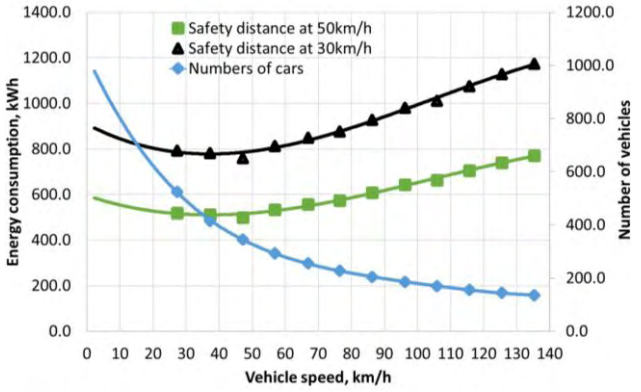

Fig. 12. Dependency of energy consumption for a fleet of electric vehicles at a constant speed of 30 km/h and 50 km/h while maintaining a safe distance

The number of vehicles in the fleet decreases as the speed increases, because the distance between vehicles increases along with an increase in speed, for which the vehicle's length must also be taken into account (4.08 m in the case of Renault Zoe). The number of vehicles travelling over a distance of 10 km at a constant speed of 30 km/h is 524 and 184 vehicles at 100 km/h. By calculating the energy consumption directly (Fig. 11) for the moving fleet, it turns out that the consumption amounts to 791.4 kWh at 30 km/h, 498.6 kWh at optimum speed (50 km/h) and 354.8 kWh at 100 km/h. The reduction in energy consumption is due to the decreasing number of vehicles in the fleet along with the increasing speed on a given road section. A detailed analysis was carried out for energy consumption if the fleet of vehicles was to cover the 10 km distance at the optimum speed (50 km/h) and at the speed limit derived from legal restrictions (30 km/h). The representative fuel will then be derived from the consumption at a given speed and number of vehicles, as shown in Fig. 12.

The energy consumption shown in the figure by the green line is presented for a fleet of 349 vehicles travel-ling at the optimum speed (50 km/h) while maintaining a safe distance. In contrast, the black line shows the consumption for a fleet travelling at 30 km/h. The differences in consumption are significant and at 50 km/h amount to ΔQ = 52.8% of the relative value, while at 30 km/h, ΔQ = 58.7%, and at 100 km/h – nearly 100% (precisely 96%).

In terms of the energy consumption of a fleet of vehicles travelling in the city, the ultimate aim should be making traffic smoother. At the same time, all the electric vehicles analysed have a significantly lower constant speeds that guarantee minimum energy consumption when compared to the internal combustion drive unit presented in papers [2, 10].

In paper [14], Mitrović pointed out that an increase from 30 km/h to 100 km/h in the case of the internal combustion drive unit results in a 93% increase in fuel consumption. A similar increase was recorded for the analysed Renault ZOE, which amounted to 90.3% and was mainly due to the vehicles' drag resistance, as shown in Fig. 7.

6. Summary

An analysis of the results obtained allows for the conclusion that the introduction of a 30 km/h speed limit causes an increase in the energy consumption of vehicle fleets. Regardless of the form of energy generation (coal, nuclear or RES), an increase in consumption always has an adverse effect on the environment. For example, it causes greater thermal and CO_2 emissions in the case of conventional coal energy, greater thermal emissions for nuclear energy and requires using more windmills or solar panels for RES. At the same time, the introduction of speed limits results in a 7.8% decrease in the number of road accidents, according to data provided by insurance companies [15].

In summary:

– 30 km/h speed-limit zones should only be introduced in particularly dangerous areas
– a reduction in speed below that which ensures minimum energy consumption results in an increased energy consumption
– the analysis carried out for a fleet of electric vehicles travelling at a safe distance from one another results in more traffic at a reduced speed, which is dangerous in itself. Therefore, these restrictions should also take traffic congestion into account
– higher energy consumption also has economic effects which should be taken into consideration.

Only a comprehensive way of considering the introduction of 30 km/h speed limits will be effective in reducing the energy consumption of electric vehicles.

Nomenclature

BEV	battery electric vehicle
ICEV	internal combustion engine vehicle
OBD	on-board diagnostic
Q	fuel consumption [l]
Qe	electric energy consumption [kWh]
Qτ	fuel flow [l/h]
V	vehicle speed [km/h]
V_{opt}	optimum speed
WLTP	Worldwide Harmonized Light Vehicles Test Procedure
WTW	well-to-wheels
ΔQ	differences in fuel consumption
τ	time [h]

Bibliography

[1] Andrych-Zalewska M, Chłopek Z, Merkisz J, Pielecha J. Determination of exhaust emission characteristics in the RDE test using the Monte Carlo method. Archives of Transport. 2023;66(2):45-60. https://doi.org/10.5604/01.3001.0016.3127

[2] Andrzejewski M, Nowak M, Woch A, Stefańska N. Analysis of pollutant emissions and fuel consumption for the use of a multi-storey carpark. Combustion Engines. 2021; 187(4):46-51. https://doi.org/10.19206/CE-141740

[3] Becker T, Sidhu I, Tenderich B. Electric vehicles in the United States: a new model with forecasts to 2030. Center for Entrepreneurship & Technology (CET), Technical Brief 2009.
[4] Bieniek A, Graba M, Hennek K, Mamala J. Analysis of fuel consumption of a spark ignition engine in the conditions of a variable load. MATEC Web Conf. 2017;118:00036. https://doi.org/10.1051/matecconf/201711800036
[5] Chłopek Z. Natural environment preservation. Motor Vehicles. WKŁ, Warsaw 2002.
[6] Chłopek Z. Evaluation of specific distance energy consumption by electric car. Car Transport/Transport Samochodowy. 2013;2:75-87.
[7] Fiori C, Arcidiacono V, Fontaras G, Makridis M, Mattas K, Marzano V et al. The effect of electrified mobility on the relationship between traffic conditions and energy consumption. Transport Res D-Tr E. 2019;67:275-290. https://doi.org/10.1016/j.trd.2018.11.018
[8] Gagan S. Unit energy consumption model of vehicles in real operating conditions. Engineering thesis, Opole University of Technology 2022. https://apd.po.edu.pl/diplomas/98969
[9] Graba M, Bieniek A, Prażnowski K, Hennek K, Mamala J, Burdzik R et al. Analysis of energy efficiency and dynamics during car acceleration. Eksploat Niezawodn. 2023;25(1): 17. https://doi.org/10.17531/ein.2023.1.17
[10] Kropiwnicki J. Comparison of energy efficiency of vehicles powered by different fuels. Combustion Engines. 2012; 150(3):34-43. https://doi.org/10.19206/CE-117029
[11] Kropiwnicki J, Furmanek M. Analysis of the regenerative braking process for the urban traffic conditions. Combustion Engines. 2019;178(3):203-207. https://doi.org/10.19206/CE-2019-335
[12] Lisowski M, Gołębiewski W, Prajwowski K, Danilecki K, Radwan M. Modeling the fuel consumption by a HEV vehicle – a case study. Combustion Engines. 2023;193(2):71-83. https://doi.org/10.19206/CE-157112
[13] Martins J, Brito FP, Pedrosa D, Monteiro V, Afonso JL. Real-life comparison between diesel and electric car energy consumption. Grid Electrified Vehicles: Performance, Design and Environmental Impacts, Nova Science Publishers, New York 2013.
[14] Mitrovic J. Optimum speed of road vehicles in terms of fuel consumption. Immissionsschutz 2020;1. https://doi.org/10.37307/j.1868-7776.2020.01.04
[15] Tutorials: the three-second-rule-on-the-road. https://mubi.pl/poradniki/zasada-trzech-sekund-na-drodze/
[16] Wang J, Besselink I, Nijmeijer H. Electric vehicle energy consumption modelling and prediction based on road information. World Electr Veh J. 2015;7(3):447-458. https://doi.org/10.3390/wevj7030447
[17] Zhang J, Wang Z, Liu P, Zhang Z. Energy consumption analysis and prediction of electric vehicles based on real-world driving data. Appl Energ. 2020;275:115408. https://doi.org/10.1016/j.apenergy.2020.115408

Prof. Jarosław Mamala, DSc., DEng. – Faculty of Mechanical Engineering at Opole University of Technology, Poland.
e-mail: *j.mamala@po.opole.pl*

Mariusz Graba, DEng. – Faculty of Mechanical Engineering at Opole University of Technology, Poland.
e-mail: *m.graba@po.opole.pl*

Prof. Jovan Mitrovic – Formerly Department of Thermal Process Engineering and Plant Technology at the University Paderborn, Germany.
e-mail: *mitrovic@tebam.de*

Krzysztof Prażnowski, DEng. – Faculty of Mechanical Engineering, Opole University of Technology. Poland.
e-mail*: k.praznowski@po.edu.pl*

Patrick Stasiak – President of the Management Board Zakład Komunalny sp. z o.o., Opole, Poland.
e-mail: *patryk.stasiak@zk.opole.pl*

Article citation info:
Szwaja M, Szymanek A. Combustion comparative analysis of pyrolysis oil and diesel fuel under constant-volume conditions. Combustion Engines. 2023;195(4):90-96. https://doi.org/10.19206/CE-169805

Magdalena SZWAJA
Arkadiusz SZYMANEK

Combustion Engines
Polish Scientific Society of Combustion Engines

Combustion comparative analysis of pyrolysis oil and diesel fuel under constant-volume conditions

ARTICLE INFO

Received: 30 May 2023
Revised: 11 July 2023
Accepted: 19 July 2023
Available online: 4 August 2023

The article discusses the research results on the combustion of pyrolysis oil derived from the pyrolysis of HDPE plastics after its distillation. The tests were carried out in a constant-volume combustion chamber in conditions similar to those in a compression-ignition engine with a compression ratio of 17.5:1. The phases of premixed and diffusion combustion and the ignition lag were determined. Then, diesel fuel combustion tests were performed under similar pressure-temperature conditions. Comparative analysis was used to draw conclusions as follows: the percentage fraction of heat released from the premixed combustion phase to total heat for pyrolysis oil was nearly 22%, whereas this parameter is 15% for diesel fuel, the maximum combustion rate for the premixed combustion phase for pyrolysis oil was approximately 27% higher than the premixed combustion rate for diesel fuel, the ignition lag for pyrolysis oil was slightly longer compared to that for diesel fuel. The presented parameters have a significant impact on both the development of combustion and the thermal efficiency of the internal combustion engine. Summing up, one can conclude, that pyrolysis oil can be applied as a substitute for diesel fuel both as a single fuel or blend component with it.

Key words: *pyrolysis oil, diesel fuel, combustion, heat release rate, IC engine*

1. Introduction

In the search for renewable fuels, more and more attention is paid to by-products generated during the thermal processing (torrefaction, pyrolysis, gasification) of organic substances. Such by-products include post-process liquid commonly referred to as pyrolysis oil. Pyrolysis oil is a condensate from liquid vapors generated during pyrolysis. Typically, biomass and organic waste (plastics, tires) are organic substances that are used as feedstock for a pyrolysis reactor. Due to the relatively well-developed technologies of torrefaction, pyrolysis, and gasification of plant biomass, attempts are made to use these technologies for the thermal processing of organic matter other than biomass, mainly car tires and plastics without the possibility of recycling them. Based on these technologies, solutions for the thermal decomposition of sewage sludge, plastics, and rubber from used tires have been successfully implemented. As discussed in the available literature [2, 10], plastic waste and used car tires, due to their high carbon and hydrogen content, are considered attractive materials for the production of liquid and gaseous substances with a satisfactory good calorific value. Hence, in the short-term future, these products may have a significant share in the fuel sector, provided that a number of changes in the waste laws are introduced in order to convert waste into a full-value material.

Currently, research is being carried out on the combustion of raw pyrolysis oil and mixtures with other fuels to enrich its combustible properties [3]. Mixing crude pyrolysis oil with another fuel substance can also be caused by reducing the content of unfavorable components, e.g. sulfur present in crude pyrolysis oil obtained from the pyrolysis of used car tires. On the basis of the studies carried out so far, there is a number of reasons to clearly confirm that pyrolysis oil should be tested in terms of its use as fuel for both automotive engines and engines in cogeneration units. Crude pyrolysis oil is a black, opaque substance with a strong characteristic odor. This oil mainly contains hydrocarbon compounds, alcohols, water, and organic acids [1]. On the other hand, due to its relatively high calorific value, pyrolysis oil is considered a potential fuel for reciprocating, piston engines and gas turbines [7, 14, 15]. Umeki [15] found that a mixture of pyrolysis oil and diesel fuel has physical and chemical properties that aspire to be directly used in a diesel engine. In addition, his research showed that the pyrolysis oil was characterized by a research octane number close to 90, i.e. such as typical gasoline for internal combustion engines of vehicles. Tudu [14] investigated and proposed a blend consisting of 50% diesel, 40% light pyrolysis oil, and 10% dimethyl carbonate. Hurdogan, after adding 10% of pyrolysis oil to diesel fuel, obtained a fuel that did not deteriorate engine performance in terms of torque and output power [7]. Furthermore, the implementation of a fuel that is a mixture of butanol (renewable fuel) and pyrolysis oil (as a product of the use of biomass/plastic waste) can be considered an innovative action [11]. The research described in this manuscript focused on the application of this fuel to a stationary engine, but the results indicate that it can also be used for automotive SI engines. Based on the literature review, a growing interest in plastic pyrolysis oil and its use as a potential primary or additional fuel for an internal combustion engine can be observed [4, 5, 8, 9, 13, 16].

A crucial environmental challenge is the analysis of exhaust gas toxicity from an engine fueled with pyrolysis oil. Due to its diverse origin, this oil may be a mixture of polycyclic aromatic hydrocarbons and may also contain chlorine which is a precursor for dioxins formation. Examination of the exhaust gas toxicity may result in supplementing the exhaust gas purity standards with compounds that may be

formed from the combustion of pyrolysis oil and are not present during the combustion of conventional fuels.

2. Methodology and test stand description

The studies presented in the article are based on experiments. These studies were conducted with the aid of comparative analysis. The results of the combustion of two liquids in a constant-volume combustion chamber were used for the analysis. One of the liquids was the tested pyrolysis oil. The reference liquid was light diesel fuel.

The constant-volume combustion chamber is a test stand where the pressure course was recorded in the time interval including injection, ignition, and flame development until its extinction for pyrolysis oil and reference fuels in conditions similar to those in a real diesel engine prevailing at the time of fuel injection into the combustion chamber and the cylinder. Techniques of testing various liquids as potential engine fuels in a constant-volume chamber assisted with high-speed video cameras is a relatively new measurement methodology, which usability was confirmed among others in work by Grab-Rogalinski [6]. Tests of injection in an oxygen-free atmosphere were also carried out to eliminate ignition and to determine the fuel flow rate from the injector nozzle and the maximum range of the injected fuel stream.

In addition, the presented phenomena were recorded using a high-speed digital camera at a frame speed of up to 20,000 fps. Figure 1 shows the combustion chamber where the injection and combustion experiment was carried out. The combustion chamber has a volume of 1.1 dm^3. Inside, the chamber is oval with a diameter of 101.6 mm.

Fig. 1. The constant volume combustion chamber

The test bench with a combustion chamber is presented in Fig. 2. The placement of both cameras and the monochromatic light source is shown. Camera 1 recorded the image in transmitted light using the Schlieren technique (Fig. 3a). This camera was set transversely to the direction of the outgoing fuel stream. Whereas, Camera 2 was positioned along the longitudinal symmetry axis of the injector and was used to record the image of self-illumination from the flame (Fig. 3b). However, in this case, the camera could also record the reflected light generated by one of the sources. It was particularly useful in the analysis of injection and spraying in an oxygen-free atmosphere, where the lack of self-luminance from the flame made the recorded image practically illegible.

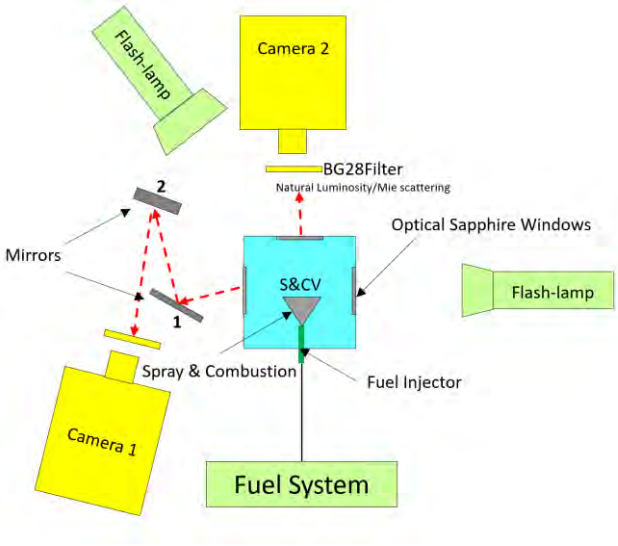

Fig. 2. The diagram of the test set-up with the constant-volume combustion chamber

The test stand consisted of two high-speed digital cameras Photron Fastcam SA1.1 with the following operational parameters:

- lenses: focal length/aperture: 85 mm/1.4 and 60 mm/1.7
- resolution: 512 × 512 pixels, monochrome image, 8-bit gray scale
- image recording speed: 20,000 fps
- shutter speed: 3.26 μs
- protective filter: 550 nm.

The methodology and the course of the experiment of combusting the tested liquid in the combustion chamber were precisely described in the procedure, the most important points of which are presented as follows:

- the combustion chamber is designed for fuel self-ignition tests at elevated temperature and pressure
- the combustion chamber is initially filled with a mixture of H_2-C_2H_2-O_2-N_2 gases in appropriate proportions
- ignition of the gas mixture is initiated from the spark plug
- as the result of the combustion of H_2 and C_2H_2 the following mixture was created: H_2O, CO_2, O_2 and N_2 with the proportions required by the experiment, especially taking part in the study, which in this case was at a concentration of 21% in terms of the total volume filling the chamber
- injection of the tested fuel is performed automatically.

The injection of the tested fuel took place after reaching the pressure in the combustion chamber at the level of, for example, 41 bar or at a temperature set-point of e.g. 1000 K, which corresponded to conditions similar to those prevailing at the end of the compression stroke in the engine with a compression ratio of 17.5:1.

The tests were carried out for pyrolysis oil and light diesel fuel according to the data shown in Table 1 and Table 2.

a)

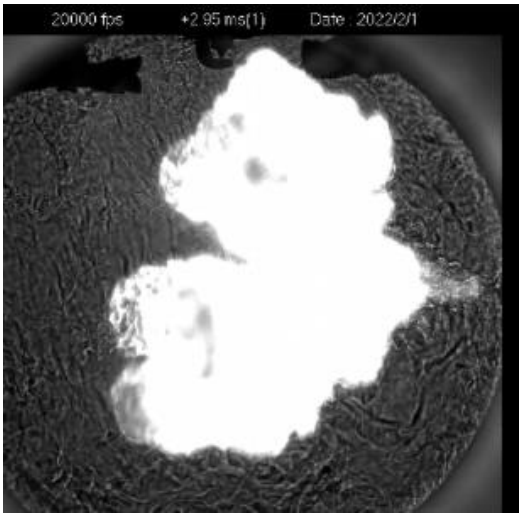

b

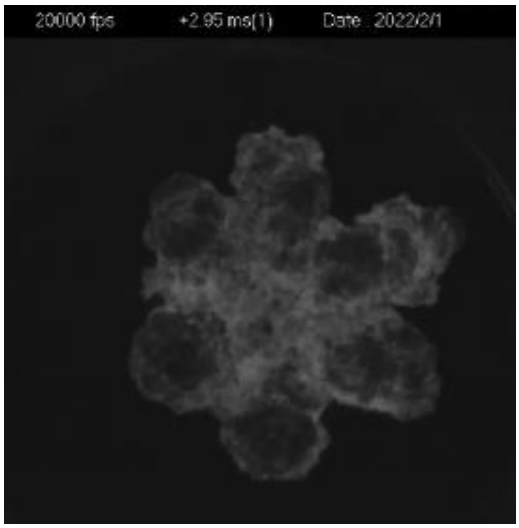

Fig. 3. Exemplary images: image from Camera 1 (a), image from Camera 2 (b)

Table 1. Selected fuel properties

		Fuel	
		Pyrolysis oil	Diesel fuel
Density	kg/dm^3	738	852
Surface tension	mN/m	22.9	27.6
Dynamic viscosity at 40°C	mPa·s	0.48	3.77
Cetane number	–	10–40	50

Table 2. Experimental matrix

		Fuel	
		Pyrolysis oil	Diesel fuel
Number of tests of combustion in the atmosphere 21% O_2		2	5 (41 bar)
Number of tests when the chamber was filled with nitrogen, without oxygen		2	2
Initial temperature	K	453	453
Injection temperature	K	1000	1000
Pressure inside the chamber during injection	bar	41	41
Injection pressure	bar	400	400

For the initial pressure of 41 bar, five tests were carried out to check the repeatability of the results and evaluate the measurement accuracy.

In the thermodynamic analysis, calculations of the heat release rate (HRR, dQ/dt) were performed. In order to calculate the heat release rate during the combustion of the tested fuel in a constant-volume chamber, a number of simplifications were adopted as follows:

- the constant-volume combustion chamber is an insulated chamber, which means that there is no heat transfer from the chamber to the environment
- gases filling the chamber are treated as an ideal gas
- the increase in mass and number of moles resulting from the injection of the tested fuel into the chamber is considered marginal and does not cause a significant change in the calculations
- the change in the chemical composition of the gases before and after the combustion of the tested fuel is irrelevant for the accuracy of the calculations, it is assumed that the mixture does not change.

The heat release rate was calculated based on the following relationships:

- equation of state for an ideal gas (1)
- relation for the universal gas constant R_u and the specific heats c_p and c_v (2)
- caloric equation for internal energy (3)
- first law of thermodynamics (4).

$$p \cdot V = n \cdot R_u \cdot T \tag{1}$$

$$\frac{c_V}{R_u} = \frac{c_V}{c_P - c_V} = \frac{1}{\kappa - 1} \tag{2}$$

$$U_i(T_i) = n_i \cdot c_{V,i} \cdot T_i \tag{3}$$

$$Q = U_2(T_2) - U_1(T_1) \tag{4}$$

After rearranging the equations (1-4) it yields

$$dQ = \frac{1}{\kappa - 1} \cdot V \cdot dp \tag{5}$$

Hence, the elementary dQ as a time-dependent variable will be proportional to the heat release rate dQ/dt, which is related to the time of 1 second.

An exemplary dQ/dt course is shown in Fig. 4. As seen from equation (5), the pressure change dp is in strict proportion to change in the heat released dQ, so does to dQ/dt. The index κ of specific heats c_p/c_v was calculated for a given pressure and temperature based on c_p and c_v for the mixture of gases filling the combustion chamber before the start of injection of the tested fuel.

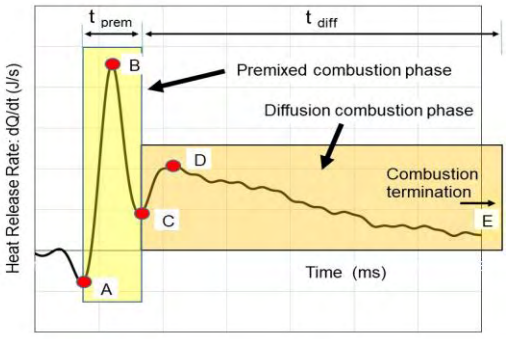

Fig. 4. Exemplary plot of heat release rate with highlighting premixed and diffusion combustion

In the initial range, a decrease in the HRR can be observed. This drop is located in the time interval when the injector opens (point A in Fig. 4) and fuel flows into the chamber. The most likely explanation for this heat loss is the evaporation of the injected fuel. In addition, it can be also assumed that the negative HRR is also influenced by chemical reactions that initiate ignition, which are usually endothermic reactions.

From the heat release rate HRR, one can read the range typical for premixed and the diffusion combustion. It is obvious that both types of combustion occur one by one in time, but it is difficult to identify when one ends and the other begins. Hence, a simplification was introduced, according to which the premixed combustion starts from point A and it goes until achieving a local minimum (point C). Diffusion combustion, on the other hand, was assumed to last from point C to the end of combustion, i.e. until dQ/dt reaches 0 at point E, the location of which is not indicated in Fig. 4.

Additionally, knowledge of the heat release rate dQ/dt will lead to determining combustion phases based on the accumulated heat Q(t) with Eq. 6.

$$Q(t) = \frac{1}{\kappa - 1} \cdot V \cdot \int_{t_0}^{t} dp \tag{6}$$

where: t_0 – start of injection.

The total heat Q released from combustion can be calculated as a maximum heat defined by Eq. 6.

On the basis of Q(t) recalculated to normalized percentage scale, the combustion phases can be introduced as follows:

- t_{0-2} – initial combustion phase measured from the start of injection to the release of 2% of heat released. This phase is usually considered a reliable parameter representing the ignition delay of the air-fuel combustible mixture
- t_{0-10} – the initial combustion phase managed as another reliable parameter to assess the ignition delay
- t_{10-90} – the main combustion phase
- t_{0-90} – the initial and main combustion phases.

Characteristics of pyrolysis oil used for tests

As a result of distillation at 280°C, the pyrolysis oil was practically free of hydrocarbons with the number of carbon atoms above 15 (Fig. 5).

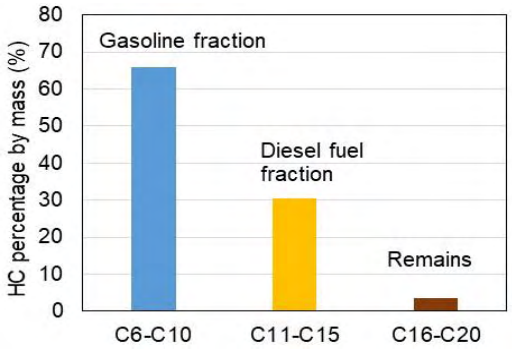

Fig. 5. Percentage hydrocarbons fractions by mass for the pyrolysis oil after distillation

Detailed analysis of processing technology of this pyrolysis oil is present in work [12]. As it results from the mass composition (Fig. 5), the fractions present in gasoline (C_6–C_{10}) are dominant. On the other hand, the fractions characteristic of diesel fuel (C_{11}–C_{15}) present in the amount of approximately 30% may adversely affect the octane number of pyrolysis oil due to their lower self-ignition temperature and thus higher tendency to generate knocking combustion.

3. Results and discussion

According to the assumptions, the heat release rate dQ/dt was determined on the basis of combustion pressure trace as depicted in Fig. 6. To avoid high numbers from deriving, the pressure was filtered.

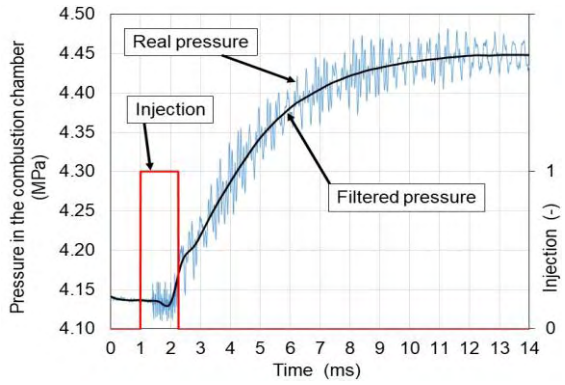

Fig. 6. Real and filtered combustion pressure trace in the combustion chamber at 41 bar initial pressure

Figure 7 shows the heat release rate dQ/dt for both tested fuels. The phases of premixed and diffusion combustion can be identified. As depicted, the premixed combustion for both fuels is faster than diffusion combustion. Additionally, higher dQ/dt is observed for pyrolysis oil, which confirms the conclusion about the higher chemical rate of reactions of substances forming pyrolysis oil.

Selected results from combustion analysis were included in Table 3.

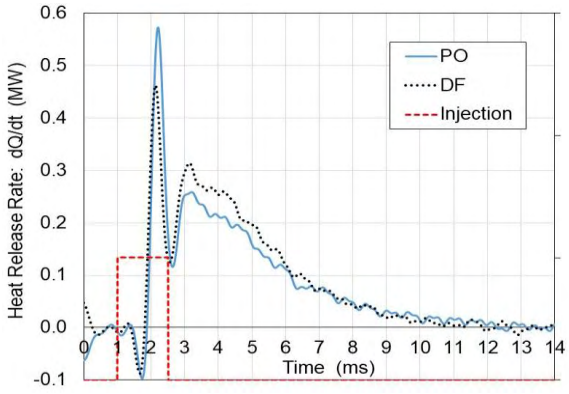

Fig. 7. Heat release rate history for pyrolysis oil and diesel fuel at initial pressure of 41 bar

Table 3. Selected combustion parameters for pyrolysis oil and diesel fuel combusted in the constant-volume combustion chamber

		Pyrolysis oil	Diesel fuel
Initial pressure	bar	41	41
$t_{0–2}$	ms	1.03	0.99
$t_{0–10}$	ms	1.22	1.21
t_{prem}	ms	0.91	0.89
t_{diff}	ms	5.06	4.55
t_{prem}/t_{diff}	%	18	20
Q_{prem}	J	202	181
Q_{diff}	J	907	997
Q_{total}	J	1109	1178
Q_{prem}	%	18.2	15.3
Q_{diff}	%	81.8	84.7
Q_{prem}/Q_{diff}	%	22.2	18.1
$dQ_{prem, max}$	MJ/s	0.57	0.46
$dQ_{diff, max}$	MJ/s	0.26	0.31

Figure 8 presents the combustion phases for pyrolysis oil and diesel fuel as follows: $t_{0–2}$, $t_{0–10}$, $t_{10–90}$, and $t_{0–90}$ for an initial pressure of 41 bar at the start of injection. As can be seen, the time intervals t_{0-2} or t_{0-10} that represent the ignition delay do not differ significantly from each other. Although, the time t_{0-10} is the time in which combusted fuel was 5 times larger of compared to the time $t_{0–2}$ as concluded from heat released. This can be explained by rapid acceleration of combustion in the initial combustion phase, caused by premixed combustion. As investigated, the main combustion phase denoted as $t_{10–90}$ is longer for pyrolysis oil. Even though, the change can be managed as insignificant, but it can affect higher soot and unburnt hydrocarbons in exhaust emissions if this pyrolysis oil would be implemented as a fuel to automotive compression ignition engines.

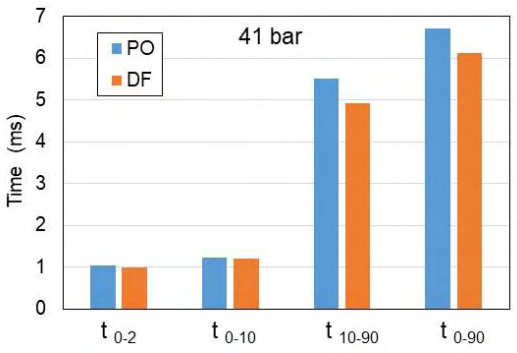

Fig. 8. Time period for combustion phases $t_{0–2}$, $t_{0–10}$, $t_{10–90}$ and $t_{0–90}$ for pyrolysis oil and diesel fuel combusted under initial pressure of 41 bar

In regards to Fig. 4, Fig. 9a shows the times of premixed t_{prem} and diffusion t_{diff} combustion phases for both tested fuels. It is obvious that the time t_{prem} is definitely shorter than the time t_{diff} as the flame at the premixed zone consumes fuel several times faster in comparison to the diffusion combustion zone. Hence, the fraction of the premixed combustion phase in relation to the diffusion combustion phase seems to be important. The percentage t_{prem}/t_{diff} quotient is shown in Fig. 10. As found, the premixed combustion is nearly five times shorter in general for both tested fuels.

a)

b)

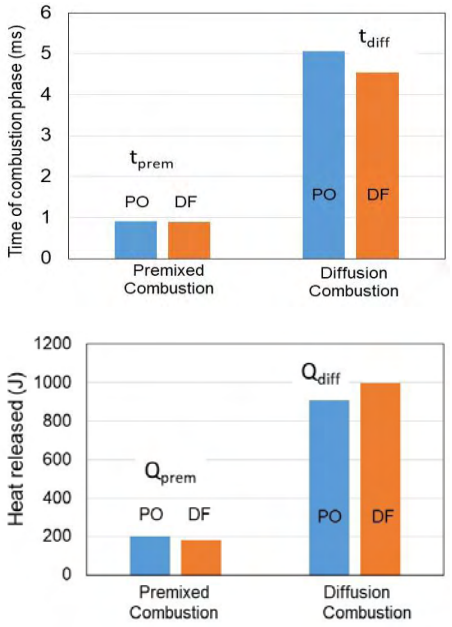

Fig. 9. Time periods for premixed and diffusion combustion phases t_{prem} and t_{diff} (a) and heat released Q_{prem} and Q_{diff} (b) for pyrolysis oil and diesel fuel combusted under initial pressure of 41 bar

In addition to comparing the time t_{prem} vs. t_{diff}, Fig. 9b depicts the amount of heat released in the premixed combustion phase Q_{prem} in relation to the diffusion combustion phase Q_{diff}. As observed, the heat contribution Q_{prem} is much higher than the time contribution t_{prem} relative to the diffusion combustion phase represented by parameters Q_{diff} and t_{diff}, respectively.

The summary of the analysis of the phases of premixed and diffusion combustion is the percentage fraction of the premixed phase referred to the diffusion phase. This comparison was made for time and heat released in these phases. As presented in Fig. 10, the time t_{prem} is nearly 5.5 times shorter than the time t_{diff} for pyrolysis oil, however, the heat released during premixed combustion is only 4.5 times lower, respectively. It means that more heat is released during premixed phase. If anyone compare these relations with diesel fuel tests, would notice opposite trend. Therefore, the maximum heat release rates dQ/dt were determined for the premixed and the diffusion combustion phases as depicted in Fig. 11. One can expect the premixed fuel burns faster if it concerns higher amount of light hydrocarbons, due to their faster evaporation.

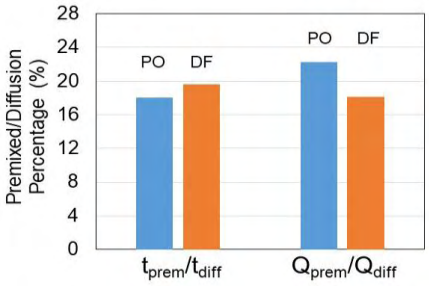

Fig. 10. Premixed to diffusion combustion percentage (t_{prem}/t_{diff} and Q_{prem}/Q_{diff}) for pyrolysis oil and diesel fuel in the combustion chamber under initial pressure of 41 bar

Thus, it is confirmed from the observation of maximum heat release rates for both tested fuels in their premixed and diffusion phases (Fig. 11). Pyrolysis oil in comparison to diesel fuel burns faster when it is premixed with air. On the other hand, pyrolysis oil burns slower in its diffusion phase in reference to diesel fuel.

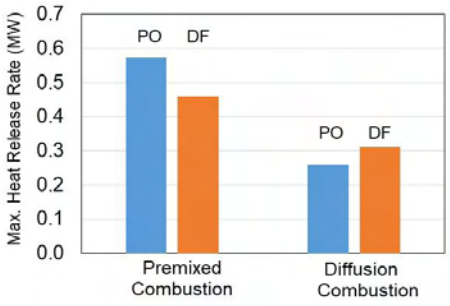

Fig. 11. Maximum heat release rate of premixed and diffusion combustion for pyrolysis oil and diesel fuel in the combustion chamber under initial pressure of 41 bar

6. Conclusions

Combustion tests were carried out on pyrolysis oil made of high density polyethylene (HDPE) as a result of pyrolysis at 575–600°C, which was then subjected to distillation in order to remove hydrocarbons with a C number above 15. The basic research tool was a comparative analysis, to which diesel fuel was used as the reference fuel. On the basis of the conducted research, the following conclusions can be drawn:

– The duration of the premixed combustion phase for pyrolysis oil is approximately 5% shorter than the premixed combustion phase for diesel fuel. Hence, this change can be considered marginal.
– The maximum combustion rate (assumed as heat release rate) for the premixed combustion phase for pyrolysis oil was approximately 27% higher than the premixed combustion rate for diesel fuel. However, the maximum rate of diffusion combustion was lower by 16% with respect to diesel fuel.
– The percentage fraction of heat released from the premixed combustion phase to total heat for pyrolysis oil was nearly 22%, whereas this parameter is 15% for diesel fuel. This is important because a bigger amount of fuel burned at the premixed phase leads to a faster pressure increase in the engine cylinder and improves the indicated efficiency of the thermodynamic cycle, which at the same time will improve the completeness of fuel combustion and reduce the specific fuel consumption.
– The self-ignition delay ($t_{0–2}$, $t_{0–10}$) for pyrolysis oil was slightly longer compared to the delay for diesel fuel. This affects the progress in further combustion, including the increase in pressure, however, in this case, it can be assumed that the ignition delay for both fuels has a similar value and in this approach, there is no significant difference between these tested fuels;
– It is proposed to use pyrolysis oil after distillation with the removal of hydrocarbons above C15 to power car engines, while for large stationary engines, attempts to burn raw pyrolysis oil can be made after examining its viscosity and sulfur content.
– It is recommended to test the exhaust gases toxicity of pyrolysis oil in stationary and dynamic load conditions.

Acknowledgements

This work was partially supported by the Polish National Agency for Academic Exchange Iwanowska program PPN/IWA/2019/1/00149/U/00001, Investigation of liquid products from thermal processing of waste as fuel to the internal combustion engine.

Special thanks for the help provided by the technical and support staff of the APSRC labs in the ME-EM and Chemical Engineering departments of Michigan Technological University, especially dr. David Shonnard and dr. Jeffrey D. Naber.

Nomenclature

c_p	specific heat at constant pressure
c_v	specific heat at constant volume
dQ/dt	heat release rate
dp	infinitesimal pressure change
$dQ_{diff,max}$	maximum heat release rate in diffusion combustion phase
$dQ_{prem,max}$	maximum heat release rate in premixed combustion phase
DF	diesel fuel
HDPR	high density polyethylene
HRR	heat release rate
κ	specific heat ratio
n	number of moles
PO	pyrolysis oil
Q	heat
Q_{diff}	heat released from diffusion combustion phase
Q_{prem}	heat released from premixed combustion phase
R_u	universal gas constant
t_0	start of injection
$t_{0–2}$	initial combustion phase
$t_{0–10}$	10% initial combustion phase
$t_{10–90}$	main combustion phase
t_{diff}	time of diffusion combustion phase
t_{prem}	time of premixed combustion phase
T	temperature
U	internal energy
V	volume

Bibliography

[1] Banar M, Akyildiz V, Özkan A, Çokaygil Z, Onay Ö. Characterization of pyrolytic oil obtained from pyrolysis of TDF (Tire Derived Fuel). Energy Convers Manag. 2012;62:22-30. https://doi.org/10.1016/j.enconman.2012.03.019

[2] Costa GA, Santos RG dos. Fractionation of tire pyrolysis oil into a light fuel fraction by steam distillation. Fuel. 2019; 241:558-563. https://doi.org/10.1016/j.fuel.2018.12.075

[3] Chwist M. Comparative analysis of heat release in a reciprocating engine powered by a regular fuel with pyrolysis oil addition. Combustion Engines. 2022;190(3):104-112. https://doi.org/10.19206/CE-146694
[4] Chwist M, Pyrc M, Gruca M, Szwaja M. By-products from thermal processing of rubber waste as fuel for the internal combustion piston engine. Combustion Engines. 2020; 181(2):11-18. https://doi.org/10.19206/CE-2020-202
[5] Damodharan D, Sathiyagnanam AP, Rana D, Kumar BR, Saravanan S. Combined influence of injection timing and EGR on combustion, performance and emissions of DI diesel engine fueled with neat waste plastic oil. Energy Convers Manag. 2018161:294-305. https://doi.org/10.1016/j.enconman.2018.01.045
[6] Grab-Rogalinski K, Szwaja S. The combustion properties analysis of various liquid fuels based on crude oil and renewables. IOP Conf Ser Mater Sci Eng. 2016;148. https://doi.org/10.1088/1757-899X/148/1/012066
[7] Hürdoğan E, Ozalp C, Kara O, Ozcanli M. Experimental investigation on performance and emission characteristics of waste tire pyrolysis oil–diesel blends in a diesel engine. Int J Hydrogen Energy. 2017;42(36):23373-23378. https://doi.org/10.1016/j.ijhydene.2016.12.126
[8] Kalargaris I, Tian G, Gu S. Experimental evaluation of a diesel engine fuelled by pyrolysis oils produced from low-density polyethylene and ethylene–vinyl acetate plastics. Fuel Process Technol. 2017;161:125-131. https://doi.org/10.1016/j.fuproc.2017.03.014
[9] Kareddula VK, Puli RK. Influence of plastic oil with ethanol gasoline blending on multi cylinder spark ignition engine. Alexandria Eng J. 201857(4):2585-2589. https://doi.org/10.1016/j.aej.2017.07.015
[10] Kumar Mishra R, Mohanty K. Co-pyrolysis of waste biomass and waste plastics (polystyrene and waste nitrile gloves) into renewable fuel and value-added chemicals. Carbon Resour Convers. 2020;3:145-155. https://doi.org/10.1016/j.crcon.2020.11.001
[11] Szwaja M, Chwist M, Szymanek A, Szwaja S. Pyrolysis oil blended n-butanol as a fuel for power generation by an internal combustion engine. Energy. 2022;261:125339. https://doi.org/10.1016/j.energy.2022.125339
[12] Szwaja M, Naber JD, Shonnard D, Kulas D, Zolghadr A, Szwaja S. Comparative analysis of injection of pyrolysis oil from plastics and gasoline into the engine cylinder and atomization by a direct high-pressure injector. Energies. 2023; 16(1):420. https://doi.org/10.3390/en16010420
[13] Szwaja S, Grab-Rogalinski K, Chwist M. Pyrolysis oil combustion in the CI engine. Combustion Engines. 2019; 179(4):126-131. https://doi.org/10.19206/CE-2019-420
[14] Tudu K, Murugan S, Patel SK. Effect of tyre derived oil-diesel blend on the combustion and emissions characteristics in a compression ignition engine with internal jet piston geometry. Fuel. 2016;184:89-99. https://doi.org/10.1016/j.fuel.2016.06.065
[15] Umeki ER, de Oliveira CF, Torres RB, Santos RG dos. Physico-chemistry properties of fuel blends composed of diesel and tire pyrolysis oil. Fuel. 2016;185:236-242. https://doi.org/10.1016/j.fuel.2016.07.092
[16] Vijaya Kumar K, Puli RK. Effects of waste plastic oil blends on a multi cylinder spark ignition engine. Abdul Amir HF, Khiew PS (ed.). MATEC Web Conf. 2017;108:08005. https://doi.org/10.1051/matecconf/201710808005

Szwaja Magdalena, MEng. – PhD student in Faculty of Mechanical Engineering and Computer Science at Czestochowa University of Technology, Poland.
e-mail: *magdaszw24@gmail.com*

Arkadiusz Szymanek, DSc., DEng. – Faculty of Mechanical Engineering and Computer Science at Czestochowa University of Technology, Poland.
e-mail: *arkadiusz.szymanek@pcz.pl*

Article citation info:
Grochowalska J, Jaworski P, Kapusta ŁJ. Analysis of the structure of the atomized fuel spray with marine diesel engine injector in the early stage of injection. Combustion Engines. 2023;195(4):97-103. https://doi.org/10.19206/CE-168394

Joanna GROCHOWALSKA
Piotr JAWORSKI
Łukasz Jan KAPUSTA

Combustion Engines
Polish Scientific Society of Combustion Engines

Analysis of the structure of the atomized fuel spray with marine diesel engine injector in the early stage of injection

ARTICLE INFO

Received: 31 May 2023
Revised: 15 June 2023
Accepted: 15 June 2023
Available online: 18 July 2023

This paper presents the results of the experimental research of the atomized fuel spray with the marine diesel engine injector in the constant volume chamber. The specificity of the phenomena occurring in the marine engine cylinder was the reason to use the optical visualisation method in the studies – the Mie scattering technique. This work presents an analysis of the influence of different geometry of outlet orifice and opening pressures of marine diesel injector on the macrostructure of the fuel spray. In the results, it was observed that the increased L/D ratio of the outlet orifice of the injector caused: an increase in the spray cone angle and a decrease in the spray tip penetration in the early stage of injection. Furthermore, it was defined that the characteristic of spray tip penetration over time was power, whereas the spray cone angle over time was a logarithmic function.

Key words: *marine diesel engine, marine diesel engine injector, early stage of injection, spray cone angle, spray tip penetration*

1. Introduction

Two- or four-stroke diesel internal combustion engines with direct in-cylinder fuel injection are used in marine ship engine rooms. A consequence of the fuel combustion process of marine engines is the emission of toxic compounds in the exhaust gases, such as nitrogen oxides (NO_x) or carbon oxides (CO_x). These marine diesel engines are usually fueled by marine diesel oil and heavy diesel oil. It should be mentioned that research is also conducted on the use of alternative fuels in marine diesel engines [28]. It is widely known that the amount of toxic compounds emitted in the exhaust of marine engines into the atmosphere is closely related to the fuel combustion process in the cylinder [8]. Consequently, the tightening requirements associated with meeting acceptable levels of toxic emissions in marine engine exhaust gases have become a major motivation for research work in this area.

The fuel injection system is responsible for the correct combustion of fuel in the cylinders of marine engines. The injectors are the main building block of the injection system, as they are responsible for the process of injecting and spraying the fuel at the correct time and dose.

The marine diesel engines use the closed injectors with a needle that opens under the force of compressed fuel [11]. The main difference in their design is using spray tips with different numbers and geometry of fuel outlet orifices. The geometry of the nozzle outlet orifice of the injector is one of the main factors determining the atomization process of the fuel spray [22]. Consequently, numerous research works are being carried out to determine the influence of various design features of the injector outlet orifice on the spray pattern of diesel engine cylinders [3–5, 27]. One such design feature considered in the research work is the ratio of outlet orifice length (L) to outlet orifice diameter (D) – (L/D). As previously mentioned, fuel injectors are used to atomize the fuel from liquid form into fine droplets. It should be noted that fuel in droplet form evaporates more quickly and mixes with air leading to an explosive mixture with the correct ratio of air and fuel masses. Therefore, the fuel atomization process is so important that it will affect the subsequent self-ignition process of the fuel-air mixture. The fuel injected under high pressure into the engine cylinder forms a cloud of droplets of varying diameter and spatial distribution.

The high injection pressure of the fuel in combination with the small outlet orifice of the injector results in the first atomization of the fuel stream into droplets, referred to as primary atomization, already during fuel flow through the orifices [21]. The fuel flowing from the spray nozzle outlet into the pressurized gas (in the cylinder) undergoes further rapid atomization into droplets. This decomposition is defined as the secondary atomization of the fuel spray into droplets [21]. The different forces govern the primary and secondary atomization process of the fuel spray. These forces are conditioned by the place of their occurrence and are classified into internal and external. The internal forces come from the fuel flow inside the injector. They include cavitation or fuel flow disturbances [2, 24, 26], and are influenced by the geometry of the injector's outlet orifices, inaccuracies resulting from the machining process of the orifice surface, or vibrations from the needle, and the injector itself [3, 5, 8]. On the other hand, the external forces result from high pressure and temperature in the cylinder.

In the fuel injection, atomization, and combustion process analysis, the information on the parameters determining the external shape and internal structure of the fuel cloud becomes crucial. This information constitutes the parameters referred to as macro and micro [16]. In the cylinder of a marine diesel engine, macro parameters provide information on the volume of the sprayed fuel. The knowledge of this geometry is required for the appropriate configuration of the injection system. The external shape of the spray cloud is characterised by macro parameters: spray tip penetration (STP) and spray cone angle (SCA).

The literature includes the mathematical models for calculating the STP and SCA, based on the results of the experimental research of the fuel injection and spray process [1, 6, 7, 14, 27]. These mathematical models are mainly

determined by: the pressures of the fuel injection process, the geometry of the injector outlets, or the density of the gas in the chamber. A pioneering two-stage model for the STP was presented in the work of Hiroyasu and Arai [12]. The two stages of the model rely on the fact that the early stage of injection of the fuel spray is directly proportional to the passage of time, and after a certain time t_{break} is proportional to the square root of time. This model was often the basis for defining new models [10, 13, 20]. It should be noted that, most mathematical models for the SCA do not account for the passage of time [12, 14, 23, 25]. This macro parameter is calculated as a constant maximum value.

The different designs of marine diesel engines with direct in-cylinder fuel injection in relation to the design of engines used in the automotive sector make it necessary to familiarise ourselves with the fuel injection and spray process in the cylinders of these engines [17, 18].

Considering the importance of the injector design parameters conditioning the fuel injection process into the cylinders of marine engines, the main aim of this paper is to analyse the effect of changing the L/D ratio of the outlet orifice of a marine engine injector on the geometry of the fuel spray. The paper particularly focuses on the early stage of atomization because, due to the relatively low rotational speed of direct-injection marine diesel engines, the fuel injection usually occurs within a few degrees of the crankshaft angular position before the TDC. This is the time when the air compressed by the piston forms the smallest volume of the high-temperature working space, which exceeds the self-ignition temperature of the fuel. As a result, the first foci of fuel spontaneous combustion appear in the cylinder space already during the initial fuel injection due to rapid processes of atomization into droplets, evaporation, and mixing with air. It is important to note that fuel combustion begins when not all the fuel has yet been delivered to the cylinder, and the fuel-air mixture formation continues throughout the fuel injection period. It is, therefore, important to carry out an analysis of the characteristics of the injected fuel spray into the cylinder at the early stage of spraying and not when the fuel spray has already developed and reached its maximum size.

2. Experimental test and method

The experimental research of the spray geometry was carried out on a laboratory bench using the constant volume chamber (CVC) presented in Fig. 1 [9, 10].

The CVC, measuring 200 mm × 200 mm in length and width, was filled with the inert gas – nitrogen. The backpressure in the chamber amounted to (P_b) 3.2 MPa. The backpressure in the chamber, corresponded to the pressures in the combustion chamber of the Sulzer 3 Al 25/30 marine diesel engine at the start of fuel injection into the cylinder, i.e. 18° before the TDC, operating at a correspondingly lower load. The diameter of the CVC access window was 100 mm. The principle of the fuel injector system was based on a common-rail system. A high-pressure fuel system (UPS – Unit Pump System) kept the fuel pressure constant at around 50 MPa. The fuel injection time was 0.04 s. A Sulzer 3 Al 25/30 marine diesel engine injector was used for the fuel injection and spray process in the CVC. The mechanical type injector was adjusted for three injector opening pressures P_o: 15, 25 and 35 MPa, respectively, by means of a needle pressure spring. The fuel pressure downstream of the injector was measured with a Kistler piezoresistive pressure sensor type 4067E designed specifically for measurements in hydraulic injection systems of internal combustion engines [15].

Only one nozzle orifice was active in the spray tip of the injector, and the others had been plugged. The dimensions of the injector orifice design parameters considered are presented in Table 1.

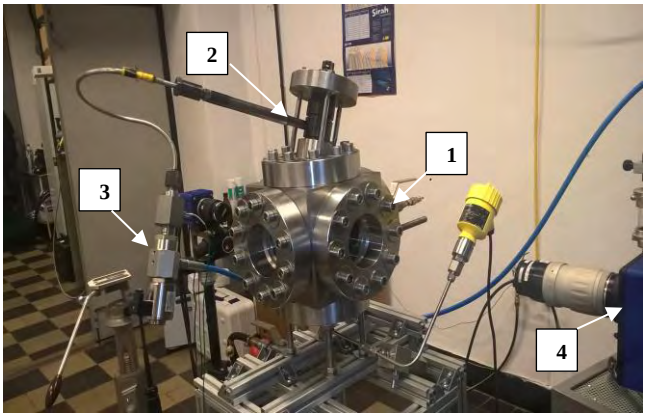

Fig. 1. Experimental laboratory set-up: 1 – constant volume chamber, 2 – marine diesel engine injector, 3 – Kistler 4067E pressure sensor, 4 – high-speed camera

The spray pattern was recorded using the Mie Scattering optical technique with a high-speed Photron SA1.1 camera with a recording frequency of 40 kHz [10, 19]. Two halogen lamps with a total output of 500 W were used to illuminate the chamber. The tests were conducted at 20–25°C. The used fuel was diesel, with a density of 816.1 kg/m^3 at 40°C.

Table 1. The nozzle dimensions

Nozzle	Diameter [mm]	Shape [-]	L/D [-]
1	0.285	cylindrical	10.9
2	0.325	cylindrical	9.5
3	0.375	cylindrical	8.3

Each measurement of the registration of the injected diesel spray into the constant volume chamber was repeated three times to eliminate coarse errors. A series of images of the injected diesel spray into the CVC were obtained from each trial. The example images for different times from the start of diesel injection are presented in Fig. 2.

The photographs of the diesel spray pattern obtained from the experimental research were subjected to image processing in the specialist software DaVis 8.4. On the basis of the graphically processed images, the geometric dimensions of the diesel spray pattern were calculated for the considered L/D ratio of the injector outlet orifices and injector opening pressures.

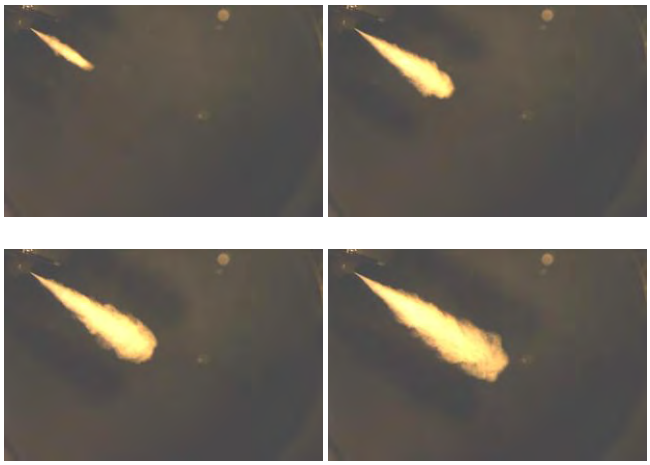

Fig. 2. The example results photos of diesel spray without outlet hole marine engine injector, L/D: 8.3; P_o: 15 MPa, P_b: 3.2 MPa

The STP is defined as the maximum reach of the fuel spray pattern in the cylinder. The SCA is the apex angle between two straight lines with a common origin at the injector outlet. The straight lines define the boundaries of the sprayed fuel in the radial direction from the spray symmetry. The definition of the STP is presented in Fig. 3a, and SCA in Fig. 3b.

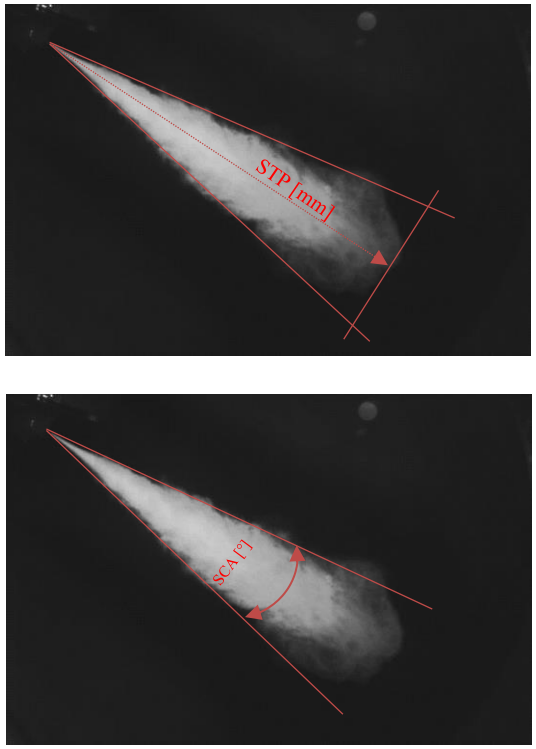

a)

b)

Fig. 3. The definition of: a) TP, b) SCA

3. Results and discussion

As part of the experimental research carried out, the STP and SCA measurement results were obtained for the spray pattern of diesel fuel from a marine diesel engine injector.

According to the example experimental results presented in Fig. 4, both the STP and SCA are time-dependent. As mentioned above, the macro parameters increase as the spray propagation time in the CVC increases. The STP characteristics of the chamber propagation were divided into three stages (Fig. 4a) and the SCA into two stages (Fig. 4b). According to Fig. 4, the stage one (I) was defined as rapid growth over a generally short period of time.

For stage (II) (Fig. 4a) for the STP, a more gentle and prolonged increase in the STP over time was observed until the stage (III), defined as "stabilisation – maximum STP", was reached. The rapid STP stage results from the initial velocity imparted to the jet by the occurring pressure difference between the injector opening pressure and the back-pressure in the CVC (P_o – P_b). During this time, the first break-ups of the spray into droplets also occur, mainly caused by the phenomena of primary atomization and secondary atomization. These phenomena include the occurrence of turbulence in the fuel jet flowing through the outlet orifice and the influence of forces from the gas medium with increased density in the CVC. In the stage (II), the diesel spray's atomization intensifies mainly due to the gas medium's aerodynamic forces in the CVC. Consequently, the stage II lasts longer than the stage I, and the STP growth during this time is more gentle. In the stabilisation stage (III), the range of the spray front reaches its maximum value. During this time, the maximum atomization of the spray into droplets occurs for the given experimental conditions.

The characteristics of the SCA over time were divided into two stages. The stage (I) similarly to the STP represents an initial rapid increase in the SCA.

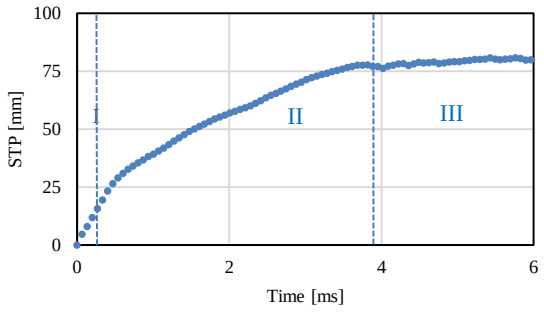

a)

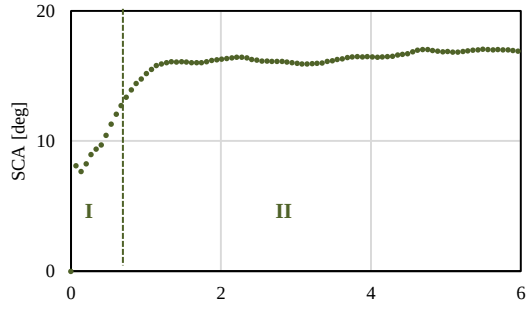

b)

Fig. 4. The example of results: L/D: 10.9; P_b: 3.2 MPa, P_o: 15 MPa, a) STP, b) SCA

The initial rapid increase in the SCA is mainly due to the difference in P_o – P_b pressure. The increased gas density in the CVC causes the diesel droplets contained in the in-

jected fuel cloud to be decelerated and deflected from the jet axis. The extremities of the spray's break-up into droplets, increasing the surface area occupied by the fuel. After approximately 1.2 ms, there is stabilisation and oscillation around a constant maximum SCA value, referred to as the stage (II) as shown in Fig. 4b.

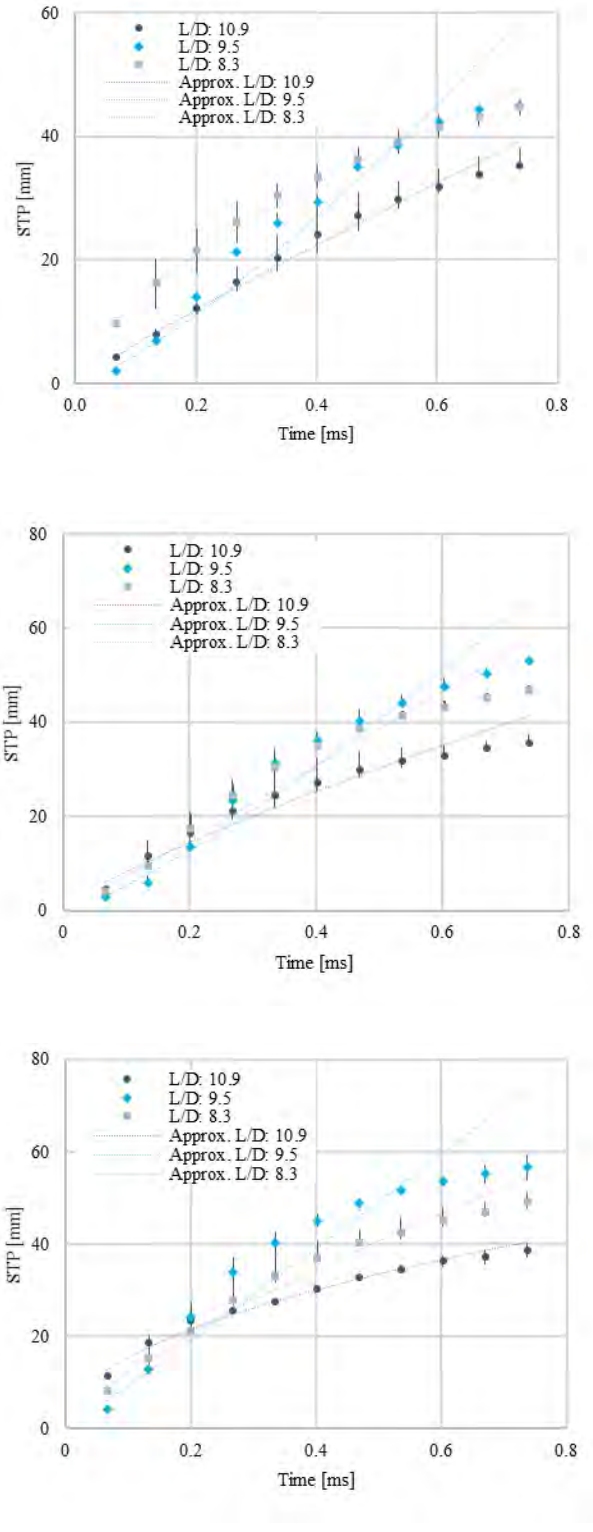

Fig. 5. The characteristics of the STP in the early stage of injection independent of different L/D ratios and opening pressures: a) 15 MPa, b) 25 MPa, c) 35 MPa

Figures 5 and 6 present the STP and SCA characteristics from injection start to 0.7 ms depending on the L/D ratio considered. The error bars present maximum and minimum values from each repeated measurement relative to the average.

In order to analyse the effect of the L/D ratio on the STP in the early stage of the spraying phase, an approximation method was applied using an appropriate mathematical function. The approximation lines are presented in Fig. 5 and 6. The best fit to the presented STP results was obtained using a power function. R^2 coefficients were calculated to assess the fit of the power function to the experimental data. The regression equations were determined for the specified functions according to the general form of the power function according to the general equation (1).

$$STP(t) = a\,t^n \tag{1}$$

where: STP – spray tip penetration; a, n – the regression coefficients; t – time [ms].

The calculated R^2 coefficients stand at 0.93–0.99, respectively, indicating a very good fit of the power function to the experimental results for time-dependent STP in the early stage of diesel spraying.

Table 3. The coefficients of regressions STP equations

P_o	L/D	a	n	R^2
15 MPa	10.9	51.67	0.91	0.99
	9.5	86.78	1.27	0.96
	8.3	58.04	0.64	0.99
25 MPa	10.9	52.88	0.80	0.95
	9.5	96.66	1.25	0.97
	8.3	78.501	1.02	0.96
35 MPa	10.9	46.90	0.49	0.98
	9.5	101.20	1.04	0.93
	8.3	68.32	0.75	0.98

Table 3 presents the calculated coefficients of the regression equations for the presented STP characteristics over time as a function of the L/D ratio and the injector opening pressures P_o considered. Based on the obtained directional coefficients "a" of the regression equations, it was observed that a change in the L/D ratio of the outlet orifice causes a change in the course of the STP characteristics during the early stage of diesel spraying.

Using Fig. 5 and Table 3, we have observed that as the L/D value of the injector fuel outlet increases, the STP decreases. For P_o: 15 MPa, the smallest STP was obtained for the L/D = 10.9 and the largest for the L/D value = 8.3. The STP for the L/D = 8.3 increased by an average of approx. 55% and for the L/D = 9.5 by 26% in relation to the STP for the L/D =10.9. However, it should be noted that for P_o: 25 and 35 MPa, the highest STP was observed for the L/D = 9.5, which increased by approximately. 35–36%, while for the L/D = 8.3, it increased by 21–24% with respect to the STP for the L/D = 10.9. An increase in L/D, i.e. a decrease in the diameter of the outlet orifice (for a constant orifice length L), results in a change in the fuel flow conditions in the orifice at certain injector opening pressure conditions. The diesel oil used in the tests is characterised by a significant viscosity and density, and therefore

a change in the outlet geometry can lead to turbulence in the high-pressure fuel flow in the injector outlet.

For P_o: 25 and 35 MPa, the initial STP (from 0 to approx. 0.2 ms) is greater for the L/D = 10.9 of the outlet hole compared to the other L/D values considered. This is the result of an intensification of the diesel spray's atomization due to the increased gas density in the chamber. The higher pressure difference (P_o – P_b) leads, for the L/D value of 10.9 of the outlet hole, to conditions in which the fuel spray atomizes faster and more intensively, which is associated with a temporary increase in the STP.

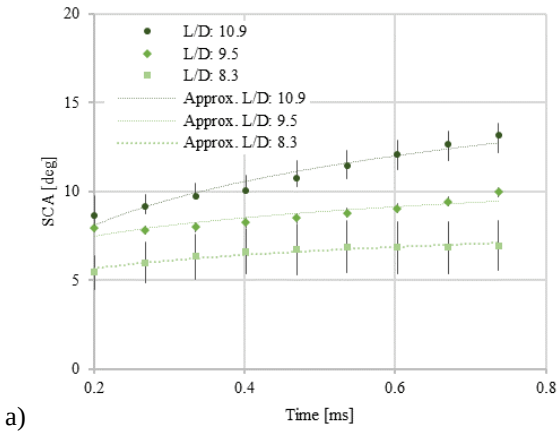

a)

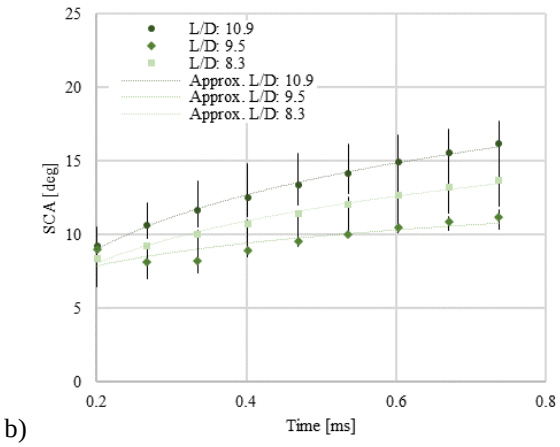

b)

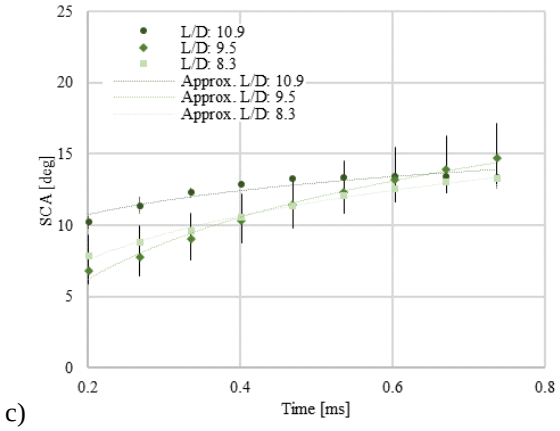

c)

Fig. 6. The characteristics of SCA in the early stage of injection in dependent of different L/D ratio and opening pressures: a) 15 MPa, b) 25 MPa, c) 35 MPa

Figure 6 presents the SCA characteristics between 0.2 and 0.7 ms. The first three measurements (at time 0–0.1 ms) were omitted from the analysis due to the difficulty in calculating the SCA of a very small fuel spray.

For the SCA, as for the diesel STP, an approximation method was applied using an appropriate mathematical function to determine the change in the L/D for the SCA during the early spraying stage. The best fit of the SCA experimental results was obtained for the logarithmic function according to the general equation (2).

$$SCA(t) = a \ln(t) + b \tag{2}$$

where: SCA – spray cone angle; a, b – the regression coefficients, t – time [ms].

The coefficient of determination R^2 for the determined cone angle characteristics was calculated and amounted to 0.82–0.99. The resulting R^2 calculations demonstrate a very good fit between the experimental results and the chosen logarithmic function.

Table 4. The coefficients of regressions SCA equations

P_o	L/D	a	b	R^2
15 MPa	10.9	3.56	13.80	0.95
	9.5	1.52	9.89	0.82
	8.3	1.10	7.42	0.91
25 MPa	10.9	5.34	17.58	0.99
	9.5	2.70	11.67	0.92
	8.3	4.15	14.72	0.99
35 MPa	10.9	2.43	14.66	0.88
	9.5	6.28	16.32	0.98
	8.3	4.42	14.71	0.99

Based on Fig. 6 and Table 4, it was observed that the SCA increases during the early stage of spraying. The highest SCA was obtained for the L/D = 10.9 for all P_o considered.

By reducing the diameter of the injector outlet, the fuel-wall friction force of the orifice increases in the wall layers, leading to an intensification of the shear forces of the spray layers. The occurrence of shear forces is a result of the viscosity effect of the diesel. Consequently, the increased disturbances occur in the injected diesel spray as a result of the intensification of the shear forces of the spray wall layers. The increased disturbance in the orifice and the smallest diameter of the outlet orifice under consideration resulted in the formation of droplets in the cloud, which lost their velocity faster and deviated from the jet axis due to the increased gas density in the CVC. Therefore, for the L/D = 10.9, a larger SCA was generally observed compared to the values of L/D = 9.5 and 8.3. A reduction in the L/D, i.e. an increase in the diameter of the injector outlet, results in a reduction in the SCA during the early stage of spraying. This is due to the occurrence of less turbulence in the spray and the formation of droplets in the cloud with greater mass and volume, which require more time to atomize and decelerate by the prevailing increased gas density in the chamber.

Conclusions

This paper presents the experimental research on the geometry of the diesel spray injected into the cylinder of

a marine engine. It should be noted that the measurement of the fuel injection and spray process in marine diesel engines requires a specialised laboratory bench fitted with equipment capable of simulating the conditions in a marine engine cylinder and measuring equipment with a wide measurement range.

On the basis of the analysis of the experimental results of the macrostructure of the diesel spray injected into the constant volume chamber, the following conclusions were drawn:

– STP and SCA of the marine diesel engine spray are time-dependent.
– The increase in the diesel STP over time in the early stage of spraying has the character of a power function, while the SCA, as a function of time, takes the character of a logarithmic function.
– The geometry of the spray pattern of diesel in the early stage of spraying is influenced by the change in the geometry of the injector outlet expressed by the L/D ratio.
– An increase in the L/D ratio of the outlet orifice resulted in an increase in the value of the cone angle of the spray over time considered.

Acknowledgements

The authors would like to thank Jerzy Kowalski, DSc., DEng., Gdansk University of Technology for their technical support and valuable remarks on the research of the fuel injection parameters in marine diesel engines.

Nomenclature

CVC	constant volume chamber
D	outlet orifice diameter
L	outlet orifice length
P_b	backpressure in the chamber
P_o	injector opening pressures
SCA	spray cone angle
STP	spray tip penetration
UPS	Unit Pump System

Bibliography

[1] Arrègle J, Pastor JV, Ruiz S. The influence of injection parameters on diesel spray characteristics. SAE Technical Paper 1999-01-0200. 1999. https://doi:10.4271/1999-01-0200
[2] Balz R, von Rotz B, Sedarsky D. In-nozzle flow and spray characteristics of large two-stroke marine diesel fuel injectors. Appl Therm Eng. 2020;180:115809. https://doi:10.1016/j.applthermaleng.2020.115809
[3] Benajes J, Pastor JV, Payri R, Plazas AH. Analysis of the influence of diesel nozzle geometry in the injection rate characteristic. J Fluids Eng Trans ASME. 2004;126(1):63-71. https://doi:10.1115/1.1637636
[4] Chang CT, Farrell PV. A study on the effects of fuel viscosity and nozzle geometry on high injection pressure diesel spray characteristics. SAE Technical Paper 970353. 1997. https://doi.org/10.4271/970353
[5] Dan T, Yamamoto T, Senda J, Fujimoto H. Effect of nozzle configurations for characteristics of non-reacting diesel fuel spray. SAE Technical Paper 970355. 1997. https://doi.org/10.4271/970355
[6] Delacourt E, Desmet B, Besson B. Characterisation of very high pressure diesel sprays using digital imaging techniques. Fuel. 2005;84:859-867. https://doi.org/10.1016/j.fuel.2004.12.003
[7] Dent JC. A basis for the comparison of various experimental methods for studying spray penetration. SAE Technical Paper 701571. 1971. https://doi.org/10.4271/710571
[8] Gopinath S, Devan PK, Sabarish V, Sabharish Babu BV, Sakthivel S, Vignesh P. Effect of spray characteristics influences combustion in DI diesel engine – a review. Mater Today-Proc. 2020;33:52-65. https://doi.org/10.1016/j.matpr.2020.03.130
[9] Grochowalska J. Analysis of the macrostructure of the fuel spray atomized with marine engine injector. Combustion Engines. 2019;179(4):80-85. https://doi.org/10.19206/CE-2019-413
[10] Grochowalska J, Jaworski P, Kapusta ŁJ, Kowalski J. A new model of fuel spray shape at early stage of injection in a marine diesel engine. Int J Numer Method H. 2022; 32(7):2345-2359. https://doi.org/10.1108/HFF-05-2021-0349
[11] Heywood JB. Internal Combustion Engine Fundamentals. McGraw-Hill, Inc. 1988.
[12] Hiroyasu H, Arai M. Structures of fuel sprays in diesel engines. SAE Technical Paper 900475. 1990. https://doi.org/10.4271/900475
[13] Jung D, Assanis DN. Multi-zone di diesel spray combustion model for cycle simulation studies of engine performance and emissions. SAE Technical Paper 2001-01-1246. 2001. https://doi.org/10.4271/2001-01-1246
[14] Kegl B, Lešnik L. Modeling of macroscopic mineral diesel and biodiesel spray characteristics. Fuel. 2018;222:810-820. https://doi.org/10.1016/j.fuel.2018.02.169
[15] Kistler. Piezoresistive High Pressure Sensor. 2014. https://www.kistler.com/?type=669&fid=61054&model=document&callee=frontend
[16] Klyus O, Rajewski P, Lebedevas S, Olszowski S. Determination of fuel atomization quality in compression ignition engines using acoustic emission signal. Combustion Engines. 2022;191(4):83-91. https://doi.org/10.19206/CE-149370
[17] Kowalski J. An experimental study of emission and combustion characteristics of marine diesel engine with fuel pump malfunctions. Appl Therm Eng. 2014;65(1-2):469-476. https://doi.org/10.1016/j.applthermaleng.2014.01.028
[18] Kowalski J. The theoretical study on influence of fuel injection pressure on combustion parameters of the marine 4-stroke engine. Journal of KONES Powertrain Transp. 2016; 23(1):161-168. https://doi.org/10.5604/12314005.1213553
[19] Lewińska J. Analysis of measurement methods for fuel injection spray parameters from marine engine injector. Journal of KONES. 2016;23(4):275-282. https://doi.org/10.5604/12314005.1
[20] Naber JD, Siebers DL. Effects of gas density and vaporization on penetration and dispersion of diesel sprays. SAE Technical Paper 960034. 1996. https://doi.org/10.4271/960034
[21] Nagasaka K, Takagi T, Koyanagi K, Yamauchi T. Development of fine atomization injector. JSAE Rev 2000;21(3): 309-313. https://doi.org/10.1016/S0389-4304(00)00049-7

[22] Payri R, Salvador FJ, Gimeno J, de la Morena J. Effects of nozzle geometry on direct injection diesel engine combustion process. Appl Therm Eng. 2009;29(10):2051-2060. https://doi.org/10.1016/j.apthermaleng.2008.10.009
[23] Reitz RD, Bracco FB. On the dependence of spray angle and other spray parameters on nozzle design and operating conditions. SAE Technical Paper 790494. 1979. https://doi.org/10.4271/790494
[24] Salvador FJ, Gimeno J, De la Morena J, González-Montero LA. Experimental analysis of the injection pressure effect on the near-field structure of liquid fuel sprays. Fuel. 2021;292: 120296. https://doi.org/10.1016/j.fuel.2021.120296
[25] Siebers DL. Scaling liquid-phase fuel penetration in diesel sprays based on mixing-limited vaporization. SAE Technical Paper 1999-01-0528. 1999. https://doi.org/10.4271/1999-01-0528
[26] Som S, Ramirez AI, Longman DE, Aggarwal SK. Effect of nozzle orifice geometry on spray, combustion, and emission characteristics under diesel engine conditions. Fuel. 2011; 90(3):1267-1276. https://doi.org/10.1016/j.fuel.2010.10.048
[27] Wakuri Y, Fujii M, Amitani T, Tsuneya R. Studies on the penetration of fuel spray in a diesel engine. Bulletin of JSME. 1960;9:123-130. https://doi.org/10.1299/jsme1958.3.123
[28] Zacharewicz M, Kniaziewicz T. Model tests of a marine diesel engine powered by a fuel-alcohol mixture. Combustion Engines. 2022;189(2):83-88. https://doi.org/10.19206/CE-143486

Joanna Grochowalska, MEng. – Faculty of Mechanical Engineering and Ship Technology, Gdansk University of Technology, Poland.
e-mail: *joanna.lewinska@pg.edu.pl*

Piotr Jaworski, DEng. – Faculty of Power and Aeronautical Engineering, Warsaw University of Technology, Poland.
e-mail: *jaworskp@icloud.com*

Łukasz Jan Kapusta, DEng. – Faculty of Power and Aeronautical Engineering, Warsaw University of Technology, Poland.
e-mail: *lukasz.kapusta@pw.edu.pl*

Article citation info:
Szwajca F, Wisłocki K. Experimental identification of the electrical discharge on a surface gap spark plug. Combustion Engines. 2023;195(4):104-108. https://doi.org/10.19206/CE-168296

Filip SZWAJCA
Krzysztof WISŁOCKI

Combustion Engines
Polish Scientific Society of Combustion Engines

Experimental identification of the electrical discharge on a surface gap spark plug

ARTICLE INFO

Received: 22 May 2023
Revised: 12 June 2023
Accepted: 13 June 2023
Available online: 14 June 2023

The main objective of the research is to assess the influence of the spark plug electrodes geometry on the structure of the electric arc. This issue is increasingly important in modern gas-fueled engines with lean and stratified air-gas mixtures. To explain the influence of electrode geometry on selected spark discharge indicators, optical tests were conducted, and the parameters of the test history, together with the movies of the discharging process, were recorded and analyzed. The tests were carried out comparatively for two types of spark plugs on the test stand: conventional spark plug and spark plug with a flat ground electrode. It has been found that using flat plug electrodes allows a larger spark area covered by the electric arc without losing the intensity of radiation. More, using an unconventional spark plug results in a shorter discharge time relative to the conventional spark plug, while the geometry of the conventional spark plug allows for maintaining a stable electric arc with a minimum tendency for creeping.

Key words: *spark discharge, spark plug geometry, ignition system, optical research, electric arc development*

1. Introduction

The development of onboard energy sources in vehicles aims to complete or significantly eliminate exhaust emissions [12, 16]. Work in this area involves improving combustion engines or implementing battery and fuel cell systems [10, 13]. According to information reported by Grand View Research, the internal combustion engine market in 2021 consisted of almost 170 million units and a growth trend of 9.3% by 2030 is predicted [9].

The internal combustion engine is a thermal machine that can be powered by fuels of very different composition and physical state, which makes it a multipurpose source of mechanical energy. The combustion of various types of gaseous fuels in internal combustion engines has positive effects on the environmental performance of the power unit and, by burning mixtures with high excess air in addition to improving environmental performance, a reduction in fuel consumption as a result of increased thermal efficiency [7].

As the excess air in the combustible mixture increases, the demand for energy for initiating the combustion process rises [11]. To increase the ignition energy in SI engines and thus improve the benefits of lean combustion, the development of modern alternative ignition systems such as laser ignition, Microwave-Assisted Spark Ignition, Radio Frequency Based Corona Ignition system or the use of a pre-combustion chamber is being carried out [18]. Studies using a Rapid Compression Machine for three configurations of the system using a pre-combustion chamber indicated a significant improvement in thermodynamic indicators and flame development under lean natural gas combustion conditions relative to a conventional SI system [4]. A limitation in using the mentioned systems is their complication and, at the moment, the fact that they are not implemented on a wide scale.

In order to improve ignition properties, it is possible to modify the widely used spark ignition, that is, the initialization of the combustion process from an electric arc. An example is Digital Twin Spark Ignition [14]. Positive results were achieved by modifying the ignition system by implementing capacitors, which resulted in increased engine stability, shortened combustion duration CA10-90, reduced emissions and fuel consumption [5]. Fiedkiewicz et al. [12] also conducted work on increasing the energy generated by a spark ignition system by using a high-voltage ceramic capacitor connected in parallel. As a result, optical and indicator tests on rapid compression machine showed a 20% reduction in combustion time and a 14% increase in flame propagation speed. Hayashi et al. [8] pointed out the possibility of improving charge ignitability by controlling the discharge current. When the intensity of charge movement is high, the discharge current should be shortened, and when it is low, it should be lengthened. As a result, it is possible to increase the limiting excess ratio by 0.2, up-to 1.8.

During engine testing, the effect of the ground electrode number on engine operation was evaluated [1]. Of the spark plugs with four, two, one and no external ground electrodes, the best results in the most stable engine operation were achieved with a plug without a side ground electrode. Another study [3] compared a conventional spark plug and one equipped with a corona ground electrode. The corona spark plug improved fuel economy and reduced hydrocarbon emissions with an undesirable increase in nitrogen oxide emissions.

Tambasco at al. [17] investigated the comparative evaluation of spark plugs with a J-shaped ground electrode and a four-electrode spark plug with flat electrodes. The research was conducted using a small constant volume chamber. Higher thermal energy and energy conversion efficiency from electricity to heat were obtained for the J-shaped electrode plug. In addition to the number of electrodes, the gap between the ground and central electrodes is also important. Optical and thermodynamic tests under different excess air ratio conditions for plugs with gaps of 1.0, 1.2 and 1.4 showed the effect of the gap on combustion, especially under stoichiometric and lean combustion conditions [2]. The worst results in terms of engine stability were obtained with a spark plug using a 1 mm gap. Energy and emission benefits increased as the gap between electrodes widened.

A simulation study comparing the effects of using an iridium spark plug with a center electrode diameter of 0.7 mm and one with a center electrode diameter of 2.5 mm showed an improvement in combustion stability of a maximum by 13.5% at partial load and low speed [15]. In addition, the possibility of reducing fuel consumption by 1.25% was indicated.

In consideration of the literature information regarding the possibility of increasing ignition energy by changing the geometry of the spark plug, the authors of this article attempted a comparative evaluation of two types of spark plugs. It was decided to answer the question of what effect the shape of the spark plug electrodes has on the discharge waveform and efficiency. It was resolved to conduct model tests using high-speed imaging and recording of electrical parameters. Two spark plugs differing in the shape of the ground electrode, and the material of the central electrode were selected for the study. The authors hypothesize that the model results correlate with the possibility of improving the combustion process in gas engines operating in lean combustion mode. In the mentioned mode of operation, ignition energy is particularly important and determines the final performance and emissions of the engine.

2. Methodology

2.1. Spark plugs geometry

The test objects accepted for investigations were two spark plugs (Fig. 1) differing in the electrodes' geometry and the central electrode's material. The first (Fig. 1a), recognized as conventional due to its wide use in SI internal combustion engines, is a spark plug with a side electrode with a truncated cone, whose central electrode is made of iridium, and the gap between the electrodes is 0.8 mm. The other one (Fig. 1b) is a spark plug with a flat side electrode that realizes a semi-surface discharge, whose central electrode is made of nickel, and the gap between the electrodes is 1.3 mm. For this paper, the conventional spark plug is designated by Z, while the spark plug with a flat ground electrode is R. Both plugs have M10 threads so that they can be used in two-stage combustion systems of high-speed engines with limited space.

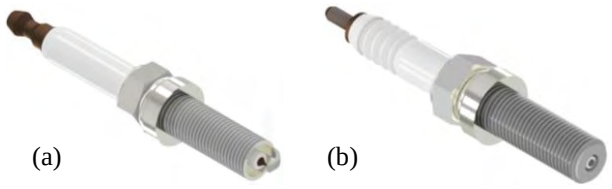

Fig. 1. Spark plug units used during testing: (a) a conventional Z spark plug and (b) a spark plug with a flat ground electrode R

2.2. Test stand and investigating apparatus

To evaluate the effect of spark plug geometry on the discharge character, a test stand fitted with a constant-volume chamber, high-speed filming equipment and electrical measurement apparatus was used (Fig. 2).

The constant volume chamber used, in which the spark plugs were installed, has a capacity of 2.2 L and optical access through 5 quartz glasses with a thickness of 30 mm. Attached to the chamber is an air pumping system consisting of a compressor, cylinder and solenoid valves. LaVision's HSS5 high-speed recording camera, an AF Nikkor prime lens, and a 700FS80-50 filter were used for optical signal recording. Electrical parameters were recorded with an eight-channel Sirius data acquisition system from DEWESoft with a maximum sampling rate of 200 kHz and voltages of 200 V and 1200 V (four channels each). Current clamp meter PP218 was used for current measurement, and capacitive pickup probe PP178 for high voltage. The voltage on the primary side was recorded directly.

A controller from the mechatronics company was used to check the ignition coil with the possibility of controlling the ignition timing and the coil charging time (up to 5 ms). A sequencer was used to initiate the operation of the camera and the ignition controller, allowing the start of the devices to be controlled with an accuracy of 1 ns.

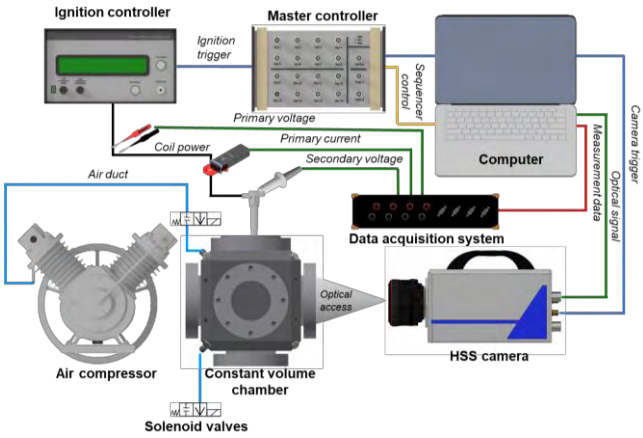

Fig. 2. Layout of test stand used to identify spark discharge

2.3. Experimental setup

The design of the spark plugs required different locations in the constant-volume chamber so that the direction of recording would remain constant and the optical system would not be affected during testing. Spark plug Z was placed in the axis of the chamber perpendicular to the direction of the camera lens so that the discharge could be recorded from the side (Fig. 3a). Spark plug R, on the other hand, was placed in the rear of the chamber in the axis of the lens to register the image from the front (Fig. 3b). During testing, the camera was moved back or forward by the difference in distance between the spark plugs as required.

The optical test plan included recording the discharge for ambient pressure and two overpressure values of 5 and 8 bar. During electrical measurements, a test point was added for 12 bar overpressure. The tests were conducted for a 4 ms constant value of the ignition coil charging time, leading to an end-charge current of 10.0 A.

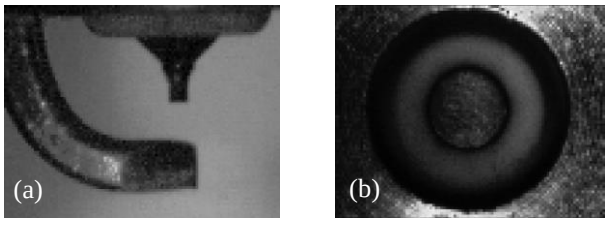

Fig. 3. View of spark plug Z from the side (a) and R from the front (b) when the discharge process is recorded optically

3. Results

3.1. Optical observations

The spark discharge at the electrodes of the analyzed spark plugs was recorded at 100,000 fps with a resolution of 128 × 80 pixels (Fig. 4-5). Due to the intensity of the discharge, an additional 700FS80-50 filter was put on the lens, and the exposure time was reduced significantly. DaVis software was used to process the images, allowing the background to be removed and the images to be parameterized to determine the intensity of the luminous and the area of the electric arc.

Figure 4 shows the first 40 μs of the spark discharge at ambient pressure in the chamber and an ignition coil charging time of 4 ms. In addition to the view of the arc, the electrode contours in the white line have been added. The first photo making the arc visible is marked as time 0. Luminous intensity is illustrated as a blue-to-red spectrum corresponding to the arc temperature, while the accurate value was not determined. In the case of the R spark plug, the arc is between the center and ground electrodes perpendicular to the axis of the spark plug, whereas in the case of the Z plug, the location is parallel. For the Z spark plug, a high concentration of energy was noted at the tip of the central electrode, which was not found for the R spark plug. However, this is probably related to the properties of the materials used for the electrodes. For the R spark plug, with time, the heat spreads over the surface of the central electrode without an expressed increase in heat density.

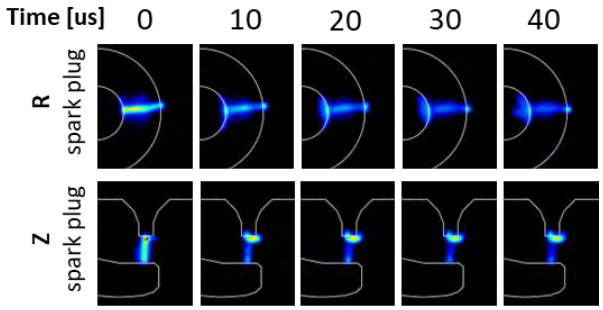

Fig. 4. Sequence of electric arc images without back pressure in a constant volume chamber

The effects of increasing the chamber pressure to 8 bar for the same ignition coil charging time are shown in Fig. 5. For this case, the sequence of images begins at 20 μs from the arc breakdown. The first two images were omitted because the luminescence intensity was too high, which led to their overexposure. In both cases, the area of the arc has increased, and the shape has changed. At the ends of the arcs, one can see a marked concentration of energy in both cases, with a longer duration for the R spark plug. The location of the arc for the R spark plug has changed relative to the position in Fig. 4. This type of geometry changes the arc's location within the electrodes from cycle to cycle, which is visible when analyzing several consecutive discharges. When the recording of the full discharge is analyzed, the change in arc location can also be seen within a cycle.

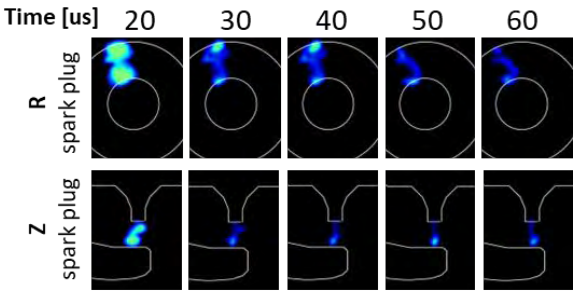

Fig. 5. Sequence of electric arc images with back pressure in a constant volume chamber of 8 bar

The previously presented images were further processed to determine the area and luminous intensity of the electric arc. In addition, the case of a 5 bar chamber pressure was also analyzed. Figure 6 shows the change in arc area for three values of pressure and both spark plugs. In all analyzed cases, the arc generated by the R spark plug has a larger surface area, and the differences range from 89 to as much as twice. The R spark plug is more responsive to pressure changes considering the surface area. In the case of the Z spark plug for different pressure values, the results are comparable.

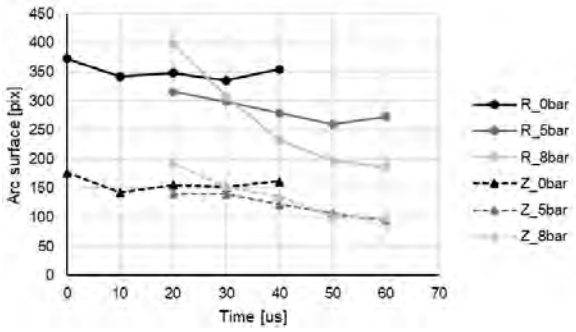

Fig. 6. Effect of pressure in the constant volume chamber on the electric arc area generated by the analyzed spark plugs

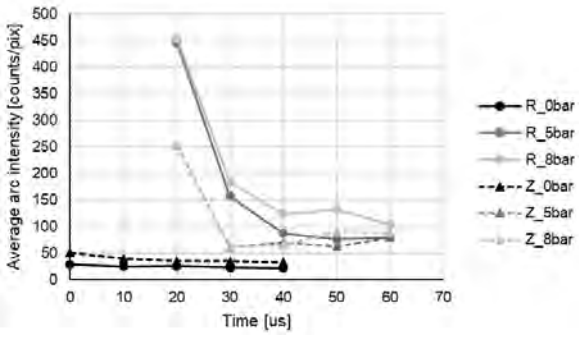

Fig. 7. Effect of pressure in the constant volume chamber on the average luminescence of the electric arc generated by the analyzed spark plugs

Each recorded pixel has a value representing the glow intensity in the range of 0 to 1023. Based on the number of pixels representing the arc area and the intensity value of each pixel, the average glow intensity of the arc was determined. For ambient pressure, a higher value of the average glow intensity was achieved with spark plug Z. As the

pressure and, thus, the air density increases, the average glow intensity increases. For higher pressure values in the initial stage of arc glowing, the R spark plug turns out to be better, and the differences range from 17% to as much as twice.

A parameter that has also been considered is the maximum illumination value for a particular image (Fig. 8). The maximum possible value is reached for overpressure values of 5 and 8 bar, considering the optics used. The trends correspond to those shown in the previous Fig. 7.

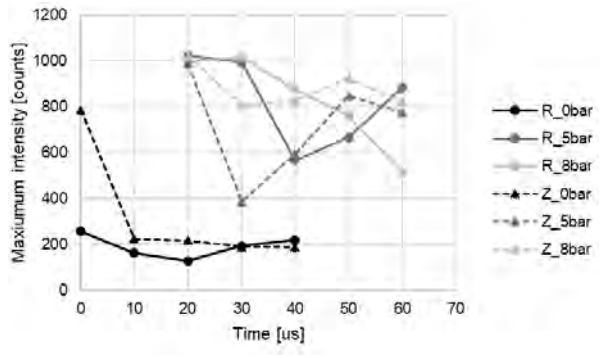

Fig. 8. Effect of pressure in the constant volume chamber on the maximum luminescence of the electric arc generated by the analyzed spark plugs

3.2. Electrical measurements

To complement the optical tests, electrical measurements were conducted. During the discharge, the voltage and current in the primary circuit and the voltage in the secondary circuit of the ignition coil were recorded (Fig. 9). For an ignition coil charging time of 4 ms, the amount of energy delivered is about 242 mJ. The energy transferred to the plug is minus the coil losses. Because the tests were conducted in a model way without combustion, the waveforms differ slightly from those obtained on a real internal combustion engine.

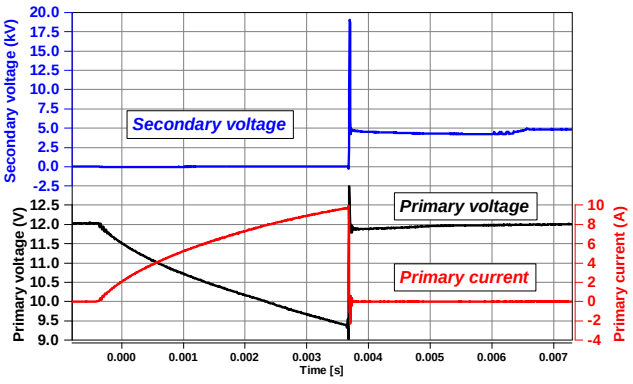

Fig. 9. History of measured electrical parameters during the process of charging the ignition coil and spark discharge

Figure 10 shows an example of the high voltage waveform in the secondary circuit of the ignition coil for an R and Z plug at 5 bar. The waveform for an R-type plug (red) during the entire discharge phase is less regular. This indicates a change in the position of the arc or, in extreme situations, an interruption. The Z spark plug is characterized by generating a more stable arc with localized interference, particularly evident at the end of the discharge. An important piece of information to obtain an explanation for the larger area of the arc and slightly higher intensity of the arc for the R spark plug relative to the Z spark plug is the duration of the discharge. For the illustrated single case, the discharge generated by the R spark plug is shorter by 0.86 ms, 70.6% of the discharge time on the Z spark plug.

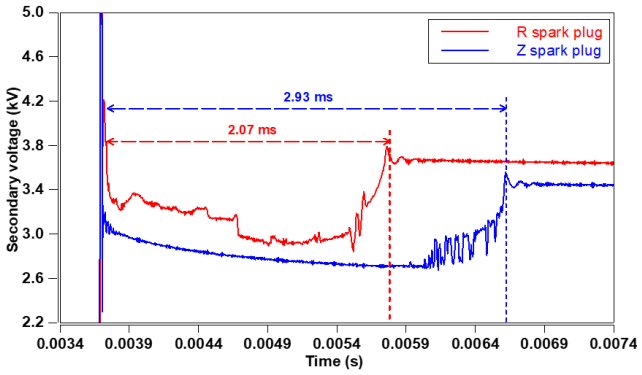

Fig. 10. High voltage waveform in the secondary circuit of the ignition coil during a spark discharge with the discharge time specified

Figure 11 shows the discharge duration relative to chamber pressure for the two spark plugs analyzed. The data shown in the diagram (Fig. 11) are averaged from five consecutive discharges at a distance of 120 ms, corresponding to 1000 rpm of a four-stroke engine speed. In the overpressure area, the discharge time decreases as the pressure increases. Throughout the analyzed area, the spark plug Z generates a discharge that lasts 4 to 30% longer. As a result of the reduction in discharge time, while supplying the same energy to the ignition coil, the physical arc breakdown processes increase in intensity. As a result, the change in the geometry of the spark plug electrodes caused an improvement in the energy density of the discharge.

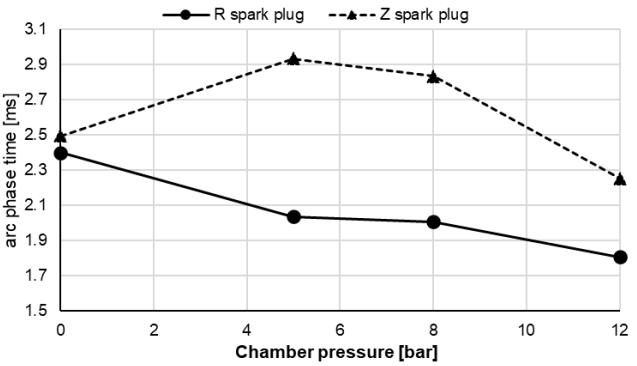

Fig. 11. Dependence of spark discharge duration on pressure in constant volume chamber

4. Conclusion

In the study presented in this paper, a model experimental study was performed to evaluate the effect of spark plug geometry on spark discharge. The tests were carried out using a constant-volume chamber, which allowed a partial reconstruction the conditions in the cylinder of an internal combustion engine. The effect of the discharge was evaluated at an ignition coil constant charging time value and a variable value of the overpressure in the Constant

Volume Chamber. According to the images of the spark discharge taken by high-speed imaging techniques and the recording of the voltage and current history of the ignition coil circuits, the following conclusions have been made:

– high luminous intensity of the spark discharge process during filming requires changes in the optical setup for the various phases of the discharge (appropriate filters, exposure time);
– surrounding pressure significantly affects the nature of the discharge, which becomes more intense as the pressure increases;
– the geometry of the spark plug significantly impacts the discharge pattern. For a conventional spark plug, the position of the arc during the discharge does not significantly change relative to the electrodes, in contrast to a plug with a flat electrode under conditions without air movement;
– using an R-type spark plug with a flat ground electrode makes it possible to increase the area of the arc while maintaining the intensity of the illumination;
– type R spark plug with a flat ground electrode is characterized by a shortening of the spark discharge leading to an increase in the concentration of energy in the electric arc which can contribute to an increase in combustion efficiency under unfavorable conditions inside the ignition chamber of a gas engines.

Acknowledgements

The research was supported by Poznan University of Technology with grant number 0415/SBAD/0338.

Bibliography

[1] Abdel-Rehim AA. Impact of spark plug number of ground electrodes on engine stability. Ain Shams Engineering Journal. 2013;4(2):307-316. https://doi.org/10.1016/j.asej.2012.09.006
[2] Badawy T, Bao X, Xu H. Impact of spark plug gap on flame kernel propagation and engine performance. Appl Energ. 2017;191:311-327. https://doi.org/10.1016/j.apenergy.2017.01.059
[3] Brereton GJ, Rahi MA. Some effects of spark plug electrode geometry and orientation on small-engine emissions. SAE Technical Paper 982057. 1998. https://doi.org/10.4271/982057
[4] Bueschke W, Szwajca F, Wislocki K. Experimental study on ignitability of lean CNG/air mixture in the multi-stage cascade engine combustion system. SAE Technical Paper 2020-01-2084. 2020. https://doi.org/10.4271/2020-01-2084
[5] Camilli LS, Gonnella JE, Jacobs TJ. Improvement in spark-ignition engine fuel consumption and cyclic variability with pulsed energy spark plug. SAE Technical Paper 2012-01-1115. 2012. https://doi.org/10.4271/2012-01-1151
[6] Fiedkiewicz Ł, Pielecha I. Optical analysis of the gas flame development in a RCM using a high-power ignition system. Combustion Engines. 2018;173(2):47-54. https://doi.org/10.19206/ce-2018-208
[7] Gracz W, Marcinkowski D, Golimowski W, Szwajca F, Strzelczyk M, Wasilewski J et al. Multifaceted comparison efficiency and emission characteristics of multi-fuel power generator fueled by different fuels and biofuels. Energies. 2021;14(12):3388. https://doi.org/10.3390/en14123388
[8] Hayashi N, Sugiura A, Abe Y, Suzuki K. Development of ignition technology for dilute combustion engines. SAE Int J Engines. 2017;10(3):984-995. https://doi.org/10.4271/2017-01-0676
[9] Internal combustion engine market size & share report, 2030. https://www.grandviewresearch.com/industry-analysis/internal-combustion-engine-market/methodology# (accessed May 10, 2023).
[10] Jeyaseelan T, Ekambaram P, Subramanian J, Shamim T. A comprehensive review on the current trends, challenges and future prospects for sustainable mobility. Renew Sust Energ Rev. 2022;157:112073. https://doi.org/10.1016/j.rser.2022.112073
[11] Moorhouse J, Williams A, Maddison TE. An investigation of the minimum ignition energies of some C1 to C7 hydrocarbons. Combust Flame. 1974;23(2):203-213. https://doi.org/10.1016/0010-2180(74)90058-3
[12] Pielecha I, Szalek A. Analysis of energy flow in the hybrid power-split (PS) system of SUV vehicle in real driving conditions (RDC). SAE Technical Paper 2022-01-1135. 2022. https://doi.org/10.4271/2022-01-1135
[13] Pielecha I, Szałek A, Tchorek G. Two generations of hydrogen powertrain – an analysis of the operational indicators in real driving conditions (RDC). Energies. 2022;15(13):4734. https://doi.org/10.3390/en15134734
[14] Ramtilak A, Joseph A, Sivakumar G, Bhat SS. Digital twin spark ignition for improved fuel economy and emissions on four stroke engines. SAE Technical Paper 2005-26-008. 2005. https://doi.org/10.4271/2005-26-008
[15] Sjerić M, Taritaš I, Kozarac D. Effect of spark plug geometry on the cyclic combustion variability and fuel consumption of gasoline engines. J Energ Eng. 2017;143(6). https://doi.org/10.1061/(asce)ey.1943-7897.0000492
[16] Skobiej K, Pielecha J. Analysis of the exhaust emissions of hybrid vehicles for the current and future RDE driving cycle. Energies. 2022;15(22):8691. https://doi.org/10.3390/en15228691
[17] Tambasco C, Hall M, Matthews R. Spark discharge characteristics for varying spark plug geometries and gas compositions. SAE Technical Paper 2022-01-0437. 2022. https://doi.org/10.4271/2022-01-0437
[18] Vedharaj S. Advanced ignition system to extend the lean limit operation of spark-ignited (SI) engines – a review. Energy, Environment, and Sustainability. 2021:217-255. https://doi.org/10.1007/978-981-16-1513-9_10

Filip Szwajca, MEng. – Faculty of Civil and Transport Engineering, Poznan University of Technology, Poland.
e-mail: *filip.szwajca@put.poznan.pl*

Prof. Krzysztof Wisłocki, DSc., DEng. – Faculty of Civil and Transport Engineering, Poznan University of Technology, Poland.
e-mail: *krzysztof. wislocki@put.poznan.pl*

Article citation info:
Sala R, Węglarz K, Suchecki A. Analysis of lubricating oil degradation and its influence on brake specific fuel consumption of a light-duty compression-ignition engine running a durability cycle on a test stand. Combustion Engines. 2023;195(4):109-115. https://doi.org/10.19206/CE-169488

Rafał SALA
Kamil WĘGLARZ
Andrzej SUCHECKI

Combustion Engines
Polish Scientific Society of Combustion Engines

Analysis of lubricating oil degradation and its influence on brake specific fuel consumption of a light-duty compression-ignition engine running a durability cycle on a test stand

ARTICLE INFO

Received: 5 June 2023
Revised: 7 July 2023
Accepted: 11 July 2023
Available online: 5 August 2023

The Euro 6 emission standard requires compliance with tough legal exhaust emissions limits for newly registered vehicles and obligates light-duty vehicle manufacturers to respect the 160,000 km durability requirements for in-service conformity. Although there is no legal limit set for fuel consumption, manufacturers are obligated to decrease the carbon footprint of vehicle fleets in order to obtain carbon neutral mobility beyond 2035.
The aim of this paper is to analyse the impact of various oils' and viscosity grades' degradation on the change in break specific fuel consumption (BSFC) measured over a standardized durability test cycle. Each oil candidate underwent 300 h of durability test running performed on a test bed without any oil changes. The purpose of the laboratory test was to reproduce the worst-case operating conditions and degradation process of the long-life engine oil type that can be experienced during extreme real life driving of a vehicle.
In order to define the influence of the engine oil deterioration on the BSFC profile, the engine operation parameters were continually monitored throughout the test run. Additionally, chemical analysis of the oil was performed and the solid deposits formed on the turbocharger's compressor side were evaluated.
The test results revealed differences up to 5% in the BSFC values between the oil candidates tested over the durability cycle. The observed BSFC increase was directly related to the decrease in engine efficiency and can cause higher fuel consumption of the engine, which in turn has an adverse effect on environmental protection goals.

Key words: *oil degradation, fuel efficiency, durability cycle, oil aging, diesel engine*

1. Introduction

Emissions limits for carbon dioxide (CO_2) and toxic exhaust compounds aim to achieve a carbon neutral and emission-free transportation sector in the coming decades.

Vehicle manufacturers have been developing new engine technologies with reduced friction and pumping losses, improved engine combustion and thermal efficiency. Coupled with such engine technologies are highly efficient exhaust aftertreatment systems (ATS) with primary operation focused on engine cold start emission and in-service conformity (ISC) compliance over the full useful lifetime of vehicle operation [1].

Modern engines and ATS technologies have to be combined with dedicated lubricating oil solutions that are enhanced with dedicated oil additives formulations. The primary role of engine oil is to protect the engine parts from deterioration due to friction, wear, corrosion, deposits, and oxidation – while at the same time providing the expected fuel efficiency effects. Anti-wear additives can protect metal surfaces from wear due to close contact. Antioxidants maintain oxidation stability and reduce the impact of oxidative decomposition. A friction modifier can reduce the coefficients of friction, improving fuel economy and helping to protect against wear. Detergent is vital in maintaining engine cleanliness from combustion contaminants and other impurities. Dispersants suspend and separate insoluble particles from fuel combustion or oil degradation [4, 11]. With a drive to lower viscosity oils for fuel economy benefits, viscosity modifiers provide more flexibility to meet those requirements [15]. To provide satisfactory performance requirements at low temperatures, pour point depressant is often blended to improve the flow properties under cold operation. When engine oil is contaminated with water, emulsifiers prevent phase separation for specific applications [7, 9, 10].

The performance of engine lubricant is expected to maintain optimum performance throughout the entire service interval – therefore, this also applies to aged oil conditions.

The term oil aging means a combination of various processes that result in changes in the chemical and physical properties of engine oil [5, 12]. Oil aging occurs for two main reasons: internal – caused by destabilization of oils (oxidation, polymerization) and external – caused by contamination of oil with mechanical impurities, as well as water or fuel [3, 8, 13]. The main lubricating oil parameters, such as: viscosity, acidity, soot content and oil dilution with fuel, change over the in-service operation of the vehicle.

Engine oil particles enter the combustion chamber through the cylinder liner-piston rings set and are burned, forming harmful side-products. [2, 6] A fraction of air-the fuel mixture or combustion gasses pass through the cylinder liner-piston rings to the engine crankcase (blow-by gas) and are recirculated back to the air intake system to reduce emissions [14]. Blow-by gasses can contaminate the intake ducts, including the compressor side of the turbocharger, causing deterioration of engine operational parameters.

This paper analyses comparative test results of eight various lubricating oils of two viscosity grades: 0W20 and

0W30, tested on an engine test bed under a durability cycle. Each oil sample was tested under a standardized durability test cycle performed on a modern light-duty Euro 6 diesel engine. The attention was paid mainly to the oil aging impact on BSFC change during the test, thus the indication of the overall deterioration in engine efficiency.

2. Test method and facilities

2.1. Test object description

The test objects were eight lubricating oils, divided into two viscosity grades and complying with the specifications listed in Table 1.

Table 1. Description of lubricating oils under test

Oil code	SAE viscosity grade	ACEA specification
Oil A	0W20	C5
Oil B	0W20	C5
Oil C	0W20	C5
Oil D	0W20	C5
Oil E	0W30	C2
Oil F	0W30	C2
Oil G	0W30	C2
Oil H	0W30	C2

For the purposes of the test, each engine oil was identified by a letter from A to H. The lubrication oils were randomly selected for the test program and derived from various manufacturers. All of them were developed for light-duty vehicles complying with Euro 6 emission requirements and were designated both for compression ignition (CI) and spark ignition (SI) engines.

The test activities were carried out on light-duty diesel engines complying with Euro 6 emission standards. The engine was installed on a test bed equipped with an eddy-current dynamometer and automation system capable of test cycle execution, engine parameters monitoring and data storage. The engine installation layout is shown in Fig. 1.

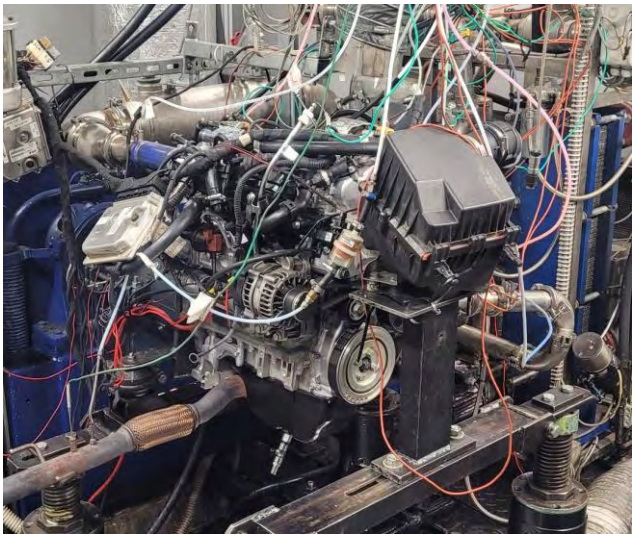

Fig. 1. Engine installation on the test bed

The engine and ATS were instrumented with temperature and pressure sensors to monitor and analyze the variations in engine operation parameters. The base engine parameters are presented in Table 2.

Table 2. Engine parameters

Engine parameters	Unit	Value
Displacement	cm^3	1248
Maximum power	kW	70
Maximum torque	Nm	200
Number of cylinders	–	4

2.2. Test methodology

Each lubricating oil under test underwent established test procedure executed on the engine dynamometer. The test procedure consisted of engine break-in, elementary durability cycle repeated for defined number of times and power curve measurement performed at the start and end of the test for engine performance verification.

The elementary durability cycle was composed of a sequence of steady-state points including engine operation at maximum power, maximum torque, partial load for emission components' loading and finally a step consisting of engine running at overspeed conditions for engine components mechanical stress.

The main criterion for lubrication oil evaluation during durability test was that the operating parameters did not exceed the engine protection limits. Another key criterion for an oil assessment was the air temperature profile at the compressor outlet, which was likely to increase due to blow-by sediments collected inside the compressor housing of the turbocharger.

The durability cycle on the test bench lasted 300 h and aimed at reproducing in an accelerated manner the distance of 30 000 km covered by the vehicle on the road.

The lubricating oil properties and elemental composition were defined based on chemical analysis performed at fresh oil conditions and during the durability cycle. The parameters analyzed included: soot content according to DIN 51452:1994 method, kinematic viscosity at 40°C and 100°C according to PN-EN ISO 3104:2021-03, TAN and TBN values.

Additionally, a chemical analysis of deposit composition collected inside the compressor housing was performed.

In order to ensure the desired repeatability of the test procedure, a brand new diesel engine unit was procured for each oil sample under test.

3. Test results and discussion

3.1. Specific brake fuel consumption results and engine performance for 0W20 lubricating oils

Four different SAE 0W20 oil samples (named A-D, respectively) were subjected to the 300 h durability cycle run on a test bed.

Figure 2 presents the variation in BSFC traces as a function of test time for A-D oil samples. Engine oil A completed the cycle; however, it did not meet the requirements due to exceeded limit of air temperature at compressor outlet. It resulted in a steady increase in the delta compressor temperature after 120 test hours, as shown in Fig. 3. The delta compressor temperature was the calculated difference between the compressor inlet and outlet temperatures.

The BSFC value of oil A was found to be increased by around 3.5% at the end of the test (EOT) compared to the best performed on oil sample C.

In the case of oil B, the durability cycle was terminated at 230 h due to activation of the engine protection limit of air temperature at compressor outlet. The temperature difference between the input and output of the compressor reached 180°C, which was an increase of over 30% compared to the start of test (SOT) condition. The increase in BSFC (compared to oil C) at the stage of test termination was near 5%.

Oil samples C and D did not reveal a significant increase in BSFC profile throughout the durability test. Also, the delta compressor temperature was found to be at a stable level for those oils.

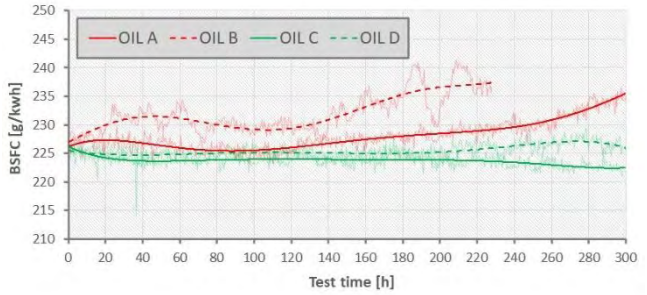

Fig. 2. BSFC change in function of the test time

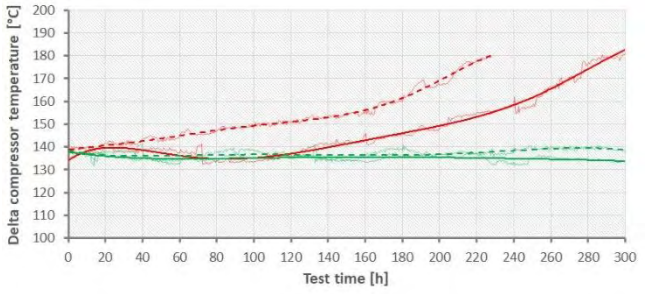

Fig. 3. Difference between compressor inlet and outlet temperature change as a function of test time

Figure 4 compares the exhaust gas pressure traces at the turbine inlet of the turbocharger. It can be noted that for oil sample A, the inlet turbine pressure exceeded 2500 mbar at EOT i.e. increasing by 25% compared to the SOT value.

Considering engine oils C and D, the exhaust gas pressure inlet turbine remained at a stable level for the entire test.

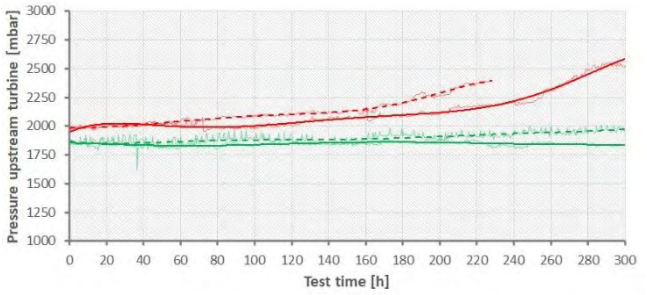

Fig. 4. Pressure upstream turbine change as a function of test time

The engine torque profiles throughout the test hours for A-D oil samples are presented in Fig. 5. For oil A that completed the test (but exceeded engine boundary condition), the relative decrease in torque was nearly 5% compared to oil C. Around 6% of engine torque deterioration was seen for oil B at the point of test termination. Engine oils C and D did not reveal a significant decrease in engine torque as a function of test time.

Figure 6 compares the calculated values of compressor efficiency for the turbocharger. The highest drop in efficiency from 0.73 to 0.54 was noticed for oil A, and it was similar in range to oil B (which did not complete the test run). The efficiency profiles for the compressor also remained almost constant in the case of oils C and D.

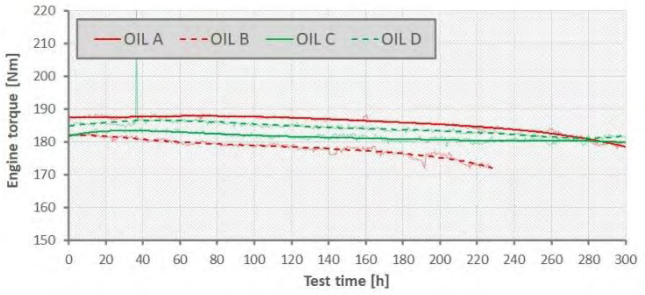

Fig. 5. Engine torque change as a function of test time

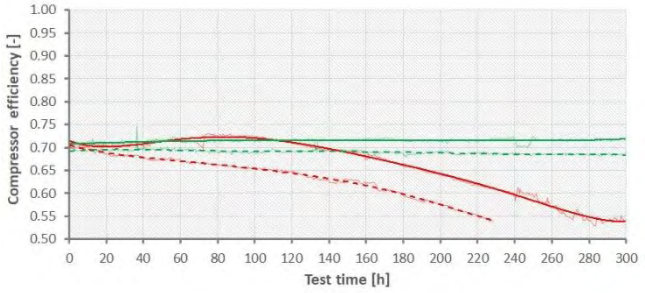

Fig. 6. Calculated compressor efficiency change as a function of test time

During the execution of durability testing, the air inlet temperature was maintained in the range of 18–22°C, as illustrated in Fig. 7. This approach was essential for test condition repeatability. Fluctuation or increase in air inlet temperature above the target values can intensify the deposit formation inside the compressor housing.

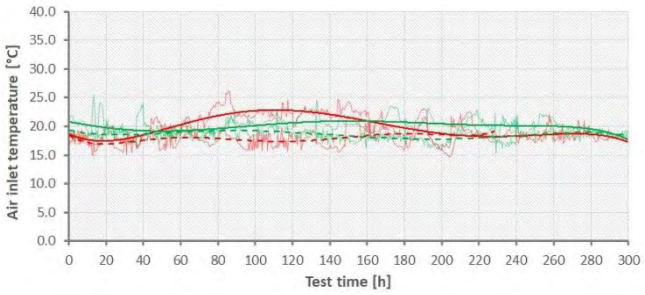

Fig. 7. Compressor air inlet temperature change as a function of test time

3.2. Brake-specific fuel consumption results and engine performance for 0W30 lubricating oils

Further lubricating oils samples named as E-H were of 0W30 viscosity grade.

Figure 8 compares the variation in BSFC behavior as a function of the durability test. Engine oils E and F did not show relevant fluctuation in the BSFC.

Oil G completed the durability test although did not meet the engine boundary conditions due to elevated air temperature at the compressor outlet. For that oil sample, the BSFC increased slightly (by around 1.5%) at EOT (compared to oil E, which was taken as a reference).

The last oil sample (code H) did not complete the durability cycle because of exceeded engine protection limit of the air temperature at the compressor outlet. This test run was terminated at 195 h. The delta compressor temperature sharply increased after 150 h and reached a value 160°C, as shown in Fig. 9. The increase in BSFC at the point of test termination was about 5% in relation to the SOT condition.

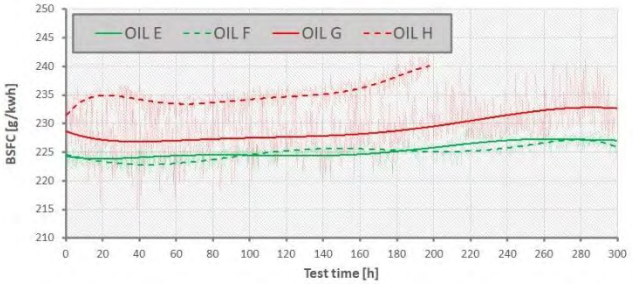

Fig. 8. BSFC change as a function of test time

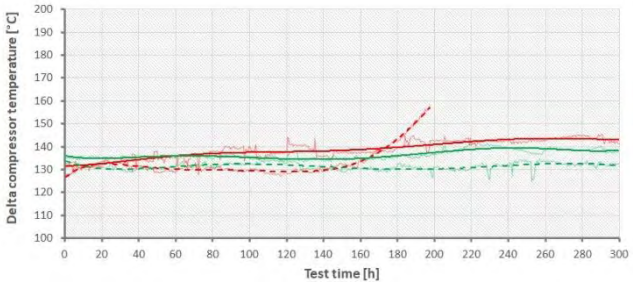

Fig. 9. Difference between compressor inlet and outlet temperature change as a function of test time

The traces of exhaust gas pressure upstream of the turbine are shown in Fig. 10. For oils E, F and G, the pressure were aligned with each other and increased by 11% at the EOT.

In terms of oil H, the pressure profile initiated from a higher level of 2050 mbar and ended up on 2300 mbar at the point of test termination (an increase of 12%).

Figure 11 illustrates the engine torque traces as a function of the test time. Oils E, F and H did not reveal a significant decrease in engine torque, in contrast to oil G for which torque decrease was 9.5% and the EOT.

Calculated compressor efficiency lines are set in Fig. 12. The greatest deterioration of compressor performance was found for oil H corresponding to values of 0.68 at SOT and 0.54 at the EOT.

The compressor air inlet temperature were adjusted in the range of 18–22°C, as shown in Fig. 13.

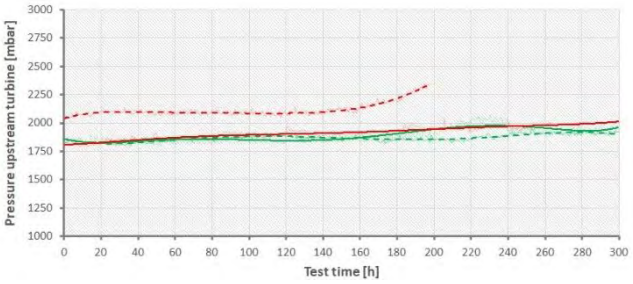

Fig. 10. Pressure upstream turbine change as a function of test time

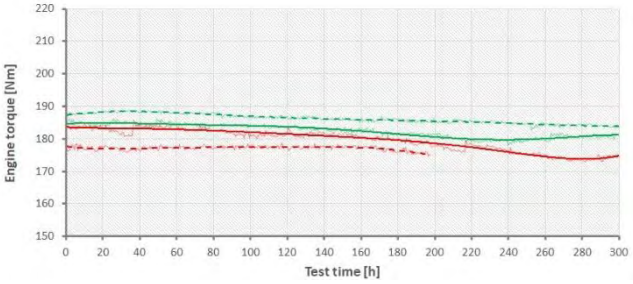

Fig. 11. Engine torque change as a function of test time

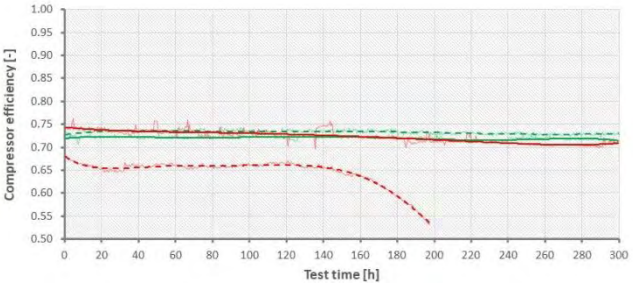

Fig. 12. Compressor efficiency change as a function of test time

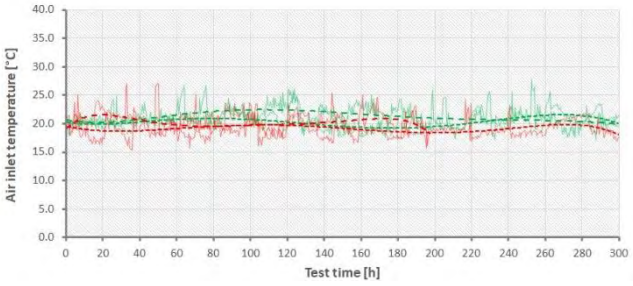

Fig. 13. Compressor air inlet temperature change as a function of test time

3.3. Chemical analysis of 0W20 engine oils

Chemical analysis of all engine oils under test were carried out periodically. Figure 14 shows a trend of soot content measured for oils A–D. The soot content did not exceed 1% for any of the oil samples A–D.

Kinematic viscosity was analyzed at oil temperature of 40°C and 100°C. In each case an increasing trend was visible over the durability test (Fig. 15 and 16).

Further investigation concerned the change in total base number (TBN) and total acid number (TAN) values over

the cycle. In the case of oil A, the traces of TAN and TBN already intersected after 85 hours of testing (Fig. 17).

The test run on oil B was stopped due to the activation of engine protection limits but the TAN/TBN traces had not yet intersected at that point.

The best performing oils (C and D) did not show any tendency for the TAN/TBN traces to intersect. This indicates that those two engine oils showed the best acid-neutralizing properties (defined by TBN), which counteracts the acidic products formed during fuel combustion and harsh operating conditions.

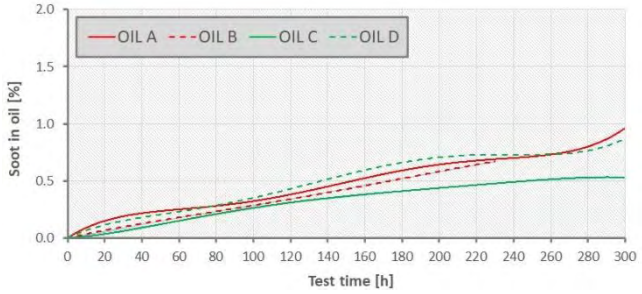

Fig. 14. Soot content change as a function of test time

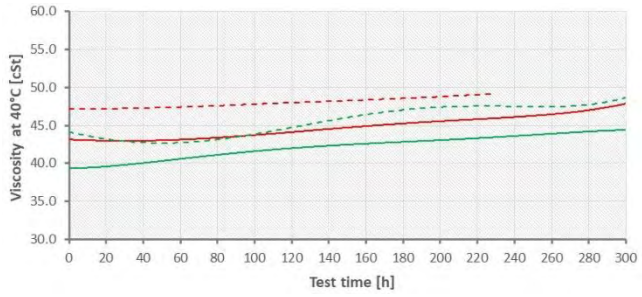

Fig. 15. Viscosity at 40°C change as a function of test time

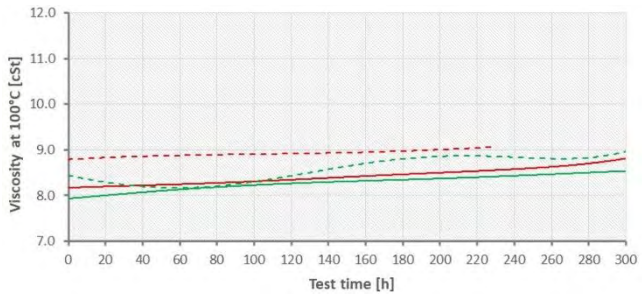

Fig. 16. Viscosity at 100°C change as a function of test time

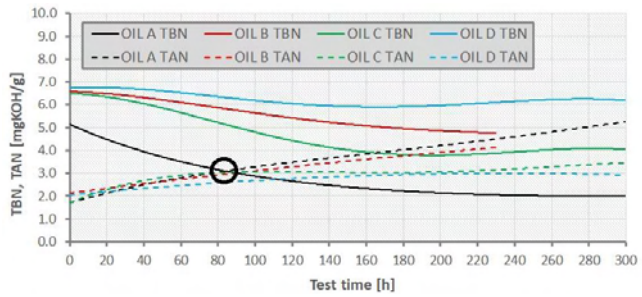

Fig. 17. TBN and TAN numbers change as a function of test time. (TBN and TAN crossover marked with a circle)

3.4. Chemical analysis of 0W30 engine oils

Figure 18 presents the trend of soot content for lubricating oils E-H. In case of oil H, the soot concentration increased by 2.5% even though the test was terminated at 240 h. For other oils, the soot level did not exceed 1% at EOT.

It was noticed that the viscosity values at 40 and 100°C were elevated for oil H, which was explained by its high soot content (Fig. 19–20).

TBN and TAN traces are presented in Fig. 21. For oils G, H and F, the crossover of TBN/TAN occurred at 150 h, 190 h, and 220 h (respectively), whereas oil E maintained the best properties in that respect.

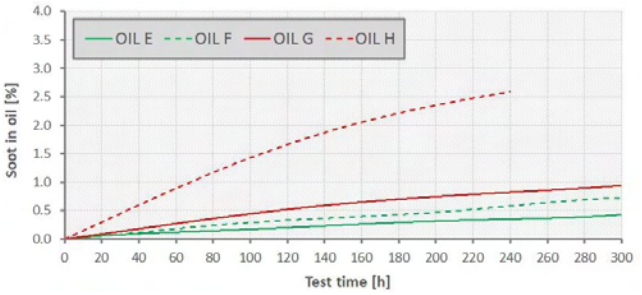

Fig. 18. Soot content change as a function of test time

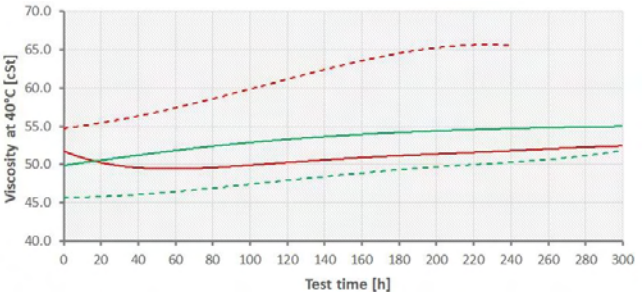

Fig. 19. Viscosity at 40°C change as a function of test time

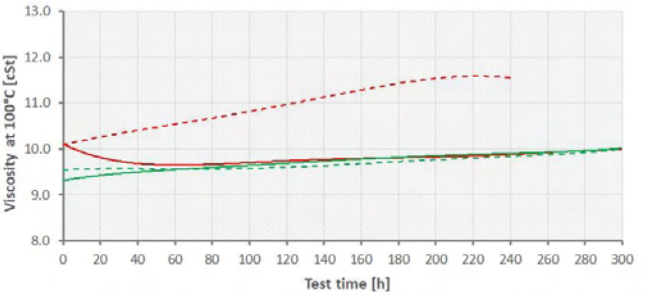

Fig. 20. Viscosity at 100°C change as a function of test time

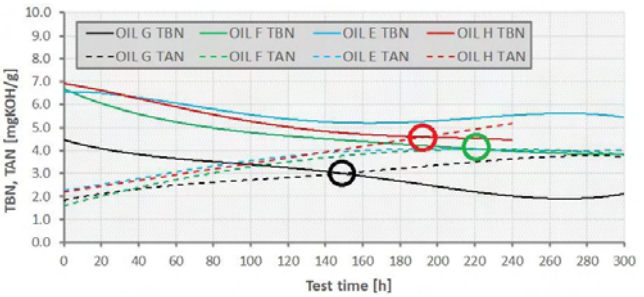

Fig. 21. TBN and TAN numbers change as a function of test time. (TBN and TAN crossover marked with circle)

3.5. Chemical analysis of lubricating oil deposits inside the turbocharger's compressor

Chemical analysis of the composition of the deposits collected inside the compressor housing revealed that nearly 92% of the material consists of carbon. The other elements found were: iron, molybdenum, calcium, phosphorus, sulfur, zinc and others, as presented in Fig. 22. The elemental composition derived mainly from the formulation of the oil additives. The analysis performed for oil H.

In principle, the reason for deposit formation inside the compressor housing is blow-by gas vapor introduced at the compressor inlet that carries over from the engine crankcase the oil fog, impurities and remnants from the combustion process. An example of a severely contaminated compressor housing and cover is shown in Fig. 23 and Fig. 24.

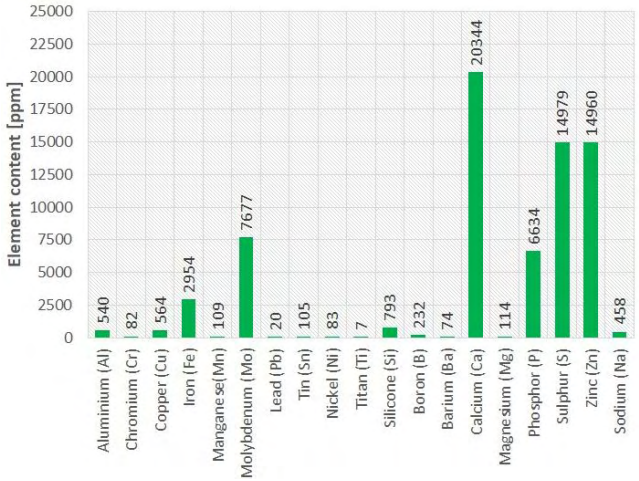

Fig. 22. Elemental content of compressor deposits after the test

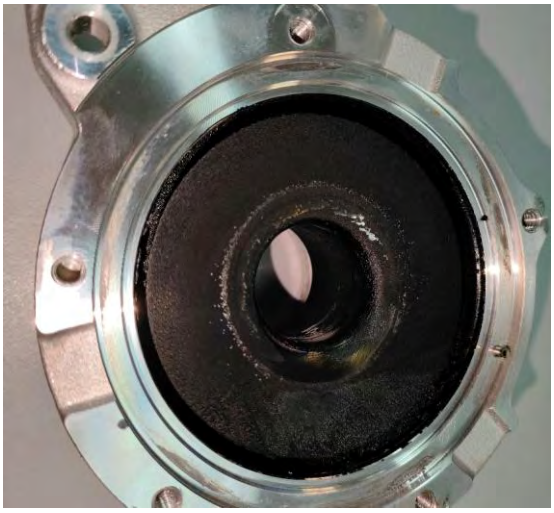

Fig. 23. Deposits collected on compressor cover after the durability test

4. Conclusion

An engine oil's resistance to aging process throughout in-service operation has an important impact on the engine operating parameters and its overall efficiency, which can be referred to as BSFC value.

Eight randomly selected oil samples of two viscosity grades (0W20, 0W30) were subjected to a 300 h durability test run, meant to reproduce in an accelerated method the distance of 30 000 km of vehicle on-road usage.

Fig. 24. Contaminated compressor housing after the durability test

It was found that within a selected batch of engine oils the maximum deterioration of BSFC reached 5%, while the decrease in engine torque was up to 6%.

Moreover, two oil samples (B and H) out of eight did not complete the durability cycle. The reason for cycle termination was exceedance of the limit for charge air temperature measured at the turbocharger's compressor outlet under full load conditions.

Elevated charge air temperature was caused by contamination of the inside of the compressor with oil-derived deposits, resulting in the deterioration of compressor efficiency.

Oil samples (C-F) successfully passed the durability run, maintaining engine operating parameters including: BSFC, engine torque, and charge air temperature at a stable level. For those oils, the engine protection limits were not surpassed.

During the durability test, physical and chemical properties of engine oils were analysed in terms of lubrication oil degradation monitoring.

In the case of four engine oil candidates (samples: A,F,G,H) crossover of TAN/TBN parameters occurred. The equilibrium of TAN and TBN values indicates that the organic and inorganic acid-neutralizing properties of the oil (as defined by the TBN value) are at its borderline value. Acidic products are mainly formed during fuel combustion and under harsh operating conditions.

A chemical analysis of the composition of deposits found inside the compressor revealed that nearly 92% of the material consisted of carbon.

From a vehicle operation perspective, inadequate quality engine oil can lead to severe contamination build up inside the turbocharger's compressor and an increase in charge air temperature. At engine full load conditions, a heavily contaminated compressor has generated charge air temperature exceeding protection limits and also a significant increase in exhaust backpressure was measured. That in turn may result in the turbocharger overstressing and its premature failure. The issue of compressor contamination can be enhanced for extended engine oil change intervals; for such applications the lubricating oil quality requirements are of key importance for faultless engine operation.

Nomenclature

ATS after-treatment system
BSFC break specific fuel consumption
CI compression ignition
CO_2 carbon dioxide
EOT end of test
ISC in-service conformity
SI spark ignition
SOT start of test
TAN total acid number
TBN total base number

Bibliography

[1] Ayodhya AS, Narayanappa KG. An overview of after-treatment systems for diesel engines. Environ Sci Pollut Res Int. 2018;25(35):35034-35047. https://doi.org/10.1007/s11356-018-3487-8

[2] Baskov V, Ignatov A, Polotnyanschikov V. Assessing the influence of operating factors on the properties of engine oil and the environmental safety of internal combustion engine. Transp Res Procedia. 2020;50:37-43. https://doi.org/10.1016/j.trpro.2020.10.005

[3] Boikov DV, Bugai TB, Mal'kov YP. Features of aging of engine oil in a gas engine. Chem Technol Fuels Oils. 2007; 43(4):299-304. https://doi.org/10.1007/s10553-007-0053-3

[4] Devlin M. Common properties of lubricants that affect vehicle fuel efficiency: A North American historical perspective. Lubricants. 2018;6(3):68. https://doi.org/10.3390/lubricants6030068

[5] Idzior M. Aging of engine oils and their influence on the wear of an internal combustion engine. Combustion Engines. 2021;185(2):15-20. https://doi.org/10.19206/CE-138033

[6] Kardos S, Pietrikova A. Evaluation of motor oil characteristics and degradation factors for possibilities of continuous diagnostics. Acta Electrotechnica et Informatica 2016;16: 20-24. https://doi.org//10.15546/aeei-2016-0010

[7] Kozak M. A comparison of thermogravimetric characteristics of fresh and used engine oils. Combustion Engines. 2019;178(3):289-292. https://doi.org/10.19206/CE-2019-350

[8] Krakowski R. Research on the effect of the effective microorganisms, silver solution and colloidal nanosilver addition on the engine oil acid number (TAN). Combustion Engines. 2021;186(3):59-63. https://doi.org/10.19206/CE-140730

[9] Liu Z, Gangopadhyay A, Lam W, Devlin M. The effect of friction modifiers and DI package on friction reduction potential of next generation engine oils: Part I fresh oils. SAE Technical Paper 2018-01-0933. 2018. https://doi.org/10.4271/2018-01-0933

[10] Sagawa T, Nakano S, Bito Y, Koike Y, Okuda S, Suzuki R. Development of low viscosity API SN 0W-16 fuel-saving engine oil considering chain wear performance. SAE Int J Fuels Lubr. 2017;10(2):469-477. https://doi.org/10.4271/2017-01-0881

[11] Shao H, Roos J, Remias J. Evaluation of the role of lubricant additives in emission control. Lubricants. 2022;10(12):362. https://doi.org/10.3390/lubricants10120362

[12] Stepien Z, Urzedowska W, Oleksiak S, Czerwinski J. Research on emissions and engine lube oil deterioration of diesel engines with BioFuels (RME). SAE Int J Fuels Lubr. 2011;4(1):125-138. https://doi.org/10.4271/2011-01-1302

[13] Tormos B, Novella R, Gomez-Soriano J, García-Barberá A, Tsuji N, Uehara I et al. Study of the influence of emission control strategies on the soot content and fuel dilution in engine oil. Tribol Int. 2019;136:285-298. https://doi.org/10.1016/j.triboint.2019.03.066

[14] Wolff A, Koszałka G. Influence of engine load on piston ring pack operation of an automotive IC engine. Combustion Engines. 2022;190(3):88-94. https://doi.org/10.19206/CE-141737

[15] Zhang Y, Ma Z, Feng Y, Diao Z, Liu Z. The effects of ultra-low viscosity engine oil on mechanical efficiency and fuel economy. Energies. 2021;14(8):2320. https://doi.org/10.3390/en14082320

Rafał Sala, DEng. – Engine Testing Laboratory, BOSMAL Automotive Research and Development Institute Ltd in Bielsko-Biała, Poland.
e-mail: *rafal.sala@bosmal.com.pl*

Andrzej Suchecki, DEng. – Engine Research Accreditation Laboratory, BOSMAL Automotive Research and Development Institute Ltd in Bielsko-Biała, Poland.
e-mail: *andrzej.suchecki@bosmal.com.pl*

Kamil Węglarz, MSc. – Engine Testing Laboratory, BOSMAL Automotive Research and Development Institute Ltd in Bielsko-Biała, Poland.
e-mail: *kamil.weglarz @bosmal.com.pl*

Article citation info:
Skonieczna D, Vrublevskyi O, Szczyglak P. Evaluation of the antiwear properties of timely changed engine oils. Combustion Engines. 2023;195(4):116-122. https://doi.org/10.19206/CE-169137

Daria SKONIECZNA
Oleksandr VRUBLEVSKYI
Piotr SZCZYGLAK

Combustion Engines
Polish Scientific Society of Combustion Engines

Evaluation of the antiwear properties of timely changed engine oils

ARTICLE INFO

Received: 31 May 2023
Revised: 28 June 2023
Accepted: 1 July 2023
Available online: 24 July 2023

The article presents the results of tests, replaced according to the vehicle manufacturer's recommendations, of engine oils. The sample of engine oils in service came from spark-ignition and compression-ignition vehicles used in urban or mixed mode. During their collection, the type of drive unit, the mileage of the car and the number of kilometers the oil was used for were recorded for each sample (this was the main criterion for differentiating samples). In addition, a control group of samples consisting of fresh oils of the same viscosity grade and distributed by the same producer was set up to observe changes in the parameters of individual lubricants after the operating period. The first part of the empirical study consisted of determining the physico-chemical properties of the lubricants, i.e.: kinematic viscosity, density and water content. The second part involved anti-wear tests using a T-02U tribometer. The use of the tribometer made it possible to record the anti-wear parameter, i.e. moment of friction, and also the load imposed on the friction node, as a result of which it was possible to calculate the friction force and friction coefficient. The research was complemented by an analysis of worn surfaces of the friction node on a microscope. The tests carried out can be used for predictive purposes, in terms of assessing the condition of a lubricant subjected to an operating process in an internal combustion engine.

Key words: *combustion engines, viscosity, density, water content, wear*

1. Introduction

It is estimated that approximately 23% of total energy consumption worldwide is related to friction. The negative effects can be reduced by using lubricants. The use of such measures, among others, can reduce the aforementioned energy consumption by 40% in the long term and by 18% in the short term [10]. In addition to its primary function – lubrication – engine oil also has the task of dissipating heat, among other things. Protection in the broadest sense also includes preventing corrosion and cleaning the interior of the engine from wear products by accumulating wear products and transferring them to the filter [17].

As the lubricant is used, its parameters change [24], which is associated with a loss of protective properties. This is influenced by the thermal oxidation process [23], which determines the darkening of the fluid and an increase in its viscosity. The products of this process contribute to the formation of viscous fractions, which can cause blockages in filter cartridges. Too low viscosity, on the other hand, can be caused by the penetration of fuel or coolant into the oil [16]. The properties of the lubricating oil are also affected by aspects such as the presence of worn particles of drive unit components, soot or exhaust gas [20]. Observing the dynamics of changes in the physico-chemical properties of engine oils can provide information about possible damage to the unit.

Because of the variable nature of lubricant viscosity during the exploitation process, researchers often refer to it. The article [13] focused on the study of viscosity changes depending on the mileage of the vehicle sampled. The experiment was conducted on oils from compression-ignition (CI) and spark-ignition (SI) engines. The analysis of the results showed that, based on this parameter for the group of oils from CI engines, it is possible to estimate the approximate mileage at which an oil change is necessary. An attempt to capture the correlation between lubricant viscosity and wear resistance of sliding nodes was made in his work by Ryniewicz [19]. He performed viscosity tests over a wide temperature range for engine oils differing in viscosity class and manufacturer. The results show that despite the same oil designation according to SAE classification, viscosity characteristics differ between samples from different manufacturers. These differences are particularly apparent in the non-catalog range for measurements at 40 and 100°C. Another paper focusing on viscosity is that of Ghannam [9]. In this case, used and fresh oil samples were juxtaposed. This approach allowed a conclusion to be drawn regarding the difference in viscosity characteristics created due to the type of power unit. Viscosity is sensitive to the lubricant's degree of wear and tear and the way it is used, which provides a reasonable basis for using this value as an indicator during research dedicated to engine oils.

The driving style of the driver influences the condition of the engine oil. The lack of smoothness of the drive unit, understood as city traffic, as well as often starting the engine at low temperatures can result in the accumulation of water in the engine. This results in an emulsion that is characterized by a higher viscosity and therefore does not lubricate the engine as effectively as fresh oil [14]. Another adverse effect of water in the lubricant is the increased danger of corrosion of system components [8]. In his work, Jakubiec [14], based on processes occurring during operation, provides a set of methods useful in assessing the properties of engine oils. One of the proposed parameters is the determination of water content in a sample following ASTM D 95. An alternative is to use the Karl Fischer coulometric titration method, which was used by Jędrychowska in her work [15]. In a subsequent paper [22], a team of researchers focused on the diagnostics of a drive unit based on lubricant properties. One of the parameters determined

was the water content, which after the test exceeded the permissible limit, which the authors considered as a reason for immediate lubricant replacement. The frequent use of water content in engine oil as an indicator of irregularities related to the operation of a drive unit, and as a parameter conditioning the reduced suitability of a lubricant to protect cooperating elements, motivates its use when analysing the impact of the value of this parameter on the antiwear characteristics of the system.

As the lubricant is used, the content of wear products from the system also increases. Such contaminants contribute to an increase in the density of the substance [23]. As presented in the article [24], increased density can be an indicator of progressive oxidation of the sample. As studies available in the literature [21] show, there is an apparent correlation between lubricant density and lubricant viscosity. This translates directly into lubricant properties in terms of friction as well as wear. This parameter can successively be used to determine the relationship between the properties of fresh and degraded oils. Such an approach was presented in their work by Landowski and Baran [17]. One type of engine oil (5W30) – fresh and used – was tested. The methodology included a comparison of three parameters with each other, which were density, viscosity and viscosity index. Based on the results, the authors conclude that the observed changes can be used as an indicator to determine the condition of the drive unit.

In addition to focusing on the properties of the lubricant, it is worth deepening the analysis by performing tests using the kinematic node that the oil protects. Machines that enable such tests are tribometers. [18]. One of the most commonly used tribometers is the T02-U four-ball tribometer. The work of Farhanah [7] was dedicated to testing engine oils of the same SAE viscosity class (10W30) from three different manufacturers. During the experiment, the temperature (40, 70, 100°C) and speed were changed stepwise. As the results show, despite the identical designation of the lubricants, they exhibit different lubricating properties. A different approach, a comparison of two groups of oils – synthetic and mineral – is presented in the paper [21].In addition to recording the basic physicochemical properties of the engine oils, the authors examined them using a T02-U tribometer. Through correlation analysis, it was proven that the frictional properties of lubricants are influenced by their viscosity. This conclusion is only possible if the analysis is extended to include wear testing. Another application of the four-ball tester in the analysis of the properties of petroleum products was the work of [11]. In this study, the effect of carbon black, on the tribological properties of engine lubricants was investigated. The result of the study was one of the conclusions indicating engine oil as having better antiwear properties than base oil.

The purpose of this study is to obtain data to develop an assessment of the condition of a lubricant subjected to service in a combustion engine. Most of the literature sources are based on the analysis of the physico-chemical parameters of fresh or used oils, or of the wear tests. Some of the tests involve artificial contamination of samples with wear products. In the present study, the focus will be on lubricants subjected to operation under real conditions, i.e. in an internal combustion engine. It is hoped that the juxtaposition of data from physico-chemical and tribological tests will contribute to the knowledge of changes in the properties of lubricants that have been subjected to service. The paper consists of four chapters. The first contains a literature review related to the issue under consideration. The second describes the methodology of the research carried out. Another, the third, is designed to present the results of the empirical research. The last chapter contains a summary and conclusions of the analysis.

2. Methodology

The experiments carried out are part of a planned comprehensive study of the effects of lubricant properties on the system in which they operate and on the components they protect from wear. Figure 1 shows in yellow the scope of the work envisaged in the current section, the results of which are described in the article, while grey shows further experiments related to the extension of the analysis.

The empirical research consisted of two parts. The first involves testing lubricants for their physico-chemical properties. This included measuring the viscosity, density and water content of fresh and used oil samples. Carrying out wear tests using a T02-U tribometer (four-ball machine) formed the second part of the laboratory tests.

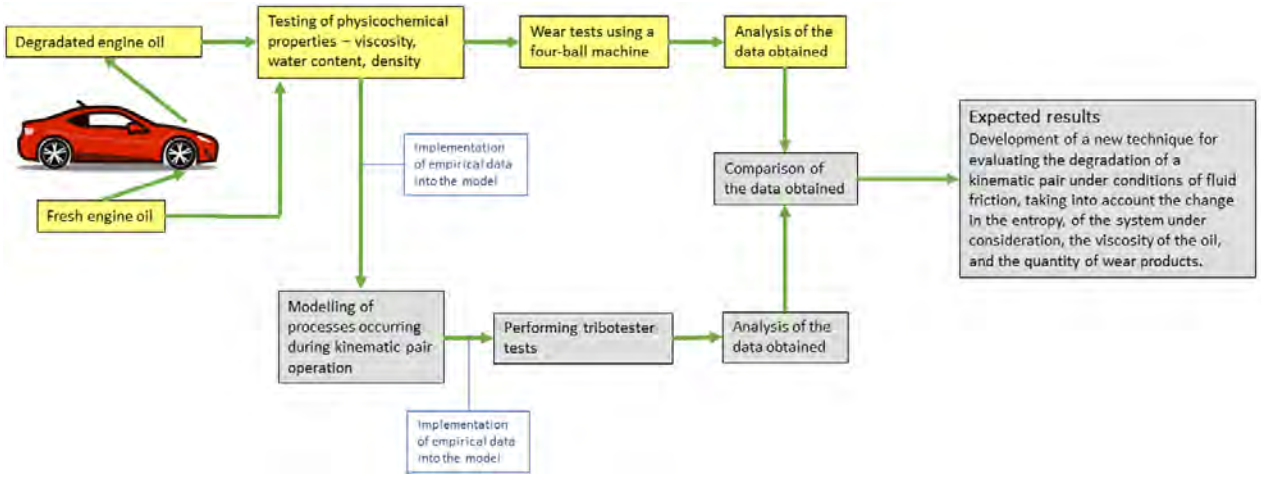

Fig. 1. Scheme of planned research

2.1. Research object

Table 1 shows eleven selected used oil samples, which were assigned fresh oil samples characterised by the same viscosity class and manufacturer (attention was also paid to the additives contained in the oil). During the collection of used oil samples, data related to the characteristics of the drive unit and its mileage was extracted. In addition, to simplify the determination of the samples, each sample was marked with an individual laboratory number, which is recorded in the first column of the table. The viscosity of the prepared samples was determined using an automatic mini AV-X viscometer. Measurements were carried out at temperatures of 40°C – under EN ISO 3104:2020 [5] – and 75°C. The higher measurement temperature provided a reference point for tribological tests, which were performed at the same temperature.

For the determination of the water content of the samples, the testing methodology was based on EN ISO 12937:2000 [3]. The Cou-Lo Aquamax KF apparatus was used for the tests. Samples for the test were fed at 1 cm^3.

The density of the samples was determined using a standardised areometer with a range of 0.8–1.0 $g \cdot ml^{-1}$. The tests were carried out taking into account the lubricant density test temperature given in EN ISO 3675:1998 [6]. Analogous to the viscosity measurement, due to tribological testing, the second density determination test was carried out at 75°C.

The tribological process test was performed following EN ISO 20623:2018 [4]. Another document that specifies the test conditions is ASTM D 4172-94 (Method B) [1]. The test time was 3600 s. The spindle speed was 1200 rpm, the node was loaded with a force of 392 N. The temperature of the lubricant was 75°C. The balls from the kinematic node were visually inspected and measured using a microscope (HUVITZ HRM 300). According to the standard, the diameter of the wear marks formed on the lower balls was measured for each test performed and the average wear diameter was determined from these.

Following the empirical tests, an analysis of the data obtained was carried out and the correlation between the physicochemical and tribological properties of the tested engine oils and their effect on the state of the kinematic junction was determined.

3. Results

A mileage index was used to compile the data, which takes into account both the P_P vehicle mileage and the P_O oil mileage. It was calculated from the equation:

$$W_p = 1 - \frac{P_O}{P_P} \quad (1)$$

where: W_P – mileage index [-], P_O – oil mileage [km], P_P – vehicle mileage [km].

This approach makes it possible to take into account both performance variables that characterise the test group. If the W_P value is close to zero, it can be concluded that the sample came from a low mileage vehicle. As this indicator increases and approaches a value equal to 1, it can be assumed that the vehicle has a lower operating potential (the operating parameters of the vehicle may be worse than those of a new vehicle).

3.1. Results of physico-chemical tests

The data obtained from the physico-chemical tests were ranked according to the adopted split concept concerning the W_P index (table 2). The oil that had the lowest mileage index is 0w30 distributed by the Volkswagen Group. The sample was characterised by the fact that it was taken from a new car and the oil change interval was within the manufacturer's recommended interval. By comparing the results of this sample with fresh oil from the control group, it can be seen that the viscosity and density parameters are similar. The fresh oil showed a 5% increase in viscosity, which was 58.96 cSt at 40°C and 19.86 cSt at 75°C (a 3% increase). For density, the values were 0.835 $g \cdot ml^{-1}$ for 15°C and 0.815 $g \cdot ml^{-1}$ for 75°C.

The next in line sample is the 5w30 grade oil distributed by Selenia. In this case, the viscosity of the used oil dropped by 37.3% (viscosity measurement at 40°C) and for 75°C the viscosity decreased by 28.3%. When comparing the density measurements of fresh and used oil, they increased slightly. For the 15°C test, it was an increase of 1.2%, and for 75°C only an increase of 0.6%. The same trend of decreasing or increasing density and viscosity was shown by another lubricant with a viscosity grade of 5W40 (Total). The viscosity values in the used oil decreased by 23.6% (at the lower test temperature) and 20.2% (at the higher test temperature). For density, there was an increase of 1.7% and 1.2% for the 15°C and 75°C measurement temperatures, respectively. Another sample showing the same trend is oil with a viscosity grade of 5W30 (Shell). The decrease in viscosity values in this case did not exceed 1% for both temperatures. In contrast, the density of the oil in service increased by 1.8% for both temperatures.

Table 1. Data on operating conditions of used oil samples

Engine oil				Vehicle			
#sample number	Manufacturer	Viscosity class SAE	Oil mileage [km]	Type of fuel to power the engine	Engine capacity [dm^3]	Nominal motor power [kW]	Car mileage at oil drain [km]
1	Fanfaro	5W30	12,650	Gasoline +LPG	1.4	63	362,211
2	Mobil	5W30	14,141	Gasoline	1.6	85	91,635
3	Shell	5W30	5,481	Gasoline	1.2	57	110,007
4	Total	5W40	7,734	Gasoline	1.6	120	60,631
5	Fanfaro	5W30	11,452	Gasoline +LPG	1.6	63	157,473
6	Selenia	5W30	14,998	Diesel	1.6	77	101,021
7	Shell	5W30	5,002	Gasoline	1.0	57	52,333
8	Mobil	10W40	6,500	Gasoline	1.6	72	330,041
9	Fanfaro	5W30	5,159	Diesel	2.5	88	196,427
10	Total	5W20	5,126	Gasoline	1.5	110	112,927
11	Volkswagen	0W30	15,000	Gasoline	1.0	95	15,000

Table 2. Physico-chemical test results sorted by mileage index

#sample number	Viscosity class SAE	W_P	μ_{40} [cSt]	μ_{75} [cSt]	δ_{15} [g·ml^{-1}]	δ_{75} [g·ml^{-1}]	Water content [µg·cm^{-3}]
11	0W30	0.00	61.97	20.44	0.850	0.810	845.14
2	5W30	0.845	70.50	22.10	0.865	0.825	643.15
6	5W30	0.851	34.07	12.04	0.860	0.825	316.46
4	5W40	0.872	61.84	20.22	0.865	0.825	740.85
7	5W30	0.904	58.20	19.29	0.855	0.815	993.16
5	5W30	0.927	54.61	17.30	0.860	0.820	1877.26
3	5W30	0.950	63.92	20.44	0.855	0.815	2124.42
10	5W20	0.954	41.40	13.93	0.855	0.820	895.86
1	5W30	0.965	61.42	19.17	0.855	0.815	825.31
9	5W30	0.973	58.35	18.47	0.855	0.815	1180.19
8	10W40	0.980	86.72	24.75	0.870	0.830	1088.63

Sample number 5, in the viscosity test run, showed a decrease in viscosity of approximately 11% for both temperatures relative to the fresh oil sample from the control group. The density measured for the dependent samples at 15°C was unchanged, while at 75°C it increased by less than 1%. A sample of oil in use with a viscosity grade of 5W20 (Total) relative to the oil in the control group showed a decrease in viscosity of 10.0% (at 40°C) and 7.7% (at 75°C). There was an increase of 0.5% in density at 15°C and a decrease of 0.6% at 75°C.

A sample of the oil 5W30 (Fanfaro) after viscosity testing at the lower temperature showed a 0.1% increase in viscosity, and a 1.1% increase for the higher temperature. Comparing the density measurements, it was found that the values at the lower temperature differed by 0.5%, while there was no change at the higher temperature. The last lubricant sample distributed by the same manufacturer and the same viscosity class (#9), with a different mileage index, showed decreases in viscosity relative to fresh oil of 4.8% for both temperatures. The density measurement at the lower temperature also showed a decrease (by 0.6%), while the measurement at 75°C was the same for both used and fresh oil.

A trend line was drawn for the ranked data, showing the relationship between the results obtained during the physico-chemical tests and the mileage index. In this way, four characteristics were obtained, which show that the trend in these parameters is similar. The mileage index of the analysed data was in the range of 0.84–0.99. From Fig. 2a, it can be determined that there is a decrease in oil viscosity in the range of 0.84–0.88. In the range 0.88–0.92, the values are lowest and then there is an increase until the W_P index value is close to 1.

Analogous ranges can be determined for the density test carried out. The middle limit denoting the range of the lowest density values of the samples is shifted slightly towards higher values and is in the range of 0.9–0.94 W_P.

When analysing the graphs presented, a characteristic point can be seen that stands out from the rest of the data, this being the point describing the viscosity measurement at 40°C for the 5W30 oil (Selenia). Such a low value for this parameter may be since the drive unit of the vehicle from which the sample came was subjected to a flushing during the lubricant change.

When analysing the results obtained from testing the water content of in-service oil samples, no correlation was found between this data and the value of the mileage index.

a)

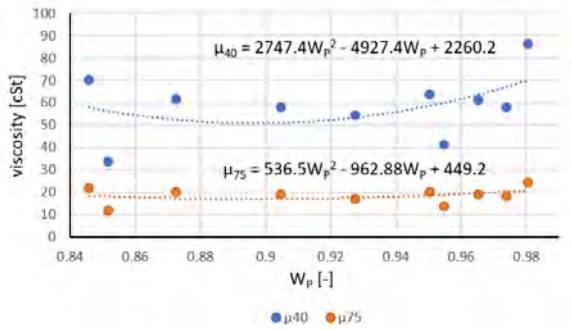

b)

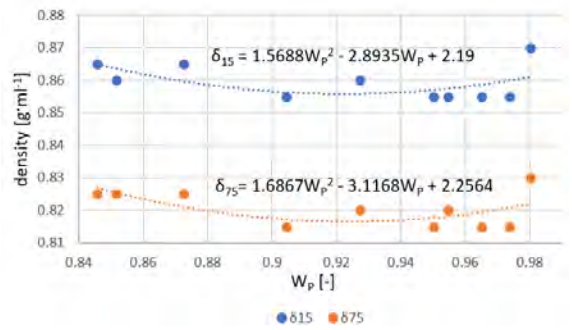

Fig. 2. Comparison of viscosity (a) and density (b) test results with trend lines

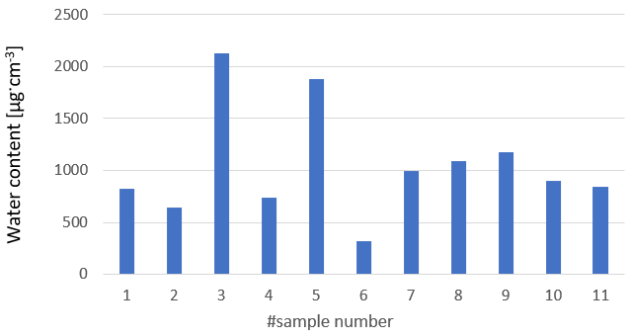

Fig. 3. Water content in samples

3.2. Results of tribological tests

The T02-U four-ball tester used in this part of the study made it possible to record test parameters such as the actual force acting on the kinematic node and the actual friction torque. These parameters were recorded at a frequency of 1 Hz. In order to take into account the load on the node and the torque acting on it, the coefficient of friction µ was calculated for each test, according to the following equation:

$$\mu = \frac{M_f}{r \cdot F}, \quad (2)$$

where: μ – coefficient of friction [-], M_f – friction torque [Nm], F – load on the kinematic node [N], r – constant moment arm of 0.15 m.

The tests on the four-ball tester consisted of three test runs for one lubricant, one hour each. The variation in time of the coefficient of friction for each sample is shown in Fig. 4. The average coefficient of friction characterising the sample was then calculated for this run.

After each test, the lower balls were visually inspected using a microscope to determine the average area of the wear mark. The data thus prepared were ranked in the same way as the results of the tribological tests (Table 3). The standard for the determination of wear traces assumes the measurement of trace diameters on the three lower balls of the kinematic node. For each ball, the measurement should be carried out twice – once along the wear traces and the second across them.

The wear marks obtained from the tests showed heterogeneity in terms of shape. Some of them were irregular (Fig. 5a), while others were close to a circle (Fig. 5b). For this reason, the diameter calculated according to the standard was not used to determine the area of the wear mark, but the image analysis methodology was used to calculate the area. This approach enabled a more accurate determination of the contact area between the lower balls (A_e – for used oil samples, A_f – for fresh oil samples) and the ball placed in the spindle of the tribometer.

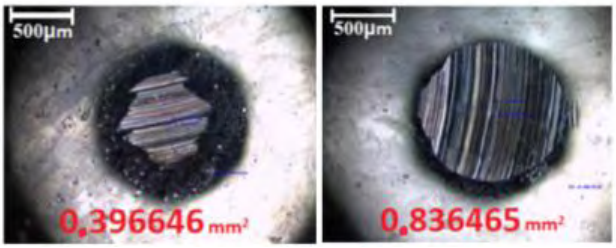

(a) (b)

Fig. 5. Example microscopic images of signs of wear

By placing the points corresponding to the mean wear trace area on the graph as a function of W_P, it was found that the trend line describing the change in mean wear trace area (Fig. 6) shows similar properties to the trend lines determined for viscosity and density. It decreases slightly in the range 0.83–0.85 W_P. In the range of 0.85–0.91 it is at a constant value (lowest). Once the W_P exceeds 0.91, the trend line manifests an increasing trend.

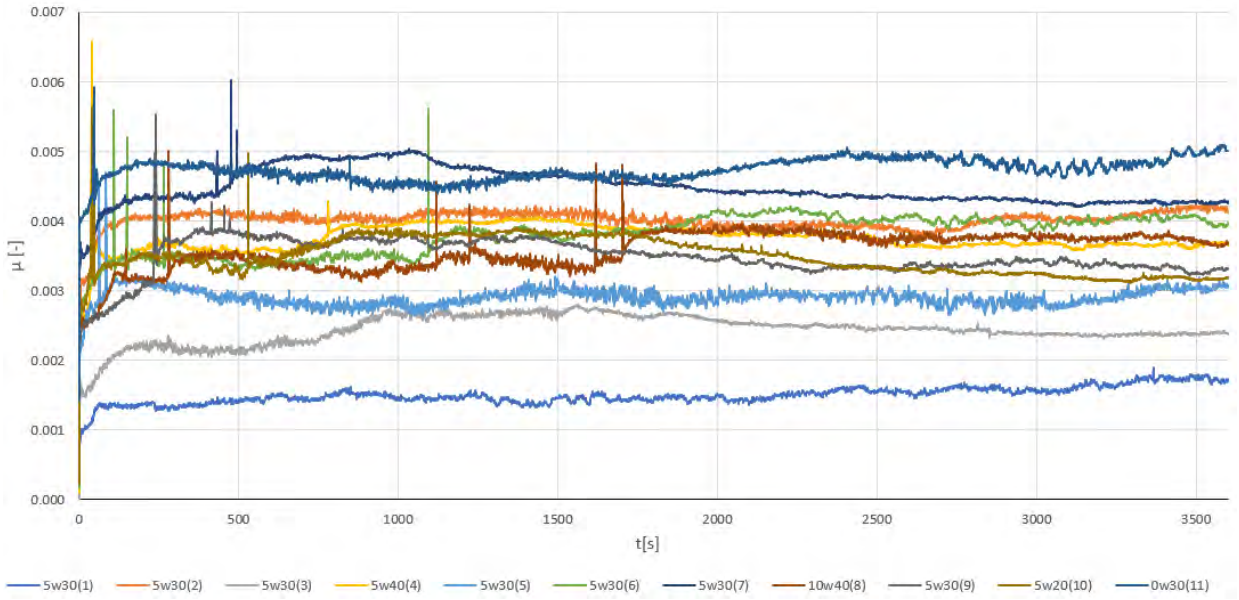

Fig. 4. The μ factor for all used oil samples

Table 3. Results of tribological tests ranked by mileage index

#sample number	Viscosity class SAE	W_p	μ	A_e [mm²]	A_f [mm²]	$\frac{A_e}{A_f}$
11	0W30	0.00	0.268	0.782631	0.234429	3.33
2	5W30	0.845	0.228	0.669358	0.405792	1.64
6	5W30	0.851	0.218	0.611117	0.318869	1.91
4	5W40	0.872	0.216	0.974916	0.200990	4.85
7	5W30	0.904	0.256	0.552152	0.220804	2.50
5	5W30	0.927	0.167	0.850034	0.166564	5.10
3	5W30	0.950	0.141	0.614777	0.220804	2.78
10	5W20	0.954	0.197	0.938673	0.202223	4.64
1	5W30	0.965	0.084	0.471683	0.166564	2.83
9	5W30	0.973	0.199	0.541008	0.166564	3.24
8	10W40	0.980	0.207	0.1073030	0.260796	4.11

The trend line drawn for the data describing the friction coefficient as a function of the mileage index did not show the same characteristics. In this case, in the range 0.84–0.87 there was an increase in the trend line. In the range 0.87–0.95, there was a decrease. This was followed by an increase once again once the run rate exceeded 0.95. Although this trend line does not show the same characteristics over the entire range as those determined previously, it is worth noting that it also shows an increase after crossing a relatively high run rate.

When analysing the data collected, it is important to note the differences in the field of wear marks obtained in the tests of used and fresh oils. In each case, the wear traces when testing fresh lubricants are smaller. When calculating the relationship between the field of the wear pattern obtained from testing fresh and in-service oils, it can be seen that the traces of the second oil group are larger from 1.6 to more than 5 times.

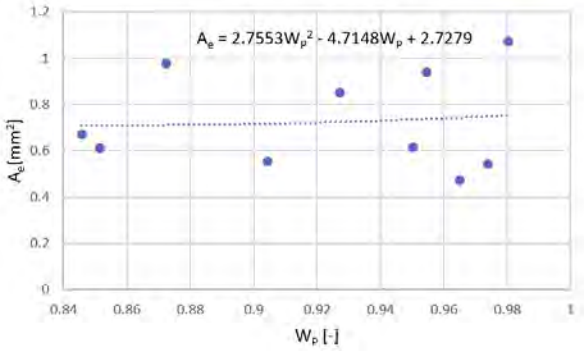

Fig. 6. Field of wear marks in relation to the mileage index

The coefficient of friction μ, calculated on the basis of the applied force and friction torque, was in most cases greater for the used oil than for the fresh oil. Only samples of oils produced by Fanfaro are inconsistent with this relationship. Due to this fact, attention was paid to the friction torque that was recorded during the test. It turns out that for all three lubricants subjected to operation, it was lower compared to the oil in the control group. Because of the dependence of the friction coefficient on the friction torque, this translated into an inverse relationship between the operated and fresh oils.

4. Conclusions

In this paper, aspects of lubricant condition assessment were developed. Based on the collected data, a synergistic W_P mileage index was determined, taking into account vehicle mileage and engine oil mileage. This enabled the research group to be ordered according to the criterion of operating conditions.

As the test results show, as the mileage index value approaches 1 (which can be defined by the near-critical condition of the drive unit), viscosity and density also increase. For proper lubrication of the drive unit, the parameters should be within the appropriate range and not increase excessively. It can therefore be concluded that, in the case of an engine in critical condition, these properties will be so high that the lubricant will not provide adequate protection for the system components. As mentioned in the introduction of the paper, the increase in these parameters may be due to excessive accumulation of wear products. In the case of water content, it was found that there was no correlation between the adopted W_P index. The values recorded during the tests for used oils were in the range of 316–2125 μg·cm^{-3}. Such a large discrepancy in results could be influenced by such aspects as the moment of oil change (hot or cold engine), the method of operation (e.g. frequent engine start-up and driving over short distances) or the water content of fresh oil fed into the system.

The relationships between the assumed W_P index and the density measured at 15°C and 75°C in the form of trend lines are similar in shape. This can be inferred from the similar coefficients of the trendline equation. In the case of the trend line describing the viscosity relationship at 40°C and 75°C and the W_P index, the discrepancy between the trend line coefficients is noticeably different. The coefficients take on a value several times greater for the trend line plotted for the viscosity measurement at 40°C.

The loss of lubricating properties by oils taken from high-mileage engines is also confirmed by tribological tests carried out. Several times larger areas of wear marks (from 1.6 to more than 5 times) in the case of testing with used oil than with fresh oil testify to less protection for the mating parts. It should be noted that in all tribological tests carried out with fresh oil, the field of the wear mark was always smaller than that of the corresponding used oil of the same viscosity grade and distributed by the same manufacturer. By comparing the wear marks of the lower balls of the four-ball tester with each other when testing a group of oils operated according to the mileage indicator, it can be deduced that, with the drive unit approaching a critical state, the wear marks will also be larger, and thus, just as in the case of the comparison with fresh oils, the engine components will be more exposed to wear.

The microscopic examination carried out showed irregular wear marks on the lower balls of the four-ball apparatus. This result may be due to the formation of lubrication channels at the lower ball – upper ball interface, which prevents the components from fully pressing against each other. It should be noted that the validity of this statement is supported by the fact that when irregularly shaped wear marks were obtained during the test, a friction torque was recorded at a very low level, at times not exceeding 0.1 Nm.

Nomenclature

A_e	area of the wear mark on the lower ball of the four-ball tester for used oil [mm^2]	F	kinematic node load [N]
A_f	area of the wear mark on the lower ball of the four-ball tester for fresh oil [mm^2]	M_f	friction torque [Nm]
		P_O	oil mileage [km]
		P_P	vehicle mileage [km]

r	friction torque arm [m]
SAE	Society of Automotive Engineers
t	time [s]
W_P	mileage index [-]
μ	coefficient of friction [-]
μ_{40}	viscosity at 40°C [cSt]
μ_{75}	viscosity at 75°C [cSt]
δ_{15}	density at 15°C [g·ml^{-1}]
δ_{75}	density at 75°C [g·ml^{-1}]

Bibliography

[1] ASTM D 4172-94 (Method B) – Standard Test Method for Wear Preventive Characteristics of Lubricating Fluid (Four-Ball Method).

[2] Chmielewski Z. Assessment of the kinetics of changes in selected physicochemical indicators of engine oil in operation. Combustion Engines. 2022;188(1):24-29. https://doi.org/10.19206/CE-1413

[3] EN ISO 12937:2000 Petroleum products – Determination of water – Coulometric Karl Fischer titration method.

[4] EN ISO 20623:2018 Petroleum and related products – Determination of the extreme-pressure and anti-wear properties of fluids – Four ball method (European conditions).

[5] EN ISO 3104:2020 Petroleum products – Transparent and opaque liquids – Determination of kinematic viscosity and calculation of dynamic viscosity.

[6] EN ISO 3675:1998 Crude petroleum and liquid petroleum products – Laboratory determination of density.

[7] Farhanah AN, Bahak MZ. Engine oil wear resistance. Journal Tribologi. 2015;4:10-20. https://jurnaltribologi.mytribos.org/v4/JT-V4-10-20.pdf (accessed on 15.05.2023).

[8] Fatima N, Minami I, Holmgren A, Marklun P, Berglund K, Larsson R. Influence of water on the tribological properties of zinc dialkyl-dithiophosphate and over-based calcium sulphonate additives in wet clutch contacts. Tribol Int. 2015; 87:113-120. https://doi.org/10.1016/j.triboint.2015.02.006

[9] Ghannam MT, Selim MYE, Khedr MAM, Bin Taleb NAG, Kaalan NR. Investigation of the rheological properties of waste and pure lube oils. Fuel. 2021;298:120774. https://doi.org/10.1016/j.fuel.2021.120774

[10] Holmberg K, Erdemir A. Influence of tribology on global energy consumption, costs and emissions. Friction. 2017;5: 263-284. https://doi.org/10.1007/s40544-017-0183-5

[11] Hu E, Hu X, Liu T, Fang L, Dearn KD, Xu H. The role of soot particles in the tribological behavior of engine lubricating oils. Wear. 2013;304:152-161. https://doi.org/10.1016/j.wear.2013.05.002

[12] Idzior M, Aging of engine oils and their influence on the wear of an internal combustion engine. Combustion Engines. 2021;185(2):15-20. https://doi.org/10.19206/CE-138033

[13] Idzior M, Wichtowska K. Study on the influence of vehicle run on changes of engine oil properties. Autobusy: technika, eksploatacja, systemy transportowe. 2016;17(6):900-904.

[14] Jakóbiec J, Budzik G. Agents influencing degree of engine oil during exploitation. Arch Automot Eng. 2007;3:209-216.

[15] Jędrychowska S. Optimalization of water determination conditions by coulometric titration method with evaporation for lubricating oils. Nafta-Gaz. 2021;7;480-489. https://doi.org/10.18668/NG.2021.07.07

[16] Landowski B, Baran M. Analysis of changes in the value of selected lubricant characteristics during use. MATEC Web Conf. 2019;302:01009. https://doi.org/10.1051/matecconf/201930201009

[17] Landowski B, Baran M. Analysys of selected results of engine oil tests. MATEC Web Conf. 2019;302:01010. https://doi.org/10.1051/matecconf/201930201010

[18] Mikołajczak J. Tribotestery. Editor PWSZ Piła 2019.

[19] Ryniewicz A, Bojko Ł, Madej T. Estimation of viscosity engine oils using rotational rheometer. SJSUTST. 2014;83: 225-234.

[20] Sejkorová M, Hurtová I, Jilek P, Novák M, Voltr O. Study of the effect of physicochemical degradation and contamination of motor oils on their lubricity. Coatings. 2021;11(1): 60. https://doi.org/10.3390/coatings11010060

[21] Thapliyal P, Thakre GD. Correlation study of physico-chemical, rheological and tribological parameters of engine oils. Adv Tribol. 2017:1-12. https://doi.org/10.1155/2017/1257607

[22] Zaharia C, Niculescu R, Clenci A, Iorga V. Analyse of used oil in order to emit diagnosis interpretations of the diesel engine operation. Rom J Automot Eng. 2019;25(1):5-11.

[23] Zaharia C, Niculescu R, Iorga-Siman V, Ducu CM. Diagnosing the operation of a locomotive diesel engine based on the analysis of used oil in the period between two technical revisions. Int Cong Automotive and Transport Engineering, Brasov, Romania. 2017. https://doi.org/10.1007/978-3-319-45447-4_36

[24] Zaharia C, Niculescu R, Năstase M, Clenci A, Iorga-Simăn V. Engine oil analysis to evaluate the degree of its wear during the period of operation of the vehicle. IOP Conf Series: Materials Science and Engineering. 2022;1220:012037. https://doi.org/10.1088/1757-899X/1220/1/012037

Daria Skonieczna, MSc. – Faculty of Technical Sciences, University of Warmia and Mazury in Olsztyn, Poland.
e-mail: *daria.skonieczna@student.uwm.edu.pl*

Piotr Szczyglak, DSc., DEng. – Faculty of Technical Sciences, University of Warmia and Mazury in Olsztyn, Poland.
e-mail: *szczypio@uwm.edu.pl*

Prof. Oleksandr Vrublevskyi, DSc., DEng. – Faculty of Technical Sciences, University of Warmia and Mazury in Olsztyn, Poland.
e-mail: *aleksander.wroblewski@uwm.edu.pl*

Article citation info:
Haller P, Haller A, Kaźmierczak A, Matla J, Sroka Z, Wróbel R. Impact of water content in fuel for smoke opacity. Combustion Engines. 2023;195(4):123-127. https://doi.org/10.19206/CE-169804

Piotr HALLER
Agata HALLER
Andrzej KAŹMIERCZAK
Jędrzej MATLA
Zbigniew SROKA
Radosław WRÓBEL

Combustion Engines
Polish Scientific Society of Combustion Engines

Impact of water content in fuel for smoke opacity

ARTICLE INFO

Received: 31 May 2023
Revised: 4 July 2023
Accepted: 19 July 2023
Available online: 2 September 2023

The development of internal combustion engines is focused at solving problems like: fulfilment with increasingly stringent requirements regarding exhaust emissions and elimination of threats to the natural environment. The subject of this thesis is to assess the impact of supplying a compression-ignition engine with hydrocarbon mixtures and to examine the impact of water on external parameters of the engine, such as smoke opacity. The main tests were carried out on a 4-cylinder VW 1.9 TDI internal combustion engine at a constant engine crankshaft speed of 3000 rpm and a variable load of 0, 30, 60, 90, 120, 150 and 180 Nm. The tests were carried out using an innovative mixture of hydrated fusel oils, ethyl alcohol and ionic and/or non-ionic emulsifiers, from which was made of microemulsions with a water content in diesel oil of 5, 10, 15, 20 and 25%. The tests carried out showed a beneficial effect of the water content in the diesel oil on the reduction of the average value of smoke opacity, which systematically decreases with the increase in the percentage of water in the diesel oil.

Key words: *combustion engines, fuel, water, microemulsion, smoke opacity*

1. Introduction

The development of internal combustion engines is primarily aimed at meeting the increasingly stringent requirements for exhaust emissions.

Currently, one of the conditions determining the use of internal combustion engines is the composition of exhaust gases emitted into the atmosphere. This is expressed in the emission of carbon dioxide CO_2, which is reflected in the level of fuel consumption, as well as the emission of toxic exhaust components in the form of carbon monoxide CO, nitrogen oxides NO_x, unburned hydrocarbons HC and particulate matter PM [8].

More and more attention is now paid to cheaper ways to reduce emissions by exploiting the potential of modifying the fuel used by shaping its composition and properties. In this way, the composition of the exhaust gas leaving the cylinder can be influenced more directly, partially eliminating the need for exhaust gas purification, thereby relieving the after-treatment equipment. One of the ways to reduce the emission of harmful compounds from diesel engines is the use of water emulsions to power them. Water in the fuel affects lower temperature in the cylinder, which has a positive effect on NO_x emissions. On the other hand, lowering the temperature should in theory cause an increase in soot in the exhaust gases.

Research on the use of water emulsions to power internal combustion engines has been conducted around the world for many years, but the scientific basis developed so far does not allow for wider technical applications. The reason is usually unfavorable results, in particular: stability of fuel-water emulsions, sensitivity to ambient temperature, possibility of corrosion of precision elements of injection equipment [8].

Currently, scientists in Asian countries are the most intensively engaged in the subject of feeding diesel engines with mixtures of fuels containing hydrocarbons and water. Over 70% of India's energy is heavily dependent on imported non-renewable fuels. This situation motivated various researchers in India to look for an alternative energy source that should be renewable and non-polluting.

In Europe, the topic was also studied. For example, in Switzerland, experimental tests and numerical calculations were carried out using standard emulsion fuel with a water content of 3 to 12%. This allowed to conclude that the use of the emulsion leads to a reduction in the emission of NO_x and CO and a reduction in the consumption of the primary fuel. The maximum reduction of emissions by 12.32 and 35.16% for CO and NO_x, respectively, and the reduction of fuel consumption by 5.46% were recorded [7, 13, 15].

In Poland, the subject of research on the impact of supplying internal combustion engines with emulsion fuels was dealt with by Jankowski [8–11]. As a result of research done by Jankowski showed that microemulsions retain the usability of the emulsion while minimizing the negative features of this type of fuel. The results of the research concerning the reduction of the emission of toxic exhaust components, in particular nitrogen oxides and particulate matter. A clear reduction of the aforementioned exhaust gas components occurs by increasing the percentage of water in the fuel. It was concluded that microemulsion fuels may contain a maximum of 30% water concentration. Above this value, liquids cease to maintain their properties and begin to stratify. Oil-water emulsions cause a simultaneous decrease in the emission of NO_x and a decrease in the smoke opacity level in the exhaust gases [2, 5, 6, 14].

2. Microemulsion of water in fuel

2.1. Obtaining microemulsions of water and fuel

One of the main problems with emulsions is that they are not stable and tend to stratify spontaneously over time. This reduces the economic viability and practical use of these fuels. There are many ways to improve the stability of

fluids, including new mixing techniques, the addition of nanoparticles, and the addition of other fluids.

The mechanical method of producing a microemulsion consists in the mechanical fragmentation of a drop of water to the size appropriate for a microemulsion (micrometres). Obtaining such an effect is possible in devices of the cavitation type or in devices with counter-rotating discs at high speed. The production of microemulsions by physicochemical methods usually consists in adding surfactant additives to the produced emulsion, which reduce the surface tension at the water-oil interface and form a layer on the water microdroplets that prevents the microdroplets from merging into larger drops. In both cases, the pre-formed oil-water emulsion contains an additive package. Depending on the type of additives and the microemulsion production technique, the additive package is introduced into water or oil [1, 3, 4, 16, 17].

2.2. Water supplying to the engine

Since the 1930s, water supplied with the fuel has been used to control the combustion process in the knocking range. As a result of adding water to the air-fuel mixture, the time of its combustion in the cylinders is reduced, which naturally prevents the conditions for detonation. The mass fraction of the fuel increases due to the microdroplets of water and steam, while the non-evaporated water increases the compression ratio. The reduction of fuel combustion temperature during the injection of water into the cylinder reduces the concentration of nitrogen oxides formed.

For the most beneficial effect, water must be supplied to the right place and at the right time to those spaces in the combustion chamber where the highest temperatures prevail. Injection of water into the intake system or direct injection of water using a separate injector may be disadvantageous because they also supply water to areas where it is inefficient [12].

Another way to put water in the combustion chamber is to feed it along with the fuel. The emulsion fuel particles sprayed as a result of the injection process contain a certain amount of water droplets in the fuel cloud. During the combustion process in the engine cylinder there are high temperatures, in which the emulsion molecule is overheated and its composition changes. As a result of the difference in boiling points, the fuel part of the droplet remains initially in a liquid state, while the other component – water – turns into a vapor state. With further heating, such a particle is atomized into finer droplets as a result of the so-called micro explosions. This phenomenon has a very positive effect on the process of mixing fuel with air. Combustion is more complete because the large amount of water vapor in the combustion chamber (in a situation of relative oxygen deficiency) promotes cracking of the fuel and gasification of the released coal, thereby reducing the number of soot particles. The addition of water has the strongest effect on reducing the emission of nitrogen oxides and this effect is maintained with an increase in the percentage of water content [9].

However, the water content in the diesel fuel must be optimized due to the overall efficiency of the engine, the degree of engine smoke and changes in the emission of toxic exhaust components. The amount of water required for a specific NO_x reduction is twice as much when injecting water into the engine's intake system than when injecting water via a diesel injector into the combustion chamber. This excess amount of water reduces the temperature level in the combustion chamber to a range where soot oxidation is inhibited, thereby increasing the level of hydrocarbon emissions, which may result in increased PM emissions. Therefore, the most advantageous method of supplying water to the combustion chamber is direct injection of the fuel-water emulsion directly into the combustion chamber [11].

3. Tests for microemulsion of water in fuel

3.1. Preparation of the microemulsions

The first tests using water microemulsions was conducted under the supervision of prof. Antoni Jankowski. As a result of the research, it was found that among all the emulsifier additives used, the best results were obtained with an ecological, hydrated fuel additive, protected by Polish patent No. PL202335. For the aforementioned research on microemulsions, this additive was modified: the fusel alcohols were removed and replaced with salts of waste fatty acids. Based on the additive prepared in this way, after mechanical mixing with fuel and water, microemulsions with a water content of 5 to 25% were created, which were then used in the research described in this article.

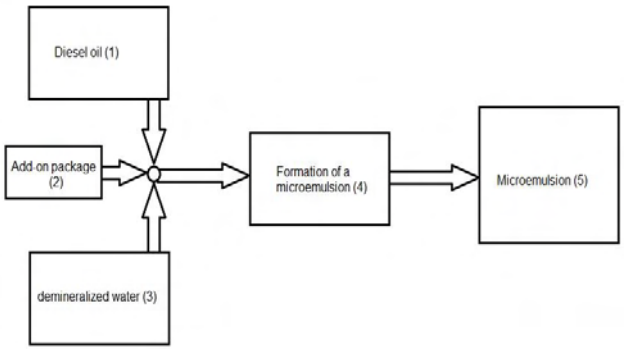

Fig. 1. Microemulsion preparation procedure

The procedure for producing the diesel oil-water microemulsion is shown in Fig. 1:

1. introduced 20 dm^3 of diesel from the tank (1) oil into the tank (4) using a drain device operating by gravity;
2. the introduced diesel fuel was then heated in the mixer (4) to the temperature of 50ºC;
3. to tank (4) containing the heated and mixed with a low-speed mechanical agitator, diesel oil was introduced from tank (2) using a gravitational drain device through a metering device: 250, 500, 750, 1000 and 1250 cm^3 (in the case of a microemulsion containing 5, 10, 15, 20, 25% water);
4. after introducing the appropriate amount of the additive package to the mixer (4), demineralized water was added from the tank (3) using a dispenser in an amount appropriate to the target water content in the microemulsion;
5. stirring at 50ºC for 30 minutes;

6. the resulting microemulsion was poured into a tank (5) and cooled to ambient temperature.

3.2. Parameters of the produced microemulsions

Fuel samples with water content of 5, 10, 15, 20 and 25% obtained in the manner described above were tested for compliance with the requirements of the standard PN-EN 590. Table 1 below presents the results of the conducted fuel tests.

Table 1. Comparison of results from laboratory tests of fuel

Tested parameter	Standard requirements PN-EN 590	Tests results for water content					
		0%	5%	10%	15%	20%	25%
Density in 15ºC [g/cm^3]	0.820–0.845	0.830	0.875	0.896	0.901	0.910	0.900
Viscosity in 40ºC [mm^2/s]	2.00–4.50	3.25	8.07	10.04	11.54	12.77	12.46
Cold filter plugging temperature [ºC]	max –22ºC	–22	–10	–6	–5	–4	–6
Ash residue [% (m/m)]	max 0.010	0.009	0.019	0.020	0.023	0.029	0.039
Water content [% (m/m)]	max 0.020	0.010	8.71	12.53	16.03	21.14	22.3
Heat of combustion [MJ/kg]	–	44.71	41.96	38.67	36.99	34.67	35.54
Calorific value [MJ/kg]	–	41.80	38.86	35.48	33.72	31.72	32.11

As can be seen, parameters such as density, viscosity at 40°C, cold filter plugging temperature and ash residue are not within the ranges provided for by the aforementioned standard.

The water content in the fuel, measured according to the PN-EN ISO 9029 standard, slightly differs from the calculated values obtained during the emulsion production process.

3.3. Measuring station and tests methodology

The basic tests were carried out on the Volkswagen 1.9 TDI engine. Engine technical data are presented in Table 2.

Table 2. Technical and operational parameters of the VW 1.9 TDI engine

Number of cylinders	4
Number of strokes	4
Cylinder diameter	95.5 mm
Piston stroke	79.5 mm
Stroke volume	1896 cm^3
Compression ratio	18.0:1
Rated power/speed	85 kW/4000 rpm
Maximum torque/speed	285 Nm/1900 rpm
Engine powered by	pump injectors
Engine type	AJM

The tests were carried out on the engine dynamometer stand at the Department of Vehicle Engineering at the Wroclaw University of Technology. This stand was placed in an isolated measuring box, where the motor and the brake were mounted on a common foundation plate. Figure 2 shows the appearance of the discussed test stand.

During the tests, one constant engine crankshaft rotational speed of 3000 rpm was used. The engine was loaded with torques of 0, 30, 60, 90, 120, 150, 180 Nm. Exhaust gas opacity was measured using an AVL type 415S G002 smoke meter. Detection limit of this device 20 μg/m^3 or 0.002 FSN. At each measurement point, the collection of concentrations of individual exhaust gas components lasted 4 minutes. The measurements at each operating point of the engine were repeated six times.

Fig. 2. Research station

Comparative tests were carried out with the engine fueled with standard diesel oil and then with microemulsion fuels with water content in diesel oil at the level of 5, 10, 15, 20 and 25%.

All tests were carried out with the factory settings of the engine, and its fuel equipment was not interfered with.

4. Smoke opacity level for tested microemulsions

The results of the tests show that for each tested engine load, the smoke opacity value for samples with water content systematically decreases with the increase in the percentage of water in the diesel oil. The addition of 5% of water in the fuel resulted in a significant decrease in smoke opacity. For loads in the range of 0 to 60 Nm, it was a decrease of about 41–51%, while for loads from 90 to 180 Nm – a decrease of about 63–72%.

Figure 3 presents graphs for all seven tested fuels, showing changes in smoke opacity level in relation to the applied rotational speeds of the test engine.

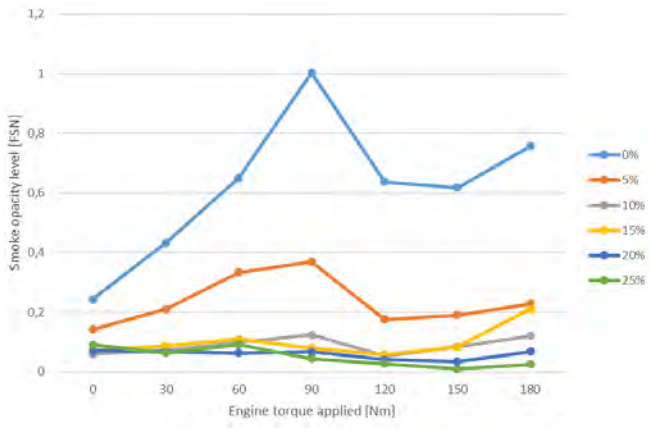

Fig. 3. The average smoke opacity values for an engine fueled with fuels with different water content depending on the engine loading torque

The Gaussian distribution is the most commonly used distribution in statistics. This is due to the fact that if a

quantity is used by many random providers, then according to their distribution, its distribution will be close to normal. If we take a closer look at the values of the Gaussian distribution, we will notice that the results obtained during the tests were close to the average values presented in Fig. 3. Especially for fuels with a water content of 10% and above, it can be concluded that the test results obtained provide a good basis for further tests on these microemulsions.

Figures 4 to 6 show the Gaussian distributions for the results obtained from the tests were repeated six times with the engine load at 30, 90 and 150 Nm. In each of the described cases, the best results were obtained for fuel with 25% water content (green line in the graphs).

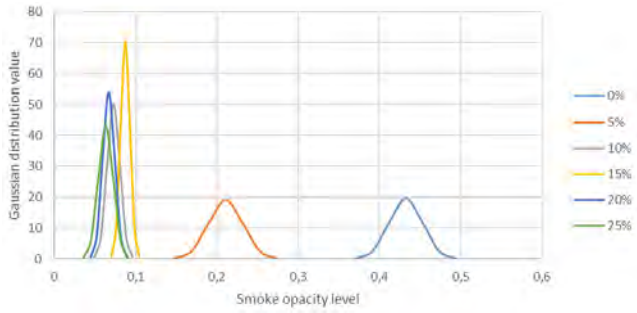

Fig. 4. Gaussian distributions for smoke opacity by the engine loaded with a torque of 30 Nm

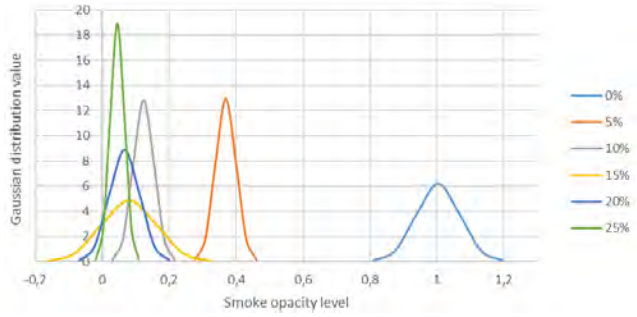

Fig. 5. Gaussian distributions for smoke opacity by the engine loaded with a torque of 90 Nm

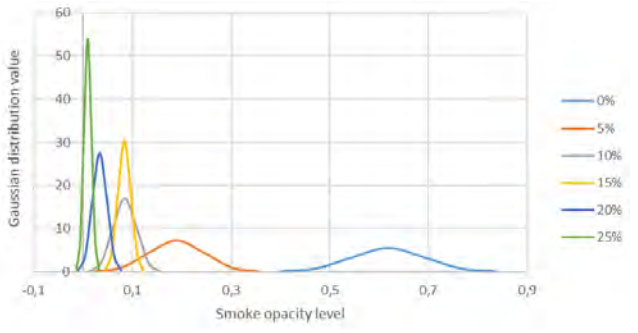

Fig. 6. Gaussian distributions for smoke opacity by the engine loaded with a torque of 150 Nm

5. Conclusions

The subject of this article was to check the effect of supplying a compression-ignition engine with hydrocarbon mixtures and to examine the effect of water on exhaust gas opacity.

Based on the research results, the following conclusions can be drawn:

- the greatest reduction of smoke opacity was obtained for the microemulsion with 25% water addition, at the engine load with a torque of 150 Nm. This value was lower by 98.5% compared to the engine fueled with standard diesel fuel
- the smallest changes in smoke opacity were recorded for tests with the engine unloaded
- tests with a set low value of the engine torque showed the highest values between the minimum and maximum for diesel fuel and emulsion with 5% water. It is shown in Fig. 4, 5, and 6 in the form of more flatter curves than for the other fuels in this test
- for the other emulsions tested, similar results were obtained, so the graphs almost overlap
- a further increase of the torque loading the engine showed similar results as in the previous tests.

Due to the reduction of smoke opacity obtained in the tests, further tests with the described emulsions are considered. The expectations regarding the addition of water in the fuel, set at the beginning of the tests, have been confirmed, which prompts further research in this area.

Nomenclature

CO	carbon monoxide
CO_2	carbon dioxide
HC	unburned hydrocarbons
NO_x	nitrogen oxides
PM	particulate matter

Bibliography

[1] Abd Razak IF, Yahya WJ, Ithnin AM, Rashid M, Zuber MA, Kadir HA et al. Effects of different water percentages in non-surfactant water-in-diesel emulsion fuel on the performance and exhaust emissions of a small-scale industrial burner. Clean Techn Environ Policy. 2021;23:2386-2397. https://doi.org/10.1007/s10098-021-02151-7

[2] Abdollahi M, Ghobadian B, Najafi G, Hoseini SS, Mofijur M, Mazlan M. Impact of water–biodiesel–diesel nano-emulsion fuel on performance parameters and diesel engine emission. Fuel. 2020;280;118576. https://doi.org/10.1016/j.fuel.2020.118576

[3] Ardabili SF, Najafi B, Aghbashlo M, Khounani Z, Tabatabaei M. Performance and emission analysis of a dual-fuel engine operating on high natural gas substitution rates ignited by aqueous carbon nanoparticles-laden diesel/biodiesel emulsions. Fuel. 2021;294:120246. https://doi.org/10.1016/j.fuel.2021.120246

[4] Dorokhov AS, Kataev YV, Gradov EA. Influence of cavitation on the working surfaces of the cylinder–piston group in a diesel engine during maintenance. Russ Engin Res. 2021; 41(11):1009-1013. https://doi.org/10.3103/S1068798X21110083

[5] Elumalai PV, Nambiraj M, Parthasarathy M, Balasubramanian D, Hariharan V, Jayakar J. Experimental investigation to reduce environmental pollutants using biofuel nano-water emulsion in thermal barrier coated engine. Fuel. 2021; 285:119200. https://doi.org/10.1016/j.fuel.2020.119200

[6] Elumalai PV, Parthasarathy M, Hariharan V, Jayakar J, Iqbal SM. Evaluation of water emulsion in biodiesel for engine performance and emission characteristics. J Therm Anal Calorim. 2022;147:4285-4301. https://doi.org/10.1007/s10973-021-10825-z

[7] Gopidesi RK, Premkartikkumar SR. Evaluating the characteristics of a diesel engine fuelled with water in diesel emulsion and hythane gas in a dual-fuel mode. International Journal of Ambient Energy. 2022;43(1):853-857. https://doi.org/10.1080/01430750.2019.1670258

[8] Haller P, Jankowski A, Kolanek C, Walkowiak W. Research of water–fuel microemulsions as fuel for diesel engine. Journal of KONES Powertrain and Transport. 2015;19:165-170. https://doi.org/10.5604/12314005.1138110

[9] Jankowski A. Influence of chosen parameters of water fuel microemulsion on combustion processes, emission level of nitrogen oxides and fuel consumption of CI engine. Journal of KONES Powertrain and Transport. 2011;18(4):593-600.

[10] Jankowski A, Kowalski M. Alternative fuel in the combustion process of combustion engines. Journal of KONBiN. 2018;48(1):69-82. https://doi.org/10.2478/jok-2018-0047

[11] Jankowski A, Sowa K, Zabłocki M. Some aspects using of micro emulsion fuel-water for supply of combustion engines. Journal of KONES 2009 Powertrain and Transport. 2009;16(4):531-538.

[12] Kaźmierczak U, Kulczycki A, Dzięgielewski W, Jankowski A. Microemulsion bioliquids (in Polish). Journal of KONBiN. 2012;21(1):141-148. https://doi.org/10.2478/jok-2013-0013

[13] Kesharvani S, Chhabra M, Dwivedi G, Verma TN, Pugazhendhi A. Execution and emission characteristics of automotive compression ignition engine powered by cerium oxide nanoparticles doped water diesel emulsion fuel. Fuel. 2023;349:128670. https://doi.org/10.1016/j.fuel.2023.128670

[14] Kornienko V, Radchenko R, Radchenko M, Radchenko A, Pavlenko A, Konovalov D. Cooling cyclic air of marine engine with water-fuel emulsion combustion by exhaust heat recovery chiller. Energies. 2022;15(1):248. https://doi.org/10.3390/en15010248

[15] Tamam MQM, Yahya WJ, Ithnin AM, Abdullah NR, Kadir HA, Rahman MM et al. Performance and emission studies of a common rail turbocharged diesel electric generator fueled with emulsifier free water/diesel emulsion. Energy. 2023;268:126704. https://doi.org/10.1016/j.energy.2023.126704

[16] Tornatore C, Marchitto L, Teodosio L, Massoli P, Bellettre J. Performance and emissions of a spark ignition engine fueled with water-in-gasoline emulsion produced through micro-channels emulsification. Appl Sci. 2021;11(20):9453. https://doi.org/10.3390/app11209453

[17] Yadykova AY, Ilyin SO. Rheological, thermophysical, and morphological features of original and hydrogenated bio-oils. Sustainable Energy and Fuels. 2021;5:4425-4433. https://doi.org/10.1039/D1SE00567G

Piotr Haller, MSc. – Wroclaw University of Science and Technology, Poland.
e-mail: *piotr.haller@pwr.edu.pl*

Agata Haller, MEng. – Wroclaw University of Science and Technology, Poland.
e-mail: *agata.haller@gmail.com*

Prof. Andrzej Kaźmierczak, DSc., DEng. – Wroclaw University of Science and Technology, Poland.
e-mail: *andrzej.kazmierczak@pwr.edu.pl*

Jędrzej Matla, MEng. – Wroclaw University of Science and Technology, Poland.
e-mail: *jedrzej.matla@pwr.edu.pl*

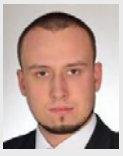

Prof. Zbigniew Sroka, DSc., DEng. – Wroclaw University of Science and Technology, Poland.
e-mail: *zbigniew.Sroka@pwr.edu.pl*

Prof. Radosław Wróbel, DSc., DEng. – Wroclaw University of Science and Technology, Poland.
e-mail: *radoslaw.wrobel@pwr.edu.pl*

Article citation info:
Adamiak B, Szczotka A, Woodburn J, Merkisz J. Comparison of exhaust emission results obtained from Portable Emissions Measurement System (PEMS) and a laboratory system. Combustion Engines. 2023;195(4):128-135. https://doi.org/10.19206/CE-172818

Borys ADAMIAK
Andrzej SZCZOTKA
Joseph WOODBURN
Jerzy MERKISZ

Combustion Engines
Polish Scientific Society of Combustion Engines

Comparison of exhaust emission results obtained from Portable Emissions Measurement System (PEMS) and a laboratory system

ARTICLE INFO

Received: 18 July 2023
Revised: 22 September 2023
Accepted: 22 September 2023
Available online: 9 October 2023

Exhaust emissions testing of vehicles under real driving conditions (real driving emissions, RDE) using portable exhaust emissions measurement systems (PEMS) was introduced a few years ago by the European Commission as a mandatory test during type approval and later also for in-service conformity. This paper compares results from mobile systems for measuring exhaust gas emissions (PEMS) with a stationary laboratory (BOSMAL's Exhaust Emissions Testing Laboratory). The tests were carried out using a passenger car equipped with a spark ignition engine, which was tested on a chassis dynamometer over the WLTC cycle. The results showed that the differences between PEMS analysers and stationary analysers range from a few percent to a dozen or so percent, depending on the component and the measurement method.

Key words: *Portable Emissions Measurement System; Worldwide harmonized Light vehicles Test Cycle; Real Driving Emissions; Conformity Factor*

1. Introduction

Environmental protection and improvement of air quality have become a major goal set by many governments around the world and by the European Commission. In many areas, the largest contributor (or one of the largest contributors) to the deterioration of air quality and greenhouse gas emissions is the road transport sector. In Europe, the road transport contributed 39% of total anthropogenic NO_x emissions and 23% of carbon dioxide emissions in 2015, reducing to 37% of total anthropogenic NO_x emissions and 18% of carbon dioxide emissions in Europe in 2020 [1, 3, 17]. In order to reduce the emission of harmful substances and greenhouse gases, exhaust emissions standards and fuel efficiency requirements for road vehicles are being tightened around the world. Over the years 2018/2019, the driving cycle in force in the EU for laboratory testing of light duty vehicles was changed from the NEDC to the WLTC, which reflected more natural/realistic driving, and Euro 6d-temp emission limits were introduced [18]. Despite the change in the driving cycle (as well as some other aspects of the test procedure), there were concerns that exhaust emissions under laboratory conditions still did not correspond to exhaust emissions under real driving conditions. For that reason, since September 2019 the regulations for measuring exhaust emissions in real-world conditions (on public roads) for all newly type-approved vehicles in accordance with EC Regulation (EU) 2017/1151 have been in force in Europe. Measurements of the emission of harmful exhaust compounds under real-world conditions (RDE) forced the manufacturers of exhaust gas analysers to develop portable exhaust emission systems (PEMS), which were initially intended for testing heavy-duty vehicles [22]. The Euro 6 standard defines the permissible emission limits for passenger cars (M1) and light commercial vehicles (N1), which include such components as CO, THC, NO_x, as well as particulate matter by mass (PM) and by number (PN) [3, 9. 11, 13, 22].

Exhaust emission tests under real-world (RDE) driving conditions are carried out on public roads in accordance with the applicable requirements within Regulation (EC) No 715/2007, with all applicable amendments. These regulations specify what devices and mobile analysers must be fitted to the vehicle during the RDE test. The PEMS system consists of portable exhaust gas analysers, an exhaust gas mass flow meter (EFM), a weather station, and a positioning monitoring system (GPS). These devices must be integrated and the control system logging their data must operate at an acquisition frequency of at least 1 Hz [22]. The regulations specify not only the devices that must be used during the RDE test, but also the route conditions such as minimum and maximum test duration, distance travelled, speed ranges and ambient conditions such as minimum and maximum altitude above sea level, as well as temperature [2, 10, 13]. For cold start testing, the regulations also specify the maximum temperature difference of the vehicle (coolant and engine oil) in relation to the ambient temperature at the start of the test. Each test route for vehicles of category M1 must include three ranges: the urban part, the extra-urban part, and the motorway part; the relative (percentage) shares of which are specified in the regulation.

Currently, Europe mandates Euro 6 emission limits, whose values for M1 vehicles are given in Tables 1–2.

Table 1. Euro 6 emission limits for M1 cars with SI engine (* GDI engine)

Parameter	Unit	Value
CO	mg/km	1000
THC	mg/km	100
NMHC	mg/kg	68
NO_x	mg/km	60
PM*	mg/km	4.5
PN*	#/km	$6 \cdot 10^{11}$

Table 2. Euro 6 emission limits for M1 vehicles with CI engine

Parameter	Unit	Value
CO	mg/km	500
NO_x	mg/km	80
THC + NO_x	mg/km	170
PM	mg/km	4.5
PN	#/km	$6 \cdot 10^{11}$

These limits apply to laboratory testing in the WLTP test. For RDE tests, emissions of two components are currently limited: NO_x and PN. These limits are closely related to (in fact, derived from) the respective Euro 6 limits. Due to methodological differences in measurement rules, Euro 6/VI introduces so-called conformity factors for LD and HD vehicles. These conformity factors reflect the additional uncertainty of the PEMS measurement compared to laboratory measurements [21]. The current conformity factors (CFs) are 1.43 for NO_x and 1.5 for PN, respectively. From September 2023 (Euro 6e) they will be 1.1 for NO_x and 1.34 for PN [8].

In order to verify the correct installation and operation of the PEMS system, it is necessary to perform a validation test for LD vehicles in accordance with Annexes XXI and IIIA of Regulation (EU) No. 2017/1151, as amended by Regulation (EU) No. 2018/1832. The validation test is the measurement of exhaust emissions from a vehicle during a laboratory test on a chassis dynamometer with the PEMS system installed on this vehicle. Emissions are measured by both systems, then the measurement results are compared with each other. The emission results from the PEMS system are compared with the results from the stationary system, while the measurement of exhaust gas emissions from the PEMS system is carried out on the basis of modal measurement of undiluted exhaust gas using fast analysers and flow meters (EFM), and the measurement from the stationary system on the basis of measurement from measuring bags diluted exhaust gases [19]. Table 3 shows the acceptable differences between the results of laboratory tests and the results of PEMS in accordance with Regulation EU 2020/49 of 21.01.2020 and new acceptable differences in accordance with Regulation EU 2023/443 of 08.02.2023 [8, 20].

Table 3. Limits for validation test limits between laboratory results

		Limit abs. 2020/49	Limit abs. 2023/443	Limit rel. 2020/49	Limit rel. 2023/443
		[±]		[%]	
Distance	km	0.250			
NO_x	mg/km	15	10	15	12.5
CO	mg/km	150	100	15	15
CO_2	g/km	10	10	10	7.5
NMHC	mg/km	20	20	20	20
CH_4	mg/km	15	15	15	15
THC	mg/km	15	15	15	15
PN	#/km	$1 \cdot 10^{11}$	$8 \cdot 10^{10}$	50	42

2. Characteristics of the emissions laboratories

BOSMAL's emissions testing laboratory is an advanced, climate-controlled facility for performing emissions, fuel consumption and performance tests over a range of driving cycles and a broad range of ambient conditions. Exhaust emissions testing is carried out with the aid of sampling bags (legislative tests), diluted and raw modal analysis (development tests) for use with CI, SI, and hybrid vehicles. These facilities permit the execution of a wide range of legislative and development emissions tests, including:

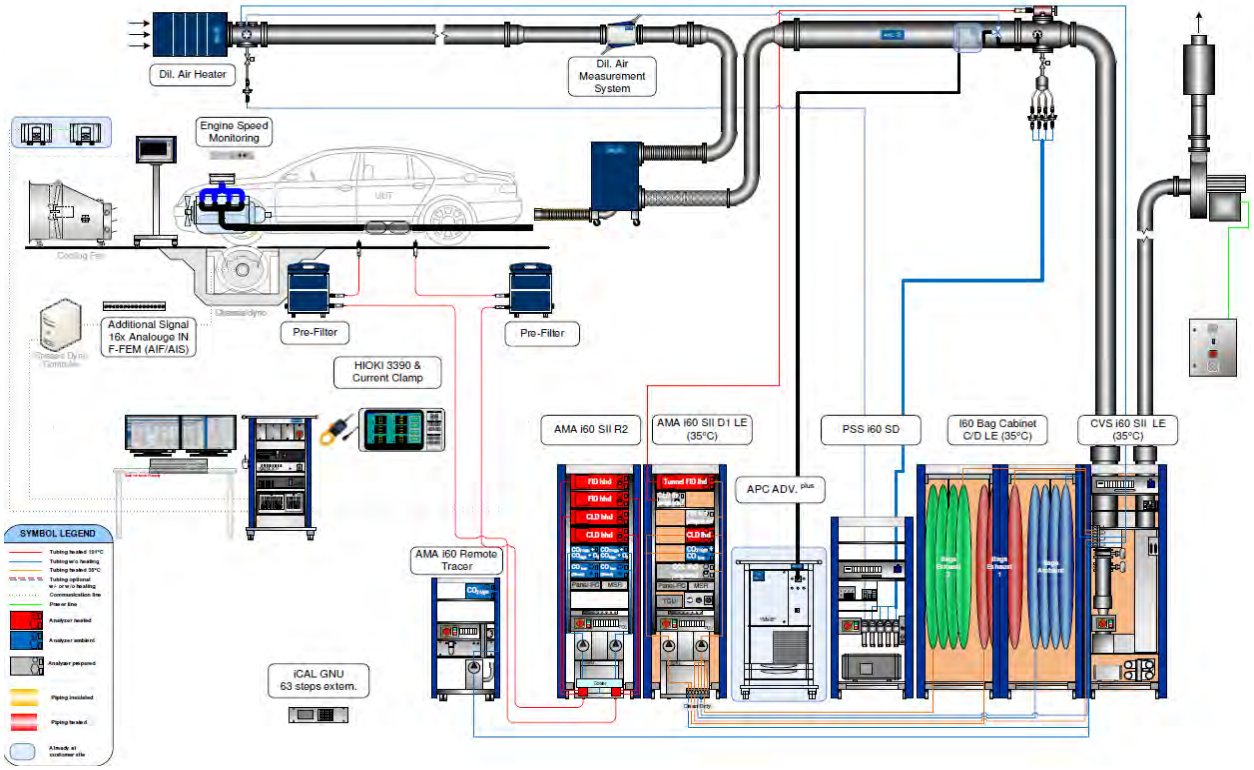

Fig. 1. Schematic laboratory

– CVS bag diluted emissions testing to international standards [6, 7]
– CO_2 emissions and fuel consumption measurement according to EU standards [20]
– gravimetric and numerical quantification of particulate matter emission according to [12, 15]
– measurement of soot and particulate matter from raw exhaust gases using additional devices.

A schematic of the Laboratory is shown in Fig. 1.

3. Emissions testing system

The emissions system in Laboratory consists of a sampling system, together with a dilution tunnel (Fig. 2), a set of exhaust analysers and a management/automation system (Fig. 3).

Fig. 2. View of the emission laboratory

Fig. 3. View of test management/automation system in the laboratory

The emissions system's bags for the sampling of diluted exhaust gas ambient and ambient air are housed in a heated, insulated unit maintained at 35°C to prevent condensation. The software (automation system) controls the analysers and their various activities during testing and analysis of bag emissions, such as calibration, purging, etc. The system automates the signals sent to the driver's aid, and include options for testing over all the test cycles previously mentioned, as well as any other cycle added to the system via the implementation of new programs. Additionally, the software monitors the laboratory's environmental parameters (temperature, pressure, humidity) as well as ambient concentrations of THC, CH_4, CO, and CO_2 within the laboratory to ensure that each test is safe, reliable, repeatable, and thoroughly documented [3]. Table 4 gives the measurement principles and analysers' ranges for stationary laboratory equipment.

Table 4. Parameters of the stationary emissions measurement system

Measuring ranges of gas analyzers of stationary systems			
Measured component (measurement method)	Bag measurement/ continuous dilution measurement		Measuring accuracy
Range	Low	High	
CO low (NDIR)	0–50 ppm	0–5000 ppm	±2% at the measuring point ±1% of scale
CO_2 (NDIR)	0–1%	0–20%	
NO_x (CLD)	0–5 ppm	0–1000 ppm	
NO (CLD)	0–5 ppm	0–1000 ppm	
THC (FID)	0–17 ppm	0–3000 ppm	
CH_4 (NMHC cutter)	0–10 ppm	0–400 ppm	
PN (condensing)	0–50000 #/cm^3		±10%

4. Research aim and research object

The aim of the research was to measure and analyse the exhaust emissions results of a passenger car (and to compare the fuel consumption) with measurements carried out over WLTC test on stationary laboratory with simultaneous measurement from a PEMS system. The test object was a PEMS system, data for which are shown in Table 5.

Table 5. Parameters of the mobile emissions measurement system

Measuring ranges of gas analyzers of mobile system		
Measured component (measurement method)	Continuous measurement of diluted exhaust gas	Measuring accuracy
CO (NDIR)	0–5%	±2% or ≤ 30 ppm
CO_2 (NDIR)	0–20%	±2% or ≤ 0.06%
NO2 (NDUV)	0–2500 ppm	±2% or ≤ 5 ppm
NO (NDUV)	0–5000 ppm	±2% or ≤ 10 ppm
THC (FID)	0–30 000 ppm C1	±2% or ≤ 5 ppm
PN (electrostatic)	0–2×10^7 #/cm^3	±10%

A brand new passenger car equipped with gasoline direct injection and fulfilling the Euro 6 norm was used for the measurements. Table 6 shows the data of the vehicle.

Table 6. Data of the test vehicle

Parameter	Value
Fuel type	Gasoline
Fuel delivery strategy	GDI
Vehicle mass [kg]	1008
Swept volume [cm^3]	1000
Power [kW]	51
Gearbox	Manual (5-speed)
Mileage [km]	170
Emission standard	Euro 6d

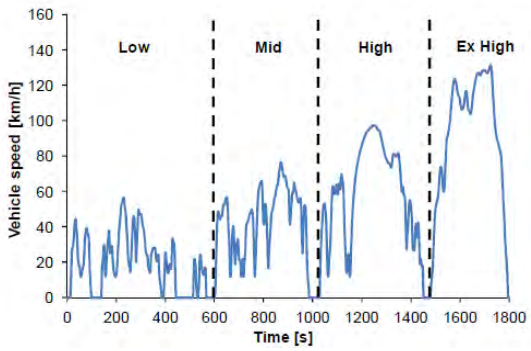

Fig. 4. The speed trace for the WLTC class 3b test cycle

The speed profile of the WLTC test, consisting of four phases: low, middle, high, and extra-high, is the legislative test for EU type approval testing of vehicles with a total weight not exceeding 3.5 t, introduced in September 2018 for all newly manufactured vehicles (Fig. 4; detailed data on test characteristics are presented in Table 7).

Table 7. WLTC test data

Parameter	Unit	Value
Distance	km	23.266
Duration	s	1800
Number of pull-away events	–	8
Pull-away events per km	km^{-1}	0.34
Length of initial idling (before first pull-away event)	s	11
Total idling time	s	234
Idling time (proportion)	%	13
Maximum speed	km/h	131.3
Mean speed (all phases, including idling)	km/h	46.50
Time at which the mean speed is first exceeded	s	217
Maximum acceleration	m/s^2	1.67
Maximum value of v·a	m^2/s^3, W/kg	20.57
Proportion of time for which speed > 100 km/h	%	10.11
Engine temperature before test start	°C	23 ±3

5. Results

Currently, in order to allow a new vehicle type to be sold for use on public roads, it is necessary to thoroughly check the exhaust emissions. For this purpose, exhaust gas analysers – both stationary and mobile – are used. The results presented below show the difference between the results from the stationary and mobile analysers. Each of the WLTC tests was performed by the same experienced driver, to minimise driver-dependent variables (and their influence on the results) as directly as possible. In addition, the test vehicle performed each test in the same selectable driving mode with the same chassis dynamometer settings. In order to eliminate additional measurement irregularities, prior to each test the vehicle was stored in a climatic chamber under constant atmospheric conditions. After each test, the vehicle was conditioned for at least 12 hours so that the temperature of operating fluids stabilized in the range of 22–24°C. The results of the three exhaust emissions and fuel consumption were averaged and then analysed and presented in the graphs below. Tests were conducted with the Start&Stop system turned off, and the results were presented without RCB and S&D corrections. In addition, the graphs showing the final exhaust emissions show the current Euro 6 exhaust gas limits as well as RDE limits and validation test limits in accordance with Regulation EU 2020/49 from 21.01.2020.

Figure 5 shows the average results of hydrocarbon emissions from the WLTC test carried out in the stationary laboratory. The results are within the Euro 6 limits and meet the validation condition. The absolute difference between the results from the stationary system and the mobile system is at a level of a few milligrams per km. Additionally, the maximum value of THC emissions is shown in purple; the minimum THC emission value is shown in yellow.

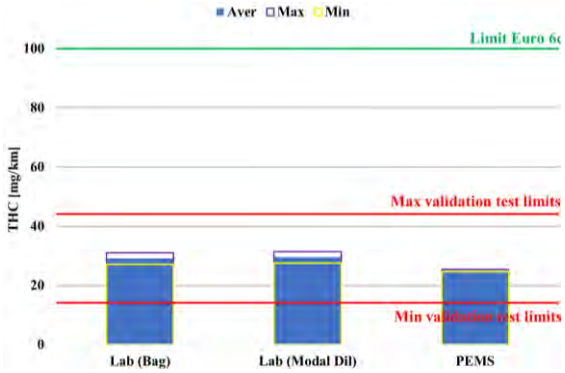

Fig. 5. THC emissions over the WLTC cycle measured by laboratory system (Bag and Modal Dil) and by PEMS

Figure 6 shows the percentage difference in the THC results from the mobile system in relation to the measurements from the stationary system, both with measuring bags (Bag) and with continuous measurement of diluted exhaust gas (Modal Dil). These differences amount to 14% in comparison with the results from the measuring bags and more than 15% compared to the results from Modal Dil.

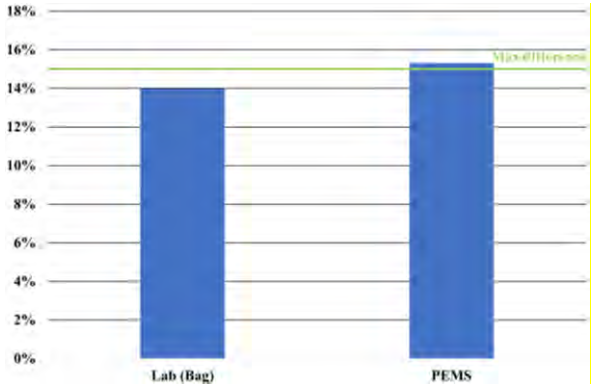

Fig. 6. Percentage differences between PEMS and results THC from Bag

Table 8. Validation test results

Inertia: 1162 kg		WLTC emissions						Remarks
Loading coefficients F0/F1/F2	km	mg/km			#/km	g/km	dm^3/100km	
	Distance	THC	CO	NO_x	PN	CO_2	FC	
18/-0,28/0.0316	23.28	29	210	14	4.18E+11	118.9	5.11	Laboratory (BAG results)
	23.28	30	211	14		119.6	5.14	Laboratory (DIL results)
	23.12	25	218	19	3.17E+11	122.9	5.26	PEMS
Difference Lab to PEMS	0.16	4	8	5	1.01E+11	4	0.15	
Maximum permissible tolerance	0.25	15	150	15	1.00E+11	11.9		

Figure 7 shows the CO_2 emissions results from the stationary system and the results from the mobile system. The validation conditions are met and the emission difference is 4 grams per km compared to the results from the measuring bags of the stationary system. The maximum CO_2 emission value is shown in purple; the minimum CO_2 emission value is shown in yellow.

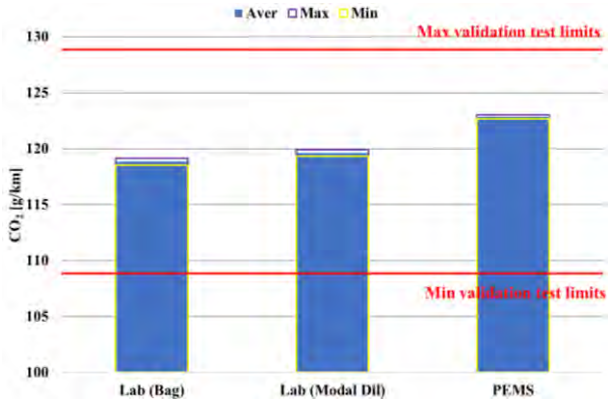

Fig. 7. CO_2 emissions over the WLTC cycle measured by the laboratory system (Bag and Modal Dil) and by the PEMS

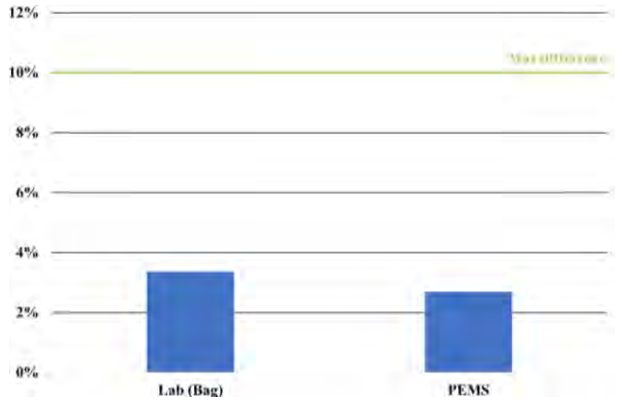

Fig. 8. Percentage differences for CO_2 results between the PEMS and Bag

Fig. 9. CO emissions over the WLTC cycle measured by the laboratory system (Bag and Modal Dil) and by the PEMS

Figure 8 shows the percentage difference in the results of carbon dioxide from the Mobile system in relation to the measurements from the stationary system, both with measuring bags (Bag) and with continuous measurement of diluted exhaust gases (Modal Dil). These differences are about 3–4% compared to the results from the measuring bags and the results of Modal Dil.

The figure below shows the results of carbon monoxide emissions. The maximum CO emission value is shown in purple; the minimum CO emission value is shown in yellow; the average emission from emission tests is marked in blue. The vehicle met the emission limits of the Euro 6 standard and the results from the mobile system met the validation condition, and the difference in CO emissions is at a level of 8 mg per km.

The figure below shows the percentage difference in the results of monoxide carbon from the Mobile system in relation to the measurements from the stationary system, both with measuring bags (Bag) and with continuous measurement of diluted exhaust gas (Modal Dil). These differences amount to 4.5% for comparison with the results from measuring bags and less than 3.5% compared to the results of Modal Dil.

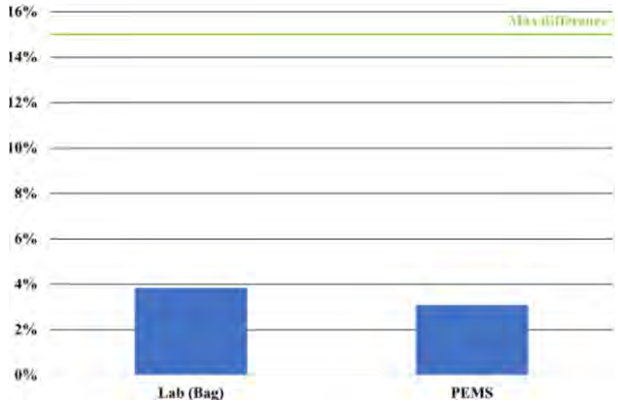

Fig. 10. Percentage differences for CO results between the PEMS and Bag

Figure 11 shows the results of nitrogen oxide emissions. The validation conditions have been met and the Euro 6 limits have not been exceeded. The difference between the results from the measuring bags and the results from the mobile system is at a level of 5 mg per km. The NO_x limit for the RDE result (with CF) is shown in blue in the graph, which for SI Euro 6d vehicles is 60×1.43 mg/km. The maximum value of NO_x emissions is shown in purple and the minimum NO_x emission value is shown in yellow.

Fig. 11. NO_x emissions over the WLTC cycle measured by the laboratory system (Bag and Modal Dil) and by the PEMS

Figure 12 shows the percentage difference in the results of nitrogen oxides from the Mobile system in relation to the measurements from the stationary system, both with measuring bags (Bag) and with continuous measurement of diluted exhaust gases (Modal Dil). The difference between the mobile system and the results from the stationary system in both methods (Bag and Modal Dil) amounts to 32%.

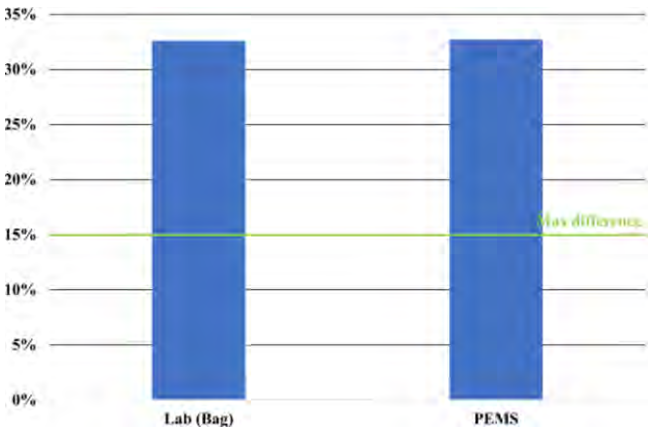

Fig. 12. Percentage differences for NO_x results between the PEMS and Bag

Figure 13 shows the particle number emission results. The validation limits of the particle number measurement are shown in red. Additionally, the maximum value of PN emissions is shown in purple; the minimum PN emission value is shown in yellow.

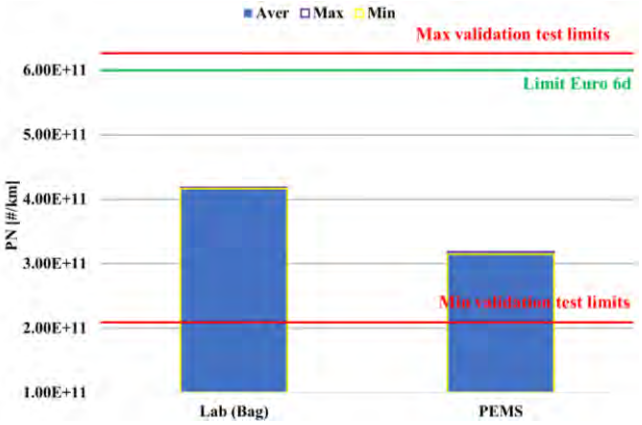

Fig. 13. PN emissions over the WLTC cycle measured by the laboratory system and by the mobile system (PEMS)

The percentage difference in the number of particles from the mobile system in relation to the measurements from the stationary system is 25%. While this relative difference is larger than for some other species measured (especially CO_2), it should be noted that differences of this magnitude may be observed for systems of the same type [4, 14].

Figure 14 shows the results of fuel consumption. The difference between the results from the measuring bags and the results from the mobile system is 0.14 dm^3/100 km.

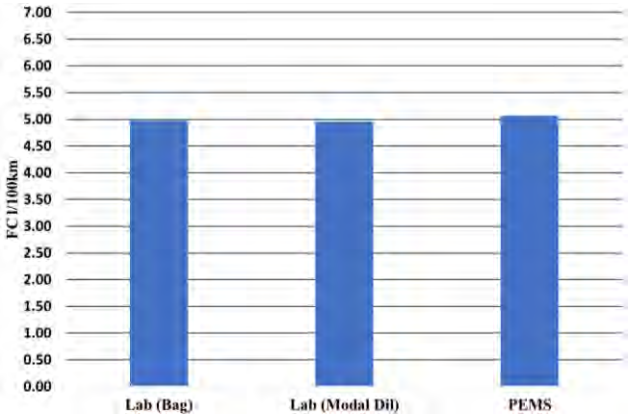

Fig. 14. FC results over the WLTC cycle by the laboratory system (Bag and Modal Dil) and by the PEMS

6. Conclusions

Based on the testing conducted, it was found that the absolute difference of a few milligrams per km for the measurement of hydrocarbons between the mobile system and the stationary system (for both measurement methods) is 14% for the measurement via bag and 15% for the continuous measurement of diluted exhaust gas. The difference at the level of 4 g per km for the measurement of carbon dioxide gives a relative value not exceeding 4% for the measurement from the bags, while for continuous measurement of diluted exhaust gas it is about 3%. In the case of carbon monoxide, the difference in relative measurements is at a level of 3–4%, which in fact gives a difference of about 8 mg per km. The results for NO_x show the largest relative difference, which is 33%, which in fact translates into a relative difference of 4.5 mg per km. The absolute difference in the concentration of particles for the mobile system is 1.01E+11 #/cm^3, which translates to a relative difference of approx. 25% compared to the PN measurement from the stationary emission system.

The research reported in this article allows it to be concluded that the absolute differences in the results of exhaust emissions between the mobile system and the measurements from the stationary system are small – and often amount to a few milligrams (or grams in the case of CO_2) per unit distance. The difference in the distance measured from the stationary and mobile system is 160 m, which may be due to the measurement of the distance traveled using the dyno for the stationary system and by speed signals from the OBD using the mobile system, but the value is within the limit of 250 m. However, the relative differences amount to several dozen percent. It can be seen that the greatest relative differences for the measurement of NO_x and the measurement of PN. These differences may result from different measurement methods for both nitrogen oxides (stationary: CLD/mobile: NDUV) and measurement of the number of particles (stationary: condensing/mobile: electrostatic). Taking into account the values measured by the mobile system (excluding measurement errors), it can be concluded that both systems are reliable and the absolute differences in the emission results do not differ significantly from the results from the stationary laboratory equipment (although the relative differences may be large for low absolute values).

Nomenclature

CF	conformity factor
CH_4	methane
CI	compression ignition
CO	carbon monoxide
CO_2	carbon dioxide
CVS	constant volume sampler
EFM	exhaust gas mass flow meter
FC	fuel consumption
GDI	gasoline direct injection
GPS	global positioning system
HD	heavy duty
LD	light duty
NEDC	New European Driving Cycle
NO_x	nitrogen oxides
PEMS	Portable Emissions Measurement Systems
PM	particle mass
PN	particle number
RDE	Real Driving Emissions
SI	spark ignition
THC	total hydrocarbons
WLTC	Worldwide harmonized Light-duty vehicles Test Cycles

Bibliography

[1] Air quality in Europe. https://www.eea.europa.eu/data-and-maps/daviz/contribution-to-eu-27-emissions#tab-googlechartid_googlechartid_googlechartid_chart_1111

[2] Baldino C, Tiegte U, Muncrief R, Bernard Y, Mock P. Road tested: comparative overview of real-world versus type-approval NO_x and CO_2 emissions from diesel cars in Europe. White Paper. International Council on Clean Transportation Europe (ICCT), Berlin 2017. https://theicct.org/wp-content/uploads/2021/06/ICCT_RoadTested_201709.pdf

[3] Bielaczyc P, Klimkiewicz D, Woodburn J, Szczotka A. Exhaust emission testing methods – BOSMAL's legislative and development emission testing laboratories. Combustion Engines. 2019;178(3):87-97. https://doi.org/10.19206/CE-2019-316

[4] Bielaczyc P, Merkisz J, Pajdowski P, Woodburn J. Correlation between two commercially available PMP-compliant particle number counting systems. Combustion Engines. 2012; 149(2):10-21. https://doi.org/10.19206/CE-117036

[5] Commission proposes new Euro 7 standards to reduce pollutant emissions from vehicles and improve air quality. European Commission; Brussels 2022. https://ec.europa.eu/commission/presscorner/detail/en/ip_22_6495

[6] Commission Regulation (EC) No 692/2008 of 18 July 2008 implementing and amending Regulation (EC) No 715/2007 of the European Parliament and of the Council on type-approval of motor vehicles with respect to emissions from light passenger and commercial vehicles (Euro 5 and Euro 6) and on access to vehicle repair and maintenance information. Official Journal of the European Union, L199, 1-136, 28.7.2008. http://data.europa.eu/eli/reg/2008/692/oj

[7] Commission Regulation (EU) 2017/1151 of 1 June 2017 supplementing Regulation (EC) No 715/2007 of the European Parliament and of the Council on type-approval of motor vehicles with respect to emissions from light passenger and commercial vehicles (Euro 5 and Euro 6) and on access to vehicle repair and maintenance information, amending Directive 2007/46/EC of the European Parliament and of the Council, Commission Regulation (EC) No 692/2008 and Commission Regulation (EU) No 1230/2012 and repealing Commission Regulation (EC) No 692/2008. Official Journal of the European Union, L 175, 1-643, 7.7.2017. http://data.europa.eu/eli/reg/2017/1151/oj

[8] Commission Regulation (EU) 2023/443 of 8 February 2023 amending Regulation (EU) 2017/1151 as regards the emission type approval procedures for light passenger and commercial vehicles (Text with EEA relevance). http://data.europa.eu/eli/reg/2023/443/oj

[9] Dornoff J. Euro 6e: Changes to the European Union light-duty vehicle type-approval procedure. 2022 International Council on Clean Transportation December 2022. https://theicct.org/wp-content/uploads/2022/12/euro6e-type-approval-dec22.pdf

[10] Giechaskiel B, Bonnel P, Perujo A, Dilara P. Solid Particle Number (SPN) Portable Emissions Measurement Systems (PEMS) in the European legislation: a review. Int J Env Res Pub He. 2019;16:4819. https://doi.org/10.3390/ijerph16234819

[11] Giechaskiel B, Casadei S, Rossi T, Forloni F, Di Domenico A. Measurements of the emissions of a "Golden" Vehicle at seven laboratories with Portable Emission Measurement Systems (PEMS). Sustainability. 2021;13(16):8762. https://doi.org/10.3390/su13168762

[12] Giechaskiel B, Lahde T, Suarez-Bertoa R, Clairotte M, Grigoratos T, Zardini A et al. Particle number measurements in the European legislation and future JRC activities. Combustion Engines. 2018;174(3):3-16. https://doi.org/10.19206/CE-2018-301

[13] Giechaskiel B, Vlachos T, Riccobono F, Forni F, Colombo R, Montigny F et al. Implementation of Portable Emission Measurement Systems (PEMS) for the Real-Driving Emissions (RDE) Regulation in Europe. J Vis Exp. 2016;118: e54753. https://doi.org/10.3791/54753

[14] Giechaskiel B, Woodburn J, Szczotka A, Bielaczyc P. Particulate Matter (PM) emissions of Euro 5 and Euro 6 vehicles using systems with evaporation tube or catalytic stripper and 23 Nm or 10 Nm counters. SAE Technical Paper 2020-01-2203. 2020. https://doi.org/10.4271/2020-01-2203

[15] Global Technical Regulation No. 15. Global technical regulation on Worldwide harmonized Light vehicles Test Procedures (WLTP). Amendment 3, Established in the Global Registry on 15 November 2017.

[16] Johnson KC, Durbin TD, Cocker DR, Miller JW, Agama RJ, Moynahan N et al. On-road evaluation of a PEMS for measuring gaseous in-use emissions from a heavy-duty diesel vehicle. SAE Int J Commer Veh. 2009;1(1):200-209. https://doi.org/10.4271/2008-01-1300

[17] Marinello S, Lolli F, Gamberini R. Roadway tunnels: a critical review of air pollutant concentrations and vehicular emissions. Transport Res D-Tr E. 2020;86:102478. https://doi.org/10.1016/j.trd.2020.102478

[18] Marotta A, Pavlovic J, Ciuffo B, Serra S, Fontaras G. Gaseous emissions from light-duty vehicles: moving from NEDC to the new WLTP test procedure. Environ Sci Technol. 2015; 49(14):8315-8322. https://doi.org/10.1021/acs.est.5b01364

[19] RDE working group. RDE – Preliminary Uncertainty. European Commission, Joint Research Centre (JRC), Institute for Energy and Transport. 14 September 2015.

[20] Regulation No 101 of the Economic Commission for Europe of the United Nations (UN/ECE) – Uniform provisions concerning the approval of passenger cars powered by an internal combustion engine only, or powered by a hybrid electric power train with regard to the measurement of the emission of carbon dioxide and fuel consumption and/or the measurement of electric energy consumption and electric range, and of categories M1and N1vehicles powered by an electric power train only with regard to the measurement of electric energy consumption and electric range. Supplement 7 to the original version of the Regulation. 18 June 2007.

[21] Valverde V, Kondo Y, Otsuki Y, Krenz T, Melas A, Suarez-Bertoa R et al. Measurement of gaseous exhaust emissions of light-duty vehicles in preparation for Euro 7: a comparison of portable and laboratory instrumentation. Energies. 2023;16(6): 2561. https://doi.org/10.3390/en16062561

[22] Varella R, Giechaskiel B, Sousa L, Duarte G. Comparison of Portable Emissions Measurement Systems (PEMS) with laboratory grade equipment. Appl Sci. 2018;8(9):1633. https://doi.org/10.3390/app8091633

Borys Adamiak, MEng. – researcher in the Engine Research Department, BOSMAL Automotive Research & Development Institute Ltd.in Bielsko-Biała. Poland.
e-mail: *borys.adamiak@bosmal.com.pl*

Joseph Woodburn, DEng. – researcher in the Engine Research Department, BOSMAL Automotive Research & Development Institute Ltd.in Bielsko-Biała, Poland.
e-mail: *joseph.woodburn@bosmal.com.pl*

Andrzej Szczotka, DEng. – Head of Exhaust Emission Laboratory in the Engine Research Department, BOSMAL Automotive Research & Development Institute Ltd in Bielsko-Biała, Poland.
e-mail: *andrzej.szczotka@bosmal.com.pl*

Prof. Jerzy Merkisz, DSc., DEng. – Faculty of Civil and Transport Engineering, Poznan University of Technology, Poland.
e-mail: *jerzy.merkisz@put.poznan.pl*

Article citation info:
Kęska A, Dziubek M, Michalik D. Market positioning of internal combustion engines and battery electric motors. Combustion Engines. 2023;195(4):136-143. https://doi.org/10.19206/CE-169803

Aleksandra KĘSKA
Mateusz DZIUBEK
Dawid MICHALIK

Combustion Engines
Polish Scientific Society of Combustion Engines

Market positioning of internal combustion engines and battery electric motors

ARTICLE INFO

Received: 30 May 2023
Revised: 18 July 2023
Accepted: 19 July 2023
Available online: 8 August 2023

To examine the current market situation of combustion and battery electric engines in vehicles and to determine the type of strategy for the development of the automotive market, a SWOT analysis was carried out. Internal strengths and weaknesses as well as external opportunities and threats on the market of internal combustion and electric vehicles were assessed. The most important areas of their operation have been designated. A weighting system and a rating scale were selected. The results of the analysis showed that combustion vehicles belong to a conservative market area which promotes the designs that have been thriving for years and maximizes their advantages. Battery electric vehicles belong to an aggressive market area, with the strategy based on a quick response to consumer needs, allowing for the maximization of profits while maintaining innovation. The future of the transport sector will be determined by the focus on the promotion of ecological transport elements.

Key words: *ICEV, BEV, types of vehicle markets, SWOT analysis*

1. Introduction

In February 2023, the governments of many European Union countries announced plans to ban the sale of new vehicles with internal combustion engines from 2030 and plans to sell hybrid electric vehicles (HEV and PHEV) with ICE only until 2035. It was planned that after 2035 only battery electric vehicles (BEVs), equipped with fuel cells and powered by hydrogen, would be allowed for sale. In March, seven EU countries, including Poland, opposed forced electrification. As a consequence, the EU authorities decided to allow the production and sale of ICE vehicles after 2035, provided that the vehicles are powered by environmentally neutral e-fuels or biofuels. However, this does not solve the problem, because the production of ecological fuels is highly energy-intensive and thus uneconomical [25].

99.7% of global transport is powered by ICE and 95% of global transport energy comes from petroleum fuels [8]. Since 2018, there has been a noticeable increase in considerations about the future of internal combustion and electric vehicles in the scientific community. Some argue that ICEs are largely responsible for environmental pollution and consider moving to fully electric mobility (zero emission vehicles – ZEV) a matter of time [4, 19]. On the other hand, some defend the sustainability of ICEs in the market, claiming that their development is the fastest way to reduce the carbon footprint of cars [9, 21]. However, the vast majority of researchers emphasize that a policy focusing solely on BEV vehicles will not be successful because it is not possible from the current technology, material resources and environmental performance point of view. Transport sustainability can only be ensured by improving ICEV efficiency and emissions, as these will drive transport significantly in the medium time perspective [9, 13]. Battery motors can realistically only power light commercial vehicles, cars and vans, which account for around 45% of global transport energy use [8]. The size and weight of the batteries needed for heavy transport, heavy sea freight and aviation would be too large to make full electrification practical, desirable or even possible [8]. A lot of hope is put in a circular economy where battery materials will be recycled. However, recovering critical metals from lithium-ion batteries is extremely difficult and energy-intensive due to their complexity and weight, and therefore these batteries are very unlikely to be recyclable even in the near future [6]. Only partial electrification, as in the case of self-charging hybrid electric vehicles (HEVs) with much smaller batteries and the energy coming from ICEVs but used more efficiently, offers readily available technology that allows for significant reductions in fuel consumption and thus CO2 emissions of petrol engines by about 25%, without the need to create new infrastructure [3]. In fact, HEVs offer a more practical prospect of lowering greenhouse gas emissions than BEVs [1, 18]. In order to avoid ecological and economic catastrophes, batteries must not become the only source of energy in transport. All available technologies, including ICEVs, BEVs, fuel cell vehicles (FCVs) [20], self-charging hybrids, and alternative fuels, should be utilized and continuously advanced to improve the sustainability of transport [18]. For a fair assessment of electrification, a full life cycle analysis of vehicles is needed [16], as the production of electric energy, not vehicle manufacturing, is the main cause of air pollution [5].

However, the development of combustion and electric engines is influenced not only by the knowledge and experience of researchers. It depends on a group of external factors, including legal, social, economic, environmental and logistic conditions. In order to study the current market situation of internal combustion engines and electric motors in motor vehicles, a SWOT analysis (an acronym for Strengths, Weaknesses, Opportunities, Threats) was conducted. The most important areas of operation of combustion and electric vehicles were determined, and a weighting system and a rating scale were developed. The current knowledge was used to determine the type of market strategy for both groups of vehicles.

2. Principles of the analysis

In the SWOT analysis, internal strengths and weaknesses as well as external opportunities and threats in a given market are assessed. Internal analysis is used to identify resources, capabilities, core competencies and competitive advantages. External analysis, on the other hand, identifies market opportunities and threats by analyzing the competitor's resources, the industry and the general environment. When conducting the analysis, the collected information should be divided into four groups (elements of the analysis) [22].

Strengths – the first internal element of the SWOT analysis describing the strengths of a given type of market. Advantage in given aspects covers the areas in which the market functions satisfactorily. The analysis should be conducted considering the microenvironment and macroenvironment. A properly implemented SWOT analysis considers the factors which shape a given market and features that correlate with different aspects of the development.

Weaknesses – the second internal element of the SWOT analysis describing the weaknesses of the operation. The study of weaknesses consists of identifying areas that are economically, technically and socially unsatisfactory. As in the case of strengths, the weaknesses should be analyzed considering the micro- and macro-environment. All activities, regardless of their size and profitability, have weaknesses.

Opportunities – the first external element of the SWOT analysis, which includes all favourable situations in the environment from which a given market can benefit. Diversification, the use of new technologies, market trends and development opportunities are identified as typical opportunities for this analysis.

Threats – the last element of the SWOT analysis covering all external threats to which a given segment is exposed. Regardless of the size of the market, all areas are exposed to threats. Threat examples can include lowering of prices on international markets or deteriorating relations with key customers. The stages of the SWOT analysis are presented in Fig. 1.

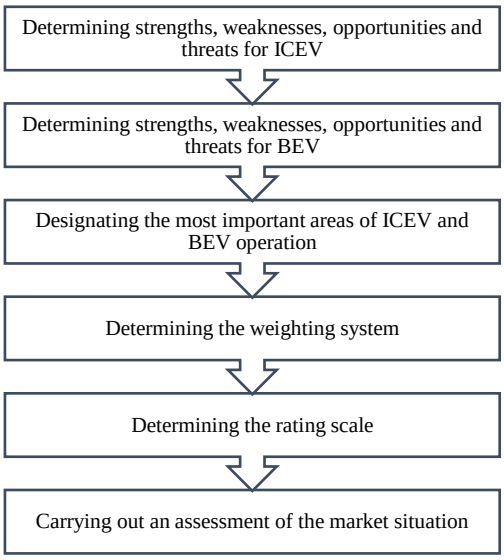

Fig. 1. Stages of SWOT analysis implementation

3. SWOT analysis

The first stage of the SWOT analysis was to identify the factors that may affect the development of the ICEV and BEV market (Table 1 and 2). They were divided respectively into strengths and weaknesses of a given market, presenting opportunities or threats to the development of a given market.

Table 1. SWOT analysis – ICEV

STRENGTHS	WEAKNESSES
1. Relatively low production cost. 2. Many years of experience in the production of ICE. 3. Availability of many types of ICE. 4. Developing industry. 5. The most common type of engines in the world. 6. Developed infrastructure. 7. Long-term improved design of the vehicle for ICE. 8. Common knowledge of engine construction. 9. Being rooted in culture, e.g. racing, rallies. 10. Easy availability of fuel. 11. Short period of filling the fuel tank. 12. Long engine life. 13. Possibility to create hybrid vehicles. 14. Lower initial purchase cost compared to BEV. 15. Known and proven ways of recycling. 16. Component availability.	1. The use phase causes environmental degradation by emitting harmful pollutants. 2. The need to install additional equipment to reduce pollution. 3. The design of the ICE requires many fluids inside the engine for efficient operation. 4. The ICE design needs servicing. 5. Maximum engine efficiency is 37%. 6. Possibility of obtaining energy mainly from hydrocarbons – crude oil. 7. A significant number of moving parts in the ICE. 8. High costs of fuels used. 9. Generating high noise levels. 10. Large size and weight of the ICE. 11. It is one of the factors causing smog in urban areas.
OPPORTUNITIES	THREATS
1. Technological progress. 2. Modernization of existing ICE units. 3. Unwillingness of vehicle users to change the existing paradigms (abandonment of the engines used so far). 4. Improving biofuel technology. 5. The possibility of using synthetic oils. 6. Probability of rejection of EV engines in favour of ICE. 7. Better driving characteristics. 8. Alternative ICE, e.g. hydrogen engines. 9. Versatility of ICE in light, heavy and specialist vehicles. 10. Consumer habits.	1. Limited oil deposits. 2. Political conditions aiming at zero greenhouse gas emissions. 3. The development of alternative forms of propulsion. 4. Users may stop using these devices for environmental reasons 5. Rising oil prices. 6. Growing restrictions in access to city centres. 7. Increase in production costs related to compliance with environmental standards. 8. Assumptions of sustainable mobility.

The analysis for combustion engines shows the advantage of strengths over weaknesses and opportunities over threats. The practical advantages of using internal combustion engines in vehicles are primarily the short time needed for refueling and the developed infrastructure. During longer journeys, the driver does not need to set the exact route. Petrol stations are widely available. Combustion engines are the most popular type of vehicle propelling devices. Currently, there are over 1.1 billion vehicles equipped with internal combustion engines [15]. This contributes to creating an environment ready for transformation. An important aspect in the scope of ICE is the product life cycle. Combustion cars have much more modern and extensive forms of recycling. Many parts are reused. In addition, the number of disposal points available is high. From the user's point of view, the operating time is an important element. Combustion engines have a long service life. Its average period is from 300 to 350 thousand kilometers.

The disadvantages of ICEVs are the high emission of pollutants during operation. The level of generating harmful substances causes non-compliance with the plans developed by the European Union in the field of zero-emission economy. This factor is decisive and has a strong impact on other areas of ICEV development. Due to the need to adapt to legal requirements, activities aimed at developing low-emission technologies are a necessary element. Nevertheless, currently used filters can negatively affect the drive unit, thus shortening its life. Adapting to EU standards requires improving individual components. All the indicated factors correlate with the high cost of purchasing ICEV. Combustion engines have a low maximum efficiency of 37%. As a result, more than half of the energy is wasted and not used for work purposes. Another aspect is the process of obtaining energy exclusively from fossil fuels. This feature prevents the production of its "pure" counterpart. Rising oil prices are transferred to end users who, in order to use vehicles, have to pay higher and higher prices for petrol and diesel fuel.

The developing automotive industry is considered the main opportunity for ICEV. The possibilities of its development correlate with the high probability of minimizing pollutant emissions for the discussed category of devices. Reducing the level of generated harmful substances will allow the use of internal combustion vehicles without a significant impact on the environment. Another important feature is the attitude of consumers towards switching to alternative forms of propulsion. User reluctance may be a decisive factor in the dominance of the ICEV market. Profit maximization is a basic element of the functioning of production enterprises. The demand in the analyzed segment can be monetized by entities with a leading position. Another factor identified in the area of opportunities is the possibility of developing alternative internal combustion engines. The use of internal combustion engines is also a very important aspect. Specialty machines and tractor units would require a radical change. The distance covered by the BEV currently prevents the installation of such solutions in trucks.

Among the potential threats to the development of ICEV may be primarily restrictions related to the availability of crude oil. Non-renewable resources are characterized by limited availability. At the current rate of oil use, it can be expected that the deposits will be exhausted in about 50 years [17]. This will result in the resignation from the solutions used so far. In addition, the European Union plans that by the end of 2050 the member states will achieve zero emissions [23].

Table 2. SWOT analysis – BEV

STRENGTHS	WEAKNESSES
1. High engine efficiency up to 85%. 2. During operation, the engine does not emit harmful pollutants. 3. Lack of engine fluids, e.g. engine oils. 4. Less frequent failures of the drive unit. 5. Less failure-sensitive gearbox. 6. Amenities in cities, such as parking lots, bus lanes. 7. Co-financing for the purchase. 8. Possibility of charging the BEV by using a household socket. 9. Rapid technological development. 10. Ability to obtain energy from many sources. 11. Energy is produced externally and the vehicle only stores and converts it into work. 12. It does not emit noise while driving. 13. Low cost of using and servicing the vehicle. 14. Power available throughout the rev range. 15. BEVs raise public awareness on environmental protection. 16. In urban conditions, it allows the recovery of a significant part of energy through recuperation.	1. High purchase cost. 2. Use of rare earth elements such as lithium or cobalt. 3. Long charging time. 4. Poorly developed charging station infrastructure. 5. The need to plan long routes due to "black spots" on the map. 6. Lack of proper recycling and reuse technology. 7. Weaker driveability. 8. The production stage emits significant amounts of harmful substances. 9. Usage gradually reduces the maximum capacity of the battery. 10. Sensitivity to cold. 11. The battery condition should be kept between 20 - 80% of the battery. 12. High production cost.
OPPORTUNITIES	THREATS
1. Dynamic development of the BEV market. 2. Increasing demand for electric cars. 3. Political orientation regarding the concept of sustainable mobility. 4. Implementation of new technologies. 5. Social pro-ecological awareness. 6. Minimization of purchase costs. 7. Manufacturers' declarations on the transition/development of EV technology. 8. The growing trend for electric vehicles. 9. Depleting oil resources.	1. Limited resources of rare earth elements. 2. Alternative forms of drive. 3. Difficulties in driving heavy and specialized vehicles (tractors or giant trucks). 4. ICE development. 5. Poorly developing infrastructure, in particular in low and medium developed countries. 6. Environmental performance depends on the energy supply structure of a given country.

The introduction of a ban on the use of internal combustion engines is one of the possible steps of the implemented policy. The ecological awareness of the society is also improving. From year to year, more and more people declare their willingness to change the form of propulsion to a more ecological one. Problems with accessibility to city centers are currently being observed. The cities of Hamburg and Stuttgart prohibit diesel vehicles [2].

The analysis carried out for electric vehicles allows to identify the dominance of the advantages of BEV vehicles over their disadvantages. Opportunities and threats, however, are on a similar level. The lack of pollutant emissions during vehicle operation is the most important strength of this category of vehicles in the context of environmental performance. This element is conditioned by the design of the car. Zero-emission vehicles are environmentally friendly when they operate. Another argument is the high efficiency of the electric engine compared to its combustion equivalent. In BEV vehicles, the engine efficiency can be as high as 85%. This translates into the level of efficiency of using the stored energy. The development of electromobility is supported by the activities of some countries regarding the co-financing of the purchase of electric vehicles. This contributes to minimizing the real costs of purchasing an electric vehicle. In Poland, the value of the subsidy may be up to EUR 4000. For comparison, in Western countries, i.e. Italy and France, the subsidy amount is EUR 6000 [12]. An important aspect is also the introduction of tax reliefs on the acquisition of BEVs. For example, some units are completely exempt from excise duty, and for the purchase of a BEV, the company can introduce almost twice as much into the business costs as compared to the purchase of a combustion vehicle. Another important factor is the versatility of the utilized energy. BEVs can draw energy entirely from renewable sources. The last important aspect is the low cost of using and servicing the vehicle. BEVs are characterized by lower repair prices than standard ICE vehicles. In addition, the price of electricity is lower than that of the liquid fuels. Assuming that the BEV will be charged at home with energy produced by installed solar panels, the energy needed to power the device may be cost-free.

Battery charging time is a significant weakness of the electric vehicles. The limited length of the power supply period is a discouraging factor for a potential group of buyers. In addition, when traveling long distances, the BEV user must take into account the charging period of the used car in the route planning process. The low level of expansion of the charging infrastructure limits the technical capabilities of electric cars. Many of the currently available points offer the users free charging. Expanding the charging infrastructure may be significantly more difficult in Eastern countries. In these regions, the availability of the number of charging points is significantly lower than in Western countries, for example Germany. Another negative feature of electric vehicles is the need to use rare earth resources. This raises questions about the actual environmental performance of BEVs. During the production of the battery, necessary for the operation of the vehicle, a significant amount of pollutants is emitted, causing degradation of the natural environment. The areas of recycling and disposal are also a barrier due to the lack of technologies enabling the recovery of elements. We should also remember about lithium greases used in BEV and HEV, for which alternative solutions should also be sought.

The dynamic development of the BEV market is the most important factor regarding possible opportunities. In recent years, the market has seen an increase of interest in BEV and a focus on expanding the existing infrastructure. These factors are an important component that contributes to achieving the goals of the Green Deal. The next chance is the legal regulations that favour the development of the electric car market. The phenomenon of globalization contributes to the increase of ecological awareness of the society. In this aspect, BEVs have an advantage over the competition being zero-emission vehicles. Over the years, one can also observe a change in the directions of activities of the leaders of the automotive industry. They focus on developing solutions based solely on electric motors. In addition, due to further EU concepts, there is a high probability of a forced departure from internal combustion engines. Depleting oil reserves are the main reason for the electrification of the automotive industry.

Depleting lithium and cobalt resources are the most important threats to the BEV market. The process of obtaining rare earth elements is characterized by complexity. Additionally, the amount of extraction of lithium and cobalt deposits is relatively low compared to other elements. Technical limitations of electric vehicles are among the factors threatening the development of BEVs. The need for high power, as in the case of trucks, can limit the use of electric engines. Increasing power is associated with the need to store more energy. Infrastructure is also a problematic area. The limited number and difficult accessibility of charging stations discourage potential consumers. In addition, in countries where energy is mainly obtained from fossil fuels, the environmental performance of vehicles with an electric engine decreases significantly.

The next stage of the analysis included the selection of the most important factors from among the strengths and weaknesses as well as opportunities and threats for ICEV and BEV. All factors were selected based on the most important areas related to infrastructure, technical aspects and environmental conditions. Then, the values of the weights (in the form of decimal fractions) were determined along with the determination of the level of importance of strengths and weaknesses as well as opportunities and threats in the development of the combustion and battery electric vehicle market (Table 3). The sum of the weights of the five selected factors for each element of the SWOT analysis must equal 1. In addition, a five-point rating scale was determined (Table 4), thanks to which it was possible to determine the impact of a given factor on the development of a given market [14]. A higher rating for strengths and opportunities is related to the positive impact of a given factor on the development of the combustion or electric engine vehicle market. A low rating for weaknesses and threats indicates a negative impact on the market. Tables 5–8 list the analyzed factors and calculated a weighted score for each of them.

Table 3. The SWOT analysis weight system

Weight	The level of importance of the factor in the development of a given market
0.1	Low
0.2	Medium
0.3	High

Table 4. The SWOT analysis rating scale

Rating	The strength of the factor's impact on the development of a given market
1	Very low
2	Low
3	Medium
4	High
5	Very high

Table 5. Weighted rating of strengths and weaknesses – ICEV

Strengths	Weight	Rating	Weighted rating	Weaknesses	Weight	Rating	Weighted rating
Well-developed infrastructure	0.3	4	1.2	The operation of the vehicle causes the emission of harmful pollutants	0.3	5	1.5
Long engine life	0.1	4	0.4	The need to install additional equipment to reduce pollution	0.3	4	1.2
The prevalence and availability of fuel	0.2	5	1	Maximum engine efficiency is 37%	0.1	1	0.1
The most common type of engine in the world	0.3	3	0.9	Possibility of obtaining energy mainly from hydrocarbons	0.1	2	0.2
Known and proven ways to recycle internal combustion vehicles	0.1	4	0.4	High costs of fuels used	0.2	2	0.4
Sum	1	–	3.9	Sum	1	–	3.4

Table 6. Weighted rating of opportunities and threats – ICEV

Opportunities	Weight	Rating	Weighted rating	Threats	Weight	Rating	Weighted rating
Unwillingness of vehicle users to change the existing paradigms (abandonment of the engines used so far)	0.3	3	0.9	Limited oil resources	0.2	4	0.8
Technological progress	0.3	4	1.2	Political conditions aiming at zero green-house gas emissions	0.3	5	1.5
Alternative combustion engines, e.g. hydrogen	0.1	3	0.3	Users may stop using electric vehicles for environmental reasons	0.1	3	0.3
Versatility of combustion engine applications in light, heavy and specialist vehicles	0.1	2	0.2	Increasing restrictions on access to city centers	0.1	3	0.3
Modernization of existing ICEVs	0.2	3	0.6	Increase in production costs related to compliance with environmental standards	0.3	3	0.9
Sum	1	–	3.2	Sum	1	–	3.8

Table 7. Weighted rating of strengths and weaknesses – BEV

Strengths	Weight	Rating	Weighted rating	Weaknesses	Weight	Rating	Weighted rating
No emission of harmful pollutants during operation	0.3	5	1.5	The use of rare earth elements, for exampl lithium or cobalt	0.2	3	0.6
Financial allowance for purchase	0.3	4	1.2	Long charging time	0.3	5	1.2
Ability to obtain energy from many sources	0.1	3	0.3	Poorly developed charging station infra-structure	0.3	4	0.8
Low cost of using and servicing the vehicle	0.2	1	0.2	Lack of proper recycling and reuse tech-nology	0.1	2	0.2
High engine efficiency up to 85%	0.1	2	0.2	The production stage emits significant amounts of harmful substances	0.1	2	0.4
Sum	1	–	3.4	Sum	1	–	3.2

Table 8. Weighted rating of opportunities and threats – BEV

Opportunities	Weight	Rating	Weighted rating	Threats	Weight	Rating	Weighted rating
Dynamic development of the BEV market	0.2	4	0.8	Limited resources of rare earth elements	0.4	3	0.6
Political conditions focused on ecology	0.3	5	1.5	Difficulties in driving heavy and special-ized vehicles (tractors and trucks)	0.2	2	0.4
Social pro-ecological awareness	0.2	3	0.6	ICE development	0.1	2	0.2
Manufacturers' declarations on transition/development of BEV technology	0.2	4	0.8	Poorly developed infrastructure, in particular in low and medium developed countries	0.2	3	0.6
Decreasing oil deposits	0.1	3	0.3	Environmental performance depends on the energy structure of a given country	0.3	5	1.5
Sum	1	–	4	Sum	1	–	3.3

4. SWOT analysis results

The analysis of the main factors influencing the market situation provided four different results for each of the discussed markets (Fig. 2 and 3). On this basis, a strategy upon the development of the ICEV and BEV markets is based was selected. The SWOT analysis distinguishes four development strategies: aggressive, conservative, competitive and defensive. If, after analyzing the results, strengths and opportunities prevail, we can be tempted to choose an aggressive strategy. It should focus on the advantages of the market and use them through strong expansion. If it turns out that strengths are the most important, but at the same time there are a lot of threats in the environment, we should choose a conservative strategy. In this case, the market will try to overcome threats using its strongest internal features. On the other hand, when we see the dominant share of weakness on the market, and at the same time there are clear opportunities outside, a competitive strategy may turn out to be the best. This means that a given market should focus on eliminating internal weaknesses in such a way as to make better use of the opportunities of the environment in the future. The last strategy - defensive - will be the best choice if we have the dominant share of weakness, and at the same time there are a lot of threats in the environment in which the market operates. When choosing it, the market focuses mainly on activities that will ensure the possibility of survival.

Fig. 2. ICEV market rating

The activity of entities using the construction of vehicles equipped with internal combustion engines is related to the established position in the automotive industry and the advantage of this type of equipment (high efficiency, low production costs). In the case of BEV, the current market depends mainly on the potential opportunities to be seized. The market assessment of ICEV is diversified depending on the considered factor. The advantages that characterize the market today show a high value of 3.9 points. What is important, however, is the threat level, which is as high as 4 points. Such a high value may indicate problems for ICEV in the future. The prospects for change are relatively low at 3.2 points. The average value of defects is 3.4 points. The ICEV market currently holds the leading position. However, the progressive threats it may face contribute to significant changes in the production and operation of ICEV.

Fig. 3. BEV market rating

In the case of electric cars, the market is shaped by seized opportunities. The value of potential opportunities is as high as 4 points. The global trend for pro-ecological activities favours zero-emission vehicles. The concept of BEV creation was developed in response to the high level of environmental pollution caused by internal combustion engines. The number of risks and disadvantages are relatively low. They are respectively 3.2 and 3.3 points. Dangers and defects mainly focus on problems related to the infrastructure and the loading process. Improving technology means that in the perspective of several years these values may decrease. The advantages of an electric vehicle on a point scale are 3.4 points. The current market and stages of BEV evolution allow predictions related to the dynamization of the growth of their advantages.

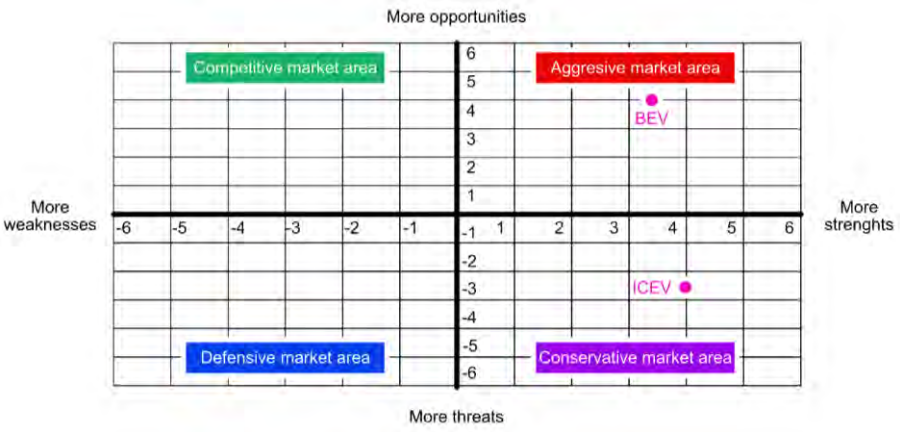

Fig. 4. Market positioning of ICEVs and BEVs

The choice of strategy is conditioned by the relationships between advantages and disadvantages as well as opportunities and threats. Figure 4 shows the types of strategies currently followed by the ICEV and BEV markets.

The market of internal combustion engine vehicles is conservative. The activities of this market are focused on generating profit from a long-term, thriving structure. The market does not show radical changes, it is stable. This effect is visible in the form of relatively stable stock quotations of concerns such as General Motors or Mercedes Benz Group AG. Capital preservation is more important here than growth or market returns. Market threats are eliminated by maximizing the use of internal strengths.

The aggressive market area that characterizes the electric vehicle market means that it is dominated by its opportunities. In addition, internal strengths are supported. It is a strategy of strong expansion and development. The marketing strategy is based on a quick response to consumer needs, which allows for maximizing profits while maintaining innovation. An aggressive strategy includes activities such as: capturing opportunities, striving to strengthen the market position and concentration of resources on competitive products. Examples of aggressive behavior of the electric vehicle market can be observed by intensifying media interest, e.g. launching the first electric car into space [10], creating stylistically unique structures (Tesla cybertruck) [7] or creating BEVs as ecological vehicles [11].

5. Conclusions

The conducted SWOT analysis allowed to identify the strengths and weaknesses of internal combustion and electric engines. The designated market areas show the current situation of ICEVs and BEVs. Electric vehicles are characterized by a rapid growth of development based on pro-ecological aspects. Conventional drives, on the other hand, use existing and prospering structures to maximize their advantages.

It is certain that in the next decade the automotive industry will develop more than in the previous century. Adapting to the current era of electromobility requires the introduction of zero-emission cars on the roads. However, caution should be exercised when identifying a single solution (BEV) as the best way to achieve the principles of sustainable development [24]. Energy policy certainly needs to be based on much greater realism, fairness and appreciation of broader global development, economic and environmental needs. It is essential to continue the research and development of all technologies that provide the world with energy, including the combustion of fossil fuels, in particular in internal combustion engines.

Nomenclature

BEV	battery electric vehicle
HEV	hybrid electric vehicle
ICE	internal combustion engine
ICEV	internal combustion engine vehicle
PHEV	plug-in hybrid electric vehicle
SWOT	strengths, weaknesses, opportunities, threats

Bibliography

[1] Abdul-Manan AFN, Gordillo Zavaleta V, Agarwal AK, Kalghatgi G, Amer AA. Electrifying passenger road transport in India requires near-term electricity grid decarbonisation. Nat Commun. 2022;13(1):2095. https://doi.org/10.1038/s41467-022-29620-x

[2] Arning K, Ziefle M. Defenders of diesel: anti-decarbonisation efforts and the pro-diesel protest movement in Germany. Energy Res Soc Sci. 2020;63:101410. https://doi.org/10.1016/j.erss.2019.101410

[3] Borkowski A, Zawiślak M. Comparative analysis of the life-cycle emissions of carbon dioxide emitted by battery electric vehicles using various energy mixes and vehicles with ICE. Combustion Engines. 2023;192(1):3-10. https://doi.org/10.19206/CE-147159

[4] Cho J, Song HH. Understanding the effect of inhomogeneous fuel–air mixing on knocking characteristics of various ethanol reference fuels with RON 100 using rapid compression machine. P Combust Inst. 2019;37(4):4911-4919. https://doi.org/10.1016/j.proci.2018.07.062

[5] Duarte Souza Alvarenga Santos N, Rückert Roso V, Teixeira Malaquias AC, Coelho Baêta JG. Internal combustion engines and biofuels: examining why this robust combination should not be ignored for future sustainable transportation. Renew Sust Energ Rev. 2021;148:111292. https://doi.org/10.1016/j.rser.2021.111292

[6] Herrington R. Mining our green future. Nat Rev Mater. 2021;6:456-458. https://doi.org/10.1038/s41578-021-00325-9

[7] Hortelano-Capetillo JG, Martínez-Vázquez JM, Baños-Lopez E, Alfaro-Ayala JA. Drag and lift force analysis for the cybertruck Tesla vehicle. Revista de Ingeniería Tecnológica. 2021;30;9-16. https://doi.org/10.35429/JTEN.2021.15.5.9.16

[8] Kalghatgi G. Is it really the end of internal combustion engines and petroleum in transport? Appl Energ. 2018;225: 965-974. https://doi.org/10.1016/j.apenergy.2018.05.076

[9] Kalghatgi G. Development of fuel/engine systems – the way forward to sustainable transport. Engineering. 2019;5(3): 510-518. https://doi.org/10.1016/j.eng.2019.01.009

[10] Kalinowska M. Tesla as an impulsive motor of future transport (in Polish). Journal of TransLogistics. 2017;3(2).

[11] Khatua A, Ranjan Kumar R, Kumar De S. Institutional enablers of electric vehicle market: Evidence from 30 countries. Transp Res Part A Policy Pract. 2023;170:103612. https://doi.org/10.1016/j.tra.2023.103612

[12] Kowalska-Pyzalska A, Kott J, Kott M. Why Polish market of alternative fuel vehicles (AFVs) is the smallest in Europe? SWOT analysis of opportunities and threats. Renew Sust Energ Rev. 2020;133:110076. https://doi.org/10.1016/j.rser.2020.11007

[13] Leach F, Kalghatgi G, Stone R, Miles P. The scope for improving the efficiency and environmental impact of internal combustion engines. Transport Eng. 2020;1:100005. https://doi.org/10.1016/j.treng.2020.100005

[14] Leigh D. SWOT Analysis. Handbook of Improving Performance in the Workplace. John Wiley & Sons, Inc. New York. 2010:115-140. https://doi.org/10.1002/9780470592663.ch24

[15] Orliński P, Gis M, Bednarski M, Novak N, Samoilenko D, Prokhorenko A. The legitimacy of using hybrid vehicles in urban conditions in relation to empirical studies in the WLTC cycle. Journal of Machine Construction and Maintenance. 2019;1:25-30.
[16] Regulski P. The material and economic assessment of the life cycle of city buses in the operational phase. Combustion Engines. 2023;192(1):50-54. https://doi.org/10.19206/CE-151942
[17] Roberts G, Barbier E, van 't Veld K. Global emissions from crude oil: The effect of oil-deposit heterogeneity. Energ Policy. 2019;132:654-664. https://doi.org/10.1016/j.enpol.2019.06.008
[18] Senecal K, Leach F. Racing Toward Zero: The Untold Story of Driving Green. SAE International; 2021.
[19] Shaheen S, Martin E, Totte H. Zero-emission vehicle exposure within U.S. carsharing fleets and impacts on sentiment toward electric-drive vehicles. Transp Policy (Oxf). 2020; 85:A23-32. https://doi.org/10.1016/j.tranpol.2019.09.008
[20] Teoh YH, How HG, Le TD, Nguyen HT, Loo DL, Rashid T et al. A review on production and implementation of hydrogen as a green fuel in internal combustion engines. Fuel. 2023;333:126525. https://doi.org/10.1016/j.fuel.2022.126525
[21] Towoju OA, Ishola FA. A case for the internal combustion engine powered vehicle. Energy Reports. 2020;6:315-321. https://doi.org/10.1016/j.egyr.2019.11.082
[22] Tylińska B. SWOT analysis as an instrument in development planning (in Polish). WSiP. Warsaw 2005.
[23] Vieira LC, Longo M, Mura M. Are the European manufacturing and energy sectors on track for achieving net-zero emissions in 2050? An empirical analysis. Energ Policy. 2021;156:112464. https://doi.org/10.1016/j.enpol.2021.112464
[24] Wanitschke A, Hoffmann S. Are battery electric vehicles the future? An uncertainty comparison with hydrogen and combustion engines. Environ Innov Soc Transit. 2020;35:509-523. https://doi.org/10.1016/j.eist.2019.03.003
[25] Website: Euronews.green, EU 2035 petrol and diesel car ban: Germany reaches deal on synthetic fuels. https://www.euronews.com/green/2023/03/22/eu-to-ban-petrol-and-diesel-cars-by-2035-heres-why-some-countries-are-pushing-back

Aleksandra Kęska, DEng. – Faculty of Mechanical Engineering, Wroclaw University of Science and Technology, Poland.
e-mail: *aleksandra.keska@pwr.edu.pl*

Mateusz Dziubek, MEng. – Faculty of Mechanical Engineering, Wroclaw University of Science and Technology, Poland.
e-mail: *mateusz.dziubek@pwr.edu.pl*

Dawid Michalik, MEng. – Faculty of Mechanical Engineering, Wroclaw University of Science and Technology, Poland.
e-mail: *gadaki198@gmail.com*

Article citation info:
Bieniek A, Graba M, Mamala J, Augustynowicz A, Szczepanek M. Analysis of passenger car powertrain system measurements in road conditions. Combustion Engines. 2023;195(4):144-151. https://doi.org/10.19206/CE-170207

Andrzej BIENIEK
Mariusz GRABA
Jarosław MAMALA
Andrzej AUGUSTYNOWICZ
Michał SZCZEPANEK

Combustion Engines
Polish Scientific Society of Combustion Engines

Analysis of passenger car powertrain system measurements in road conditions

ARTICLE INFO

Received: 2 June 2023
Revised: 31 July 2023
Accepted: 31 July 2023
Available online: 19 August 2023

The paper is focused on presenting a methodology for measuring power and torque based on diagnostic equipment available in most diagnostic workshops, such as OBD interfaces or the CAN Bus on-board data transmission network, under real-world road conditions. The publication presents an algorithm for calculating the powertrain's torque and power based on measurements of changes in vehicle speed or acceleration recording during a two-phase road test. The results presented, based on the method described, apply to both the internal combustion and electric vehicle. Common powertrain operating parameters, such as maximum power, maximum torque and the powertrain's flexibility parameters described in the literature, are proposed for the final evaluation of the vehicle's traction system.

Key words: *power and torque measurement, drive system, powertrain, road conditions, electric drive*

1. Introduction

Recently, there has been a definite increase in the market share of hybrid and electric drives [2]. However, regardless of the vehicle's powertrain, the issues of its diagnostics and verification of whether its current operating parameters correspond to the original designers' assumptions remain. The powertrain's operating parameters are linked to the vehicle's dynamic properties [11, 15] and often determine the choice of a particular vehicle. Modern powertrains generate higher torques than units produced a decade earlier, and the drive system's operation is controlled by sophisticated control systems. If their operation is disrupted, for example by faulty sensor readings, the disruption causes a reduction in the powertrain's torque and power, but often also results in an uncontrolled increase in environmental emissions [12, 16]. The powertrain's related malfunction is then recorded as a fault in the OBD network [13]. Once the fault has been removed, not only should a repeated diagnosis be carried out to verify the repairs under workshop conditions, but, more importantly, a test drive should be carried out in real-world road conditions by qualified workshop personnel.–In such conditions, it is possible to check the available sensors' readings using a diagnostic device to make sure they correspond to the set values. However, all diagnostic tests are carried out without any load on the powertrain, corresponding to real-world driving conditions. Only a check of the powertrain's parameters and operating parameters under load gives true information about its technical condition. The reason for this is the lack of appropriate workshop equipment, such as a chassis dynamometer. Such a dynamometer also requires the preparation of proper technical infrastructure and the employment of staff suitably trained to operate it. Hence, dynamometers are often reserved for workshops specialising in the optimisation and verification of the operating parameters of sports vehicle powertrains.

Nevertheless, most mechanical workshops verify the repairs by performing a test drive under real-world road conditions, during which an acceleration test is carried out to subjectively assess the correct functioning of the drive system and other components. The acceleration test is a process of vehicle acceleration from a standstill to a preset target speed using specific transmission gear ratios. It is also possible to carry out a so-called flexibility test [19]. The flexibility test can be perceived as the process of vehicle acceleration while driving in one selected gear. In both cases, the proper implementation of such a defined acceleration process most often requires the powertrain's power supply control equipment to be set to full power. In the case of manual transmission and acceleration through gears, the ratio must be changed at a strictly defined speed that characterises the powertrain's operation. In this case, the outcome of the acceleration process is assessed subjectively and depends on the experience of the workshop personnel performing the test. Its assessment is mainly based on the feeling of the vehicle's acceleration dynamics, i.e. the increase in speed over time. The assessment is less frequently done by measuring the acceleration time to reach the target speed or the time needed to travel a certain distance [4]. Time is a measurable index, but it does not directly determine the drive system's operating parameters and has no direct reference to its external characteristics. A fundamental question can then be formulated: Is it possible to assess the correctness of a powertrain's repairs under road test conditions with the common diagnostic equipment used in workshops? At the same time, can the powertrain's basic operating parameters in the form of power, torque and flexibility be determined? In this respect, the authors of this elaboration carried out comparative measurements of the operating parameters in a passenger vehicle's internal combustion and electric drive system during a road test using a workshop diagnostic device.

2. Operating parameters and the powertrain's flexibility

Carrying out the acceleration test at full intensity in a road test, especially within a single gear, is an example of loading a vehicle's drive system, not only by the basic

forces of rolling drag and aerodynamic drag, but also by the load associated with mass inertia in progressive motion and the inertia of rotating components [17]. The inertia force counteracts the vehicle's acceleration process and its value is directly proportional to the product of the vehicle's mass and the resulting acceleration. The vehicle's mass is constant and the greater the acceleration, the higher the inertia force. The inertia force is the apparent force that maintains the power balance in the drive system (1).

$$N_n = N_{op} \tag{1}$$

where:

$$N_n = F_n \cdot v \tag{2}$$

$$N_{op} = (F_t + F_p + F_i) \cdot v \tag{3}$$

where: N_n – traction power, kW; N_{op}– motion drag, kW; F_n – driving force, kN; v – vehicle speed, m/s; F_t – rolling drag, kN; F_p – air resistance, kN; F_i – inertia force, kN.

Such a test involves using all available power in the drive system to accelerate the vehicle at maximum intensity. In such a test, the vehicle mass is accelerated in a progressive motion and rotating masses are accelerated, while the increase in the vehicle's speed is a measure of the power applied to the vehicle's driven wheels. Full acceleration intensity allows the powertrain to operate on an external speed characteristic curve which can be used to determine interesting powertrain operating parameters, such as power and torque as a function of drive shaft speed. Detailed analysis allows for assessing the vehicle's traction properties and determining the drive system's flexibility field. The powertrain's flexibility is the ability to change its load as represented by the torque waveform between the values of the drive shaft speed at maximum torque (n_{Mmax}) and maximum power (n_{Nmax}). This property is expressed by the torque and speed flexibility index and is widely described in the literature [14, 17] as the powertrain's shaft speed flexibility:

$$e_n = \frac{n_{N_{max}}}{n_{M_{max}}} \tag{4}$$

and torque flexibility

$$e_M = \frac{M_{max}}{M_{Nmax}} \tag{5}$$

where: $n_{N_{max}}$ – speed at maximum power, rpm; $n_{M_{max}}$ – speed at maximum torque, rpm; M_{max} – maximum torque, Nm; M_{Nmax} – torque at the powertrain's maximum power, Nm.

On other hand, total flexibility was written down as:

$$e_c = e_n \cdot e_M \tag{6}$$

The flexibility coefficients of many modern powertrains depend on the external torque and power curves in the speed characteristics and the possible interoperation between the powertrains used (Fig. 1).

The rapid development of powertrains, and in particular their hybridisation, is changing their flexibility and even enabling vehicle manufacturers to shape it through appropriate control of the individual power units interoperating in a given drive system. The combination of an internal combustion engine and an electric engine that interoperate in a single drive system is also an answer to the challenge faced by the automotive industry in the modern world. On the one hand, it reduces emissions of pollutants into the environment and, on the other hand, allows the power in the drive system to be shaped accordingly. Determining the powertrain's flexibility and, therefore, the power's and torque's flexibility in the drive system by means of a road test is possible for any configured passenger vehicle drive system. The determination of these parameters requires carrying out a test involving vehicle acceleration from a pre-set initial speed to the target speed with a fixed drive system transmission ratio. Hence, such a test can be performed under real-world road conditions during a test drive. However, the element essential to ensure the test's correctness is to read the data at a frequency that allows the dynamics of the vehicle's speed changes to be identified. The time required to reach the target speed (not necessarily the maximum speed) enables the tested powertrain's operation to be assessed. It is therefore, possible to monitor in detail the acceleration's waveform and its instantaneous declines in value. The results of speed changes recorded only during the acceleration process are insufficient to determine the powertrain's operating parameters due to the losses occurring in the drive system. This depends on the transmission's type, the mass inertia in the drive system, the losses from the vehicle's turning wheels and the impact of atmospheric conditions on the vehicle. The test is therefore complemented with an idle run from the end speed to the flexibility test's starting speed.

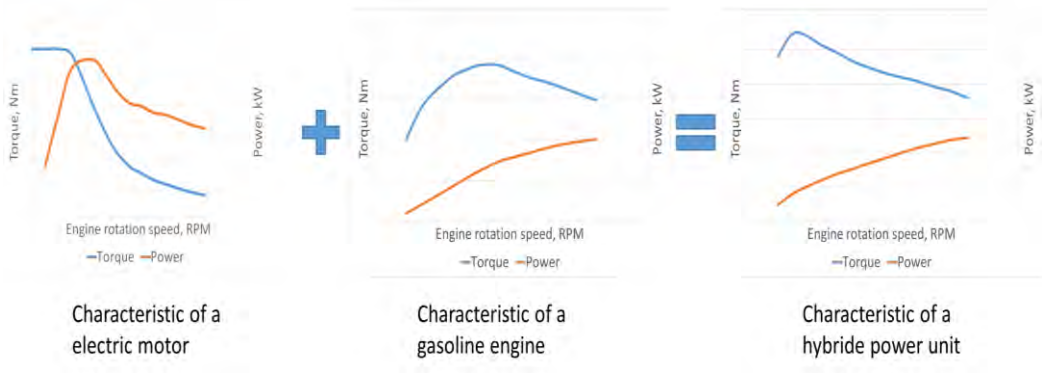

Fig. 1. External characteristics of various powertrains in passenger cars

As demonstrated by the authors of [6, 10], a two-phase road test allows for the compensation of the vehicle's motion drag, mass inertia (and masses in rotary motion) in the powertrain and the impact of environmental conditions on the powertrain's determined operating parameters and flexibility. At the same time, it is recommended that the flexibility test in the road test be carried out on a road section with a constant slope. Measurement sections based on a flat horizontal road surface enable obtaining repeatable and reliable results.

3. Measurements of operating parameters in the road test

A number of measuring devices are used in the measurement methods intended for determining the powertrain's operating parameters and flexibility in the proposed two-phase acceleration and idle run test. These devices allow changes in the vehicle's speed, and consequently changes in its acceleration to be measured by direct and indirect methods. The direct methods include measuring the vehicle's longitudinal acceleration using an accelerometer attached directly to its body. In this context, it is not only the recording of the changes in acceleration over time that is important, but also the accelerometer's mounting position and method, the sampling frequency, the road surface's condition, the centre of gravity or the vehicle's suspension system. The effects of the above-mentioned factors on the recorded acceleration require the development of a suitable calculation algorithm related to the change in the measuring axes' orientation relative to the road in the X-Z plane due to the change in the vehicle suspension's deflection during acceleration and idle run.

The application of indirect methods to measure acceleration requires using specialised measuring equipment. Very good results for measuring the vehicle's speed and then calculating the acceleration can be obtained by using the Peiseler 5th wheel, Correvit optical head, radar or GPS devices, by measuring the vehicle's wheel speed or using information from the OBD network [3, 18]. All these methods show varying accuracy in terms of speed measurement, which often depends on the device's sophistication and price.

4. Research methodology

4.1. Test objects

The flexibility test was carried out with the use of two test vehicles, i.e. passenger vehicles, the basic technical data of which are presented in Table 1. The Audi vehicle was equipped with an internal combustion engine (ICE), while the Renault Zoe was powered by an electric engine (full BEV – Battery Electric Vehicle).

The flexibility test in the road test was carried out on a closed road section of 4 km, with a constant road slope close to zero and a good road surface. The ambient temperature was 15–19^{o}C, atmospheric pressure amounted to 1014 hPa, while wind speed was 1.67 m/s, and its direction was perpendicular to the test road.

Table 1. Basic parameters of test objects

	Parameter	Unit	AUDI A4 B6	Renault ZOE
1.	Maximum power	kW	96	68
2.	Speed at max power	rpm	4000	8000
3.	Maximum torque	Nm	310	210
4.	Speed at max torque	rpm	1900	0
5.	Vehicle mass during test	kg	1705	1725
6.	Wheel size	–	235/40 R18	195/55 R16
7.	Main transmission ratio	–	3.444	-
8.	3/4 gear ratio	–	1.360/ 0.903	-
9.	Total gear ratio	–	4.683/ 3.110	9.300
10.	Torque flexibility	–	1.240	2.58
11.	Crankshaft speed flexibility	–	2.110	∞
12.	Total flexibility	–	2.616	∞

4.2. Measurement equipment

The study utilised a two-phase test to determine the operating parameters of two different passenger vehicle drive systems using workshop diagnostic equipment. A diagnostic device intended for reading data from the OBD network and an interface for reading parameters from the CAN BUS on-board data transmission network were used in the tests. The proposed two-phase test was used for both measuring devices and was carried out at a constant drive system ratio.

The research was carried out during road tests, involving recording the powertrain's operating parameters with a diagnostic device which enabled saving the data in a data file. Once connected to the on-board diagnostic network via the OBD socket and logged into the measured value block, selected parameters of the tested powertrain, such as time, engine crankshaft speed and vehicle speed during the test, can be recorded. A complication of this measurement method is the need to develop a measurement algorithm to determine the powertrain's operating parameters from the obtained measurement data [8], obtained, for example, with the use of the inertia method [1, 9] or the load method [5, 7]. An interface for reading the parameters from the CAN BUS on-board data transmission network can also be used to measure the powertrain's operating parameters. The interface also allows for recording many other parameters.

4.3. Two-phase test method for determining the powertrain's operating parameters

The two-phase road test method is based on carrying a run-in and idle run during a single measurement (Fig. 2). An important rule is to carry out the acceleration at full intensity with a constant ratio in the transmission that does prevents the driving force limit to be exceeded (prevents wheel slip) under the prevailing road conditions, taking into account the driven wheels' traction. Irrespective of the measuring device used, exceeding the driving force limit has an adverse effect on the accuracy of the measurement of the powertrain's operating parameters or even makes this measurement impossible.

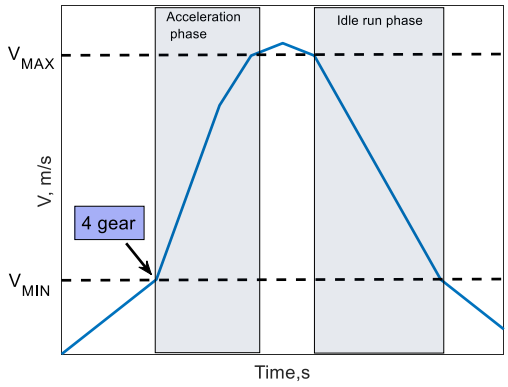

Fig. 2. Speed profile in the flexibility test

During acceleration, it is necessary to measure such parameters as time, vehicle speed or acceleration. These parameters are needed to determine the basic operating parameters, such as the power expended to change the vehicle's kinetic energy at the given acceleration (1). Since the vehicle's kinetic energy is obtained during the acceleration measurement in the first acceleration phase, it is reduced in the subsequent idle run phase by the energy associated with the basic motion drag, and the mass inertia drag in progressive and rotational motion. The second phase should be carried out under the same road and ambient conditions, preferably immediately after the acceleration phase (Fig. 2).

$$\Delta E_{k(V)} = \\ = \frac{m(v_{R(n)}{}^2 - v_{R(n-1)}{}^2)}{2} + \frac{m(v_{w(n-1)}{}^2 - v_{w(n)}{}^2)}{2} \quad (7)$$

where: $\Delta E_{k(V)}$ – kinematic energy change in the speed range, m – vehicle mass, V_R – vehicle linear speed during acceleration, V_W – vehicle linear speed during idle run, n – matrix index.

The final results of the powertrain's operating parameters are obtained in the proposed calculation algorithm (Fig. 3).

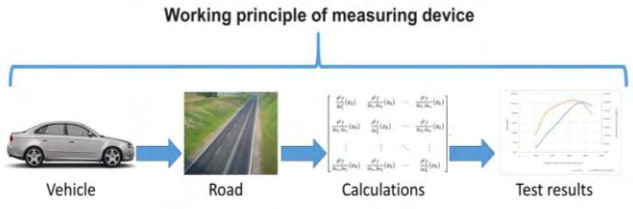

Fig. 3. Calculation algorithm for determining the powertrain's operating parameters and flexibility

The calculations of the powertrain's operating parameters and flexibility rely heavily on the measurement of the vehicle's kinematic parameters and the continuous measurement of its linear speed v, time, as well as other drive system operating parameters, such as accelerator pedal opening angle, shaft speed, intake air pressure, airflow pressure or fuel pressure. Recording of these parameters can be performed from the vehicle's OBD network [13] or from the on-board data transmission network. Due to the data transmission rate, it is a good idea to limit the amount of data recorded to the minimum necessary for the OBD system. The instantaneous values of the flexibility test's measurement parameters are simultaneously recorded as matrix elements labelled for the acceleration phase with the subscript R, and for the idle run phase with the subscript W (Fig. 4).

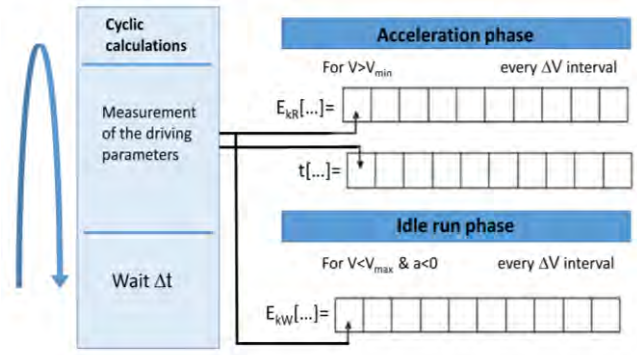

Fig. 4. Algorithm for matrix data storage during the two-phase test

At the same time, the recording's increment determinant for both matrices is the change in the vehicle's linear speed v (Fig. 5). It should be noted that the kinetic energy state and other recorded operating parameters at which the instantaneous kinetic energy states E_{kR} and E_{kW} were determined are stored in the matrix for velocity v under the same index.

Finally, at the end of the test, the change in the vehicle's kinetic energy is obtained with a corresponding change in vehicle speed. This allows for recording the dependency enabling the determination of the powertrain's operating parameters and flexibility in the given time interval. Equation (8) allows to determine the power.

$$N = \frac{|\Delta E_{kR}|}{|\Delta t_R|} + \frac{|\Delta E_{kW}|}{|\Delta t_W|} \quad (8)$$

where: $\Delta E_{kR/W}$ – change in energy for the given linear speed range, $\Delta t_{R/W}$ – change in time for the given linear speed range.

The power determined by the two-phase method takes into account changes in the vehicle's kinematics separately for the acceleration and idle run phases. The main advantage of this method is that carrying out a test of the correct operation of the drive system does not require the possession of specialized test stands, but only the available diagnostic equipment. Additionally, the proposed method takes into account the basic resistances occurring during the movement of the vehicle, which should give results much closer to the real ones in comparison to the simplified methods on which some diagnostic testers are based. However, the interpretation of the results obtained during the road test requires a deeper analysis. and comparisons to the drive system performance indicators provided by the manufacturer. Further mathematical operations, according to equation (9), enable the determination of the torque:

$$M = \frac{N}{2 \cdot \pi \cdot n} \quad (9)$$

The maximum power and torque values incremented for the nth matrix element in the form of the powertrain's shaft

speed allow for the determination of the powertrain's flexibility and its external speed characteristics curve waveform.

5. Analysis of results – the powertrain's operating parameters and flexibility

5.1. Internal combustion powertrain

As standard, the powertrain or other vehicle components diagnostics can be carried out via the diagnostic interface using the OBD diagnostic connector with the VCDS diagnoscope. At the same time, it is possible to save the values measured in the on-board diagnostic network in a file while driving on the road. In this case, the data so recorded for the test car was used in the flexibility test, and the test run was carried out for gears 3 and 4. Figure 5 shows the test for gear 3.

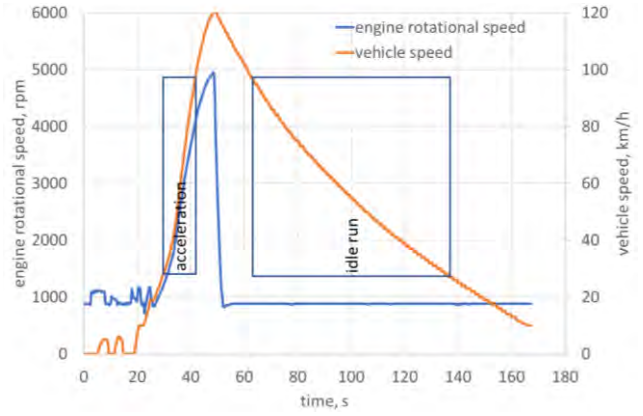

Fig. 5. Flexibility test demonstrating the speed change over time for the VCDS at gear 3

Once the calculations have been made according to the algorithm shown in Fig. 4, the waveform of the powertrain's operating parameters for full acceleration intensity can be determined. It is important to linearize and condense the measurement points in the flexibility test analysis process for both the acceleration and idle run phases, as the VCDS interface records the data at a frequency of approx. 3 ±1 Hz. Figures 6 and 7 show the waveform of the powertrain's operating parameters for gears 3 and 4.

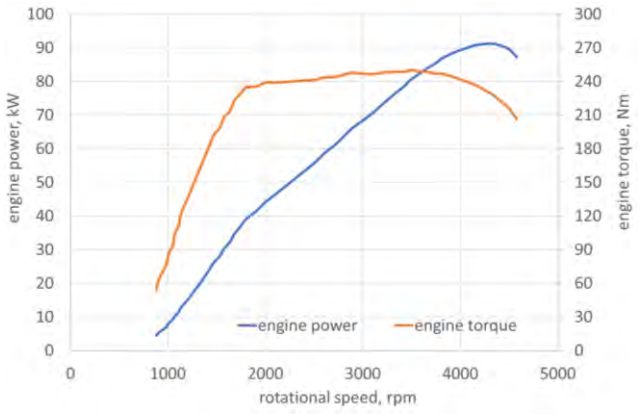

Fig. 6. Speed characteristics of power and torque in the flexibility test for gear 3

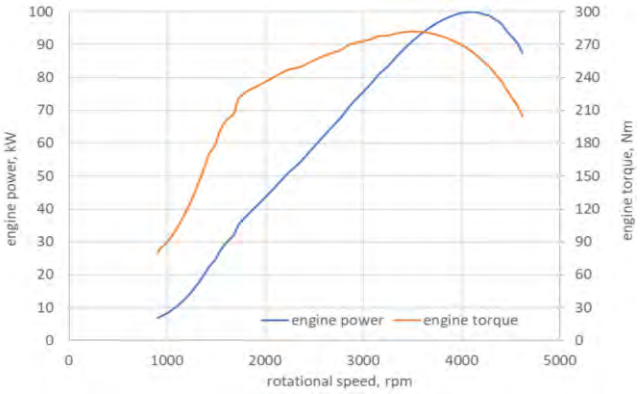

Fig. 7. Speed characteristics of power and torque in the flexibility test for gear 4

The flexibility test was repeated multiple times and the average values are presented in Table 2.

Table 2. Maximum parameters obtained using the VCDS interface for the Audi A4

Measured gear	N_{max}, kW	n, rpm	M_{max}, Nm	n, rpm	M_{Nmax}, Nm
3	91.16	4326	249.72	3486	228.22
4	99.94	4074	281.67	3591	265.66

An analysis of the discrepancies between the data reported by the manufacturer (Fig. 8) and that obtained in the road test using the VCDS diagnostic interface is shown in Tables 3 and 4.

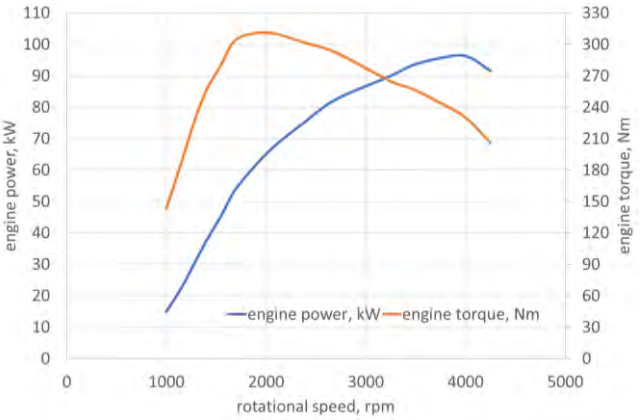

Fig. 8. Manufacturer speed characteristics of power and torque

Table 3. Absolute differences in the parameters compared to the nominal (factory) values for the Audi A4

Measured gear	ΔN_{max}, kW	Δn, rpm	ΔM_{max}, Nm	Δn, rpm	ΔM_{Nmax}, Nm
3	–4.84	326	–60,28	1586	–21.78
4	3.94	74	–28.33	1691	15.66

Table 4. Relative differences in the parameters compared to the nominal (factory) values for the Audi A4

Measured gear	ΔN_{max}, %	Δn, %	ΔM_{omax}, %	Δn, %	ΔM_{Nmax}, %
3	–5.04	8.15	–19.45	83.47	–8.71
4	7.34	1.85	–9.14	89.00	6.26

An analysis of these differences shows the occurrence of significant differences, mainly for rotational speeds, whose values are higher than 80% and for engine torque the differences are between 9.14 to 19.45% to nominal values (Table 4). This affects subsequent parameters, such as flexibility. The maximum values of power show a slight deviation of a few percent from the nominal values provided by the manufacturer, and their nature (both positive and negative deviations) may suggest, on one hand, that the road method isn't perfect by pointing to its measurement accuracy related to the frequency of recording the operating parameters from the OBDII diagnostic network, lower accuracy of used sensors and, on the other hand, that real-world values are very close to the nominal values. In addition, it should be noted that many manufacturers allow slight deviations of several percent of individual parameters, such as power, torque or rotational speeds values at which individual operating indicators are achieved in cars of the same series and model, which is confirmed by tests carried out on certified research test stands.

During the measurement carried out at the set ratio, high repeatability of the results was achieved. The relative difference in power measurement for each test did not exceed 1% of the average value obtained in all tests. Therefore, the calculations for each of the tests provided almost identical results. However, the results for individual gears shown differences in both engine power and torque. These values vary considerably: the maximum values for power at gear 3 are 5.04% lower and at gear four the values are 7.34% higher than the nominal values provided by the manufacturer. The different waveforms of the powertrain's operating parameters also resulted in a change in total flexibility, which was 48.1% lower for gear 3 and 54.0% lower for gear four than the values derived from the factory data. The discrepancies obtained are mainly due to differences between the respective reference speeds (as stated by the manufacturer) and those actually obtained due to the dynamics of the acceleration process. The individual flexibility parameters are summarised in Table 5.

Table 5. Flexibility parameters obtained using the VCDS interface for the Audi A4

Measured gear	e_M	e_n	e_c	Difference in e_c, %
gear 3	1.094	1.241	1.358	–48.1
gear 4	1.060	1.134	1.203	–54.0

These differences are the result of the selected gear during the flexibility test, which was carried out at the same, i.e. maximum, intensity in both cases.

5.2. Electric powertrain

The two-phase test was used to determine the powertrain's operating parameters and flexibility for another vehicle, i.e. the Renault ZOE. The flexibility tests were carried out for the drive system's Eco and Normal control modes. The Eco mode limits the available power in the drive system while limiting the temperature inside the car to 21°C. The Normal mode is characterised by the drive system's full power availability.

During the measurement carried out on the electric vehicle, high repeatability of the results was achieved and the relative error in power measurement for each test did not exceed 1% of the average value obtained in all tests (Table 6). These measurements were made with CAN BUS onboard data transmission network via the SYS TEC interface, where the highest recording frequency was close to 100 Hz.

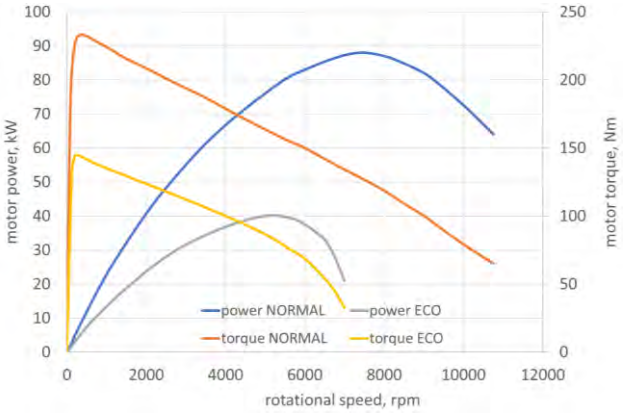

Fig. 9 Speed characteristics of power and torque in the flexibility test for the electric vehicle's Eco and Normal modes

Table 6. Maximum parameters obtained for the Renault Zoe

Designation	N_{max}, kW	n, rpm	M_{max}, Nm	n, rpm	M_{Nmax}, Nm
Eco	40.00	4950	144.52	150	77.20
Normal	88.00	7650	231.66	225	126.72

Table 7. Absolute differences in the parameters compared to the nominal values for the Renault ZOE

Designation	ΔN_{max}, kW	Δn, rpm	ΔM_{max}, Nm	Δn, rpm
Eco	0.00	–50	0.2	150
Normal	20.00	–350	21.66	225

Table 8. Relative differences in the parameters compared to the nominal values for the Renault ZOE

Designation	ΔN_{max}, %	Δn, %	ΔM_{max}, %
Eco	0	–1.00	0.26
Normal	29.41	–4.45	10.31

A summary of the flexibility parameters for the electric vehicle is presented in Table 9.

Table 9. Flexibility parameters for the Renault Zoe

Designation	e_M	e_n	e_c
Eco	1.872	34.000	63.648
Normal	1.828	34.000	62.152

As demonstrated in Table 6, the maximum torque and power values in the electric drive system vary considerably depending on the drive mode used. In the Eco mode, the maximum drive power has been limited to 40 kW, which is about 45% of the nominal power. A reduction of the maximum torque to 62% of the nominal value was also noted. At the same time, it should be noted that the electric powertrain can be briefly loaded above its nominal value without adversely affecting its durability. The Normal mode allowed for obtaining almost 30% more power compared to the nominal value during acceleration at maximum intensity and the higher power was available in the first acceleration

phase. Also, the maximum torque was more than 10% higher than its nominal value. The tested drive system does not have a gearbox, so both Eco and Normal modes measurements were carried out at the same overall gear ratio. The flexibility parameters for the two drive modes are very similar and the difference between the total flexibility index is approximately 2%. A comparison of the total flexibility parameters e_c shows that the electric passenger vehicle has higher (up to about 40 times) flexibility than the internal combustion vehicle.

6. Summary

The subject matter presented in the paper concerned the determination of power and torque and was aimed to verify their maximum values in a road test. The results obtained are largely consistent with the technical parameters specified in the factory data of the passenger vehicles tested. The small discrepancies of a few per cent for the internal combustion engine, being both positive and negative in nature, may indicate that the tested powertrain's real-world maximum operating parameters are very close to the nominal values stated by the manufacturer. Such values may suggest a good overall technical condition of the entire drive system, in particular the absence of significant mechanical faults. The determined power maximal values show that they are close to factory data without value fluctuations or significant differences. However, a significant shift in the maximum value was noticed, especially in terms of engine torque, towards much higher rotational speeds and lower maximal value (up to 20%) in relation to the data provided by the manufacturer. When analyzing the total elasticity index in this case, there are clear differences between the factory data and those obtained during the test, amounting to about 50% of the discrepancy between the factory and test values. This may indicate improper control, e.g. of the amount of air flowing to the engine related to the operation of the supercharging system. In the case of the electric drive system, the possibility of temporarily overloading the powertrain beyond the nominal values of power (by about 30%) and torque (by about 10%) also points to its good technical condition. Repeated measurements show significant repeatability under the same road conditions and on the same device. At the same time, the high frequency of the recorded data allows for determining very even and smooth power and torque characteristics. This allows for the conclusion that the proposed methodology, which utilises workshop diagnostic equipment and a two-phase road test, has satisfactory accuracy for obtaining basic torque and power parameters for different types of powertrains. The waveforms obtained can be used to assess the technical condition and in extended diagnostics of the vehicle's drive system. At the same time, the flexibility parameters determined on their basis deviate from the original data due to the reading of specific maximum values from the characteristics, which are influenced by many factors such as recording speed or process dynamics.

Acknowledgements

The paper is co-funded by the "DELTA" programme of the Opole University of Technology for researchers in 2021.

Nomenclature

BEV	battery electric vehicle
CAN	controller area network
ICE	internal combustion engine
OBD	on-board diagnostics
VCDS	VAG-COM diagnostic system

Bibliography

[1] Bździuch D. Measurement of engine operating parameters and diagnostic tests of motor vehicles on the VT-2 chassis dynamometer (in Polish). Autobusy: technika, eksploatacja, systemy transportowe. 2007; 6:560-568. bwmeta1.element.baztech-e4923386-3ba6-4208-9932-e5faf2878296

[2] Energy Agency I. Global EV Outlook 2022 Securing supplies for an electric future. 2022.

[3] Gardulski J. The fifth wheel as a part of a data acquisition system for diagnostic testing of car shock absorbers with vibroacoustic methods. Biuletin WAT 2011:1:83-91. bwmeta1.element.baztech-article-BWAW-0006-0041

[4] Graba M, Mamala J, Bieniek A, Sroka Z. Impact of the acceleration intensity of a passenger car in a road test on energy consumption. Energy. 2021;226: 120429. https://doi.org/10.1016/j.energy.2021.120429

[5] Haller P, Wróbel R, Dimitrov R, Michaylow V. Introducing new engine performance lab at the Department of Motor Vehicles and Combustion Engines of Wroclaw University of Technology. Combustion Engines. 2013;154(3):549-555.

[6] Hayes JG, Davis K. Simplified electric vehicle powertrain model for range and energy consumption based on EPA coast-down parameters and test validation by Argonne National Lab data on the Nissan Leaf. 2014 IEEE Transportation Electrification Conference and Expo. 2014:1-6. https://doi.org/10.1109/ITEC.2014.6861831

[7] Kolator B, Janulin M. Methodology for measuring car traction parameters. MATEC Web Conf. 2018; 182:02001. https://doi.org/10.1051/matecconf/201818202001

[8] Kubiak P, Krzemieniewski A, Lisiecki K, Senko J, Szosland A. Precise method of vehicle velocity determination basing on measurements of car body deformation–non-linear method for 'Full Size' vehicle class. Int J Crashworthiness. 2018;23(3):302-310. https://doi.org/10.1080/13588265.2017.1331692

[9] Kuranc A. Vehicle engine power tests using inertial methods (in Polish). Autobusy: technika, eksploatacja, systemy transportowe. 2012:13(10):119-124. bwmeta1.element.baztech-fd47b0d8-256a-48d9-8c7f-72f3c51f7f11

[10] Ligterink NE, van Mensch P, Cuelenaere RFA, Hausberger S, Leitner D, Silberholz G. Correction algorithms for WLTP chassis dynamometer and coast-down testing. 2014. https://climate.ec.europa.eu/system/files/2016-11/wltp_correction_algorithms_en.pdf

[11] Mamala J, Graba M, Bieniek A, Prażnowski K, Hennek K, Kołodziej S et al. Evaluation of energy consumption in the acceleration process of a passenger car. Combustion Engines. 2022;190(3):35-44. https://doi.org/10.19206/CE-142553

[12] Merkisz J, Rymaniak Ł. The assessment of vehicle exhaust emissions referred to CO_2 based on the investigations of city buses under actual conditions of operation. Eksploat Niezawodn. 2017;19(4):522-529. https://doi.org/10.17531/ein.2017.4.5

[13] Merkisz J, Mazurek S. On board systems for passenger vehicles (in Polish). WKiŁ. Warsaw 2002.

[14] Mysłowski J. The flexibility of modern spark ignition engines (in Polish). Autobusy: technika, eksploatacja, systemy transportowe. 2011;12(5):307-311. bwmeta1.element.baztech-article-BWAN-0021-0046

[15] Pielecha I, Pielecha J. Simulation analysis of electric vehicle energy consumption in driving test. Eksploat Niezawodn. 2020;22(1):130-137. https://doi.org/10.17531/ein.2020.1.15

[16] Pielecha J, Skobiej K, Kurtyka K. Exhaust emissions and energy consumption analysis of conventional, hybrid and electric vehicles in real driving cycles. Energies. 2020;13(23):6423. https://doi.org/10.3390/en13236423

[17] Prochowski L. Movements Mechanics (in Polish). WKiŁ. Warsaw 2016.

[18] Sapundzhiev M, Evtimov I, Ivanov R. Determination of the needed power of an electric motor on the basis of acceleration time of the electric car. IOP Conf Ser Mater Sci Eng. 2017;252:0120636. https://doi.org/10.1088/1757-899X/252/1/012063

[19] Szpica D. Coefficient of engine flexibility as a basis for the assessment of vehicle tractive performance. Chin J Mech Eng. 2019;32(1):1-9. https://doi.org/10.1186/s10033-019-0352-8

Andrzej Bieniek, DEng. – Faculty of Mechanical Engineering, Opole University of Technology, Poland.
e-mail: *a.bieniek@po.edu.pl*

Mariusz Graba, DEng. – Faculty of Mechanical Engineering, Opole University of Technology, Poland.
e-mail: *m.graba@po.opole.pl*

Prof. Jarosław Mamala, DSc., DEng. – Faculty of Mechanical Engineering, Opole University of Technology, Poland.
e-mail: *j.mamala@po.opole.pl*

Prof. Andrzej Augustynowicz, DSc., DEng. – Faculty of Mechanical Engineering, Opole University of Technology, Poland.
e-mail: *a.augustynowicz@po.opole.pl*

Michał Szczepanek, Eng. – Student in the Faculty of Mechanical Engineering, Opole University of Technology, Poland.
e-mail: *michal.szczepanek@student.po.edu.pl*

Ergonomics and automation

Compliance: UE regulations 2017/1151, EN 12341:2014, US EPA 40CFR 1065, 40CFR part 50

- Automation of measurement
- On-line measurement d
- Air buoyancy correctio
- Dynamic analysis of the quality of weighing
- Environmental conditions module

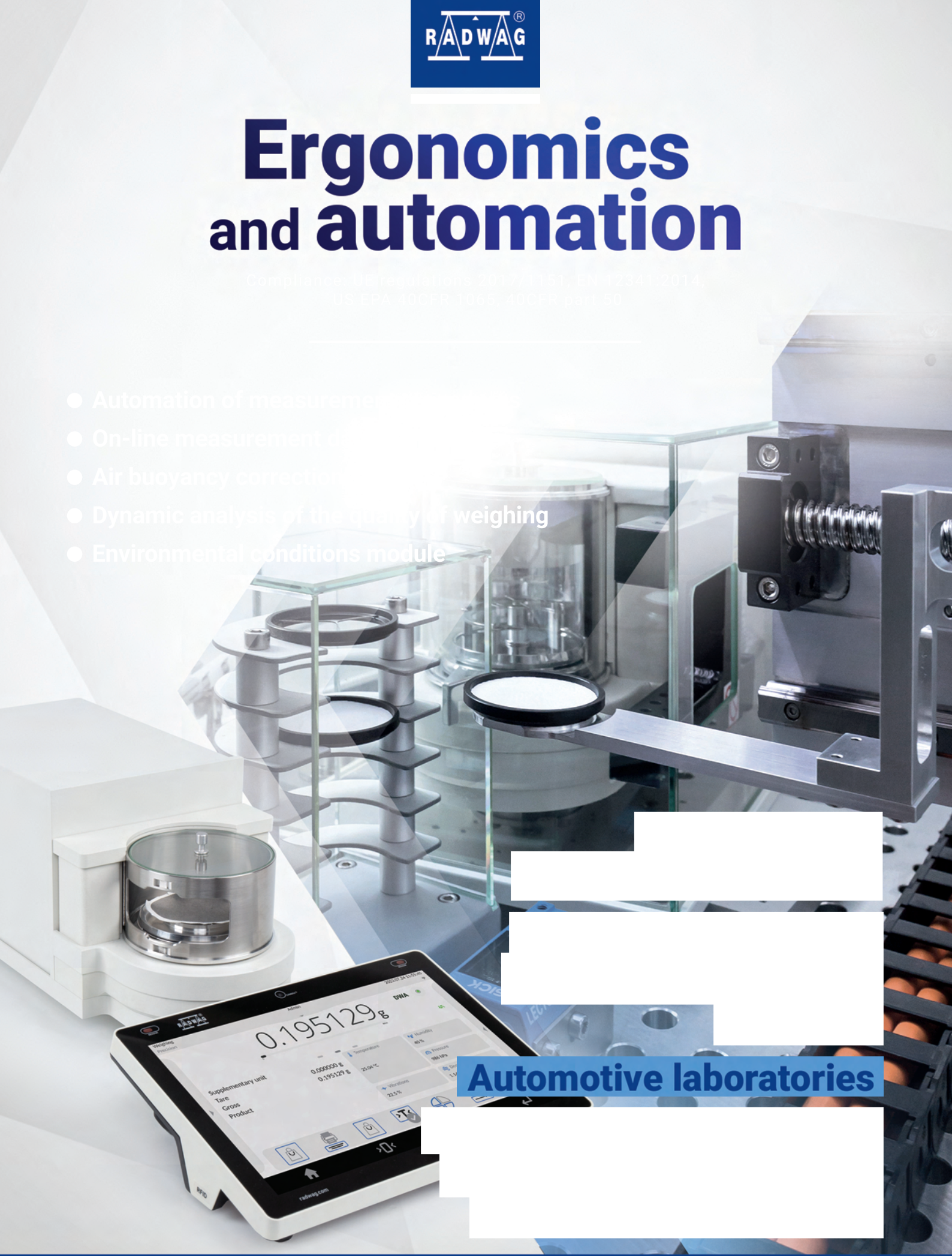

Automotive laboratories

RADWAG Wagi Elektroniczne
26-600 Radom, ul. Toruńska 5
tel. 48 386 60 00, e-mail: radom@radwag.pl

radwag.com

Poznan University of Technology

Faculty of Civil and Transport Engineering

Institute of Combustion Engines and Powertrains

- Emissions of combustion engines and hybrid powertrains
- Energy consumption of HEV, FCHEV, EV
- Hydrogen and multi-fuel combustion engines
- Maintenance of aircraft propulsion
- Vehicle and aircraft simulators
- Unmanned aerial vehicles
- Combustion systems
- Fuel cells

Institute of Combustion Engines and Powertains
Division of Combustion Engines | Division of Alternatives Powertrains | Division of Aircarft
Piotrowo 3 street, 60-965 Poznan, Poland
Phone: +48 61 665-2207; office_ice@put.poznan.pl

Publisher:

Polish Scientific Society of Combustion Engines

Combustion Engines

Polskie Towarzystwo Naukowe Silników Spalinowych

ISSN: 2300-9896
eISSN: 2658-1442

www.combustion-engines.eu